Elektrochemie von „trockenen“ Metalloberflächen im Hinblick auf atmosphärische Korrosion

Dissertation

zur

Erlangung des Grades

Doktor-Ingenieur

der

Fakultät für Maschinenbau

der Ruhr-Universität Bochum

von

Cristiano Kasdorf Giesbrecht

aus Bagé, Brasilien

Bochum 2023

Dissertation eingereicht am: 30.05.2023

Tag der mündlichen Prüfung: 08.08.2023

Erstgutachter: PD Dr. rer. nat. Michael Rohwerder

Zweitgutachter: Prof. Dr. rer. nat. Martin Stratmann

Electrochemistry of “dry” metal surfaces with regard to atmospheric corrosion

Cristiano Kasdorf Giesbrecht

RUHR
UNIVERSITÄT
BOCHUM

RUB

Fakultät Maschinenbau
fortschritt studieren

MAX-PLANCK-INSTITUT
FÜR EISENFORSCHUNG GmbH

Acknowledgements

In the year of 2008, I had the pleasure to make my internship at the Max-Planck-Institut für Eisenforschung GmbH (MPIE), in Düsseldorf, taking part of Dr. Michael Rohwerder’s group. It was my first international scientific experience. Back to Brazil to finish my Chemistry Course, I always remembered the good time spend in the MPIE. In 2017, after finishing my Master in Chemistry at the Federal University of Santa Maria (UFSM), Brazil, I received the opportunity to start a doctorate in Dr. Rohwerder’s group. My special thanks to him for this opportunity, for his teachings and suggestions in my work and dissertation.

I also want to thank the MPIE, for the structure, high tech instrumentation and possibility to make the research which led to this dissertation and for the financial support at my stay in Germany. My thanks to the Fakultät für Maschinenbau of the Ruhr-Universität Bochum (RUB) for accepted me as a PhD student. I am also thankful to Prof. Dr. Martin Stratmann and Prof. Dr. Andreas Ostendorf for taking part in my PhD defense.

Special thanks to Dirk Vogel and Alexandra Vogel for the support by assembling the new instrumentation in the laboratory. I am also thankful to Petra Ebbinghaus and Martin Rabe for the suggestions and discussions regarding the optical spectroscopy instruments, to Philipp Kerger for the supporting with the XPS technique, to Eberhard Heinen for the sample preparation in the PVD instrument and to the workshop team for manufacturing some instrumentation components.

The start of a new life, in other country, far away from family and friends may not be an easy process. In this sense, my thanks to all people from the MPIE and RUB who helped me with the bureaucracies and for giving me answers and tips for many questions about “living in Germany”, especially to Brigitte Kohlhaas. My thanks to all employees and students for the friendship and assistance in my research.

Now, a very special thank to my wife Bruna Mohr Giesbrecht, which came from Brazil to support and live here in Europe with me and to my family, especially my parents Walter Giesbrecht and Anneliese Kasdorf Giesbrecht for all support and encouragement in this step of my academic and personal life.

“Great minds discuss ideas;
Average minds discuss events;
Small minds discuss people.”

Anna Eleanor Roosevelt

Abstract

In this dissertation a methodology for tailoring the electrochemical double layer of electrodes covered by electrolyte layers in the sub-monolayer and monolayer range was developed. It is based on the emersion of electrodes under potential control from the electrolyte into inert atmosphere of different relative humidity. By adjusting the relative humidity to different levels, the thickness of the resulting double layer of the emersed electrode can be controlled. Furthermore, a simple Kelvin probe-based approach for determining the kinetics of important electrochemical reactions on such electrodes was developed. Thus, it should be possible to correlate kinetics and structure in an unprecedented way, since the whole double layer region is directly accessible for surface analytical methods. Such correlation should not only be of importance for providing deeper insight into fundamental electrochemistry, but also for applications such as electrochemical reactions on catalysts in fuel cells or surfaces of technical materials exposed to atmospheric corrosion conditions, where in both cases electrochemical reactions underneath ultra-thin electrolyte layers play a crucial role. In this work the studies were mainly carried out on gold electrodes emersed from aqueous electrolytes. More precisely, the samples consisted of a 200 nm gold layer deposited by physical vapor deposition (PVD) on glass substrates. Electrolytes with different anions and pH values were chosen: 0.1 mol L^{-1} $NaClO_4$, 0.05 mol L^{-1} H_2SO_4 and 0.1 mol L^{-1} NaOH. A complex instrumentation system was assembled for this study, as part of dedicated a laboratory concept. For this, a three-electrode electrochemical cell, a Kelvin probe and a Fourier-transform infrared spectrometer (FT-IR) were combined, between which samples could be transferred without exposure to atmosphere, thus preserving the prepared double layer. Furthermore, a spectroscopic ellipsometer and a Near Ambient Atmosphere (NAP) X-ray Photoelectron Spectrometer (XPS) were employed. The Kelvin probe and the NAP-XPS analysis chambers allow *in operando* studies (at different atmosphere conditions). As reference for the electrochemical cell and for the Kelvin probe calibration Ag/AgCl/3M KCl reference electrodes were chosen (all potentials presented in the results and discussion sections are referred against this electrode).

Potentials applied on the sample during immersion were stepped in a wide range: from -0.4 until 1.3 V (positive direction) and from 1.3 until -0.4 V (negative direction). Different atmospheric conditions were adjusted for the studies on the emersed sample surface: relative humidity values of 1-3%, 65-70% and 90-95% and nitrogen or synthetic air were investigated. The Volta potential difference was determined by Kelvin probe technique and a linear range with unity slope after emersing the electrode from the electrolyte was generally observed for applied potentials between about 0.1 until 1.0 V, depending on the electrolyte and atmospheric condition. This potential range corresponds to the potential window from PZC to gold oxidation. When the measured values were calibrated vs the Ag/AgCl reference electrode, the resulting potential values where close to the applied values or higher, depending on the relative humidity. This is attributed to the role of amount water molecules and their orientations and corresponding dipole moments to the potential. Increases in the Volta potential difference up to 0.2 V were observed when stepping the potentials during the polarization in the negative direction compared to the experiments in which the potentials were stepped in positive direction. Around PZC and towards potentials below PZC the measured potential values suggest a re-orientation of the water molecules. Some characteristics in the diagrams $\Delta\Psi$ vs E suggest a dependence on the electrolyte anions. The FT-IR spectra show the presence of hydroxide group from water molecules adsorbed on the emersed gold electrode surface and a possible reorientation around the PZC. The results obtained by ellipsometry suggest a layer thickness in sub-monolayer range adsorbed on the gold surface.

Contents

Acknowledgements…… c
Abstract…… e
Glossary…… V
List of Figures…… XIII
List of Tables…… XXVII
1 Motivation…… 1
2 Introduction…… 5
  2.1 Corrosion…… 5
    2.1.1 Thermodynamics and kinetics related to corrosion…… 6
    2.1.2 The Pourbaix diagram…… 9
    2.1.3 Corrosion types…… 13
  2.2 Hydrogen…… 17
    2.2.1 Innovation involving hydrogen energy…… 18
    2.2.2 Hydrogen negative effect on metals…… 19
  2.3 Electrodes, potentials and the electrochemical double layer…… 22
    2.3.1 Nernst equation and the cell potential…… 25
    2.3.2 Reference electrodes…… 27
    2.3.3 Working and counter electrodes…… 28
  2.4 Kelvin probe…… 29
    2.4.1 Measurement of the Volta potential…… 29
  2.5 Fourier-transform infrared spectroscopy…… 33
  2.6 Spectroscopic ellipsometry…… 37
  2.7 X-ray photoelectron spectroscopy…… 38
  2.8 Potential of zero charge…… 41
  2.9 The idea of electrodes emersed from aqueous electrolytes…… 42
    2.9.1 The role of humidity inside the analysis chamber…… 43
  2.10 Gold employed as electrode…… 44
  2.11 Choosing the electrolyte: $NaClO_4$, H_2SO_4, NaOH…… 45
3 Experimental…… 47
  3.1 Equipment…… 47

3.1.1 Kelvin probe system…………..……………………………….…….……. 47

3.1.2 FT-IR spectrometer……………………….………………………..………. 49

3.1.3 Electrochemical cell.………….……………………………….….…………. 49

3.1.4 Laboratory concept: combining electrochemical cell, Kelvin probe and FT-IR……………………………………………………………………… 54

3.1.5 Spectroscopic ellipsometer……..…………………………………………… 60

3.1.6 NAP-XPS spectrometer…………………………………….…………… 62

3.1.7 Other devices……………..…..…………………………………………… 66

3.2 Reagents and gases.……………………………………………………………… 67

3.3 Samples…………………………..………………………………………… 68

3.4 Cleaning procedures………………..………………………………………… 69

3.5 pH determination of the electrolyte....…………………………………………… 69

3.5.1 pH values of different electrolyte concentrations………………………. 70

3.6 Sample preparation and introducing into the electrochemical cell…….……… 72

3.7 Calibrating the Kelvin probe……………………………………………………… 74

3.8 Open circuit potential measurement……………………………………..……… 78

3.8.1 Open circuit potential measured on the gold sample in the main electrolytes used in this work…………………………………………..... 79

3.9 Cooling the sample down to achieve higher RH values…...…………………… 79

3.10 Measurement of the potential of the emersed samples as function of the potential applied during immersion……………………………...…………….. 80

3.11 FT-IR measurements on gold surfaces after applying potentials in the electrochemical cell….…………………………………………………...……… 81

3.12 Ellipsometry determinations…………………………………………………… 82

3.13 XPS measurements on gold surfaces after applying potentials in the electrochemical cell….…………………………………………………...……… 82

3.14 Flowchart of the processes involved in this work..……………………………… 83

4 Results and discussions...…………………………………………………...……… 85

4.1 Kelvin probe calibration by “dry” Ag/AgCl reference electrodes……………… 85

4.1.1 Background …………...……………………..85

4.1.2 Results on stability of HOPG vs changes of relative humidity and partial pressure of oxygen………………………………………………………88

4.1.3 Results of stability of “dry” Ag/AgCl vs changes of relative humidity and partial pressure of oxygen…………………………………………….……… 90
4.2 Measurement of the correlation between applied potential and the potential of the emersed gold electrode……………………………………………………100
4.2.1 Comparing the Volta potential difference when potentials were stepped in positive and in negative direction………...................................111
4.2.2 Potential of zero charge and specific anion adsorption……………..113
4.2.3 Water molecules orientation on the metal surface and the role of specifically adsorbed anions……………………………………………119
4.2.4 Alkaline media solution as electrolyte……………………...…………..122
4.2.5 Bromide anion solution as electrolyte with higher specific adsorption…………………………………………………………..……..…….125
4.2.6 Evaluation of the addition of N_2 atmosphere inside the electrochemical cell during the emersing process…………...………...…………..132
4.3 Preliminary investigation on electrochemical reactivity of the emersed electrodes…………………………………………………………...…..……….134
4.4 Results obtained by FT-IR measurements on the gold electrodes after emersion……………………...……………………...……………….……….146
4.4.1 FT-IR spectra from gold surfaces employing $NaClO_4$ solution as electrolyte…………………...…………………………….…………...152
4.4.2 FT-IR spectra from gold surfaces employing H_2SO_4 solution as electrolyte …………………...…………………………………………...160
4.4.3 FT-IR spectra from gold surfaces emersed into humid atmosphere.171
4.5 Results obtained by ellipsometry..……………………………….……..176
4.6 Preliminary investigations by XPS……………………………………….179
4.7 Measurement of OCP after stopping polarization without removing the electrolyte from the electrochemical cell and after emersion and re-immersion of the sample……………………………………………………179
5 Summary and Outlook…………………………………………………………189
Bibliography………………………………………………………………………….195
Appendix A: Configuring and testing the electrochemical cell…………...………..207
Curriculum Vitae………..………………………………………………………...……213

Glossary

Abbreviations and chemicals formula:

AC	Alternating field
AgCl	Silver chloride
APXPS	Ambient pressure x-ray photoelectron spectroscopy
CE	Counter electrode
ClO_4^-	Perchlorate ion
CHA	Concentric hemispherical analyzer
CPD	Contact potential difference (is equivalent to Volta potential difference)
CPS	Counts per second
e^-	Electron
ESCA	Electron spectroscopy for chemical analysis
FIR	Far infrared
FT-IR	Fourier-transform infrared spectroscopy
HCl	Hydrochloric acid
$HClO_4$	Perchloric acid
H_2O_2	Hydrogen peroxide
H_2SO_4	Sulfuric acid
H_{ab}	Absorbed hydrogen
H_{ad}	Adsorbed hydrogen

HgO	Mercury oxide
Hg_2Cl_2	Mercurous chloride (calomel)
Hg_2SO_4	Mercurous sulfate
HOPG	Highly oriented pyrolytic graphite
HSA	Hemispherical sector analizer
IR	Infrared
KBr	Potassium bromide
KCl	Potassium chloride
KP	Kelvin probe
LN-MCT	Liquid Nitrogen cooled HgCdTe detector
Me	Representation of a metal in reactions
MEA	Membrane Electrode Assembly
MIR	Mid infrared
NaCl	Sodium chloride
$NaClO_4$	Sodium perchlorate
NaOH	Sodium hydroxide
Na_2SO_4	Sodium sulfate
NAP	Near ambient pressure
NAP-XPS	Near ambient pressure x-ray photoelectron spectroscopy
NIR	Near infrared
OCP	Open circuit potential
ORR	Oxygen reduction reaction

ppb	Parts per billion
ppm	Parts per million
PTFE	Polytetrafluorethylene
PVD	Physical vapor deposition
PZC	Potential of zero charge
RE	Reference electrode
RH	Relative humidity
rpm	Rotations per minute
SCE	Saturated calomel electrode
SE	Spectroscopic ellipsometry
SHE	Standard hydrogen electrode
Std	Standard deviation
UHV	Ultra-high vacuum
UV	Ultraviolet
WE	Working electrode
XPS	X-ray photoelectron spectroscopy

Formula abbreviations and parameters:

C	Capacitance
E	Electrode potential, electric field
E^0	Standard potential
E_{abs}	Absolute electrode potential
E_{b}	Electron binding energy
E_{F}	Fermi energy level
E_{j}	Liquid junction potential
E_{k}	Electron kinetic energy
E_{vac}	Vacuum level
E_{ip}	Incident electric wave amplitude (parallel)
E_{is}	Incident electric wave amplitude (perpendicular)
E_{rp}	Reflected electric wave amplitude (parallel)
E_{rs}	Reflected electric wave amplitude (perpendicular)
F	Faraday constant (9.64853 x 10^4 C mol^{-1})
ΔG	Gibbs free energy change
h	Planck constant (6.62608 x 10^{-34} J s)
H	Enthalpy
ΔH	Enthalpy change
ΔH_{f}^0	Standard enthalpy of formation
i	Current density

I	Current
k_0	Standard rate constant
k_d	Mass transfer coefficient
n	Number of transferred electrons
p	Pressure
R	Gas constant (8.31451 J K^{-1} mol^{-1}), ohmic resistance, reflection coefficient
ΔS	Entropy change
tan	Tangent
T	Temperature
U	Internal energy, potential
ΔU	Internal energy change
V	Potential
ΔV	Volume change
α	Activity
β	Geometric factor
σ	Surface charge
Δ	In ellipsometry, the phase difference between the two polarized incident waves and the two polarized reflected waves; difference (change) in a variable
δ	In infrared spectroscopy, deformation vibration; in the electrical double layer theory, dipole moment
η	Overpotential
μ_e	Chemical potential
ν	Radiation frequency

ν_a	Antisymmetric stretching vibration
ν_s	Symmetric stretching vibration
ρ	In ellipsometry, the complex ratio of the total reflection coefficients
$\Delta\varphi$	Galvani potential
$\Delta\varphi^{Me}_{El}$	Potential drop across the metal/electrolyte layer interface
ϕ	Work function
χ	Surface potential (also χ_S)
$\Delta\chi$	Surface potential difference
Ψ	Volta potential
$\Delta\Psi$	Volta potential difference
Ψ	In ellipsometry, correspond to the amplitude ratio between “p” and “s” polarizations

List of Figures

Figure 1. Scheme of the electrochemical process of steel corrosion 6

Figure 2. Example of energy balance in the life cycle of iron 7

Figure 3. Pourbaix diagram (*E* vs pH) for gold at 25 °C. In the diagram, the domain hatched with ▦ represents the immunity region (corrosion not possible); the domain hatched with ▨ represents the regions where corrosion is possible (in the $Au(OH)_3$ region some degree passivity is expected) 10

Figure 4. Pourbaix diagram (*E* vs pH) for water and its decomposition products..11

Figure 5. Scheme representing the main constituents responsible for atmospheric corrosion...14

Figure 6. Instrument set-up example for the hydrogen electrode in the “dry” concept: a) potentiostat; b) reference electrode; c) counter electrode; d) connection to the working electrode; e) gas inlet; f) gas outlet; g) electrolyte; h) working electrode (sample); i) Kelvin probe tip; j) Kelvin probe; k) gas inlet; l) gas outlet 21

Figure 7. Schematic sketch of Galvani potential (composed by the surface potential difference and the Volta potential difference) at electrode with positive charge..23

Figure 8. Scheme of a three-electrode cell: a) voltmeter (potentiostat); b) commercial Ag/AgCl reference electrode; c) working electrode; d) counter electrode; e) inert gas inlet; f) gas outlet; g) Luggin capillary; h) electrolyte 25

Figure 9. Kelvin probe: a) schematic of the principle with a vibrating tip; b) diagram representing the Fermi energy levels of the Kelvin probe tip (E_F

$_{\text{KP}}$) and the sample ($E_{\text{F Sample}}$), the work functions of the Kelvin probe (ϕ_{KP}) and the sample (ϕ_{Sample}) and the contact potential difference (V_{CPD}, also called $\Delta\Psi$) between tip and sample. E_{vac} represents the vacuum level. The tip represented in b) is drawn inverted to facilitate interpretation of the diagram…………………………………….………30

Figure 10. Electron energy level diagram for Kelvin probe tip and sample: a) without electrical contact between them; b) with electrical contact between them …………………………………………………………….…32

Figure 11. Representation of periodic motions of water molecule (a – c) and carbon dioxide (d – g), where ν_s represents the symmetric stretching vibration, ν_a represents the antisymmetric stretching vibration and δ represents the deformation vibration; the representations f) and g) are the same, but viewed from two different perspectives ……………......34

Figure 12. Diagram of the interferometer parts in a FT-IR spectrometer: a) IR beam coming from the source; a_x) part of the IR beam reflected by the beamsplitter; a_y) part of the IR beam transmitted through the beamsplitter; b_y) the "a_y" beam reflected by the fixed mirror; b_x) the "a_x" beam reflected by the movable mirror; b) combined beam of "b_x" and "b_y" reaching the sample surface; c) beam reflected on the sample surface reaching the instrument detector……………………….………36

Figure 13. Schematic principle of the ellipsometry technique, where "p" and "s" represent the parallel and the perpendicular waves, respectively …….37

Figure 14. Schematic representation of an XPS system with four differential pumping stages; p_0, p_1, p_2, p_3 and p_4 represents the pressure in each of the chamber/stages, where $p_0 > p_1 > p_2 > p_3 > p_4$. This instrumentation was also used in the present work and is described in section 3.1.6. The differential pumping depicted here is necessary to achieve so called Ambient Pressure XPS (APXPS) …………………………………………………..39

Figure 15. The Kelvin probe system: a) probe retract manipulator; b) tip; c) sample; d) sample holder; e) KP grounding; f) sample grounding; g) adjustable probe retract manipulator ……………………..……………………...……48

Figure 16. The electrochemical cell: a) electrochemical cell; b) gas inlet and c) outlet into the electrochemical cell; d) gas inlet for the electrolyte flask; e) drying N_2 inlet for drying the sample surface after contact with the electrolyte; f) Ag/AgCl reference electrode; g) working electrode connection; h) electrolyte inlet in the electrochemical cell; i) counter electrode connection; j) electrolyte waste outlet valve; k) diaphragm pump for the electrolyte; l) potentiostat connected to the electrochemical cell via reference electrode, working electrode and counter electrode; m) valve for changing the electrolyte flow from the electrochemical cell back to the electrolyte flask; n) control valve to controlling the flow of the “removing electrolyte”; o) glass trap containing inert oil to prevent entrance of atmospheric air in the electrochemical cell; p) flask for waste (electrolyte leaking) collecting; q) valve for overpressure releasing; r) electrolyte refill system; s) electrolyte flask; t) drain system for clean out the electrolyte flask and the electrochemical cell hoses; u) glass traps with the second trap containing inert oil to prevent entrance of atmospheric air in the electrolyte flask; v) flask for collecting mixture of electrolyte and inert oil in case of overpressure in the system. Hoses and cables in the drawing may differ in length from the real equipment. All valves are represented in “closed” mode……………………………..……………………………………..51

Figure 17. Layout of the electrochemical cell: a) device extremity for sample introduction in the cell with a sample (yellow detail); b) counter electrode (platinum foil); c) Luggin capillary ending with a small platinum wire at the extremity; d) electrochemical cell itself; e) electrolyte inlet and outlet (when removing electrolyte from the cell); f) electrolyte outlet; g) counter electrode (platinum wire); h) Ag/AgCl reference electrode.

This system is represented slightly tilted as in the real instrumentation…………………………………………………………...53

Figure 18. Technical drawing of the FT-IR spectrometer with microscope and macro imaging chamber, the electrochemical cell and the Kelvin probe mounted on the SPECS structure: a) FT-IR external detector; b) Kelvin probe manipulator; c) IR beam guide chamber (equipped with a light polarizator); d) FT-IR spectrometer; e) microscope; f) macro imaging chamber. Some cables and hoses were neglected in this representation……………………………..……………...………...55

Figure 19. Top view perspective of the system: a) sample manipulator (with inlet and outlet for cooling water); b) Kelvin probe/infrared beam chamber; c) “quick-closing” door to connecting a vacuum suitcase; d) electrochemical cell; e) FT-IR external detector; f) sample transfer with storage (for up to three samples) chamber. Cables and hoses were neglected in this representation ……………………..……………….56

Figure 20. Lateral view of the vacuum suitcase: a) removable sample vessel; b) hook for connection to the desired system; c) UHV valve; d) transferring bar ..……………………………………………………………………….57

Figure 21. Humid atmosphere control system for the Kelvin probe/infrared beam chamber: a) gas inlet in the system; b) wet atmosphere mass flow meter/controller; c) dry atmosphere mass flow meter/controller; d) Kelvin probe; e) Kelvin probe/infrared beam chamber; f) connection to the FT-IR external detector; g) connection to the FT-IR spectrometer; h) dew point meter (chamber outlet); i) dew point sensor; j) dew point meter (chamber inlet); k) chilled mirror hygrometer; l) oxygen measuring transmitter; m) water flasks for the humid atmosphere; n) glass traps with the second trap containing inert oil to prevent entrance of atmospheric air in the system. Hoses and cables in the representation may differ in length from the real equipment. All valves are represented in “closed” mode……………………………………………………………59

Figure 22. Spectroscopic ellipsometer device: a) gas inlet in the system; b) manipulator (*x*, *y* and *z* axes); c) analysis chamber; d) receiver unit; e) input unit; f) control box; g) optical fiber cables; h) gateway to the sample transferring chamber, in which is located the gas outlet………62

Figure 23. Top view perspective of the NAP-XPS device (first level): a) UHV manipulator with *in-situ* reactor NAP cell; b) focused monochromatic X-ray source; c) X-ray monochromator; d) first pumping stage; e) UHV pump on the second pumping stage; f) UHV pump on the third pumping stage; g) hemispherical energy analyzer; h) gas handling system; i) analysis chamber; j) X-ray source; k) fourth pumping stage; l) detector. The major part of cables and hoses were neglected in this representation…………………………………………………………….64

Figure 24. Top view perspective of the second level of the system composed by: a) electrochemical cell; b) buffer chamber; c) transfer/storage chamber; d) load lock; e) preparation chamber; f) load lock compatible with a vacuum suitcase. Cables and hoses were neglected in this representation ………………………………………………..…………..65

Figure 25. a) measured potential of the pH meter vs the pH of the pH buffers with trend line (in black color); b) concordance of measured pH buffers; c) measured pH for different $NaClO_4$ concentrations …………………...…71

Figure 26. Representation of the electrochemical cell with the device for sample introduction into the system: a) device pulled back; b) enlarged view of the device extremity (without sample/sample holder); c) device with sample (yellow detail) connected to the other side (sample in contact with electrolyte); d) enlarged view of a gold sample fixed on the sample holder 73

Figure 27. Sketch of the electrochemical cell set-up used for the preparation of the Ag/AgCl/KCl reference electrodes: a) Ar inlet; b) working electrode (Ag sample); c) reference electrode; d) counter electrode; e) electrochemical cell; f) electrolyte. The gas outlet is placed on the rear of the cell ……………………………………………………………………….76

Figure 28. Schematic representation of the Kelvin probe calibration process: a) the homemade Ag/AgCl/KCl reference electrode is removed from the electrochemical cell, dried and the Volta potential difference determined using the Kelvin probe providing the calibration of the tip; b) a sample is polarized in the electrochemical cell; c) the same polarized sample has the potential determined by the previously calibrated Kelvin probe. Cables and hoses were neglected in this representation………..…….77

Figure 29. OCP of the gold sample for 24 h. For a) 0.1 mol L^{-1} $NaClO_4$ and b) 0.05 mol L^{-1} H_2SO_4 solutions, purged with N_2 at a flow rate of 250 mL min^{-1} during the whole time of measurement………………………………..…79

Figure 30. Flowchart of the processes involved in the dissertation work ………....84

Figure 31. Diagrams representing the Volta potential difference measured between Kelvin probe tip and HOPG sample during: a) 40 min while changing the atmosphere conditions every 10 min (dry N_2 and dry synthetic air) and b) 20 min while changing the atmosphere conditions every 10 min (dry N_2 and wet N_2). Picture in c) is the real HOPG sample fixed on a sample holder and employed in the experiments presented in this section ……...………………………..…………..………..…………….…..89

Figure 32. Diagram representing the current (*I*) vs the potential (*E*) typical behavior along time during the Ag/AgCl reference electrode fabrication process………………………………………………………………… … 91

Figure 33. Prepared Ag/AgCl electrode measured in humid N_2 atmosphere inside the SKP chamber for 50 min (Ag/AgCl electrode vs SHE calibrated against $Cu/CuSO_4$)…………………..…………..……………………..92

Figure 34. Volta potential difference determined by Kelvin probe on Ag/AgCl reference electrode in changing atmosphere conditions: a) dry (1-3%

RH) and wet (65-70% RH) N_2 and b) wet (65-70% RH) N_2 and wet (65-70% RH) synthetic air atmosphere ...…………...…………………………..93

Figure 35. Volta potential difference measured between Kelvin probe tip and HOPG sample during 120 min while changing the atmosphere conditions every 30 min: a) dry N_2 and dry synthetic air and b) wet N_2 and wet synthetic air…………………………………………...…………96

Figure 36. Volta potential difference measured between Kelvin probe tip and HOPG sample during 120 min while changing the atmosphere conditions every 30 min (wet N_2 and wet synthetic air). Experiment carried out some months later…………...……………………………..…97

Figure 37. Diagrams representing a long-term determination of the Volta potential difference between the Kelvin probe tip and the HOPG sample surface…………………………………………………………………….99

Figure 38. Plots of the potential measured by KP on the emersed electrode (vs Ag/AgCl) vs the potentials applied on evaporated gold for emersion into nitrogen atmosphere of different relative humidity. Electrolytes were 0.05 mol L^{-1} H_2SO_4 solution (a) and b)) and 0.1 mol L^{-1} $NaClO_4$ solution (c) and d)), with the potentials stepped in a) and c) positive and in b) and d) negative direction………………………………...……………104

Figure 39. Schematic explanation of the probable dependence of the potential measured on the emersed electrode and relative humidity: a) clean gold (i.e. without any ions or water molecules adsorbed) in vacuum, where the measured potential is corresponding to the work function of the clean gold, b) gold polarized (anion adsorbed and corresponding positive charge on the gold surface) in UHV condition (without water molecules), c) same as b) but with a presence of a minimum amount of water molecules, assumed to be adsorbed preferentially to the charges, d) very low humidity (of 1-3% RH, which is the dry condition in this work), e) intermediate relative humidity of 65-70% RH, f) higher humidity of 90-95% RH (and with d)-f) indicated by 1-3), g) experimental example demonstrating the corresponding difference observed between the three different humidity conditions analyzed in this study……….108

Figure 40. Comparison of potentials applied in positive and in negative direction with different electrolytes and atmosphere (RH values) conditions.…112

Figure 41. Plots of potential of the emersed electrode vs the applied potential, for the different electrolytes and relative humidity: in a), b) and c) 0.05 mol L^{-1} H_2SO_4 solution and in d), e) and f) 0.1 mol L^{-1} $NaClO_4$ solution as electrolyte. The black vertical dashed lines represent the probable PZC; the red dashed lines represent a “potential variation” around the PZC value.………………………………………………………….……..……115

Figure 42. Sketches of possible water molecule orientation on metal surfaces: a) “ice-like” structure, with the blue dashed lines representing hydrogen bonds; b) water molecule in the vicinity of an adsorbed anion, oriented with the oxygen atom towards the metal surface and the hydrogen atom towards the specific adsorbed ion. The metal surface is represented positively charged in both cases only for illustration …..………………120

Figure 43. a) Electrode potential measured by Kelvin probe in dry N_2 atmosphere vs potential applied in 0.1 mol L^{-1} NaOH solution as electrolyte; b) pictures taken from gold samples emersed from H_2SO_4 and NaOH electrolytes ………………………..…………………………………....123

Figure 44. Another example for electrode potential measured by Kelvin probe in dry N_2 atmosphere vs potential applied in 0.1 mol L^{-1} NaOH solution as electrolyte……………………………………………………………..…124

Figure 45. Potential of the emersed gold sample (calibrated vs Ag/AgCl) as function of applied potential during immersion, measured by Kelvin probe in different RH conditions. As electrolyte was used 0.1 mol L^{-1} KBr solution, with the potentials stepped in a) positive and in b) negative direction……………………………………………………..………...128

Figure 46. Comparison of measured potentials in positive and in negative direction for the electrolytes employed in this work……….……………………..131

Figure 47. Potentials of the emersed gold electrode vs applied potential obtained with additional blowing of dry nitrogen. Electrolyte was 0.1 mol L^{-1} $NaClO_4$ solution. The electrolyte was removed from the electrochemical cell before the sample polarization was stopped ...….………….…..133

Figure 48. Volta potential difference behavior during atmosphere changing experiments. The vertical dashed lines represent the atmosphere changing time and the horizontal dashed lines represent the maximal difference between the highest and the lowest Volta potential difference value……………………………………………………..…………...135

Figure 49. Volta potential difference behavior during atmosphere changing experiment. The vertical dashed line represents the atmosphere changing time……………………………………………………………...136

Figure 50. Volta potential difference between emersed electrode and Kelvin probe for different gas change experiments and for applied potential of -0.3 V corresponding to potential change: a) in positive and b) in negative direction ………………………………………………………………….138

Figure 51. Volta potential difference between emersed electrode and Kelvin probe for different gas change experiments and for applied potential of +0.4 V corresponding to potential change: a) in positive and b) in negative direction ………………………………………………………………….140

Figure 52. Potential change of the emersed electrode during change of the atmosphere between nitrogen and synthetic air for different humidity (see indicated in the figure), corrected vs the tip (Volta potential change obtained on electrodes emersed at +0.4 V vs Ag/AgCl). The vertical dashed lines represent the atmosphere changing time. The applied potential during immersion was -0.3 V vs Ag/AgCl adjusted in: a) positive and b) negative direction. The dashed red curve indicates the fitting curve used further below for calculating Tafel plots……..……..142

Figure 53. d*E*/d*t* vs *E* plots for a) the electrode emersed at -0.3 V vs Ag/AgCl into a) high humidity of 90-95% RH and b) intermediate humidity of 65-70% RH. The data were obtained from the data of potential vs time upon switching to synthetic air (between 60 and 120 min; data from Figure 52a))……………………………………………………………………...145

Figure 54. FT-IR spectra obtained stepwise with an emersed gold sample surface, after polarizing stepwise from -0.2 until 1.0 V employing 0.1 mol L^{-1} $NaClO_4$ solution as electrolyte………..…………………………..……147

Figure 55. Infrared beam path guided outside the spectrometer through the IR beam guide chamber and analysis chamber (sample location) with the instrumentation optical components …..…………………………..……148

Figure 56. FT-IR spectra of a gold sample surface polarized from -0.2 until 1.0 V using 0.1 mol L^{-1} $NaClO_4$ solution as electrolyte and spectrometer aperture configured to 4.0 mm……………………...………………..149

Figure 57. Single beam spectra of a gold sample surface polarized from -0.2 until 1.0 V using 0.1 mol L^{-1} $NaClO_4$ solution as electrolyte ……….………150

Figure 58. LN-MCT detector stability test experiment along 5 days. A gold sample was polarized using a) 0.1 mol L^{-1} $NaClO_4$ and b) 0.05 mol L^{-1} H_2SO_4 solution as electrolyte. As reference the spectra from the previous day was employed (resulting in a perfect horizontal line, signaling high reproducibility and stability) and the next day spectra can be directly compared……………………………….………………..………...…151

Figure 59. FT-IR spectra obtained on gold surface after polarizing the sample in 0.1 mol L^{-1} $NaClO_4$ solution with the potentials stepped in: a) positive and b) negative directions……………...………………..………………153

Figure 60. FT-IR spectra obtained on gold surface after polarizing the sample in 0.1 mol L^{-1} $NaClO_4$ solution with the potentials stepped in positive direction. As reference spectra were used: a) spectra of clean sample (background) and b) spectra obtained after emersion from 0.0 V (PZC region)……………………………………..………………………156

Figure 61. FT-IR spectra obtained on gold surface after polarizing the sample in 0.1 mol L^{-1} $NaClO_4$ solution with the potentials stepped in negative direction. As reference spectra were used: a) spectra of clean sample (background) and b) spectra obtained after emersion from 0.0 V (PZC region) ……………………………………...........……………….159

Figure 62. FT-IR spectra obtained on gold surface after polarizing the sample in 0.05 mol L^{-1} H_2SO_4 solution with the potentials stepped in: a) positive and b) negative directions…………..………………..…………………161

Figure 63. FT-IR spectra obtained on gold surface after polarizing the sample in 0.05 mol L^{-1} H_2SO_4 solution with the potentials stepped in: a) positive and b) negative directions. Same data as used for Figure 62 above, but as reference were employing the 0.1 V (PZC region) spectra……….163

Figure 64. FT-IR spectra presenting the sulfate vibrational assignments around 770 – 620 cm^{-1} obtained on gold surface after polarizing the sample in 0.05 mol L^{-1} H_2SO_4 solution with the potentials stepped in positive direction…………………………………………………………………166

Figure 65. FT-IR spectra obtained on gold surface after polarizing the sample in 0.05 mol L^{-1} H_2SO_4 solution with the potentials stepped in positive direction. As reference spectra were used: a) spectra of clean sample (background) and b) spectra obtained after emersion from 0.1 V (PZC region)……………………………………………..….………………168

Figure 66. FT-IR spectra obtained on gold surface after polarizing the sample in 0.05 mol L^{-1} H_2SO_4 solution with the potentials stepped in negative direction. As reference spectra were used: a) spectra of clean sample (background) and b) spectra obtained after emersion from 0.1 V (PZC region)..…..…………………170

Figure 67. FT-IR spectra obtained on emersed gold surface after polarizing the sample in 0.1 mol L^{-1} $NaClO_4$ solution with the potentials stepped in positive direction. The atmosphere inside the analysis chamber was set to humid N_2 (65-70% RH)……..…..…………………………………..…172

Figure 68. FT-IR spectra obtained on emersed gold surface after polarizing the sample in 0.1 mol L^{-1} $NaClO_4$ solution with the potentials stepped in positive direction (between -0.4 and 0.6 V). The atmosphere inside the analysis chamber was set to humid N_2 (65-70% RH) ………………...173

Figure 69. FT-IR spectra obtained on gold surface in humid atmosphere after polarizing the sample in 0.05 mol L^{-1} H_2SO_4 solution with the potentials stepped in positive direction. As reference spectra were used: a) spectra of clean sample (background) and b) spectra obtained after emersion from 0.1 V (PZC region)……………………………………175

Figure 70. Thickness of the water layer adsorbed on gold surface after applying 0.1 V and emersion from 0.1 V. Prior to the measurements, the ellipsometry chamber was flushed for 24 h with N_2 atmosphere with following RH values: 1-3, 65-70 and 90-95%, which were thus maintained at high stability throughout the according measurement. It should be noted that while the relative difference of thickness obtained at different relative humidity is quite reliable, the value at 1-3 % RH is subject to high uncertainty, i.e. there might be an offset error............178

Figure 71. OCP measurement on the unpolarized gold sample: a) without emersion; b) with emersion and re-immersion; c) after 5 or 10, 60, 300 and 600 s. The red dashed lines in b) represents the start of the emersion and re-immersion processes……………………………...…181

Figure 72. OCP determination on the polarized gold sample: a) and b) without emersion; c) and d) with emersion and re-immersion. Electrolyte was 0.05 mol L^{-1} H_2SO_4……………………………………..……….……..183

Figure 73. Plots of OCP at different waiting times after the polarization was stopped vs applied potential during polarization, with the potentials stepped in positive and in negative directions. Electrolyte was 0.05 mol L^{-1} H_2SO_4 …………………..…………………..…………………………185

Figure 74. Plots of OCP of re-immersed samples at different waiting times after emersion vs applied potential during polarization, with the potentials stepped in positive and in negative directions. Electrolyte was 0.05 mol L^{-1} H_2SO_4 ………………………………..……………......……………186

Figure 75. Schematic representation of water adsorption at different relative humidity and how it is affecting the potential of the emersed electrode (1, 2, 3 denoting 1-3% RH, 65-70% RH and 90-95% RH, respectively)……………………………………………………………..192

List of Tables

Table 1. Some reactions for gold and for water and their standard reduction potentials ………………………………………………………………12

Table 2. Moisture and the amount of water correlated ……………………………15

Table 3. Some secondary reference electrodes and its related standard potentials...……………………………………………………………..28

Table 4. Vibrations and the respective wavenumbers present in water and carbon dioxide molecules …………..……………………………………35

Table 5. Determined pH values in different electrolytes …………………….....72

Table 6. Potentials of the emersed electrode measured by Kelvin probe and referenced vs Ag/AgCl vs the potentials applied during immersion, for stepwise polarization into the positive direction, for H_2SO_4 and $NaClO_4$ solutions as electrolyte and N_2 atmosphere with different RH values .101

Table 7. Potentials of the emersed electrode measured by Kelvin probe and referenced vs Ag/AgCl vs the potentials applied during immersion, for stepwise polarization into the negative direction, for H_2SO_4 and $NaClO_4$ solutions as electrolyte and N_2 atmosphere with different RH values .102

Table 8. Polarization stepped in positive and negative directions on gold surfaces in contact with KBr solution as electrolyte and the correspondent potential measured by Kelvin probe in N_2 atmosphere with different RH values ………………………………………………..……126

Table 9. Difference of the potentials measured by Kelvin probe on the emersed electrodes when employing 0.1 mol L^{-1} KBr solution compared to 0.1 mol L^{-1} $NaClO_4$ and 0.05 mol L^{-1} H_2SO_4 solutions (in the linear range with slope around 1 for all experiments) ……………………………….130

Table 10. SiO_2 layer thickness determined by ellipsometry in N_2 atmosphere of different relative humidity…………………………………..……………..177

1 Motivation

Electrochemistry is playing a crucial role in many important technical processes and in corrosion and last but not least plays a key role in transforming our current economy based on fossil fuels into an economy free of carbon dioxide emissions. Although our understanding of electrochemistry is already quite advanced, deeper insight of the molecular structure of the double layer region and the correlation of structure and interfacial kinetics is still of great importance to further advance our knowledge. However, the electrochemical layer region is buried underneath an analytical barrier of bulk water. Over the last decades this problem gave rise to a variety of different research approaches aimed at making the electrochemical double layer region more accessible. One is the approach of the emersed electrode, which is based on emersion of an electrode under potential control into an inert atmosphere, aiming at preserving the electrochemical double layer while stripping the bulk electrolyte. More recent is the concept of the electrode in the "dry"[1,2,3], which is based on polarizing the electrode from its backside by permeation of hydrogen.

To make the interface accessible was already an idea behind the development of the so called emersed electrodes, which refers to electrodes that are pulled out of the electrolyte under potential control. The idea is that thus the double layer is preserved. Indeed, the first investigations on composition and structure of electrodes and the electrochemical double layer were performed on electrodes emersed under potential control into UHV (Ultra High Vacuum). This ex-situ surface science approach, performed the first time by Hansen *et al.*[4], was extremely important for the development of modern electrochemical science.[5] Although for emersion into UHV it was found that for samples polarized during immersion within the potential window of ideal polarizability (i.e. in absence of Faraday processes), a 1:1 correlation between applied potential and measured work function is usually obtained, indicating that the double layer was transferred intact, usually no water or only very low amount of water was detected, i.e. during transfer into UHV the water in the double layer is lost.[6] Interestingly, although a 1:1 correlation between applied potential and measured work function was observed, the corresponding absolute potential was estimated to be up to 400 mV more positive than the one of the applied potential.

Emersion into inert atmosphere (nitrogen) of high relative humidity (close to 100% RH) seems to preserve water in the double layer region at least to some extent, leading to significantly lower potentials compared to what was obtained from the work function measurements for emersion into UHV.[7] Samec *et al.* proposed that while both emersion into UHV and emersion into nitrogen atmosphere of high relative humidity showed a 1:1 correlation of potentials measured on the emersed electrode vs the applied potential, the offset in the values should be caused by the difference in adsorbed water.[7]

It seems intriguing to have a closer look into the role of water on the potential of then preserved electrochemical double layer, i.e. how will the potential change when water is gradually added into double layer of surface charge and counter ions. Hence, in this work for the well-established example of gold as electrode material, the emersed electrode was re-investigated again, but this time with different relative humidity of the inert nitrogen atmosphere. As will be seen in this work, a quite complex dependence was found and also a significant effect on the resulting electrochemical activity, e.g. for the case of oxygen reduction reaction on emersed electrodes.

The results will be certainly of great importance for a better fundamental understanding of electrochemistry, but maybe also of considerable practical relevance. Ultra-thin electrolyte layers play a crucial role e.g. in fuel cells and atmospheric corrosion. In fuel cells based on reacting hydrogen and oxygen, these gases have to be able to freely diffuse through a porous network in the gas diffusion layers, but also the membrane electrode assemblies, which means that catalyst particles are not immersed in bulk electrolyte but covered by ultra-thin electrolyte layers. For oxygen reduction reaction (ORR) on a “bare” catalyst particle in a Membrane Electrode Assembly (MEA), protons have to be delivered from the ionomer in the vicinity.[3] It is reported that proton transport can readily occur on the surface of the metallic catalyst, e. g. for Pt via Pt-OH or Pt-H.[8,9,10]

Furthermore, the results reported here should be of importance for obtaining a better understanding also of atmospheric corrosion. For instance, besides the cathodic activity in micro-droplets that are forming around the larger primary droplets, it might be also important to consider the activity in the seemingly inactive area between them, which is just covered by ultra-thin electrolyte layers in the monolayer range.[11] Atmospheric corrosion is highly researched due to the high variety of applications of metals in this environment, such as for buildings, bridges, cars, ships, airplanes and so on.

In this sense, the concept of the electrode in the “dry” emersed from aqueous electrolytes and relating the applied potentials with the potential obtained by Kelvin probe technique may be of great importance for a better understanding corrosion/electrochemical processes. The necessary development of new experimental approaches developed in this PhD study provided some great challenges. The combination of different non-destructive measurement techniques in this dissertation allows the study of water layers adsorbed on the metal/electrode surface (i.e. the electrical double layer) even in the range of few monolayers and below, i.e. in the nanometer and sub-nanometer range. This approach only is possible after emersing an electrode from the electrolyte under potential control, avoiding the presence of bulk water, which is a barrier for analyzing the electrochemical interface.

The experimental development work of this study made possible the combination of the traditional electrochemical cell (three-electrode cell) with the Kelvin probe, X-ray Photoelectron Spectroscopy (XPS), ellipsometry and infrared spectroscopy, also allowing *in operando* experiments. Especially, the use of Fourier-transform infrared spectroscopy enables a wide spectral range of analysis with high sensitivity. Coupling all these techniques in a closed system under vacuum or controlled atmosphere made possible the study without exposure of the samples to the environment, avoiding not only according contamination but also any possible discharging of the electrochemical double layer transferred during the emersion of the electrodes.

The wide range of analytical techniques from Kelvin probe, ellipsometry, infrared and X-ray spectroscopy used in this work, was fundamental for this research and helped to understand the electrochemical behavior of such electrode in the “dry”.

2 Introduction

In this section of the dissertation some background information about the subjects involved in this work will be presented and discussed, especially on the emersion of electrodes from aqueous electrolytes and what is known so far about the correlated potentials of the emersed electrodes compared to the ones applied during immersion. General aspects of metallic corrosion processes (i.e. electrochemical processes), relevant key methods and techniques, such as Kelvin probe and its principles, electrochemical cell set-up and spectroscopic techniques, such as infrared spectroscopy, ellipsometry and X-ray photoelectron spectroscopy will be shortly discussed. Also described are some aspects of thermodynamics and kinetics in electrochemistry.

2.1 Corrosion

Ideas about corrosion emerged with the beginning of metallurgical process, ore extraction and its processing to obtain metals. Corrosion is a natural process that affects all materials, especially metals.[12] According to the European Federation of Corrosion (EFC), *"corrosion processes may be considered as reactions of metals with species in the environment to form chemical compounds"*.[13] Metal corrosion is an electrochemical process, characterized by oxidation and reduction reactions occurring on the metal surface (metal/electrolyte interface).[14] While in homogeneous corrosion both anodic and cathodic reactions are evenly distributed, in heterogeneous corrosion some areas on these surfaces act as net anode (oxidation reaction) and some as net cathode (reduction reaction) with respective ionic current exchange between them through the electrolyte.[12] Generally, an electrolyte is composed by a solvent with dissolved species (cations and anions). Water is the most usual solvent in corrosion.[15] In order for electron transfer to occur, it is necessary that a correspondence between the energies of the orbitals in which the transfer takes place in the involved species exists. In a metal it is the Fermi energy level (E_F). Already in soluble species it is the orbital of the valence electron.[16] A common example of heterogeneous -here caused by different access of oxygen to the surface- corrosion of steel is the scheme presented in Figure 1.

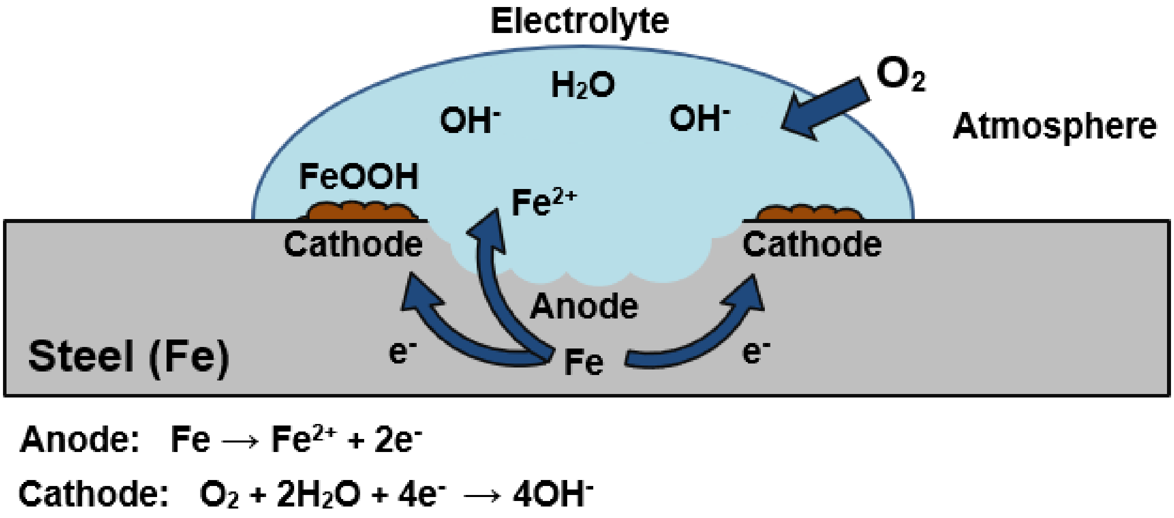
Electrolyte
O_2
Atmosphere
H_2O
OH^-
OH^-
FeOOH
Fe^{2+}
Cathode
Cathode
Anode
Steel (Fe)
e^-
Fe
e^-
Anode: $Fe \rightarrow Fe^{2+} + 2e^-$
Cathode: $O_2 + 2H_2O + 4e^- \rightarrow 4OH^-$

Figure 1. Scheme of the electrochemical process of steel corrosion.

From economic aspects, estimates reveal that corrosion is responsible for a loss of about 3.5% of the national gross product in industrialized countries.[14,15] Some of these economic losses are related to plant downtime, loss of products, loss of efficiency and contamination. Corrosion has also a very important significance regarding human health and safety.[17]

2.1.1 Thermodynamics and kinetics related to corrosion

In this section some characteristics of thermodynamics and kinetics related to corrosion are shortly described. From a thermodynamic aspect, corrosion is necessary for the energy balance. Metals are extracted from minerals, and the same (or similar) amount of energy necessary to extract these metals from the respective minerals is released during the corrosion reactions, producing chemical compounds that are similar or identical from the original mineral.[17] This means the stored energy acquired in the extraction and refining process is available to supply the driving force when the metal returns to the native (original) state.[18] In Figure 2 as an example the thermodynamic energy balance for iron is displayed, synthetized from hematite (Fe_2O_3) and producing rust (FeOOH) after corrosion process.

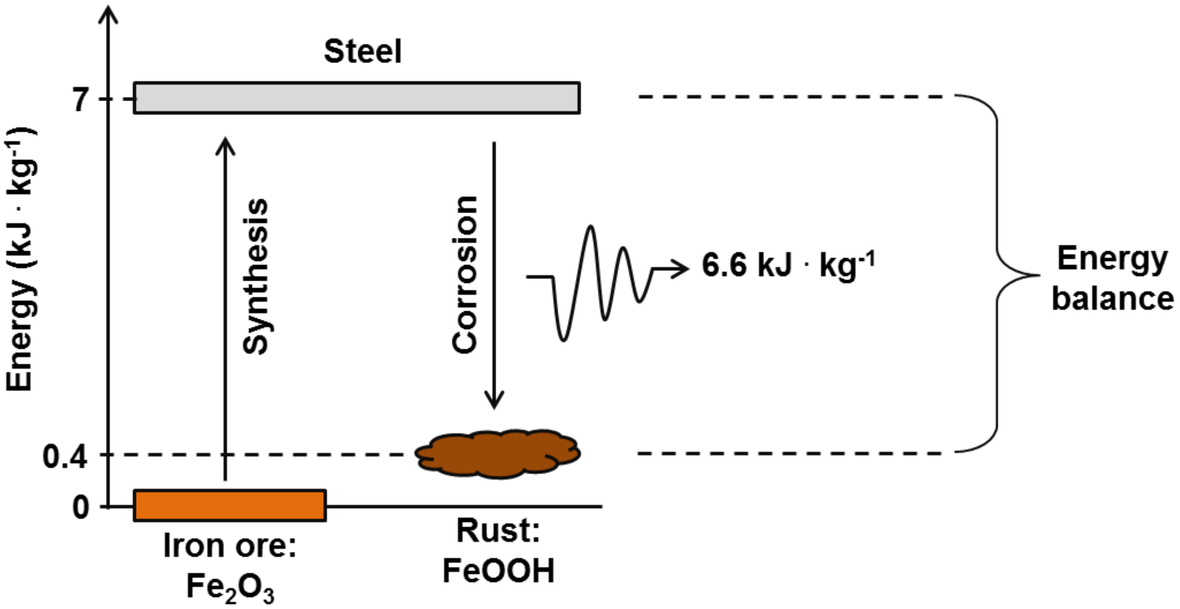

Figure 2. Example of energy balance in the life cycle of iron.

Chemical and electrochemical processes in corrosion are influenced by their thermodynamic characteristics which can explain if a process may or not occur under some conditions. The rates of the reactions involved on the metal surface are determined by the corresponding kinetics, which determine whether the process will actually occur and how fast.[14]

The energetics involved in a chemical reaction are described by internal energy (U) and enthalpy (H).[15] The change of these energetics is internal energy change (ΔU) and enthalpy change (ΔH). When a reaction involves only solid, liquid or dissolved species, then ΔU is equal ΔH.[14] If volume changes are involved, i.e. especially for gases, then the following equation is valid:[14]

$$\Delta H = \Delta U + p\Delta V \qquad \text{(Equation 1)}$$

where ΔV and p are the volume change and the pressure, respectively.

The enthalpy of a reaction, in stoichiometric conditions, can be calculated as the standard enthalpies of formation (ΔH_f^0) of the species involved. The ΔH_f^0 correspond to the formation of the involved species from the elements for temperature T = 298 K and pressure p = 1.013 x 10^5 Pa (standard conditions).[14] If $\Delta H^0 < 0$, the reaction is exothermic, i.e., energy is lost to the surroundings and if $\Delta H^0 > 0$, the reaction is endothermic, i.e., energy is supplied in order to the reaction occur.[19]

The Gibbs free energy change (ΔG) is one parameter to give the driving force of a chemical reaction, according to the next equation:[14]

$$\Delta G = \Delta H - T\Delta S \qquad \text{(Equation 2)}$$

where ΔS is the change of entropy of a reaction.

For a spontaneous process in an isolated system, ΔS is positive.[14] With respect to Gibbs free energy change, if $\Delta G < 0$ than the reaction is possible; if $\Delta G > 0$ the reaction will not occur and $\Delta G = 0$ represents an equilibrium.[15]

Corrosion involving metals normally consists of an anodic dissolution (metal) and a cathodic process, such as reduction of dissolved oxygen or hydrogen evolution. The measured current density is the superposition of the anodic dissolution and the cathodic deposition with $i = 0$ at the corrosion potential.[14]

The concentration of species at the electrochemical interface is dependent on the mass transport of these species from the solution. It can be described by the mass transfer coefficient (k_d). By an irreversible reaction, a high kinetic barrier has to be overcome, which is reached by the application of an extra potential (overpotential, η). In this situation, $k_0 << k_d$, where k_0 is the standard rate constant (kinetics are expressed by this constant). When the reaction is reversible, then $k_0 >> k_d$ (the kinetics of the electrode reaction is much faster than the transport).[16]

2.1.2 The Pourbaix diagram

When it comes to thermodynamics, the Pourbaix diagram shows the Thermodynamically expected states of an element and its ions, solids and gaseous compounds in an aqueous electrochemical system.[17,20] In corrosion science, a Pourbaix diagram is a potential – pH equilibrium diagram (*E* vs pH) which represent corrosion and non-corrosion domains, i.e., the diagram makes a clear distinction between domains where corrosion is or is not possible to occur. Corrosion is impossible in the region of immunity (where the metal is in its metallic state) and in the region(s) of passivation (oxides, hydroxides, hydrides or salts of the metal). In the latter situation, the metal will be coated with the oxide, hydroxide, hydride or salt layers formed on the metal surface as non-porous or a porous film. When these films are non-porous they protect the underlying metal and thus can significantly slow down corrosion. In general, the metals are resistant to pure water around 25 °C when they cross perpendicularly at pH = 7 only the regions of immunity and/or passivation at potential between -0.8 and +0.7 V. Titanium and gold, for example, have the possibility to be corroded at high electrode potentials, and a slight dissolution can be observed at highly oxidizing situations.[20] In Figure 3 as example the Pourbaix diagram for gold at 25 °C is shown, as gold is the main metal investigated in this thesis as electrode material.

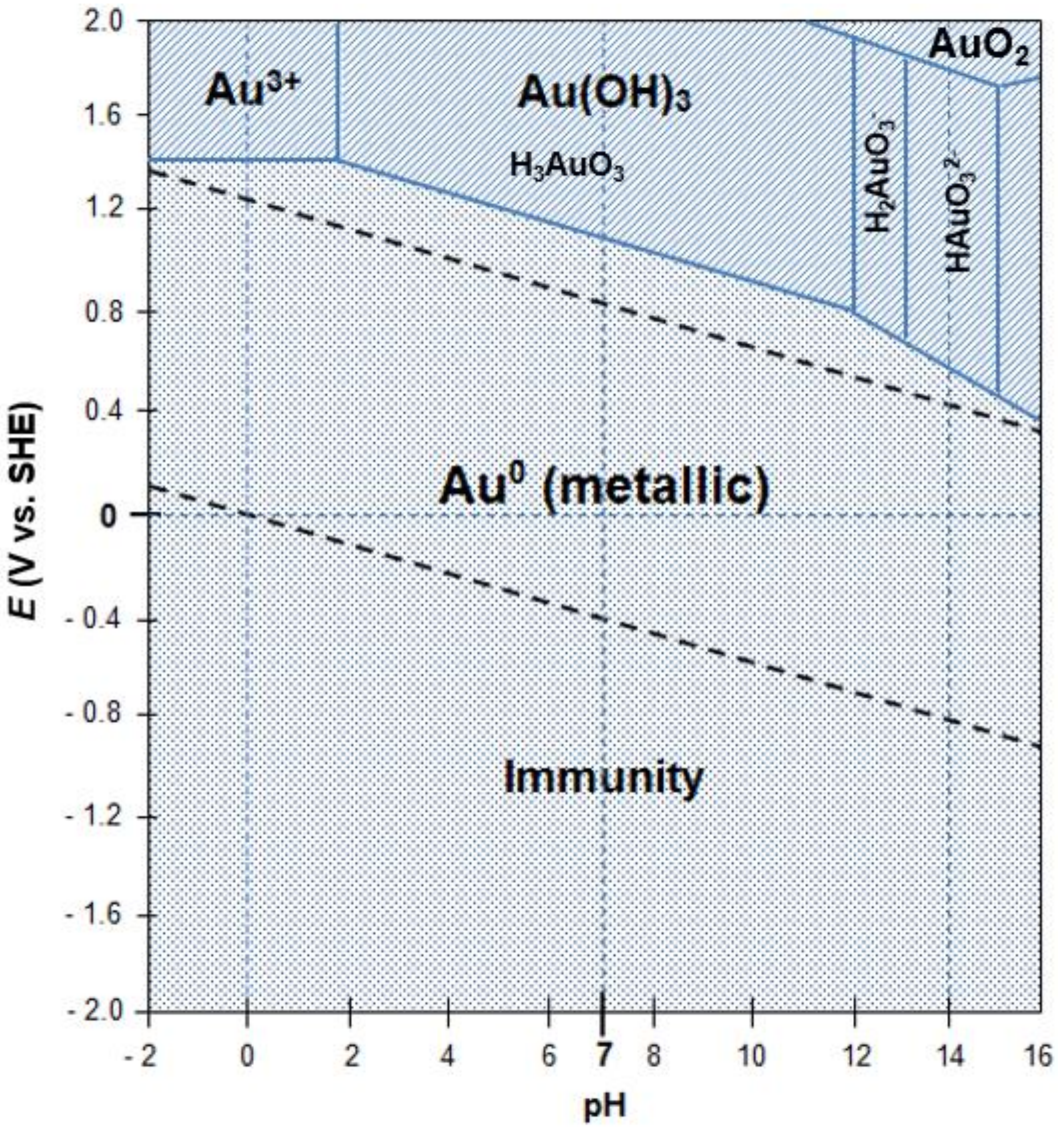

Figure 3. Pourbaix diagram (*E* vs pH) for gold at 25 °C. In the diagram, the domain hatched with ▩ represents the immunity region (corrosion not possible); the domain hatched with ▨ represents the regions where corrosion is possible (adapted from references 20,21; in the $Au(OH)_3$ region some degree passivity is expected).

The two parallel and diagonal dashed lines (in black color) in Figure 3 represent the equilibrium conditions of the reduction and oxidation of water.[20] This situation is explained next in another Pourbaix diagram shown in Figure 4, representing water and its decomposition products.

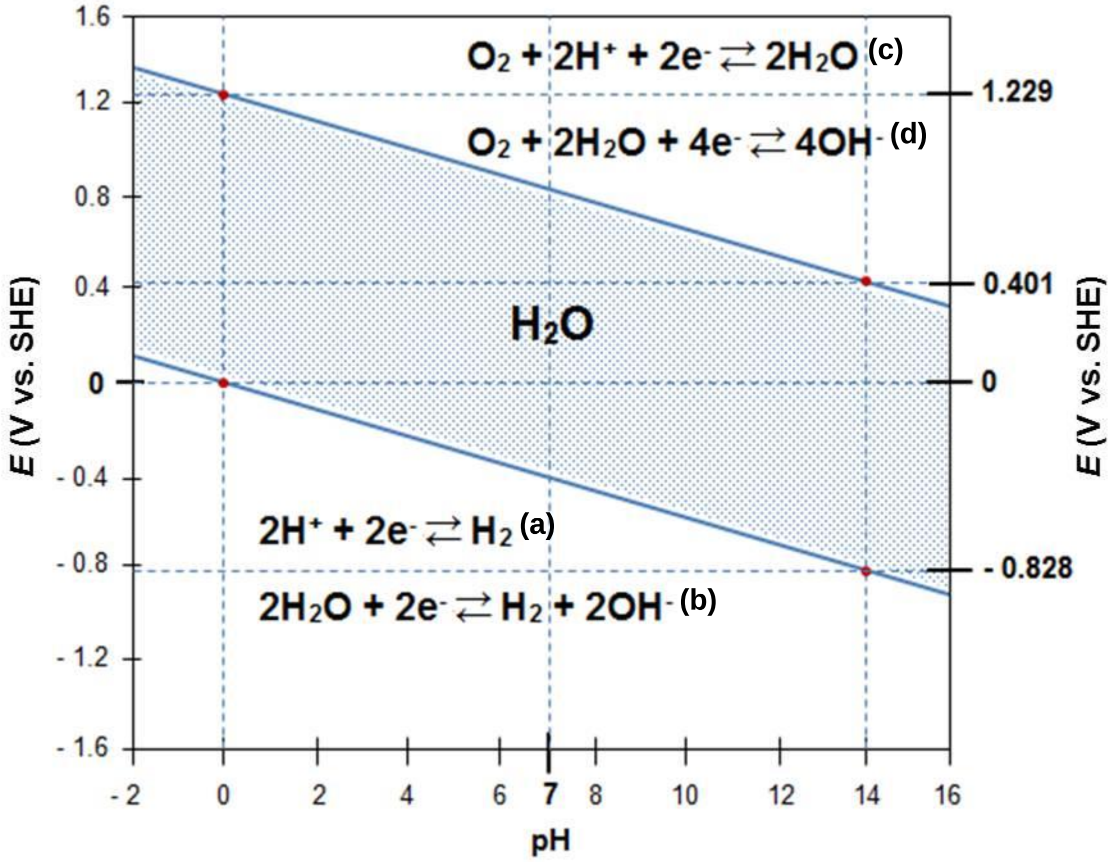

Figure 4. Pourbaix diagram (*E* vs pH) for water and its decomposition products (adapted from reference 17).

In Figure 4 for the hydrogen electrode (a) the Nernst equation (will be presented and explained in section 2.2.1.1) after substituting the constants with the appropriate values (at 25 °C temperature and 1 atm pressure) is used according to: $E = E^0 - 0.059 \log \alpha$. The pH is defined as $- \log \alpha$, then $E = E^0 - 0.059$ pH.[17] Following is demonstrated the relation of the Nernst equation with some data from the Pourbaix diagram:

For reaction (a): $E = 0.000 - 0.059$ pH. If pH = 0, $E = 0.000$; if pH = 14, $E = - 0.828$;

For reaction (c): $E = 1.229 - 0.059$ pH. If pH = 0, $E = 1.229$; if pH = 14, $E = 0.401$.[17,20]

The three regions in the diagram shown in Figure 4 represent the domain where water can be electrolyzed anodically and form oxygen (upper region), the domain where water is stable (center) and the domain where water can be electrolyzed cathodically and form hydrogen (lower region). The two parallel and diagonal lines representing the equilibrium potentials for hydrogen electrode (reactions (a) and (b)) and the oxygen electrode (reactions (c) and (d)) (shown here in blue color) are normally inserted on the Pourbaix diagrams for metals.[17] Additional to Figures 3 and 4 in Table 1 some standard potentials related to reduction reactions for gold and for water are shown.

Table 1. Some reactions for gold and for water and their standard reduction potentials (adapted from reference 22).

Substance	Reaction	E^0 (V vs. SHE)
Gold	$Au^+ + e^- \rightleftarrows Au$	+ 1.680
	$Au^{3+} + 3e^- \rightleftarrows Au$	+ 1.420
	$Au^{3+} + 2e^- \rightleftarrows Au^+$	+ 1.290
Water	$O_2 + 2H^+ + 2e^- \rightleftarrows 2H_2O$	+ 1.229
	$O_2 + 2H_2O + 4e^- \rightleftarrows 4OH^-$	+ 0.401
	$2H^+ + 2e^- \rightleftarrows H_2$	+ 0.000
	$2H_2O + 2e^- \rightleftarrows H_2 + 2OH^-$	– 0.828

One important practical function of the Pourbaix diagram is related to the domains where corrosion is thermodynamically impossible. In other words, in some cases potential and/or pH values can be adjusted to prevent corrosion thermodynamically.[17] Unfortunately there are some limitations of these diagrams. No information about behavior of alloys is provided, only for pure metals and non-metals.[20] Furthermore, no information related to corrosion rates (kinetics aspects) are given by Pourbaix diagrams.[17]

2.1.3 Corrosion types

Many forms of corrosion are possible to occur. Uniform corrosion, where the corrosive environment has the same access to the entire homogeneously reactive metal surface; galvanic corrosion, which occurs when two different metals/alloys are in contact with the electrolyte and one of these metals are preferentially corroded; pitting corrosion, where the corrosive attack is localized;[17] crevice corrosion, which is a localized corrosion occurring in areas of restricted flow and where the metal surface is in contact with a small confined liquid volume.[23] The environmentally induced cracking may be responsible for failures, like stress corrosion cracking, corrosion fatigue cracking and hydrogen-induced cracking. All those are originated in the presence of an environment that causes some uniform corrosion. Another type of corrosion, common in many alloy systems, is the intergranular corrosion, induced by the presence of reactive impurities (like chromium).[17] The erosion-corrosion occurs by the growth of the mechanical abrasion/friction of the metal simultaneously to the corrosion attack.[12] However, since this thesis is focused on electrochemistry and the electrochemical double layer of non-immersed electrodes, -besides its relevance for a fundamental understanding of electrochemistry- its main relevance for corrosion will be on atmospheric corrosion.

Atmospheric corrosion has been intensely studied around the world, especially because of the many applications of metals in outdoor structures, such as bridges, buildings, cars, ships, for example.[24] This corrosion type, caused by weather action, is responsible for the main part of economic losses attributed to corrosion. The atmosphere is a very complex environment due to the variation related to time and location.[25] In a perfectly dry atmosphere, the metallic corrosion has a very slow rate and may be considered negligible for practical purposes.[26]

Atmospheric corrosion occurs in a complicated system composed by the metal, corrosion products, electrolyte and the atmosphere surrounding this system.[24] Many environmental variables are involved and cause influence on the atmospheric corrosion. The most significant influences are from temperature, sunlight, wind, moisture and contaminants. Another aspect to be taken in consideration is the site nature, i.e., the environment where the metal structure is situated, for example, marine or industrial environment. In these situations, chlorides and sulfur dioxide are present, in marine and industrial environments, respectively.[27] In countries with temperatures below freezing in the winter, salts for de-ice are commonly used. Acid rain condition (due to anthropogenic activity) combined with marine environments, deicing salts and humidity were shown as responsible for severe atmospheric corrosion on a bridge in New York.[28]

Precipitation water (rain, snow, fog) is not pure in the atmosphere; however, it is a complex chemical solution composed by water, radicals, ions and reactive molecules. Great part of the corrosion is caused by the interaction of these trace species present in precipitation water with the metals. To evaluate atmospheric corrosion it is necessary detail the following factors: precipitation frequency, chemical compounds present in the precipitation water and the susceptibility of the metal to react with these chemical compounds.[29] In the scheme in Figure 5 the main variables responsible for atmospheric corrosion are schematically explained.

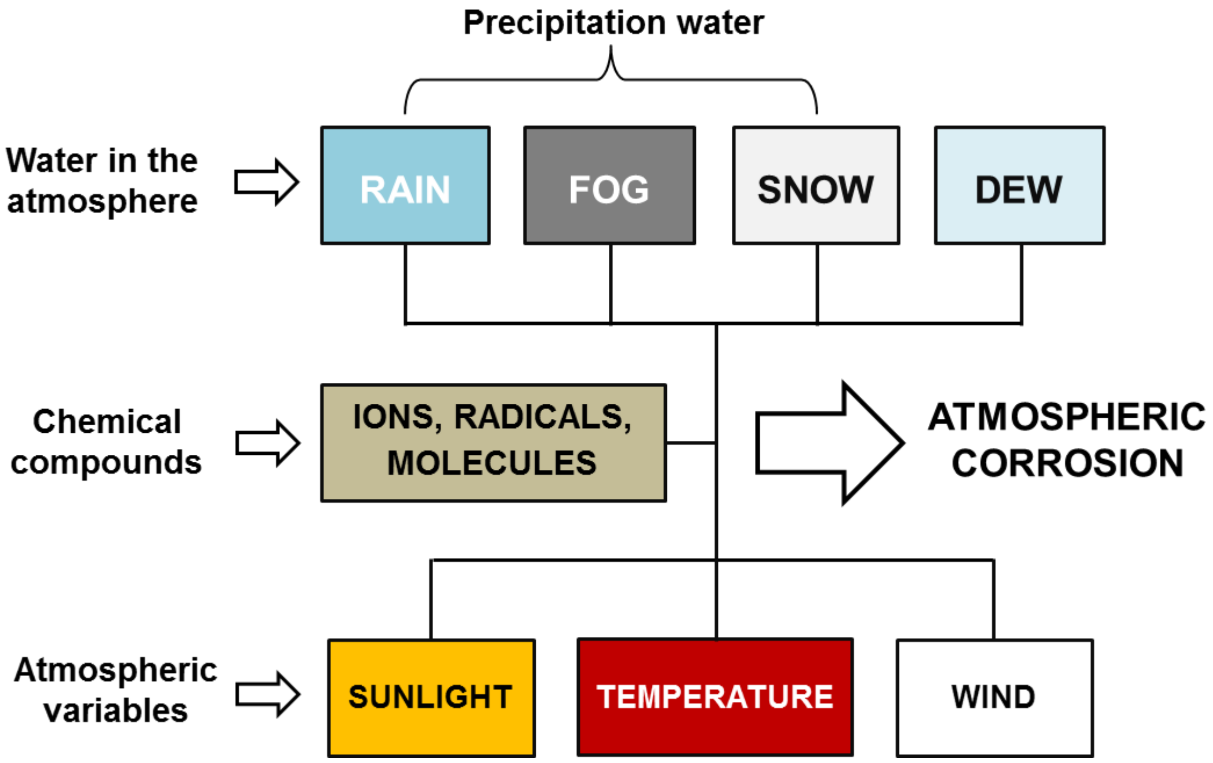
Precipitation water
Water in the atmosphere
RAIN
FOG
SNOW
DEW
Chemical compounds
IONS, RADICALS, MOLECULES
ATMOSPHERIC CORROSION
Atmospheric variables
SUNLIGHT
TEMPERATURE
WIND

Figure 5. Scheme representing the main constituents responsible for atmospheric corrosion.

Dew formation on metallic surfaces occurs when the surface temperature is below the dew point of the atmosphere. It is an important cause of corrosion under sheltered situations and dew periods are considered as very corrosive. Around 10 g of dew water covers a surface of 1 m^2, that can be considered more than the amount of adsorption layers covering metal surfaces.[24]

Rain promotes two different situations: firstly, it creates electrolyte layers with about 100 g m^{-2} and affects the corrosion by adding some corrosion stimulators (for example, H^+ and SO_4^{2-}); on the other hand, rain washes the metal surface, removing away contaminants accumulated during dry periods.[24] In an industrial site, sulfur dioxide in the atmosphere causes acid rain, which is very corrosive.[27] In Table 2 are presented the amount of water values related to different moistures.

Table 2. Moisture and the amount of water correlated (adapted from reference 24).

Moisture	**Amount of water (g m^{-2})**
Critical relative humidity	0.01
100% relative humidity	1
Covered by dew	10
Wet from rain	100

Sunlight is a variable that affects the degree of wetness on a surface as well as the performance of some nonmetallic species and coatings. In this sense, it is important to monitor the extent of the sunlight at atmospheric test sites.[27] The ambient atmosphere temperatures maintain corrosion rates relatively low; on the other hand, it may increase condensation of water on the metal surface and the corrosion rate. In addition, higher temperatures will dry the metal surface, and so, reduce corrosion.[17]

The principal chemical constituents involved in atmospheric corrosion are different compounds containing sulfur, nitrogen and chlorine. Sulfur is the most important gaseous stimulant in the atmospheric corrosion process, proceeding from oil and coal burning emissions, petrochemical and pulp and paper industries.

Nitrogen compounds, especially NO and NO_2, are mainly formed in combustion reactions in power plants and vehicles. The chlorides mainly are provided from marine atmospheres (aerosols) and from de-icing salts, coal burning and incinerators emissions. Furthermore, Cl_2 from industrial processes can photo-dissociate into radicals which can lead to form HCl.[30]

One important question not much addressed up to now in the research on atmospheric corrosion is how important electrochemical reactions on metal surfaces just covered by electrolyte in the monolayer and maybe even sub-monolayer range may be. This is because often atmospheric corrosion does not take place beneath homogeneous films of electrolyte, but on surfaces covered by a high density of larger and smaller droplets. Besides the cathodic activity in micro-droplets that are forming around the larger primary droplets[11], it might in such case be also important to consider the activity in the seemingly inactive area between them, which is just covered by ultrathin electrolyte layers in the monolayer range.[3]

For instance, the so-called cathodic spreading of droplets[11] might be driven by cathodic oxygen reduction on that “dry” surface area in the vicinity of these droplets. This can be enabled by cation migration from the droplets into this surrounding area, which was e.g. recently investigated by Prabhakar *et al.*[31], a process which is similar as to cathodic delamination of organic coatings.[32] In both processes cations (accompanied by electrons in the metal underneath) migrating into the yet unaffected surface/interface result in a pull down of the electrode potential, enabling onset of oxygen reduction, which then occurs on the “dry” surface or buried coating/metal interface.

Electrochemistry on “dry” surfaces may not only be of interest for atmospheric corrosion, but might also play a crucial role e.g. in fuel cells, where the catalyst particles in the porous catalyst layers are not immersed in bulk electrolyte, as this would block the gas transport through the pores. Instead they are just covered by an ultra-thin electrolyte film most likely in the monolayer range.[3] This is suggested by the fact that in fuel cells current densities for oxygen reduction are observed that are significantly higher than what is expected, as oxygen reduction at high rates is limited by transport processes. In bulk electrolyte this is the oxygen diffusion towards the surfaces, which for thin electrolyte layers shows a dependence inverse to the thickness of the electrolyte layer. However, for layers below a thickness in the range of about 10 micrometers that dependence is lost and the rate is determined by the oxygen uptake kinetics at the electrolyte/gas interface.[33,34,35,36,37] This raises the question why much higher reaction rates than expected from this observed uptake limitation in the range of a few mA/cm^2 are possible (see Zhong *et al.*[3]).

The reason may be that the main part of the ORR in fuel cells occurs of the surface of catalyst particles just covered by such ultra-thin electrolyte layers, as it was observed that then no uptake reaction at the surface exists.[3]

The methodology developed by Zhong *et al.* for measuring ORR on surfaces covered by ultra-thin electrolyte layers, however, relies on a known hydrogen permeation rate from the backside of the sample that is correlated with the potential - established as equilibrium potential of ORR and HOR- measured by Kelvin probe on the surface (concerning Kelvin probe, see section 2.4). This demonstrates that electrochemistry on “dry” surfaces plays a real role in practical applications. In fact, the concept of the “electrode in the dry” was first reported in the context of a novel Kelvin probe-based approach for the high sensitive and highly resolved detection of hydrogen, as will be discussed in the following.

2.2 Hydrogen

Hydrogen is the most abundant element in the entire universe, representing more than 90% of overall composition. This is due its presence in the stars (in form of plasma) and in the interstellar matter (mostly as atomic hydrogen). On the planet Earth, hydrogen is the ninth most abundant element, present in the water molecule and in organic compounds, for example.[38] Hydrogen is considered environmentally friendly and nonpolluting for atmosphere as well as for water.[39]

An important application for hydrogen is as fuel. In the past, the NASA Space Shuttle booster rockets and the Apollo missions rockets used a combination of liquid hydrogen and liquid oxygen as fuel.[38] Another application of hydrogen, in gas form, is in meteorological balloons.

2.2.1 Innovation involving hydrogen energy

For aviation and aerospace industry enthusiast like me, Airbus announced in September 2020 very great news: the ZEROe concept, a new concept for three airplanes powered by hydrogen.[40] This concept idea is based on reducing aviation's CO_2 emissions to the atmosphere by up to 50%. By 2035, three different commercial aircraft models, called Airbus ZEROe, are planned to be available. These aircrafts will be powered by a hybrid propulsion system: liquid hydrogen combustion and hydrogen fuel cells. The gas turbine engines will be modified to burn liquid hydrogen as fuel; complementing the propulsion, hydrogen fuel cells will generate electrical power.[40]

The employment of liquid hydrogen as fuel is a solution for aerospace and also other industries to achieve neutral climate targets.[41] According the reaction below[38], the combustion of liquid hydrogen fuel generates only water vapor and energy (heat) as products:

$$2H_2 + O_2 \rightarrow 2H_2O + \text{heat} \qquad \text{(Reaction 1)}$$

Hydrogen fuel cells combine hydrogen and oxygen to produce electric power. It is an electrochemical process in which hydrogen is fed to the anode and oxygen to the cathode.[42] The chemical reaction involved in this process also produces water and heat:[43]

$$2H_2 + O_2 \rightarrow 2H_2O + Q + W \qquad \text{(Reaction 2)}$$

where H_2 is the fuel, O_2 is the oxidant, Q is the heat transferred and W is the rate of electrical work produced by the system.[43]

2.2.2 Hydrogen negative effect on metals

Despite all benefits of hydrogen that were shortly discussed above, this chemical element also causes serious problems in metals. Atomic hydrogen that is formed during processing (such as e.g. chemical or electro-chemical cleaning steps, electro-galvanizing etc.) or during the lifetime (e.g. during corrosion) can get absorbed into the metal. In circumstances with sufficient hydrogen solubility on the metal, with low obstruction of hydrogen entrance into the metal, with high diffusion rate of atomic hydrogen and by high coverage of the metal surface with atomic hydrogen, adsorbed hydrogen from the metal surface will be absorbed into the metal interior ($H_{ad} \rightarrow H_{ab}$).[44]

Serious degradation of metals due to strong hydrogen absorption can cause decreased mechanical strength and may induce embrittlement and stress corrosion cracking.[14] The high hydrogen mobility causes the main problem in materials prone to hydrogen embrittlement. The hydrogen solubility and diffusivity, the possibility to react and form hydride or react with impurities and alloying elements are some factors related to the effect of hydrogen in metals.[45] When atomic hydrogen migrates from the surface into internal defects are created voids, where molecular hydrogen can nucleate and form enough internal pressure to rupture the metal locally.[17]

A metal can absorb hydrogen along many processes, like casting, forging, heat treatment, welding, finishing or during service. In order to obtain thermodynamic equilibrium, if the external pressure is reduced after the hydrogen absorption, diffusion from the metal is necessary. This equilibrium is a function of temperature.[45]

Analyzing the Pourbaix diagrams for corroding metals, the two parallel and diagonal lines shows conditions that will promote hydrogen evolution and/or reduce dissolved oxygen.[17]

Given the great importance of hydrogen in materials, being able to measure hydrogen permeation through and effusion out of materials is of great importance, at high sensitivity and if possible even with high lateral resolution. Such a method was developed based on the so called hydrogen electrode in the “dry” concept.

The concept of the hydrogen electrode in the “dry” was presented by Evers and Rohwerder[1] as an approach to determine mobile hydrogen in metals and its permeation through metals by measuring the work function utilizing the Kelvin probe technique. The origin of this were experiments, where it was found that the work function measured on one side of the sample -exposed to dry nitrogen- was found to be correlated 1:1 to the potential applied on the other side by electrochemical polarization. This was initially observed for palladium (25 µm membrane) and a “sandwich” sample (25 µm Pd membrane coated by 1 µm of Fe and 100 nm of Pd). The explanation is, that hydrogen is in chemical equilibrium throughout the system, where the hydrogen activity controls the potential. Consequently, on the surface exposed to the dry nitrogen there is a hydrogen electrode in the “dry”: the electrode surface is covered by water in the monolayer and sub-monolayer range.[1] A set-up example of the system is presented in Figure 6. Hydrogen transport trough metals like palladium is very fast.[39]

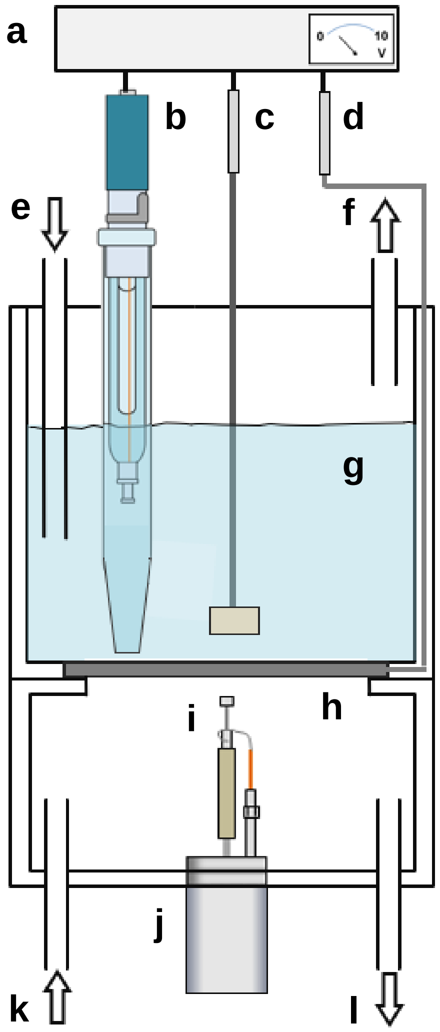

Figure 6. Instrument set-up example for the hydrogen electrode in the “dry” concept: a) potentiostat; b) reference electrode; c) counter electrode; d) connection to the working electrode; e) gas inlet; f) gas outlet; g) electrolyte; h) working electrode (sample); i) Kelvin probe tip; j) Kelvin probe; k) gas inlet; l) gas outlet (adapted from reference 1).

As mentioned, the work function was measured on the palladium membrane side exposed to dry N_2 atmosphere (Figure 6k) represents this gas inlet). Hydrogen has a high solubility in palladium and the work function measured shows linearity with applied potentials in a wide range. Such behavior is similar if the palladium membrane was totally immersed and both sides were in contact with electrolyte (electrochemical double cell), i.e., there is an electrochemical equilibrium between the applied electrode potential (on the entry side/electrolyte contact) and the other side of the palladium membrane (“dry” side, represented in Figure 6h)).[1] Hence, it was proposed that a hydrogen electrode is forming.

According the authors, the linear wide range was achieved between approximately 0 and 400 mV (SHE); above 400 mV (SHE) the hydrogen activities are too low and the work function stops to correlate. Under 0 mV (SHE) the linear correlation between the applied potentials and the work function measured by the Kelvin probe is lost, because of the formation of a binary phase of Pd with dissolved hydrogen and Pd hydride, pinning the hydrogen activity to the equilibrium activity for the co-existence of the two phases.[1]

As the example of the work by Zhong *et al.* discussed above this shows that electrodes covered by electrolyte layers in the monolayer or even sub-monolayer range are relevant and “real” electrochemistry occurs there. An obvious advantage of such “dry” electrodes is that the electrochemical double layer range is directly accessible by standard surface analytical tools, such as photoelectron spectroscopy (XPS). However, the hydrogen electrode in the “dry” does not contain ions that can be analytically detected by methods such as XPS, as only H^+ cations are expected.

In the present PhD study, the idea of these electrode in the “dry” was therefore combined with the emersed electrodes concept, that will be described further below. The aim was to prepare electrodes, where the double layer region is accessible, such as in these electrodes in the “dry” and where electrochemical reactions can be investigated.

2.3 Electrodes, potentials and the electrochemical double layer

In the following some short overview of the electrochemical double layer will be given. An electrochemical double layer can be defined as an electrically neutral system in which a layer of positive and a layer of negative charges are opposed. Furthermore, layers of oriented polar molecules and/or polarized atoms are present in this system. The electrochemical double layer is composed of two charge layers with thickness and distance apart in the atomic dimension.[46] In Figure 7 is represented schematically an electrochemical double layer system.

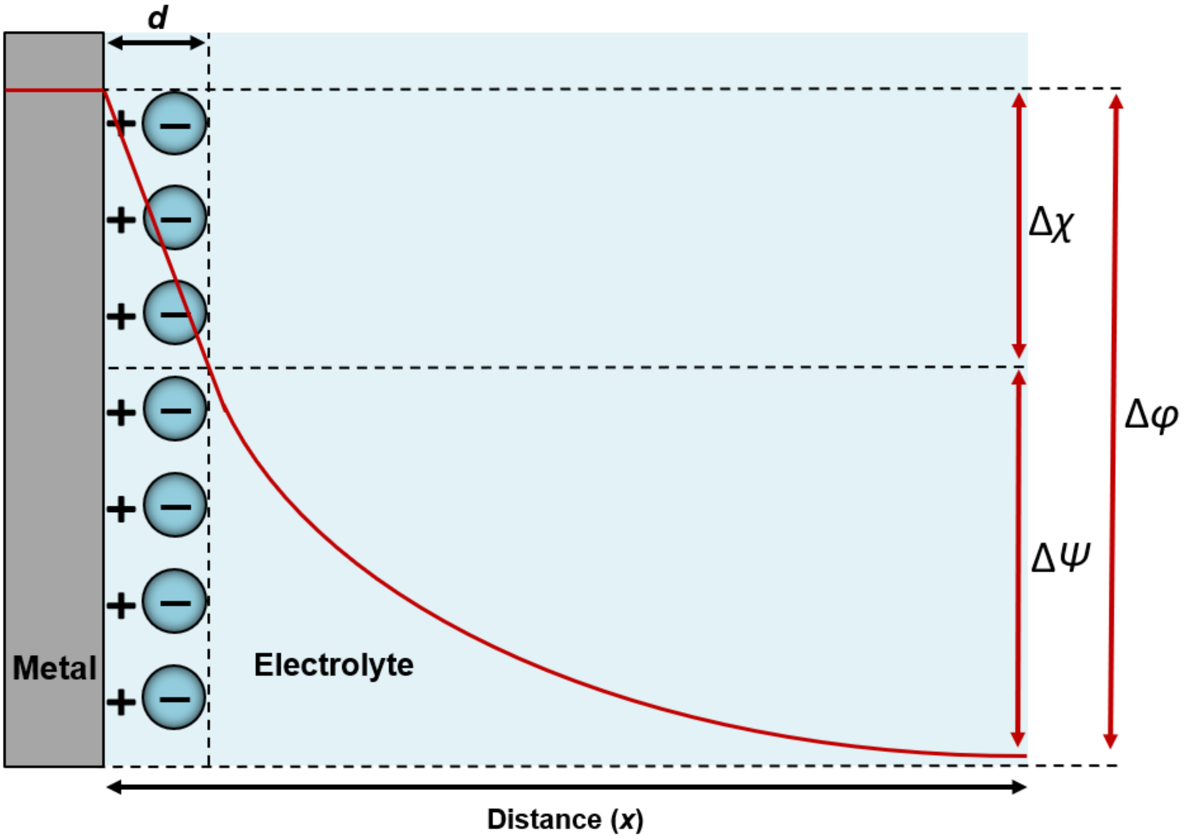

Figure 7. Schematic sketch of Galvani potential (composed by the surface potential difference and the Volta potential difference) at electrode with positive charge.

In Figure 7 is represented the Galvani potential ($\Delta\varphi$), i.e., the potential difference between the interior of two substances which is defined as:[46]

$$\Delta\varphi = \Delta\Psi + \Delta\chi \qquad \text{(Equation 3)}$$

where $\Delta\Psi$ represents the Volta potential difference (which can be directly determined by Kelvin probe measurement and will be described in section 2.4.1) and $\Delta\chi$ represents the surface potential difference.

The distance represented by "*d* " in Figure 7 correspond to the double layer thickness. Its measure is in angstroms order (1 Å correspond to 10^{-8} cm or 0.1 nm) and was deduced by Thomson as the minimum distance between two charged layers.[46]

Usually electrodes are polarized and investigated in electrochemical cells. Usually this is a three-electrode cell, composed of a reference electrode (RE), a counter electrode (CE) and a working electrode (WE).[14] The CE is an inert conductor which supplies the current (flowing to the WE) for the electrochemical cell.[47] The cell is purged with an inert gas, like argon or nitrogen to remove the oxygen dissolved in the electrolyte.[14,15]

In laboratory studies, normally the electrochemical process of interest is occurring on the WE over the potentiostatic control, i.e., controlling the potential of the WE and measuring the current it passes, or over the galvanostatic control, i.e., controlling the current which the WE pass and measuring its potential. The resistance between WE and RE has to be the smallest possible to ensure accurately potential on the WE.[16] When carrying out potentiodynamic experiments, a linear sweep of the electrode potential with time is required.[14] In Figure 8 is represented a scheme of a three-electrode cell. The electrodes are briefly described at sections 2.3.2 and 2.3.3.

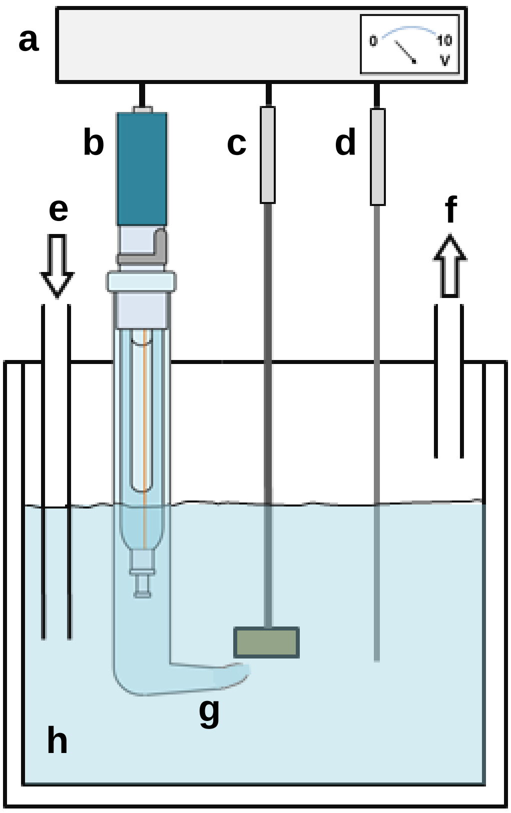

Figure 8. Scheme of a three-electrode cell: a) voltmeter (potentiostat); b) commercial Ag/AgCl reference electrode; c) working electrode; d) counter electrode; e) inert gas inlet; f) gas outlet; g) Luggin capillary; h) electrolyte.

2.3.1 Nernst equation and the cell potential

The Nernst equation provides the relation between electrode potential and the oxidizing and reducing species in the electrolyte.[48] As example are shown the reaction of iron in water (neutral pH):

Anodic semi-reaction: $Fe_{(s)} \rightarrow Fe^{2+}_{(aq)} + 2\ e^-$ (Reaction 3)

Cathodic semi-reaction: $O_{2(aq)} + 2\ H_2O_{(l)} + 4\ e^- \rightarrow 4\ OH^-_{(aq)}$ (Reaction 4)

Global reaction: $2\ Fe_{(s)} + \frac{1}{2}\ O_{2(aq)} + H_2O_{(l)} \rightarrow Fe(OH)_{2(aq)}$ (Reaction 5)

The activities of the species involved in the cell reaction are related to the Gibbs energy change of the related reaction according to:[48]

$$\Delta G = \Delta G^0 + RT \ln \alpha \qquad \text{(Equation 4)}$$

where α is the quotient of the activities of the involved species.

The cell potential is given by:[16,48]

$$\Delta G = -\, nFE_{cell} \qquad \text{(Equation 5)}$$

Dividing both sides of Equation 4 by ($-\, nF$) and combining with Equation 5, the following equation is obtained:[48]

$$E_{cell} = -\frac{\Delta G^0}{nF} - \frac{RT}{nF} \ln \alpha \qquad \text{(Equation 6)}$$

where n is the electrons stoichiometric coefficient in the half-reaction.[48]

The standard cell potential can be defined as:[48]

$$E^0{}_{cell} = -\frac{\Delta G^0}{nF} \qquad \text{(Equation 7)}$$

Finally, with combination of Equations 6 and 7 is formed the Nernst equation (Equation 8), i.e., an equation for the cell potential related to its composition:[48]

$$E_{cell} = E^0{}_{cell} - \frac{RT}{nF} \ln \alpha \qquad \text{(Equation 8)}$$

The Nernst equation also can be formulated in terms of log α. For temperature of 298.15 K and replacing the constants R and F for the corrects values, then the equation is written as:[17]

$$E_{cell} = E^0{}_{cell} - \frac{0.059}{n} \log \alpha \qquad \text{(Equation 9)}$$

2.3.2 Reference electrodes

A standard hydrogen electrode (SHE) establishes, by definition, the zero point on the electrochemical scale. This electrode is called primary reference. The hydrogen half-cell reaction has a potential, $E_{H^+/H_2} = 0$, defined for reactants and products at the standard state.[17]

For the major part of electrochemical experiments secondary reference electrodes are used.[17] These electrodes have a reproducible and stable potential relative to the SHE. Some secondary reference electrodes are Hg_2SO_4, HgO, the calomel and the Ag/AgCl electrodes.[14] The both last are shortly described here.

A much known secondary reference electrode is the saturated calomel electrode (SCE), composed by Hg_2Cl_2 with a mixture of a paste and liquid Hg. The Hg is in contact with a saturated KCl solution and a platinum wire immersed in the Hg made electrical contact. The SCE potential of 0.241 V is lower than the standard potential of 0.268 V from the calomel half-cell reaction ($Hg_2Cl_2 + 2e^- \rightarrow 2Hg + 2Cl^-$). This happens due to the saturation of chloride, i.e., the Cl^- activity is greater than 1 and influences the result at the Nernst equation.[17]

A Ag/AgCl electrode is composed of a silver wire covered with AgCl in contact with a chloride solution.[14] Platinum wire can also be employed for an electroplated silver coating. The Cl^- can be provided from HCl (used to oxidizing the silver surface) or from KCl (electrode solution). The half-cell reaction ($AgCl + e^- \rightarrow Ag + Cl^-$) gives the potential of 0.222 V and the electrode potential is given by $E_{Ag/AgCl} = 0.222 - 0.059 \log [Cl^-]$ (Nernst equation).[17] In Table 3 are presented some secondary reference electrodes with the related standard potentials.

Table 3. Some secondary reference electrodes and its related standard potentials (adapted from reference 14).

Electrode	E^0 (V vs. SHE)
Ag/AgCl electrode	+ 0.222
Calomel electrode	+ 0.268
Hg_2SO_4 electrode	+ 0.615
HgO electrode	+ 0.926

A Luggin capillary (as shown previously in Figure 8g)) is applied to ensure a resistance as small as possible between reference and working electrodes. The reference electrode is inserted into the capillary (normally made of glass) which is positioned near the working electrode.[16] The use of excess of salts where cations and anions have the same mobility, like KCl, provides a small liquid junction potential (E_j). The E_j difference occurs at the contact between electrolytes with different diffusion mobilities of cations and anions due to the concentration gradients. Therefore, solutions of these kinds of salts, like KCl, are used in the reference electrodes and in electrolyte bridges.[14]

2.3.3 Working and counter electrodes

Most working electrodes are solid, but there are also some liquid electrodes (at room temperature); the most common is the mercury electrode used as a dropping electrode.[16] The sample in study can also be the working electrode, like palladium.[49] The surface of a solid working electrode has to be free of physical defects, i.e., the surface has to be polished.[16] Counter electrodes normally are made of inert materials, such as platinum[16] or gold[49] and are used to complete the electrical circuit.[16]

2.4 Kelvin probe

The Kelvin probe (KP) is a device able to measure the potentials of local electrodes or corrosion without touching the surface under study. The measure occurs across a dielectric environment with infinite resistance[50] and is also a non-destructive technique.[51] Furthermore, KP measurements allows the electrode potential determination at buried interfaces beneath coatings and at ultrathin electrolyte layers covering the electrode.[52] Principles and applications of the KP will be described next.

2.4.1 Measurement of the Volta potential

Basically, the KP is composed by a metallic reference electrode (tip) connected to the sample by a metallic wire. KP tip and sample are separated by a dielectric medium.[50] The Kelvin probe measures the Volta potential difference ($\Delta\Psi$) between the tip and the sample.[52] Before explaining the measurement of $\Delta\Psi$, it is necessary to define some concepts.

The work function (ϕ) is defined as the least amount of energy necessary for the removal of an electron from a solid surface just outside this material.[51,53] The true work function can also be defined (at uniform surfaces of an electric conductor) as the electrochemical potential (Fermi energy level) difference of the electrons just inside the conductor and the electrostatic potential energy of an electron just outside the conductor (in the vacuum).[54] In Figure 9 the principles of a Kelvin probe are represented schematically.

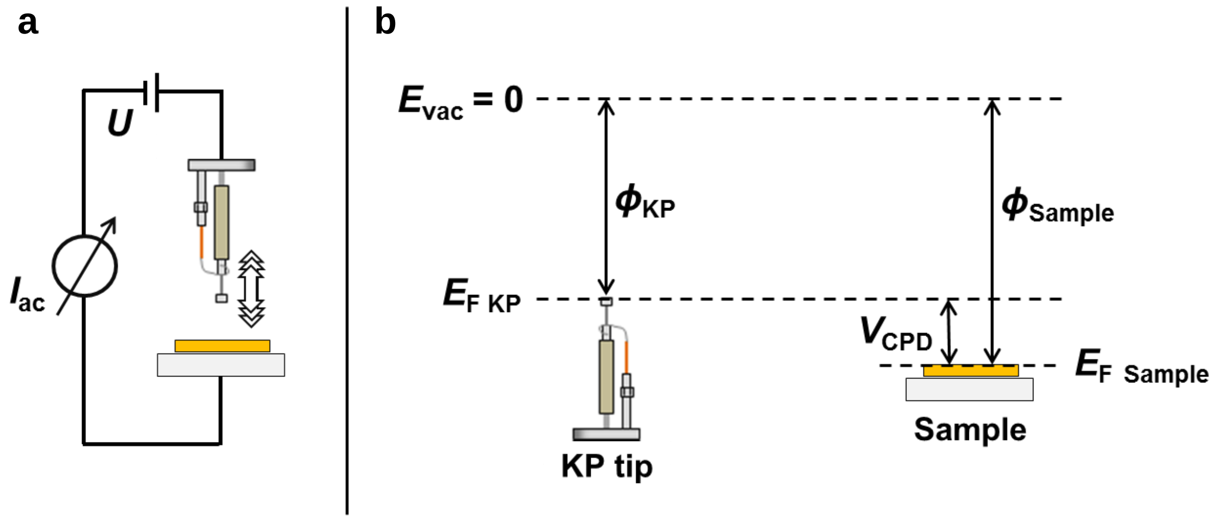

Figure 9. Kelvin probe: a) schematic of the principle with a vibrating tip (adapted from reference 52); b) diagram representing the Fermi energy levels of the Kelvin probe tip ($E_{\mathrm{F\ KP}}$) and the sample ($E_{\mathrm{F\ Sample}}$), the work functions of the Kelvin probe (ϕ_{KP}) and the sample (ϕ_{Sample}) and the contact potential difference (V_{CPD}, also called $\Delta\Psi$) between tip and sample. E_{vac} represents the vacuum level. The tip represented in b) is drawn inverted to facilitate interpretation of the diagram (adapted from reference 55).

If the work functions of the sample and the KP tip are, respectively ϕ_{Sample} and ϕ_{KP}, the electrochemical potentials of the electron (Fermi energy levels) in the sample and in the KP tip are, respectively $E_{\mathrm{F\ Sample}}$ and $E_{\mathrm{F\ KP}}$, the chemical potentials of the electron in the sample and in the KP tip are, respectively μ_e^{Sample} and μ_e^{KP}, the surface potentials of the sample and the KP tip are, respectively χ^{Sample} and χ^{KP}, then:[50]

$$\phi_{\mathrm{Sample}} = -E_{\mathrm{F\ Sample}} = -(\mu_e^{\mathrm{Sample}} - F\,\chi^{\mathrm{Sample}}) \qquad \text{(Equation 10)}$$

$$\phi_{\mathrm{KP}} = -E_{\mathrm{F\ KP}} = -(\mu_e^{\mathrm{KP}} - F\,\chi^{\mathrm{KP}}) \qquad \text{(Equation 11)}$$

where F is the Faraday constant. The E_{F} are also called absolute electrode potentials according to Trasatti.[56]

The μ_e represents the chemical work necessary to transfer one electron from the infinity into the sample and – μ_e represents the chemical work necessary to transfer one electron from the sample to the infinity.[57]

When KP tip and sample shown in Figure 9b) are connected by a wire, then their Fermi energy levels are equal, i.e., $E_{\mathrm{F\ Sample}} = E_{\mathrm{F\ KP}}$ [58] and a charging on one of them (KP tip or sample) regarding to the other will cause a Volta potential difference:[50]

$$E_{\mathrm{F\ Sample}} = -\phi_{\mathrm{Sample}} - F\,\Psi_{\mathrm{Sample}} \qquad \text{(Equation 12)}$$

$$E_{\mathrm{F\ KP}} = -\phi_{\mathrm{KP}} - F\,\Psi_{\mathrm{KP}} \qquad \text{(Equation 13)}$$

$$\Delta\Psi = \Psi_{\mathrm{KP}} - \Psi_{\mathrm{Sample}} \qquad \text{(Equation 14)}$$

where $\Delta\Psi$ is the Volta potential difference between the Kelvin probe tip and the sample under investigation.

According to the diagram represented in Figure 9b), the energy difference between the Fermi energy levels from the Kelvin probe tip and the sample is equal to the Volta potential difference:[55]

$$\Delta\Psi = E_{\mathrm{F\ KP}} - E_{\mathrm{F\ Sample}} \qquad \text{(Equation 15)}$$

The scheme represented in Figure 10 shows an electron energy level diagram for the Kelvin probe tip and a sample without and with electrical contact.

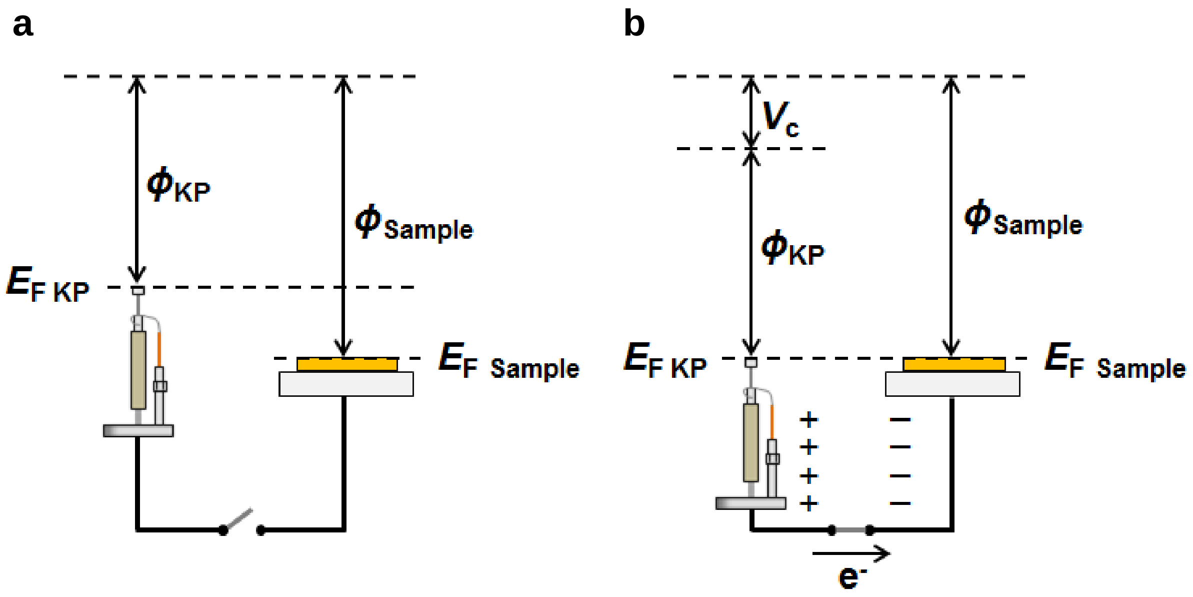

Figure 10. Electron energy level diagram for Kelvin probe tip and sample: a) without electrical contact between them; b) with electrical contact between them (adapted from references 51,55).

The electrical contact between Kelvin probe tip and sample results in a transfer of electrons from the lower work function (KP tip) to the higher work function (sample)[55] and the Fermi energy levels equalizes ($E_{F\ Sample} = E_{F\ KP}$).[55,58] The term V_c in Figure 10b) is called contact potential and is resulted by the correlated flow of charge between tip and sample.[51] To measure the contact potential the distance between Kelvin probe and sample is modulated harmonically and an external potential is applied (backing potential V_b) until no displacement current can be measured anymore, i.e. the surface charge was revoked ($V_b = -V_c$).[51,59]

The Kelvin probe tip has to be calibrated against a known surface (determining the work function) to calculate the work function of the sample.[51] This calibration is possible using readily available reference electrodes, for example, Ag/AgCl/KCl.[52] The calculation can be done using the following equations:[51]

$$\phi_{KP} = \phi_{Test\ sample} - \Delta\Psi \qquad \text{(Equation 16)}$$

$$\phi_{Sample} = \phi_{KP} + \Delta\Psi \qquad \text{(Equation 17)}$$

The tip of a Kelvin probe can be made of different materials. The use of nickel, Ni/Cr, gold and stainless steel as material for Kelvin probe tips have been reported.[52] Tips can have different diameters. As some examples, 125 µm [60], 300 µm [61], 400 µm [1], about 500 µm [52] and 2.0 mm [55] diameter tips were employed in different studies. Tips made of Ni are apparently more stable in variable atmospheric conditions when compared to tips made of Ni/Cr, gold or stainless steel.[52]

2.5 Fourier-transform infrared spectroscopy

The connections between the atoms in a molecule in a way behave like elastic bonds and can perform periodic motions (vibrations). Polyatomic molecules composed by *n* atoms have 3*n*-6 normal vibrations, whereas linear molecules have 3*n*-5. These vibrations will define the vibrational spectra of a molecule. The spectra present characteristic vibrations which are particular of some functional groups of atoms. Infrared (IR) spectroscopy is one of the most important methods of vibrational spectroscopy.[62] It is also an analytical technique for surface analysis involving photons.[63] The infrared radiation comprehends the range of wavelengths between the visible and microwaves of the electromagnetic spectrum. For many years the dispersive spectrometers were used to obtain the infrared spectra[64], where prisms or diffraction gratings disperse the radiation.[65]

The relative motions of the atoms in a molecule and the corresponding frequencies of that motions are defined by the molecular geometry, by the atoms masses and by the bonds force constants. These vibrations can be symmetric (ν_s) or antisymmetric (ν_a) stretching and deformation vibration (δ) of the OH bonds in the water molecule.[62] In Figure 11 vibrations characteristic for water and carbon dioxide molecules are schematically sketched.

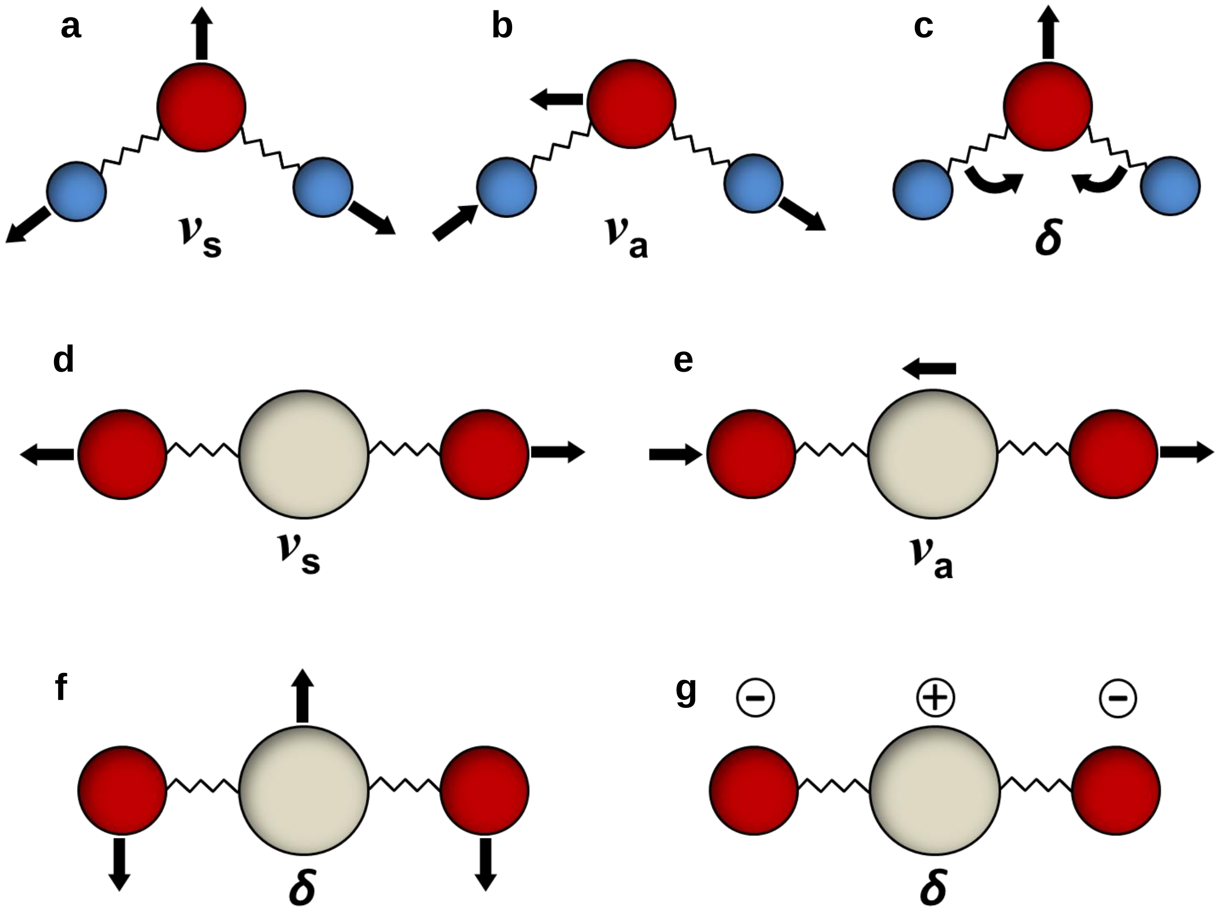

Figure 11. Representation of periodic motions of water molecule (a – c) and carbon dioxide (d – g), where ν_s represents the symmetric stretching vibration, ν_a represents the antisymmetric stretching vibration and δ represents the deformation vibration; the representations f) and g) are the same, but viewed from two different perspectives (adapted from references 62,64).

The absorption of light in the infrared region of the electromagnetic spectrum covers the wavelengths range from 0.78 until 1000 μm, with wavenumber from 12800 until 10 cm^{-1}. In this region, the far infrared (FIR) comprehends the absorption spectrum between 200 and 10 cm^{-1}. Mid infrared (MIR) are the wavenumbers between 4000 and 200 cm^{-1}. The region from 12800 until 4000 cm^{-1} is called near infrared (NIR).[66] In Table 4 are listed the vibrations and the respective wavenumbers present in the infrared spectrum of water and carbon dioxide molecules. These wavenumbers are of interest due to the presence of both substances in the atmosphere.

Table 4. Vibrations and the respective wavenumbers present in water and carbon dioxide molecules (adapted from reference 64).

Substance	Vibration	Wavenumber (cm^{-1})
Water	ν_a OH	3756
	ν_s OH	3652
	δ OH	1596
Carbon dioxide	ν_a CO_2	2350
	ν_s CO_2	1340
	δ CO_2	665

For the present work, some other substances were of high importance, for example, the perchlorate ion. In this case, wavenumbers from 1130 – 1090 cm^{-1} are attributed to perchlorate ion adsorbed on gold surfaces.[67]

The Fourier-transform infrared spectroscopy is an infrared technique with many advantages: the wavelengths are very accurate and all elements (vibrations and deformations from the molecules) providing from the IR source reach the detector simultaneously. Huge advantages of the FT-IR spectroscopy compared to conventional spectroscopy is the shorter measurement time and also a better relation signal/noise.[66]

In the FT-IR spectroscopy, the radiation is separated in two beams. One beam reaches a fixed mirror and the other one reaches a movable mirror.[64] A beamsplitter, composed by two semitransparent mirrors with a multiple constructive interference for all wavelengths in the middle[62] is responsible for dividing the IR beam in two beams. All these components together compose the interferometer, also called

Michelson interferometer.[66] A diagram representing the interferometer in a FT-IR spectrometer is presented in Figure 12.

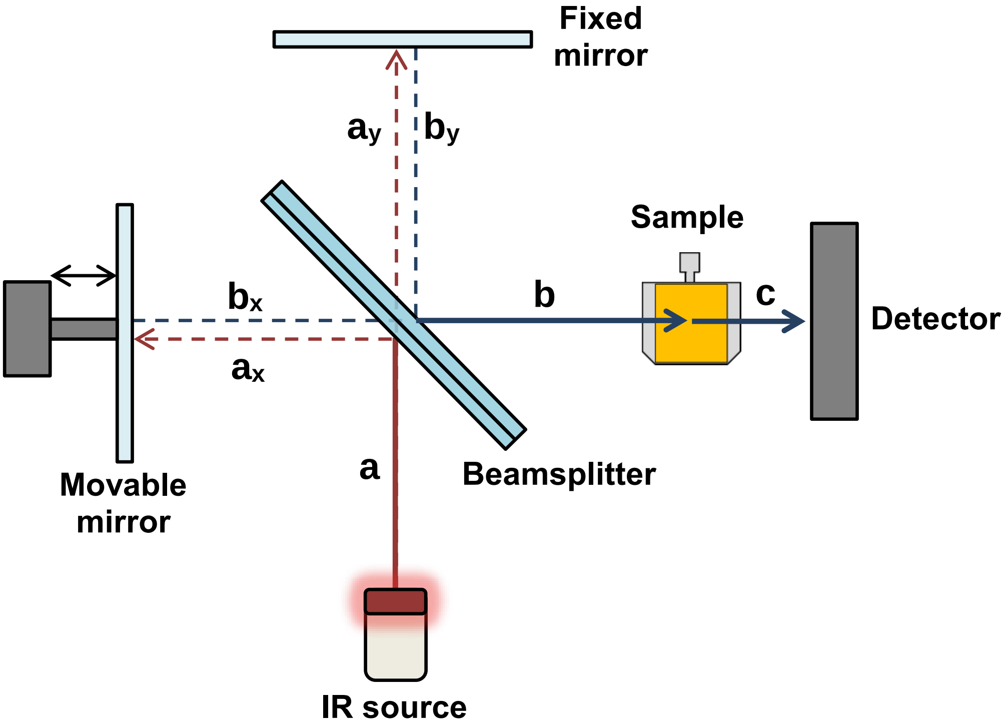

Figure 12. Diagram of the interferometer parts in a FT-IR spectrometer: a) IR beam coming from the source; a_x) part of the IR beam reflected by the beamsplitter; a_y) part of the IR beam transmitted through the beamsplitter; b_y) the “a_y” beam reflected by the fixed mirror; b_x) the “a_x” beam reflected by the movable mirror; b) combined beam of “b_x” and “b_y” reaching the sample surface; c) beam reflected on the sample surface reaching the instrument detector (adapted from references 62,64).

While the movable mirror is moving, constructive and destructive interferences are generated. This creates variations of the IR radiation that reaches the sample and the detector, the called interferogram (in time domain), which is converted trough the Fourier-transform in an interferogram in frequencies domain. The continuous movement of the movable mirror then modifies the beam (b_x) travelled distance and these movements generates the whole infrared spectra.[64]

2.6 Spectroscopic ellipsometry

The spectroscopic ellipsometry (SE) technique employs light as measurement probe (optical measurement technique). In ellipsometry, polarized light waves irradiates the sample surface at a specified angle. The polarization (reflection or transmission) will be changed by the surface film thickness and by the optical constants.[68] Polarized light (oriented in two perpendicular planes) is focused on the sample surface; in Figure 13, E_{ip} represents the incident electric wave amplitude in the same plane of incidence as the sample surface (horizontal, in this case) and E_{is} represents the incident electric wave amplitude perpendicular to E_{ip}.[68,69] The subscript "i" is referred to incident light[68] and the subscripts "p" and "s" are referred to "parallel" and "senkrecht", respectively (German words for parallel and perpendicular).[69] The ellipsometry name is attributed to the "elliptical form" of the light waves after been reflected/transmitted by the film on the sample surface, like presented in Figure 13.

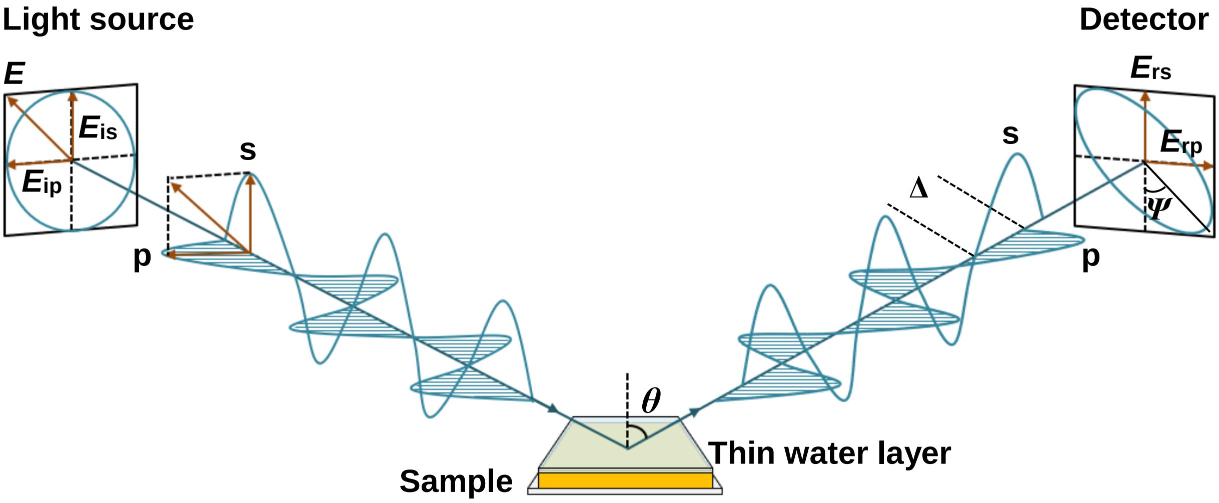

Figure 13. Schematic principle of the ellipsometry technique, where "p" and "s" represent the parallel and the perpendicular waves, respectively (adapted from references 68,69).

After reaching the sample/surface film, the incident polarized light is reflected; E_{rp} for reflected electric wave amplitude (parallel) and E_{rs} for reflected electric wave amplitude (perpendicular). The phase difference between the two polarized incident waves and the two polarized reflected waves is called "delta" (Δ). This phase shift is induced by the reflection of the light on the sample/surface film.[69] Another important parameter in ellipsometry is "psi" (Ψ), which correspond to the amplitude ratio between "p" and "s" polarizations.[68] The total reflection coefficient is the ratio between the amplitudes of outgoing and incoming waves, and this is generally a complex number. Therefore, the magnitudes of these amplitude diminutions are $|R^p|$ and $|R^s|$ and the following equations can be written:[69]

$$\tan \Psi = |R^p|/|R^s| \qquad \text{(Equation 18)}$$

$$\rho = R^p/R^s \qquad \text{(Equation 19)}$$

where ρ is a complex number (the complex ratio of the total reflection coefficients).[69]

Now it is possible to define the fundamental equation of ellipsometry:[68]

$$\rho \equiv \tan \Psi \exp(i\Delta) \qquad \text{(Equation 20)}$$

Example of the application of ellipsometry in electrochemical studies are investigation of the electrochemical oxidation of gold which is accompanied by chemisorbed species and leads to a change of the optical properties.[70] Of great relevance for this thesis are examples where the thickness of an adsorbed water layer on gold surfaces at different humidity is revealed by ellipsometry.[3] Another work of ellipsometry application on gold surfaces show results between 0.2 and 0.5 nm.[71]

2.7 X-ray photoelectron spectroscopy

The X-ray photoelectron spectroscopy (XPS) is a common technique employed for surface analysis and often used in replacement of the older name "electron spectroscopy for chemical analysis" (ESCA). In the XPS technique, the sample surface is irradiated with photons of characteristic energy, which interact directly with core electrons present in the sample atoms. This interaction produces ionized states in which a photoelectron is emitted; the kinetic energy of this photoelectron is approximately the difference between the photon energy and the electron binding energy.[72] In Figure 14 the key components and the trajectory of impinging X-ray and emitted photo-electron in the XPS instrument are shown.

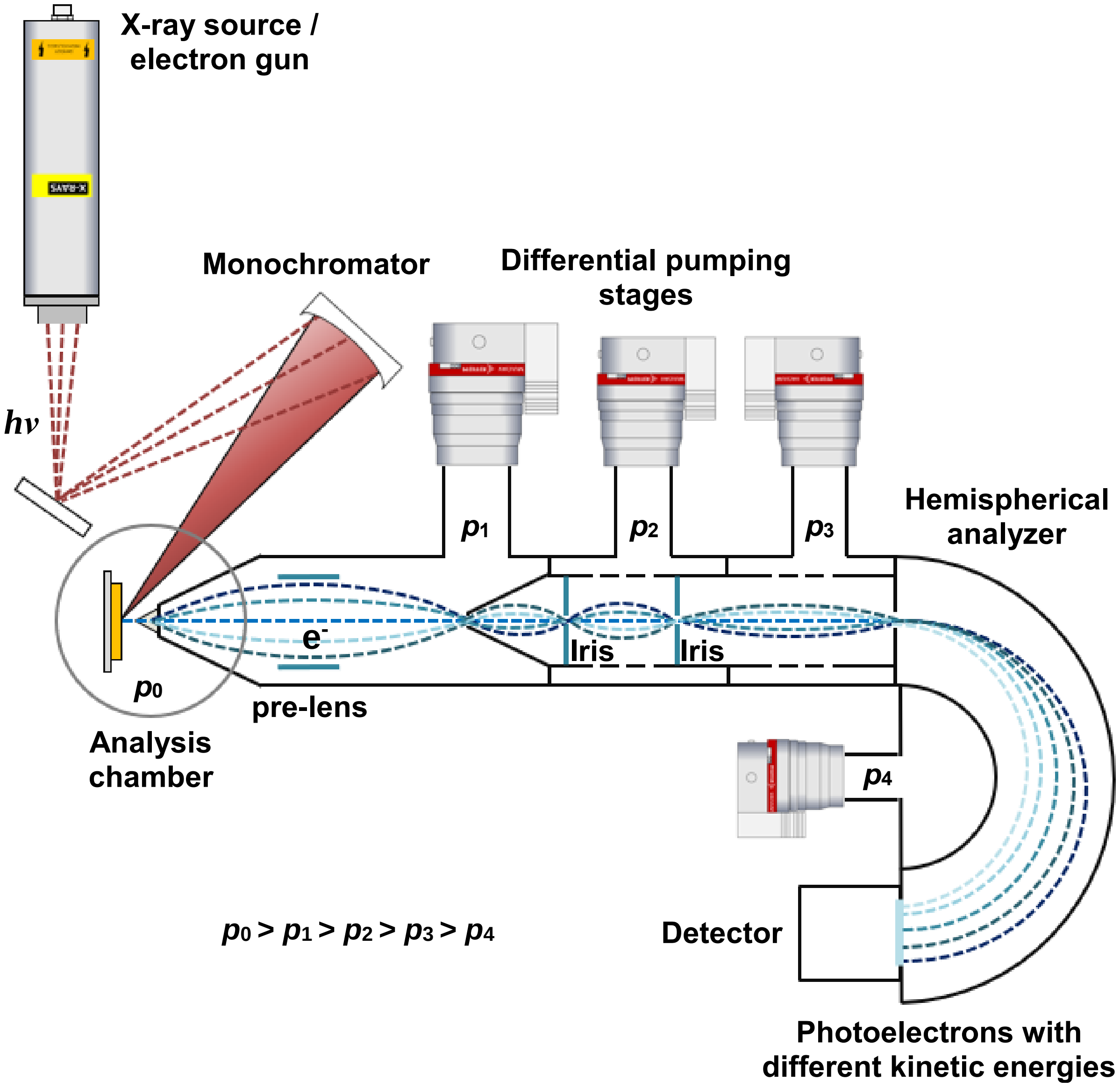
X-ray source /
electron gun
X-RAYS
Monochromator
Differential pumping
stages
hv
p1
p2
p3
Hemispherical
analyzer
e-
Iris
Iris
p0
pre-lens
Analysis
chamber
p4
p0 > p1 > p2 > p3 > p4
Detector
Photoelectrons with
different kinetic energies

Figure 14. Schematic representation of an XPS system with four differential pumping stages; p_0, p_1, p_2, p_3 and p_4 represents the pressure in each of the chamber/stages,

where $p_0 > p_1 > p_2 > p_3 > p_4$. This instrumentation was also used in the present work and is described in section 3.1.6 (adapted from references 72,73,74). The differential pumping depicted here is necessary to achieve so called Ambient Pressure XPS (APXPS).

In Figure 14 is shown the energy ($h\nu$) route from the X-ray source through the monochromator and the focused radiation hitting the sample (represented in yellow color). After the interaction of the photons with the sample surface, the photoelectrons from the sample are guided through the nozzle (small cone placed near the sample) into the differential pumping stages (p_1, p_2, p_3 and p_4) in ultra-high vacuum (UHV) conditions. This is necessary for so called Ambient Pressure XPS (APXPS), where the sample can be exposed to pressure up to a few mbar and for some instruments already up to 1 bar. The sample surface has to be very close to the entrance nozzle of the analyzer, in order to prevent collision of the photoelectrons with gas molecules. Going through the hemispherical energy analyzer, the photoelectrons with different kinetic energies reach the detector.

Besides the UHV pumps in the XPS system, some other important components can be mentioned, such as the X-ray source and the energy analyzer. X-rays are generated when a sufficiently energetic electron beam hits a metallic solid, called X-ray anode. As X-ray anodes commonly employed in XPS systems are the Al-$K\alpha$ X-rays. These anodes present some advantages, such as high robustness, high energy and intensity, minimal energy spread and Al is also a good heat conductor.[75] With respect to the energy analyzers, only the hemispherical analyzer shall be mentioned in this section due its application in the present work. The hemispherical sector analyzer (HSA), also called concentric hemispherical analyzer (CHA), is one of the mostly employed electron energy analyzers in commercial XPS systems.[72,75] One advantage of the HSA is a better energy resolution than provided by other analyzers. Resolution values of < 0.01 eV can be achieved with HSA analyzers.[75] HSA analyzers are composed of two concentric hemispheres, where on the outer hemisphere a negative potential ($-V$) against the inner hemisphere is applied.[72] Applying specific potentials to the hemispheres will result in deflection of the electrons (with accordingly specific energies) onto the detector.[75]

The photoelectron spectrum from the XPS analysis represents a direct indication of the binding energies from the different core electron levels in the atoms. The higher the electron binding energy, the lower the photoelectron kinetic energy.[72] The kinetic energies of the electrons emitted from the sample are measured and their binding energies are determined using the following equation:[76]

$$E_b = h\nu - E_k + \Delta\phi \qquad \text{(Equation 21)}$$

where E_b is the electron binding energy in the solid, $h\nu$ is the incident photon energy, E_k is the electron kinetic energy and $\Delta\phi$ is the work function difference between sample and detector material (assuming that there is no charge at the sample surface).[76]

The XPS technique is able to identify and quantify the elemental composition of solid surfaces (electrons of the outer 10 nm or less) of the majority of chemical elements, with exception of H and He (this is attributed to the fact that XPS is sensitive to core electrons, not to valence electrons; furthermore, their photoelectron cross-sections yields are below the XPS limits of detection).[75]

2.8 Potential of zero charge

Potential of zero charge (PZC) is considered, according the International Union of Pure and Applied Chemistry (IUPAC), "*the value of the electric potential of an electrode at which one of the charges defined is zero. The reference electrode against which this is measured should always be clearly stated. The potential difference with respect to the potential of zero charge is defined by:* $E_{pzc} = E - E_{\sigma = 0}$ *, where the potential at the point of zero charge is that for the given electrode in the absence of specific adsorption".*[77] The electrode (sample surface) is charged negatively below the PZC and positively above the PZC.[67] The PZC value also is important due information about species orientation/reorientation on an electrode surface/electrolyte interface, which can be studied, for example, employing infrared spectroscopy techniques[67] and will be further discussed in section 4.2.2.

2.9 The idea of electrodes emersed from aqueous electrolytes

In the early 80s, Neff and Kötz[6] proposed a study to a surface science approach to the electric double layer (solid/liquid interface). In their experiment, gold samples (electrodes) were emersed under control of the electrode potential from acid aqueous electrolytes into UHV conditions and the samples were investigated by ultraviolet photoelectron spectroscopy, with which the adsorbed species on the surface were analyzed and also the work function was determined.[6] In another study, in the 90s, Samec *et al*.[7] determined the Volta potential difference between a Kelvin probe tip and gold or platinum electrodes emersed from different aqueous electrolytes into a water saturated nitrogen gas phase (around 99% RH). A wide pH range was employed for such studies. As example, acid solutions (H_2SO_4 and HCl)[6,7] and neutral solutions (NaCl and KCl)[7] were employed. Alkaline solutions, such as NaOH, were also used in investigations of the electrochemical double layer on silver electrodes.[78]

All these investigations show (for polarization in the ideally polarizable range) a linear behavior between the applied potentials on the sample surface (for example, gold) and the related Volta potential difference determined after the emersion from the electrolyte. The experimental procedures of such experiments carried out in this PhD work are presented in section 3.10 and the results in section 4.2.

Concerning, water molecules in the double layer, in the experiments by Neff and Kötz[6] no indications for water present on the electrodes emersed into UHV, while in the experiments carried out by Samec *et al.*[7] water was definitely present on the electrodes emersed into nitrogen of high relative humidity and is proposed to play a role in the observed significantly overall lower potentials than observed by Neff and Kötz. For immersed polarized electrodes, it is suggested that on metal surfaces, uncharged or charged positively, the water molecules form a structure called “ice-like” (*in situ* study for the determination of water molecules orientation).[67]

2.9.1 The role of humidity inside the analysis chamber

According a study proposed by Heras and Viscido,[79] the presence of water layers on clean gold surfaces in vacuum conditions was not detected at room temperature, once adsorbed water molecules start to desorb at temperatures around – 73 °C.[79] With respect the vacuum, experiments carried out in the 70’s by Wells and Fort Jr.[80] presented detectable water adsorbed on gold surfaces only at pressures around 10^{-9} bar and higher.[80] As mentioned, also for emersed electrodes the study conducted by Neff and Kötz under UHV conditions and at room temperature gives no proof for the emersion of an intact (i.e. still containing the water molecules of the double layer region) electrochemical double layer; probably most part of the water in this double layer desorbs.[6] In other words, the structure of the double layer could not be considered totally retained.[7]

The desorption of water under UHV conditions can be expected from a thermodynamic point of view in which the desorption will be faster with the presence of low solvation free energy ions adsorbed.[7] Experiments show the influence of water vapor (to form water layers) on the dielectric constant behavior: for the first monolayer, the water molecules adsorbed on surface of α-Fe_2O_3 were observed to be quite rigid on a solid surface (in this case, a surface of α-Fe_2O_3), i.e. these molecules cannot orient with an applied alternating field (AC) and, consequently, will not contribute to the system capacitance. With the presence of a second layer, the dielectric constant rises up; this behavior is due the ability of adsorbed water molecules to respond to the AC field. The experiment proposed that the relative change in the dielectric constant after the formation of approximately three layers levels off. With this study it was possible to notice that the multilayers are more mobile than the first adsorbed layer.[81]

Wells and Fort Jr.[80] show in their study that the water vapor adsorption on gold surfaces follows two steps: first, a fast physical adsorption and second, a slow chemisorption.[80] As conclusion about all the studies shortly presented in this section: one good alternative to “preserve” or contour the desorption situation is to emerse the electrode in study into an inert atmosphere saturated with water vapor.[7]

This was the case in the experiments carried out by Samec *et al.*[7] on electrodes emersed into high humidity inert nitrogen atmosphere, where water was definitely present on the samples. Hence, since in both cases a linear dependence of the work function (for emersion into UHV) and of potential (emersion into high humidity) on the potential applied during immersion was observed, the question is what role of the water molecules in the electrochemical double layer play on potential and reactivity of electrochemical reactions. This is a key question of this PhD thesis.

2.10 Gold employed as electrode

For the investigation of an electrode/electrolyte interface, gold is chosen due its wide double layer potential range. This means that the water molecule orientation can be investigated over a wide potential range without Faraday reactions such as surface oxidation or hydrogen evolution.[67] Although gold is considered the noblest and most inert of the metals and is mentioned as the ideal solid electrode for fundamental electrochemistry studies due the absence of Faraday reactions -referred to as ideally polarizable- in the wide range of potential region, i.e., approximately 0.0 to 1.3 V (SHE) and 0.0 to 1.2 V (SHE) in acid and alkaline media, respectively, there are studies presented in the literature suggesting the formation of oxygen species in this ideally polarizable potential range.[82] In one interesting study, as an example employing combined electrochemical and spectroscopic techniques, the authors observed slow adsorption reaction on 10 to 20% of the gold surface caused probably by the specific adsorption of hydroxide anion (from NaOH) in neutral and alkaline media and adsorption of water in acid media electrolytes[83] (more information regarding specific ions adsorption will be presented/discussed in section 4.2).

A model of gold dissolution was proposed by Cherevko *et al*.[84] The authors suggest two dissolution mechanisms: at low anodic potentials, gold and adsorbed hydroxide anions and oxygen ions are exchanged; on the other hand, at higher potentials (in the oxygen evolution reaction area), the dissolution takes place on the gold oxide surface initiating gold losses.[84]

2.11 Choosing the electrolyte: $NaClO_4$, H_2SO_4, NaOH

Solutions containing perchlorate ions (ClO_4^-) are used as supporting electrolyte with different electrodes in electrochemical research.[85] The perchlorate ions, in $HClO_4$ or $NaClO_4$ aqueous solutions, for example, weakly adsorb on gold surfaces at more positive potentials than the PZC.[67,86,87] In studies of water molecule orientation on gold, these ions also are used in order to minimize the influence of specific adsorption of electrolyte anions.[67]

Sulfate anions (SO_4^{2-}) are described as presenting similar specific adsorption to the perchlorate anions.[88] Specific adsorption plays an important role in the electrode surface/interface; specifically adsorbed anions are responsible for the local electric field. This promotes the orientation of molecules with their negative dipole moment towards the electrolyte solution.[89] In the present PhD work, diluted sulfuric acid solution was employed as electrolyte. The use of sulfuric acid as electrolyte for the passive behavior of gold was studied by Zhang *et al*.[90] The authors identified by XPS analysis the presence of gold ions (Au^+ and Au^{3+}) after applying 1.4 V (SHE) during 2 h on the gold surface; this could indicate the formation of $Au(OH)_3$ or Au_2O_3 films on the gold electrode surface.[90] These trivalent gold compounds are also compatible with predictions provided by the Pourbaix diagram.[20]

Regarding the hydroxide anion (OH^-), it has been suggested that this anion adsorbs specifically on gold surfaces.[78,91] In a work proposed by Bodé Jr. *et al.*[88] was concluded that hydroxide anions are significantly adsorbed on gold surfaces and these anions are more pronounced then less adsorbable anions, such as ClO_4^- and SO_4^{2-}, for example.[88] More discussions involving on electrolytes (ClO_4^-, SO_4^{2-} and OH^- anions) will be provided in section 4.2.

3 Experimental

In this section details on the materials used, such as reagents, substrate materials and other materials and the equipment used in this work will be described. Also, the methodologies used to preparing the samples, the assembly of the set-ups and the operational procedures to obtain the results will be discussed. All potentials applied in the experiments presented in this section are referred against the Ag/AgCl/3M KCl reference electrode.

3.1 Equipment

The equipment and instruments employed for this work and the corresponding laboratory concept (combination of different analytical techniques, such as Kelvin probe and infrared spectroscopy) are described at the following sections.

3.1.1 Kelvin probe system

An ultra-high vacuum Kelvin probe system, model UHV-KP020-50 / UHV-KP020-100, KP Technology Ltd., Wick (Scotland), United Kingdom, http://www.kelvinprobe.com, was used for the measurement of the Volta potential difference between sample and Kelvin probe. This system was set-up by the manufacturer to operate with amplitude 50, frequency 70 Hz and gradient 300.[51] The Kelvin probe tip was made of stainless steel and had a diameter of 4.0 mm. The Kelvin probe was connected to a Digital Control Unit, model DCU Series 10, KP Technology Ltd. and to an oscilloscope, model Smart DS5032EV, Owon Technology Inc., Zhangzhou, P. R. China, http://www.owon.com. The computer connected to the Kelvin probe system was equipped with the software Kelvin Probe Measurement

System Version 11.30b, KP Technology Ltd. In Figure 15 a drawing of the Kelvin probe system is shown.

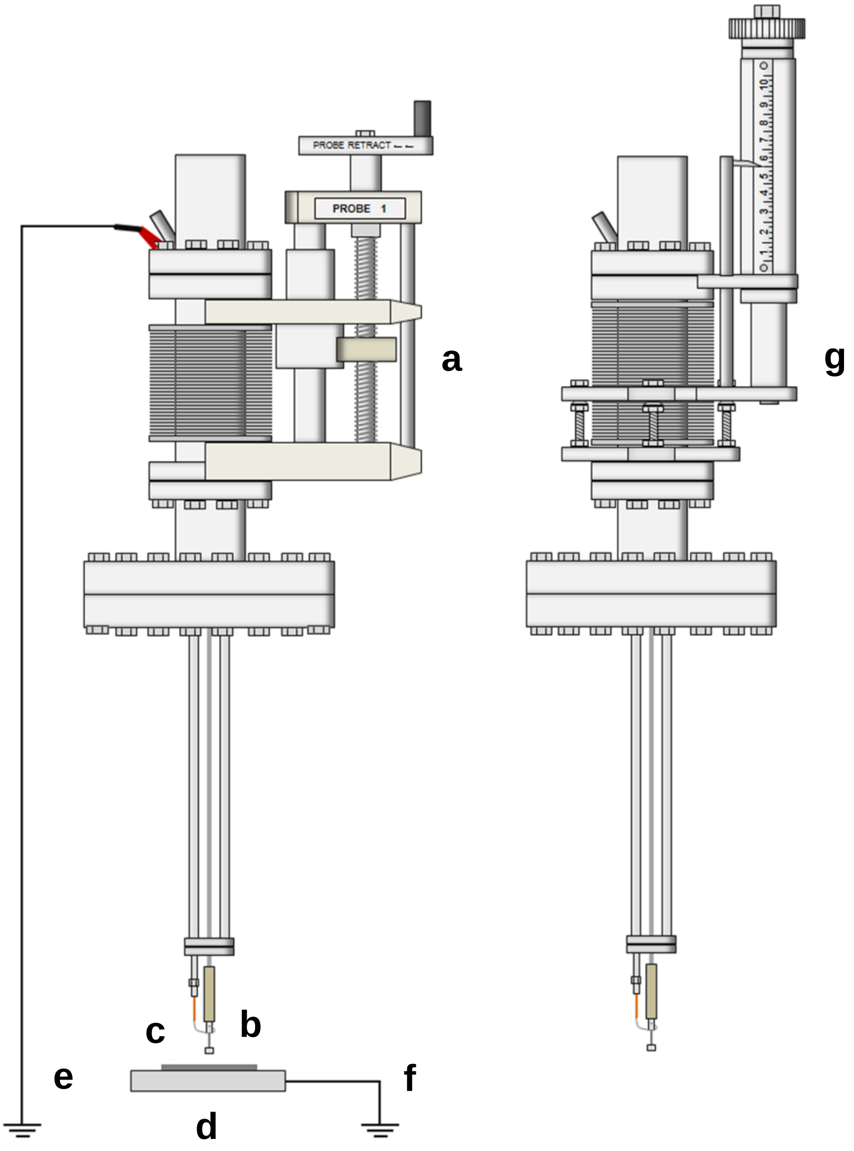

Figure 15. The Kelvin probe system: a) probe retract manipulator; b) tip; c) sample; d) sample holder; e) KP grounding; f) sample grounding; g) adjustable probe retract manipulator.

In order to improve a better adjustment of the tip position over the sample, the original probe retract manipulator was exchanged by an adjustable manipulator, VAb

(Vakuum-Anlagenbau GmbH), Elmshorn, Germany, http://www.vab-vakuum.com (Figure 15g)). This manipulator is equipped with three adjustable screws, allowing the placement of the tip at a desirable position/angle. Furthermore, the manipulator has a numerical scale for distance control.

An anti-static wrist strap was used while handling the Kelvin probe as a recommendation from the manufacturer.[51]

3.1.2 FT-IR spectrometer

A Fourier-transform infrared spectroscopy (FT-IR) equipment, model VERTEX 70v, Bruker Optik GmbH, Ettlingen, Germany, http://www.bruker.com, was employed for the sample surface analysis. An LN-MCT (Liquid Nitrogen cooled HgCdTe) detector, model ID316, InfraRed Associates, Inc., Stuart, USA, http://www.irassociates.com, was installed in the external detector chamber (see section 3.1.4). This detector was used for the infrared determinations in this work. The FT-IR equipment was controlled by OPUS Spectroscopy Software version 7.5. According the manufacturer, the FT-IR covers a spectral range from 8000 cm^{-1} to 350 cm^{-1} (using the standard optical components, like KBr beamsplitter, DLaTGS detector and MIR source).[92] To evacuate the FT-IR spectrometer and the external detector chamber a mechanical pump was used, model nXDS15i, Edwards Limited, Burgess Hill, United Kingdom, http://www.edwardsvacuum.com.

3.1.3 Electrochemical cell

The electrochemical cell (made of PTFE) was inserted in a glass chamber cross containing six windows (for x, y and z axes). One of these windows was used for placing the working electrode, which was connected to a potentiostat, model Compactstat Electrochemical Interface, Ivium Technologies B. V., Eindhoven, Netherlands, http://www.ivium.nl. The computer connected to this potentiostat was equipped with the software IviumSoft, release 2.828(3), Ivium Technologies B. V. For testing the potentiostat, a testcell, model Testcell 1, Ivium Technologies B. V. operating at 1000 Ω resistivity was employed.[93] In the opposite window the counter electrode (platinum) and the reference electrode were placed. This last electrode was from the model 6.0726.107, Ag/AgCl/3M KCl, Metrohm AG, Herisau, Switzerland, http://www.metrohm.com. This electrode features a potential of approximately +0.211 V (SHE) at 20 °C.[94] On the top window of the chamber a gas inlet/outlet system for purging the electrochemical cell was installed. The rear window was connected to the Kelvin probe/infrared beam chamber (passing through the sample transfer chamber) and the front window was connected to a sample manipulator. The bottom window was closed, opened by a valve only for cleaning when electrolyte was leaked out from the electrochemical cell. The electrolyte for the experiments in the electrochemical cell was stored in a PTFE flask with approximately 200 mL volume capacity. The flask cap had four entrances/exits. Two of them were for entrance and exit of N_2 (inert atmosphere) and the other two were for entrance and exit of the electrolyte. In this case, a Diaphragm Laboratory Pump, model Liquiport® NF 100 KT.18S, KNF FLODOS AG, Sursee, Switzerland, http://www.knf-flodos.ch, was employed to carrying the electrolyte until the electrochemical cell. The gas valves, connections and hoses for N_2 were from Sang-A, Sang-A Pneumatic Co., LTD., Daegu, South Korea, http://www.sanga2000.com and the valves, connections and hoses for electrolyte were from BOLA, Bohlender GmbH, Grünsfeld, Germany, http://www.bola.de. These valves, connections and hoses employed for electrolyte were all made of PTFE, which due to its high degree of inertness helps to avoid unwanted reactions between this material and the electrolyte. A scheme of the electrochemical cell is presented in Figure 16.

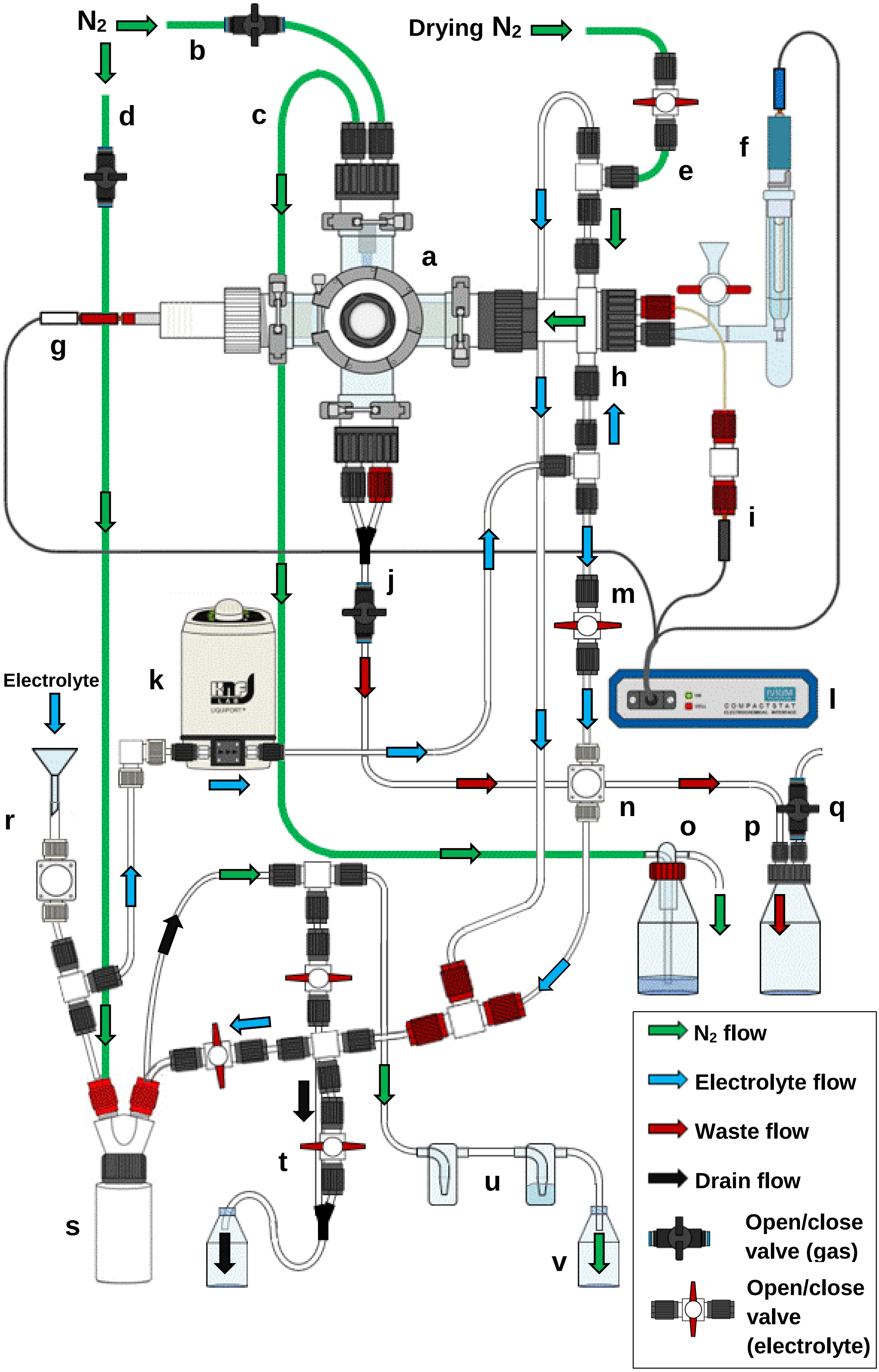
N₂
b
d
c
Drying N₂
a
e
f
g
h
i
j
m
Electrolyte
k
l
n
o
p
q
r
s
t
u
v
N₂ flow
Electrolyte flow
Waste flow
Drain flow
Open/close valve (gas)
Open/close valve (electrolyte)

Figure 16. The electrochemical cell: a) electrochemical cell; b) gas inlet and c) outlet

into the electrochemical cell; d) gas inlet for the electrolyte flask; e) drying N_2 inlet for drying the sample surface after contact with the electrolyte; f) Ag/AgCl reference electrode; g) working electrode connection; h) electrolyte inlet in the electrochemical cell; i) counter electrode connection; j) electrolyte waste outlet valve; k) diaphragm pump for the electrolyte; l) potentiostat connected to the electrochemical cell via reference electrode, working electrode and counter electrode; m) valve for changing the electrolyte flow from the electrochemical cell back to the electrolyte flask; n) control valve to controlling the flow of the “removing electrolyte”; o) glass trap containing inert oil to prevent entrance of atmospheric air in the electrochemical cell; p) flask for waste (electrolyte leaking) collecting; q) valve for overpressure releasing; r) electrolyte refill system; s) electrolyte flask; t) drain system for clean out the electrolyte flask and the electrochemical cell hoses; u) glass traps with the second trap containing inert oil to prevent entrance of atmospheric air in the electrolyte flask; v) flask for collecting mixture of electrolyte and inert oil in case of overpressure in the system. Hoses and cables in the drawing may differ in length from the real equipment. All valves are represented in “closed” mode.

The valve presented in Figure 16e) was chosen as “for electrolyte” in order to prevent some electrolyte remnants went in contact with a gas valve (if one of these would be employed here). The glass device for the reference electrode shown in Figure 16f) was filled with the respective electrolyte in study (this part of the device was directly connected to the electrochemical cell); the other side of the device (with the electrode) was filled with a 3.0 mol L^{-1} KCl solution. The counter electrode was made of platinum wire and platinum foil. The oil used to fill the glass traps (Figures 16o) and 16u)) was the DIFFELEN ultra pump fluid, Ref.-No. 176 71, Leybold Vakuum GmbH, Köln, Germany, http://www.leybold.com.

A more detailed layout of the electrochemical cell is shown in Figure 17. The cell was assembled slightly tilted on the system to facilitate the electrolyte outflow when it was removed from the cell. Moreover, reference and counter electrodes were placed near the bottom of the cell and near the sample (working electrode) in order to maintain the potential control up to the end of the electrolyte removal step.

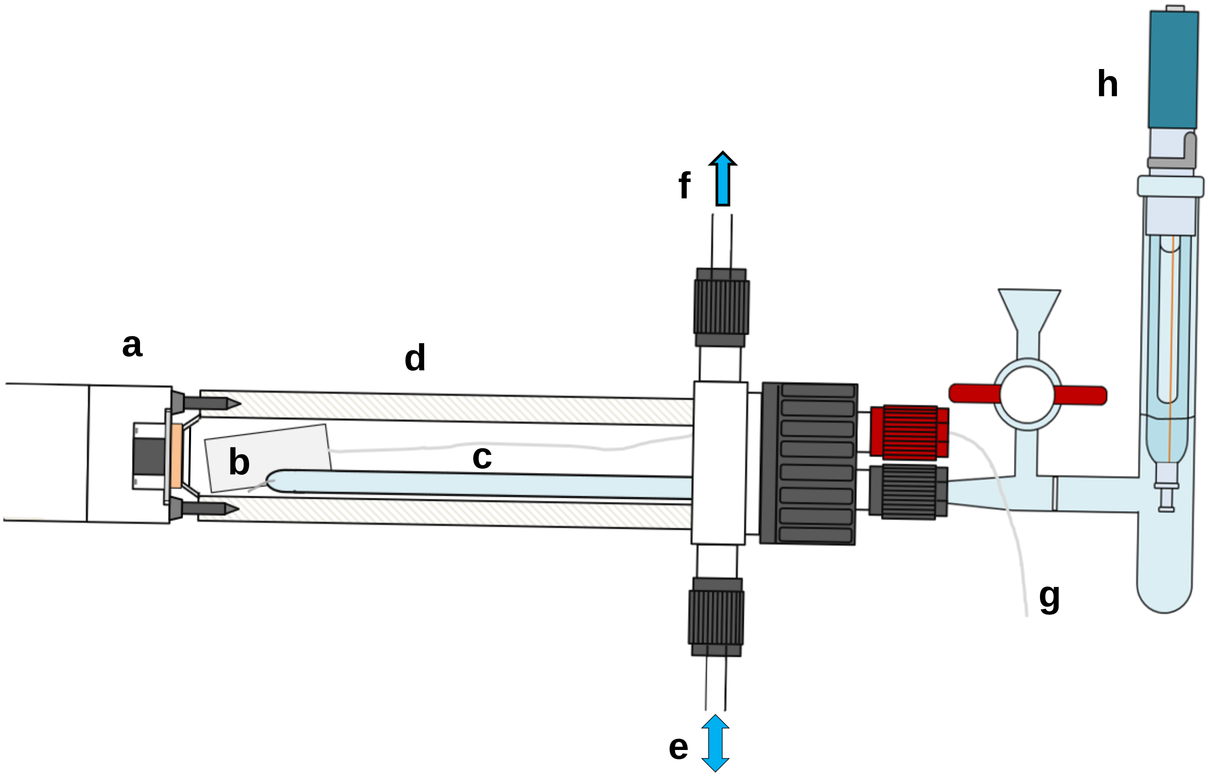

Figure 17. Layout of the electrochemical cell: a) device extremity for sample introduction in the cell with a sample (yellow detail); b) counter electrode (platinum foil); c) Luggin capillary ending with a small platinum wire at the extremity; d) electrochemical cell itself; e) electrolyte inlet and outlet (when removing electrolyte from the cell); f) electrolyte outlet; g) counter electrode (platinum wire); h) Ag/AgCl reference electrode. This system is represented slightly tilted as in the real instrumentation.

The parts a) with the sample and d) are “sealed” with a PTFE O-ring. Some more details and operational parameters involving the electrochemical cell are described in appendix A.

3.1.4 Laboratory concept: combining electrochemical cell, Kelvin probe and FT-IR

The electrochemical cell, the Kelvin probe and the complete FT-IR system were mounted on a steel and aluminum frame structure provided by SPECS Surface Nano Analysis GmbH, Berlin, Germany, http://www.specs.de, as shown in Figure 18. This configuration is able for *in operando* experiments, as will be presented later in this dissertation.

In Figure 18 is also represented a FT-IR microscope, model HYPERION 3000, Bruker Optik GmbH and a macro imaging chamber, model IMAC, Bruker Optik GmbH, however this instrumentation was not employed for sample analysis in this PhD study.

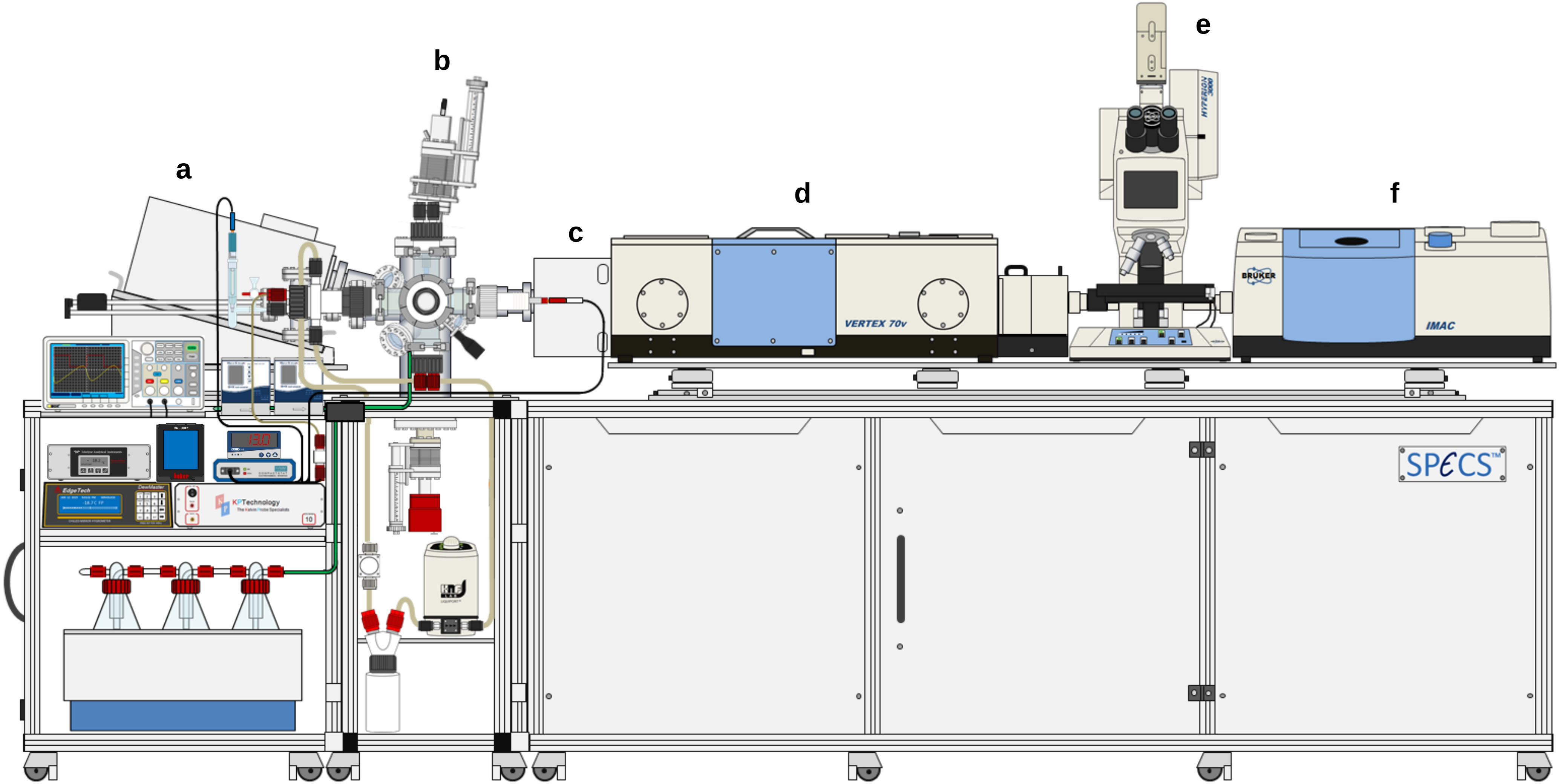
a
b
c
d
e
f
VERTEX 70v
HYPERION 3000
BRUKER
IMAC
SPECS™
KPTechnology
The Kelvin Probe Specialists
EdgeTech
DewMaster

Figure 18. Technical drawing of the FT-IR spectrometer with microscope and macro imaging chamber, the electrochemical cell and the Kelvin probe mounted on the SPECS structure: a) FT-IR external detector; b) Kelvin probe manipulator; c) IR beam guide chamber (equipped with a light polarizator); d) FT-IR spectrometer; e) microscope; f) macro imaging chamber. Some cables and hoses were neglected in this representation.

This complete instrumentation was part of the new “laboratory concept”, built up during the PhD study at the MPIE and which contributed to acquire so to speak “industrial experience”, a very important opportunity and knowledge about laboratory organization and instrumentation assembling, complementing the PhD work.

In order to improve the visualization of the electrochemical cell, the sample transfer chamber and the Kelvin probe/infrared beam chamber, a representation of these devices is shown as from an on top view perspective in Figure 19.

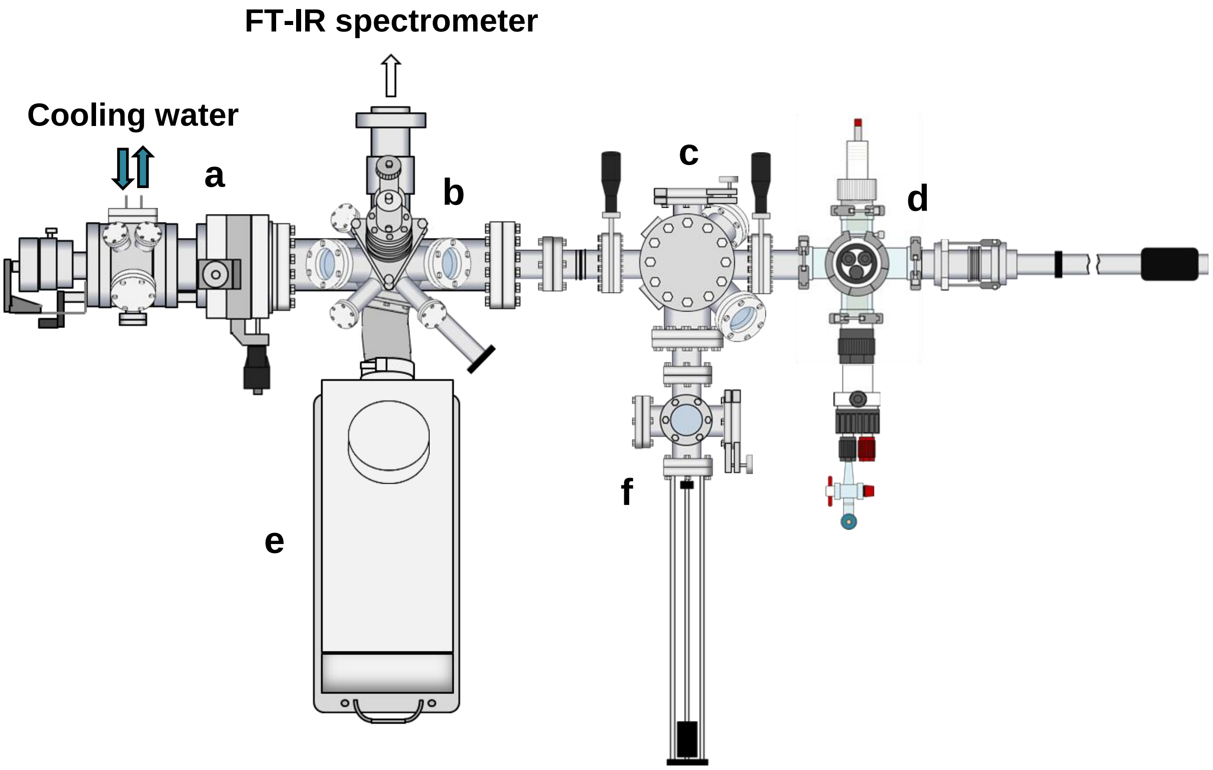

Figure 19. Top view perspective of the system: a) sample manipulator (with inlet and outlet for cooling water); b) Kelvin probe/infrared beam chamber; c) “quick-closing” door to connecting a vacuum suitcase; d) electrochemical cell; e) FT-IR external detector; f) sample transfer with storage (for up to three samples) chamber. Cables and hoses were neglected in this representation.

The sample manipulator presented in Figure 19a) was provided by VAb (Vakuum-Anlagenbau GmbH) and is adjustable in the *x* and *y* axes and also in the inclination for the correct sample positioning under the Kelvin probe tip and the IR beam. Furthermore, this manipulator allows cooling down the sample temperature when connected to a water chiller.

For the purpose of transfer samples from this system to the NAP-XPS system (see section 3.1.6), a vacuum suitcase, model V2, SPECS Surface Nano Analysis GmbH, with a removable sample vessel was employed. This suitcase, also compatible with UHV conditions, is connected (hooked) to the system through a “quick-closing” door (for example, on the door in Figure 19c)). It allows transporting up to three samples at time and is represented in Figure 20.

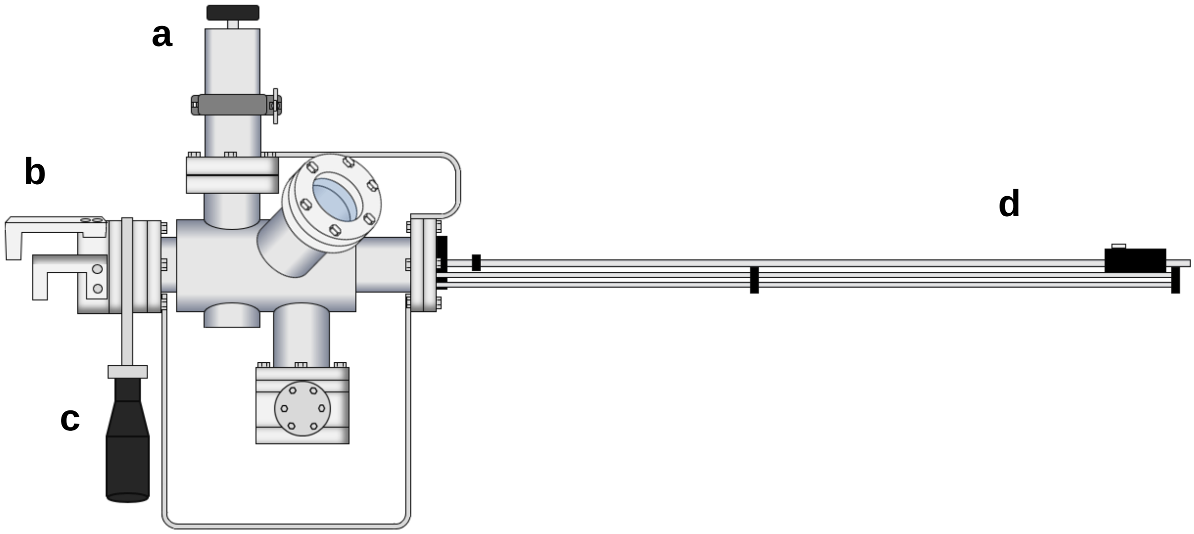

Figure 20. Lateral view of the vacuum suitcase: a) removable sample vessel; b) hook for connection to the desired system; c) UHV valve; d) transferring bar.

Wet atmosphere (N_2 or synthetic air) was adjusted employing six water (“washing”) bottles where gas was run through and then introduced into the Kelvin probe/infrared beam chamber (Figure 19b)). A chilled mirror hygrometer, model DewMaster, Edgetech Instruments Inc., Hudson, USA, http://edgetechinstruments.com, was installed in order to control the humidity through the dew point inside this chamber (chamber gas inlet). The chamber´s gas outlet was also connected to a trace moisture analyzer, model 8800A, Teledyne Analytical Instruments, City of Industry, USA, http://www.teledyne-ai.com, via a hybrid dew point transmitter, model XTR-100 sensor, COSA Xentaur Corporation, Yaphank, USA, http://www.cosaxentaur.com. The oxygen concentration inside the chamber (less than 10 ppm during dry or wet N_2 flow) was monitored by an oxygen measuring transmitter (chamber gas outlet), model Insta-Trans, Teledyne Analytical Instruments. The flow of dry and wet atmosphere to the chamber was controlled by two mass flow meter/controller, model Mass-Stream D-6311, M+W Instruments GmbH, Leonhardsbuch, Germany, http://www.mw-instruments.com. This flow was set around 40 L h^{-1}, independently when only “dry” or when combining “dry and wet” atmosphere was employed to achieve the desired humidity inside the Kelvin probe/infrared beam chamber. A layout of the system is presented in Figure 21.

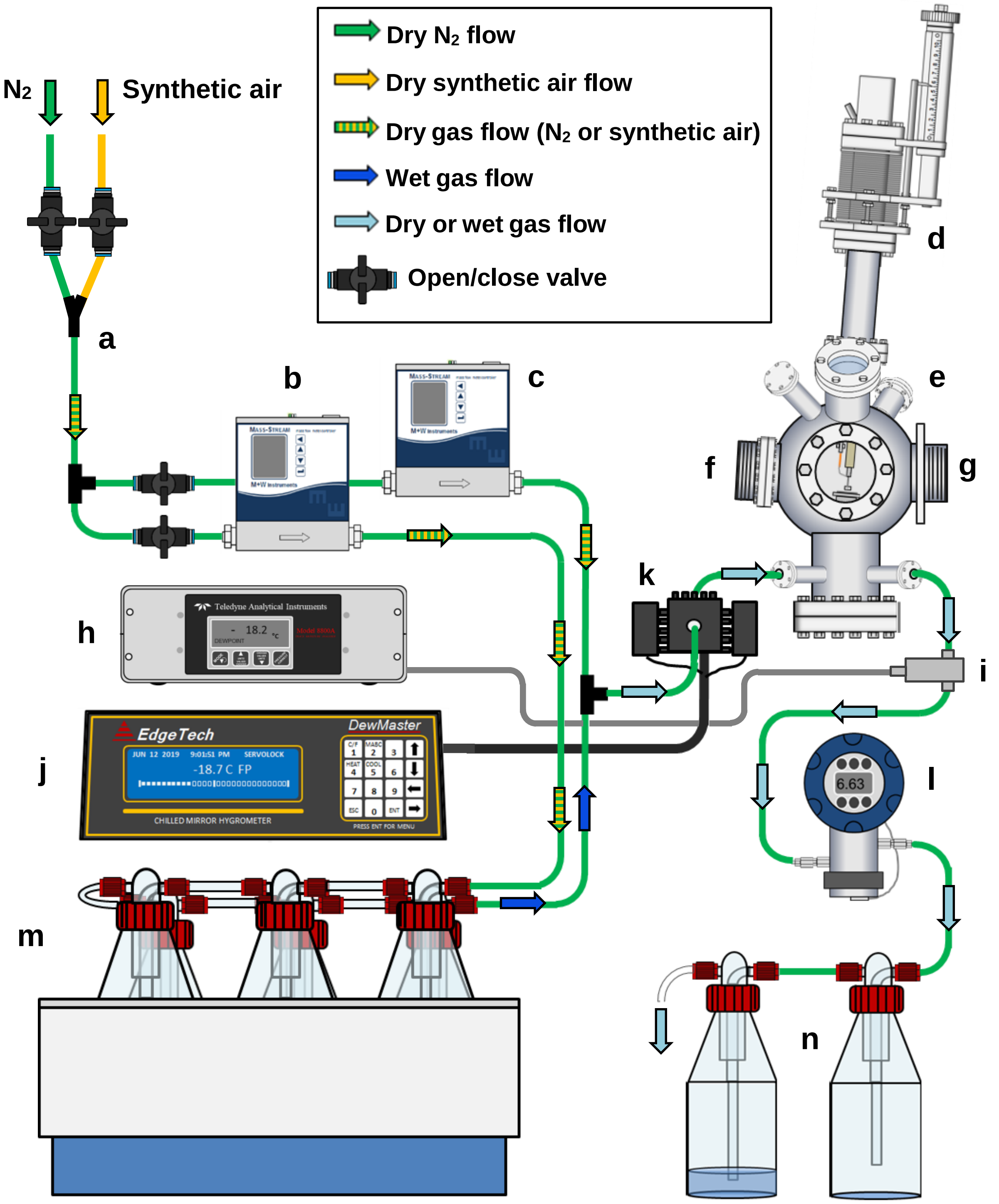
Dry N_2 flow
Dry synthetic air flow
Dry gas flow (N_2 or synthetic air)
Wet gas flow
Dry or wet gas flow
Open/close valve
N_2
Synthetic air
a
b
c
d
e
f
g
h
i
j
k
l
m
n
MASS-STREAM
M+W Instruments
Teledyne Analytical Instruments
18.2
DEWPOINT
EdgeTech
DewMaster
JUN 12 2019 9:01:51 PM SERVOLOCK
-18.7 C FP
CHILLED MIRROR HYGROMETER
PRESS ENT FOR MENU
6.63

Figure 21. Humid atmosphere control system for the Kelvin probe/infrared beam chamber: a) gas inlet in the system; b) wet atmosphere mass flow meter/controller; c) dry atmosphere mass flow meter/controller; d) Kelvin probe; e) Kelvin probe/infrared beam chamber; f) connection to the FT-IR external detector; g) connection to the FT-IR spectrometer; h) dew point meter (chamber outlet); i) dew point sensor; j) dew

point meter (chamber inlet); k) chilled mirror hygrometer; l) oxygen measuring transmitter; m) water flasks for the humid atmosphere; n) glass traps with the second trap containing inert oil to prevent entrance of atmospheric air in the system. Hoses and cables in the representation may differ in length from the real equipment. All valves are represented in “closed” mode.

High values of humidity, such as e.g. 90% RH or more (for Kelvin probe measurements, for example), were achieved cooling the sample down: a cooling circulator, model Ministat 240, Huber Kältemaschinenbau AG, Offenburg, Germany, http://www.huber-online.com, was connected to the sample manipulator (Figure 19a)) and the sample was cooled down while wet atmosphere was provided from the humid atmosphere system (previously presented in Figure 21). This circulator operates between - 45 °C (cooling) and 200 °C (heating) and was controlled by the Pilot ONE® system, Huber Kältemaschinenbau AG. The humidity inside the Kelvin probe/infrared beam chamber was then calculated based on the dew point and cooled sample temperatures using the software PST Michell Humidity Calculator, Michell Instruments Ltd., http://www.processsensing.com/en-us/humidity-calculator/. This software was also used to calculate all RH values when employing the humid atmosphere system. The sample temperature inside the Kelvin probe/infrared beam chamber was monitored by a digital microprocessor indicator, model JUMO di 08, JUMO GmbH & Co. KG, Fulda, Germany, http://www.jumo.de, connected to the sample manipulator.

3.1.5 Spectroscopic ellipsometer

An *in-situ* spectroscopic ellipsometer (iSE) device, model iSE, J.A. Woollam Co., Lincoln, USA, http://www.jawoollam.com, inserted into a chamber located over the sample transferring chamber was employed to determine the thickness and optical properties of films on the sample surface (the transfer chamber was previously presented in Figure 19 and the ellipsometer was placed over the fictitious blind flange (shown to avoid overlap) between positions c) and f) in Figure 19). The light source (quartz tungsten halogen lamp; wavelength range: 399.9 – 997.1 nm) was situated in a control box, model CCE-200, J.A. Woollam Co., and the light beam was guided to the input unit (source) through an optical fiber cable. The source and the receiver units were separated from the chamber with UV fused silica (quartz) windows and the light incident angle was around 68° from the sample surface normal vector. For the ellipsometer operation RH values between 20 and 80% were recommended.[95] The computer connected to the ellipsometer was equipped with the CompleteEASE Software, J.A. Woollam Co. A 25 nm SiO_2 layer on Si calibration wafer, J.A. Woollam Co., with 20 – 25 nm SiO_2 thickness was cut into a rectangle shape and fixed on a sample holder with conductive silver paint. This SiO_2 reference wafer was employed for the ellipsometer calibration/system check.

The ellipsometer device was not presented in Figures 18 and 19 in order to avoid overlap with other parts of the entire system (Kelvin probe, for example); therefore, the ellipsometer is shown in Figure 22. The ellipsometer chamber can also be flushed with dry or wet N_2 atmosphere in the same way as the Kelvin probe/infrared beam chamber (sample cooling, however, is not possible).

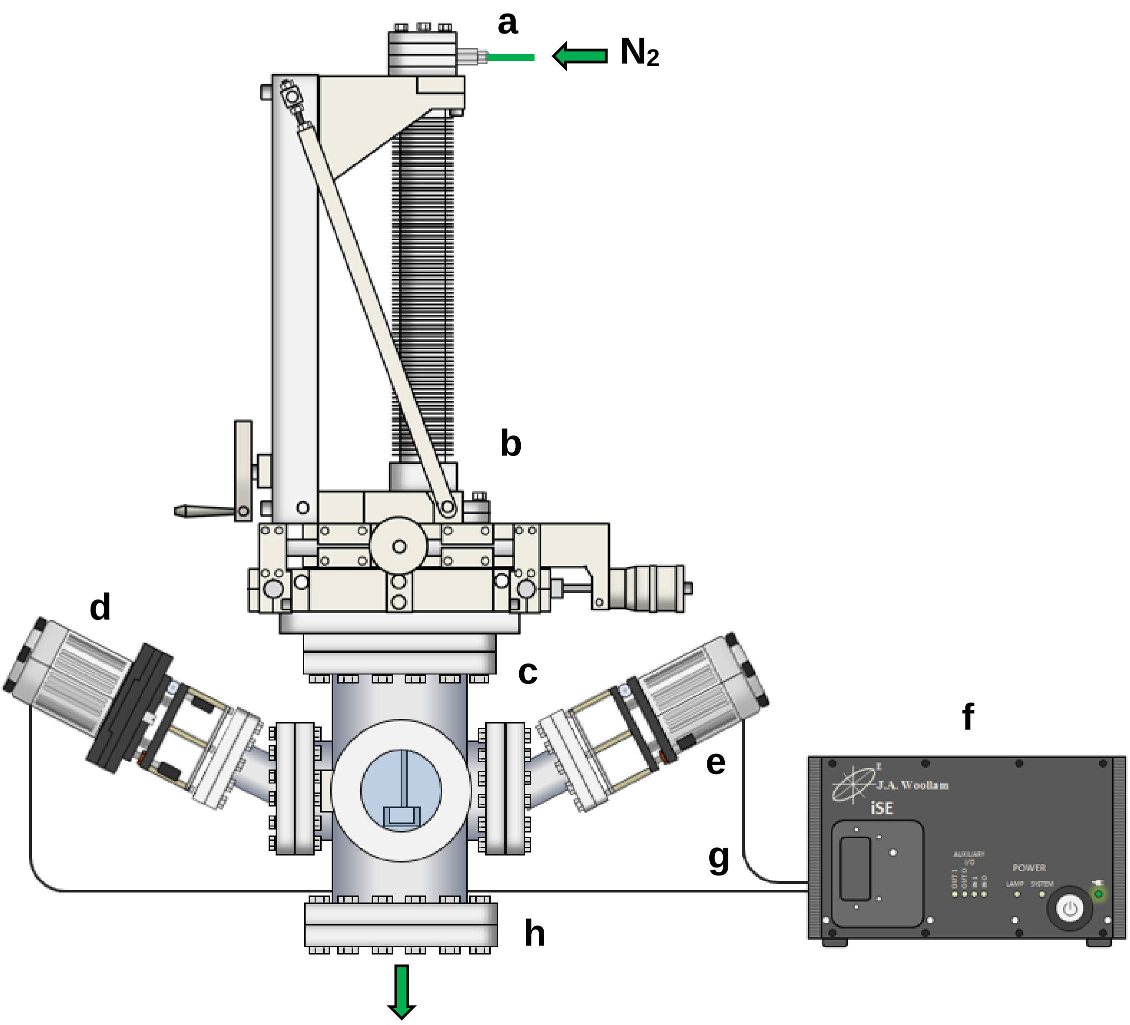

Figure 22. Spectroscopic ellipsometer device: a) gas inlet in the system; b) manipulator (*x*, *y* and *z* axes); c) analysis chamber; d) receiver unit; e) input unit; f) control box; g) optical fiber cables; h) gateway to the sample transferring chamber, in which is located the gas outlet.

3.1.6 NAP-XPS spectrometer

A Near ambient pressure X-ray photoelectron spectroscopy (NAP-XPS) device from SPECS Surface Nano Analysis GmbH was employed for sample surface analysis. This NAP-XPS device was composed by an UHV manipulator (*x*, *y* and *z* axes), model DeviSim NAP, with *in-situ* reactor NAP cell and a custom gas handling system; a twin anode X-ray source, model XR 50; an X-ray monochromator suitable for NAP conditions, model µ-FOCUS 600, with aluminium excitation line (Al-*K*α X-rays); a 180° hemispherical energy analyzer, model PHOIBOS 150 NAP, with a 2D-DLD (delayline) detector. A nozzle, with 300 µm aperture diameter, was the "entrance" for the photoelectrons into the energy analyzer, which was equipped with four differential pump stages. The vacuum in the chambers/stages were provided by turbomolecular pumps achieving around 10^{-10} mbar. The first stage was equipped with an UHV pump, model HiPace® 700, Pfeiffer Vacuum GmbH, Aßlar, Germany, http://www.pfeiffer-vacuum.com; the second and third stages were equipped with the model HiPace® 300 and the fourth stage was equipped with the model HiPace® 80. The models HiPace® 700, HiPace® 300 and HiPace® 80 provides a rotation speed of 49200, 60000 and 90000 rpm (± 2%), respectively.[96,97,98] As pre-pumps for the UHV pumps were used mechanical pumps, model nXDS15i, Edwards Limited.

The NAP-XPS device with its main components is represented in form of a top view perspective in Figure 23. Shown is the so-called first level (analysis level). The top of the analysis chamber (Figure 23i)) is represented as a blind flange in order to avoid overlap with other parts of the system, but in the real instrument it is the connection between this chamber, the second level of the system and an UHV sample manipulator from VAb (Vakuum-Anlagenbau GmbH). This manipulator was adjustable in *x*, *y*, *z* axes and variable in the *y* axe angle.

Furthermore, an electrochemical cell, similar to the system presented previously in section 3.1.3, was attached one level above the NAP-XPS device (not represented in Figure 23 to avoid overlap with other parts of the system). After the polarization in the electrochemical cell, the sample was first transferred to a buffer chamber, in which UHV conditions could be provided (10^{-6}-10^{-7} mbar) in order to prevent transferring impurities (electrolyte) and humidity to be carried into the NAP-XPS device. After this stage, the sample was transferred to the analysis chamber (10^{-10} mbar), passing through the transfer/storage chamber (10^{-9} mbar) and the preparation chamber (10^{-9} mbar).

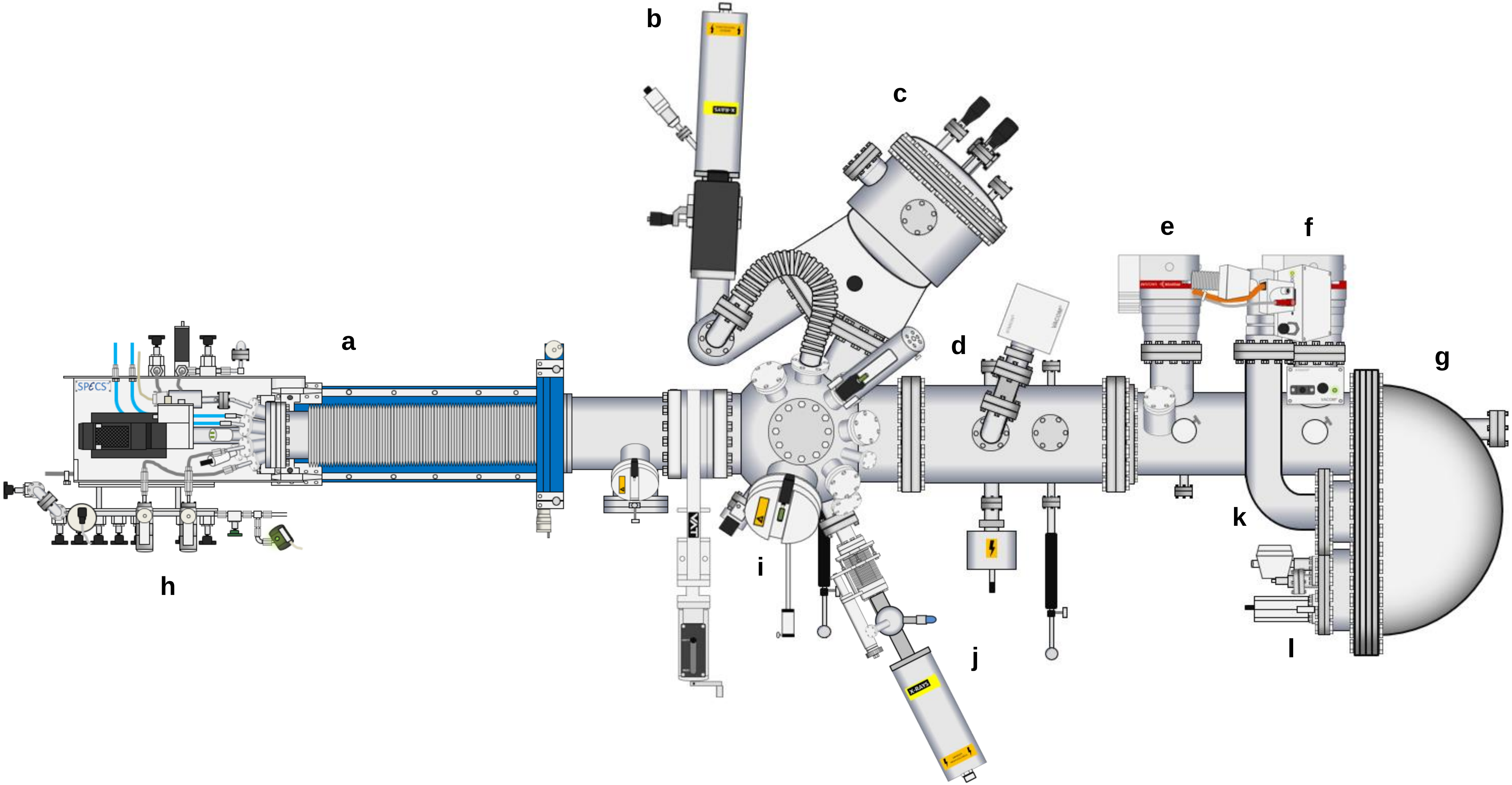

Figure 23. Top view perspective of the NAP-XPS device (first level): a) UHV manipulator with *in-situ* reactor NAP cell; b) focused monochromatic X-ray source; c) X-ray monochromator; d) first pumping stage; e) UHV pump on the second pumping stage; f) UHV pump on the third pumping stage; g) hemispherical energy analyzer; h) gas handling system; i) analysis chamber; j) X-ray source; k) fourth pumping stage; l) detector. The major part of cables and hoses were neglected in this representation.

In Figure 24 the chambers composing the second level of the system are schematically shown (preparation level).

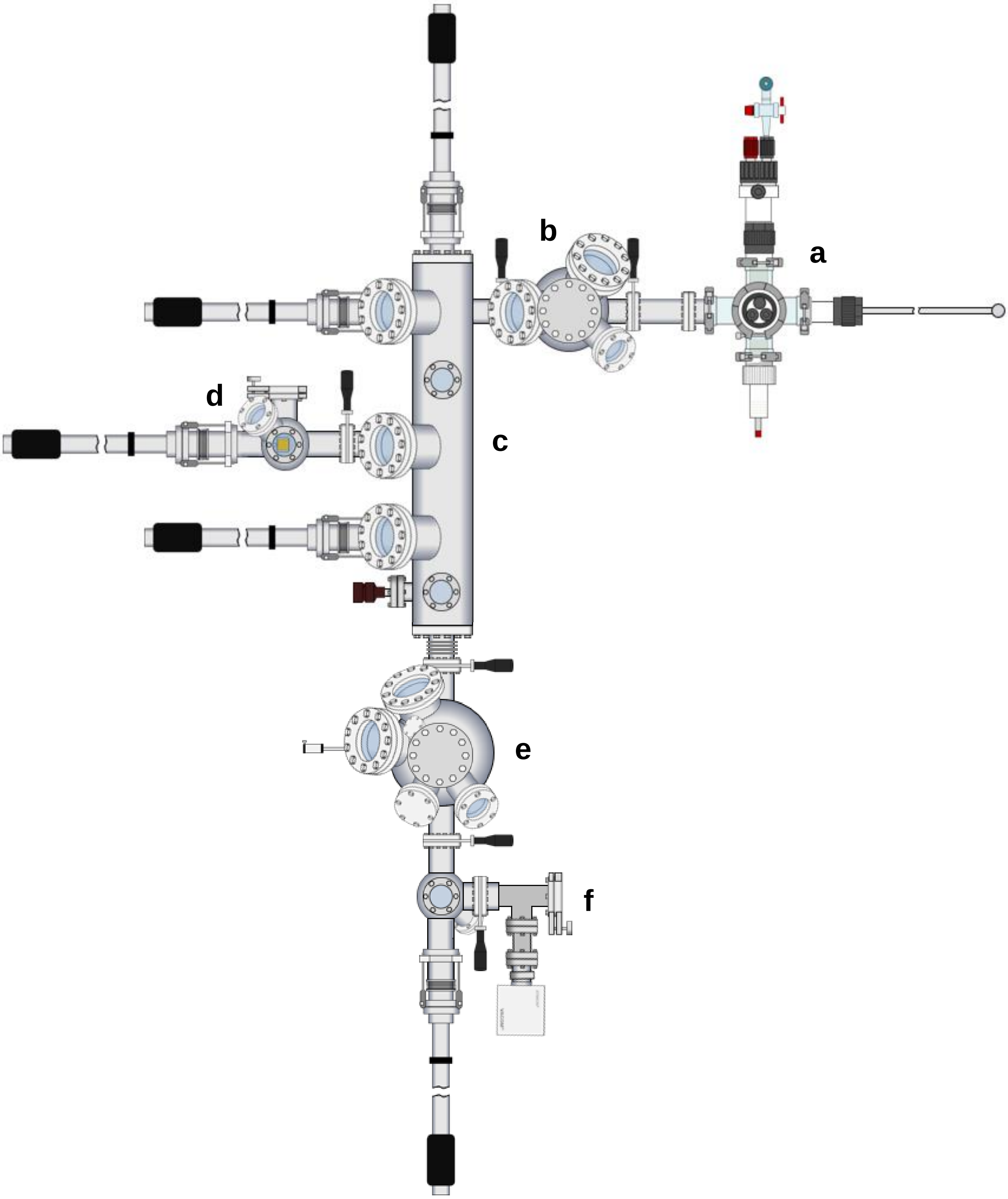

Figure 24. Top view perspective of the second level of the system composed by: a) electrochemical cell; b) buffer chamber; c) transfer/storage chamber; d) load lock; e)

preparation chamber; f) load lock compatible with a vacuum suitcase. Cables and hoses were neglected in this representation.

Only components used for experiments in this PhD study are represented in Figure 24. The top of the buffer chamber (Figure 24b)) is represented with a blind flange; in the real instrument is inserted a Kelvin probe (as described in section 3.1.1). Also, the top of the preparation chamber (Figure 24e)) is represented with a blind flange; here is placed the manipulator in which is inserted the sample and then transferred to the first level (analysis chamber).

For a better signal/noise ratio, the X-ray source shown in Figure 23j) was employed for characterization of ions in the double layer of the emersed electrodes, as this source provided a much higher intensity, with 12 kV anode voltage and 400 W power (this source with aluminium excitation line provides up to 400 W power with a 10 mm spot size).

3.1.7 Other devices

A physical vapor deposition (PVD) device, model Univex 450, Leybold AG, Köln, Germany, http://www.leybold.com, was used to evaporate chromium or titanium (as adhesion layers) and, posteriorly, gold on the glass substrates. For grinding and polishing sample holders (used in the NAP-XPS device as samples covered with gold), a grinding/polishing machine was employed, model Forcipol 2V, Metkon Instruments Inc., Bursa, Turkey, http://www.metkon.com.

Reagents for preparation of the aqueous solutions were weighed with a milligram balance (readability of 0.001 g and maximal weighing capacity of 210 g), model Quintix 213-1S, Sartorius Lab Instruments GmbH & Co. KG, Göttingen, Germany, http://www.sartorius.com. The measurement of the pH of the electrolyte was done with a pH measuring instrument, model SevenCompact pH/Ion S220, Mettler-Toledo AG, Schwerzenbach, Switzerland, http://www.mt.com, equipped with a pH electrode, model InLab® Expert PRO-ISM pH, Mettler-Toledo AG, operational at pH range 0-14 (temperature between 0 °C and 100 °C). The device is also equipped with a temperature compensation system.

3.2 Reagents and gases

All the reagents used in this work were of analytical grade. The water for preparing the electrolyte solutions was purified by an ultrapure water system, model Milli-Q® Reference A+, Millipore SAS, Molsheim, France, http://www.merckmillipore.com, presenting final resistivity around 18.2 MΩ cm at 25 °C and Total Oxidizable Carbon (TOC) below 5 ppb.[99] This ultrapure water was also used to rinse the laboratory glassware.

As electrolyte for the first experiments in the electrochemical cell sodium perchlorate monohydrate ($NaClO_4 \cdot H_2O$) was used, cod. A11243, ≥ 97%, Alfa Aesar, Kandel, Germany, http://www.alfa.com. The $NaClO_4$ was dissolved in ultrapure water and stored in a polyethylene flask, a concentration of 0.1 mol L^{-1} was employed. Electrolyte solution of potassium chloride (KCl), cod. 83605.290, AVS TITRINORM, 3.0 mol L^{-1}, VWR International, Leuven, Belgium, http://www.vwr.com, was used for the preparation of reference electrodes for the Kelvin probe calibration.

Sulfuric acid (H_2SO_4), cod. 1.00731.1000, EMSURE®, 95-97%, Merck KGaA, Darmstadt, Germany, http://www.merckmillipore.com, hydrogen peroxide (H_2O_2), cod. 8.22287.1000, 30%, Merck KGaA, acetone (CH_3COCH_3), cod. 1.00014.1000, EMSURE®, Merck KGaA and ethanol (C_2H_5OH), cod. 1.00983.1011, EMSURE®, Merck KGaA, were used for cleaning the laboratory glassware, the polyethylene flasks and the glass samples. The same H_2SO_4 was also used to prepare electrolytes with lower pH values. For the cleaning procedure of sample holders used in the NAP-XPS device as samples, Extran® (laboratory cleaning agent composed by ionic and non-ionic surfactants, phosphates and excipients) was employed, cod. 1.07553.2500, Extran® MA 02, liquid neutral concentrate, Merck KGaA. Sodium hydroxide (NaOH), cod. 1.06462.1000, pellets pure, ≥ 99%, Merck KGaA, was used as electrolyte with higher pH values. Potassium bromide (KBr), cod. 1.04907.0100, Uvasol®, Merck KGaA, was also employed as electrolyte for some experiments.

As internal electrolyte for the Ag/AgCl/3M KCl reference electrode (inside the Luggin capillary) a 3.0 mol L^{-1} KCl solution was used, InLab® Solutions, Mettler-Toledo AG. For the pH measuring instrument calibration technical buffer solutions (pH 2.00, 4.01, 7.00, 9.21 and 11.00 at 25 °C) were employed, Mettler-Toledo AG.

For grinding the sample holders silicon carbide grinding paper was used, CarbiMet (P1000), CarbiMet (P2500) and MICROCUT (P4000), Buehler Ltd., Lake Bluff, USA, http://www.buehler.com; for polishing these holders a polishing disc was used, model MD Plus, 1 µm grain size, Struers Inc., Cleveland, USA, http://www.struers.com. This polishing procedure was supported by a water-based monocrystalline diamond suspension, cod. 39-410-M, DIAPAT-M (1µm), Metkon Instruments Inc. and a water-based diamond lubricant, cod. 39-502, DIAPAT, Metkon Instruments Inc.

Nitrogen (N_2), 99.999%, Nippon Gases Deutschland GmbH, Düsseldorf, Germany, http://www.nippongases.com, was used to purge the electrochemical cell, the electrolyte flask and to dry the rinsed glassware and samples. This nitrogen was also used as liquid nitrogen for cooling down the LN-MCT detector. Argon (Ar), 99.999%, Air Products GmbH, Hattingen, Germany, http://www.airproducts.de, was also employed to dry glassware and samples. Synthetic air, (20.5 ± 0.5% O_2 in N_2), Air Liquide, Düsseldorf, Germany, http://www.airliquide.com was employed in some experiments in the Kelvin probe/infrared beam chamber.

3.3 Samples

Glass samples (approximately 15 mm x 12 mm x 3 mm) were used as substrate for deposition of a gold layer as they present a smooth surface. This gold layer (200 nm) was deposited on the glass substrate surface by PVD, as described in section 3.6.

Stainless steel sample holders were covered with gold when used in the NAP-XPS device as samples. This was done in order to avoid using silver paint or another adhesive that eventually could cause some contamination inside the vacuum chambers of the system.

3.4 Cleaning procedures

The laboratory glassware and polyethylene flasks were decontaminated using a freshly prepared piranha solution. This solution was composed by 70% of H_2SO_4 (95-97%, v/v) and 30% of H_2O_2 (30%, v/v). Afterwards, the glassware and flasks were rinsed many times and filled with ultrapure water and sonicated for 10 min in an ultrasonic bath, model Elmasonic P, Elma Schmidbauer GmbH, Singen, Germany, http://www.elma-ultrasonic.com. The ultrapure water was changed and another ultrasonic cycle was carried out. Then, the glassware and flasks were rinsed many times again with ultrapure water and dried with Ar or N_2 stream. When some of the glassware or flasks were employed for hydrophobic solutions, they were also rinsed with ethanol before drying with Ar or N_2.

3.5 pH determination of the electrolyte

The pH value of 0.01, 0.05, 0.1, 0.5 and 1.0 mol L^{-1} $NaClO_4$ solutions was determined. The pH measuring instrument was previously calibrated with pH 2.00, 4.01, 7.00, 9.21 and 11.00 buffer solutions, and then tested with pH 4.01 and 7.00 buffer solutions. Furthermore, pH values of 0.05 mol L^{-1} H_2SO_4, 0.1 mol L^{-1} NaOH and 0.1 mol L^{-1} KBr solutions were determined. In this way, electrolytes with a wide pH range were evaluated.

3.5.1 pH values of different electrolyte concentrations

The calibration of the instrument for measuring the pH was performed with buffer solutions of pH 2.00, 4.01, 7.00, 9.21 and 11.00 (see Figure 25a)). In order to check the calibration, the pH 4.01 and 7.00 buffer solutions were measured after the calibration and the concordance is presented in Figure 25b). The pH values of 0.01, 0.05, 0.1, 0.5 and 1.0 mol L^{-1} $NaClO_4$ solutions are presented on the graphic in Figure 25c).

The laboratory and solutions temperature were around 19.5 °C and compensated by the instrument. The pH values of the different $NaClO_4$ concentrations vary from 5.55 (1.0 mol L^{-1}) until 5.91 (0.05 mol L^{-1}). Therefore, no expressive differences of the pH values from $NaClO_4$ solutions between 0.01 and 1.0 mol L^{-1} were observed, as presented in Figure 25c).

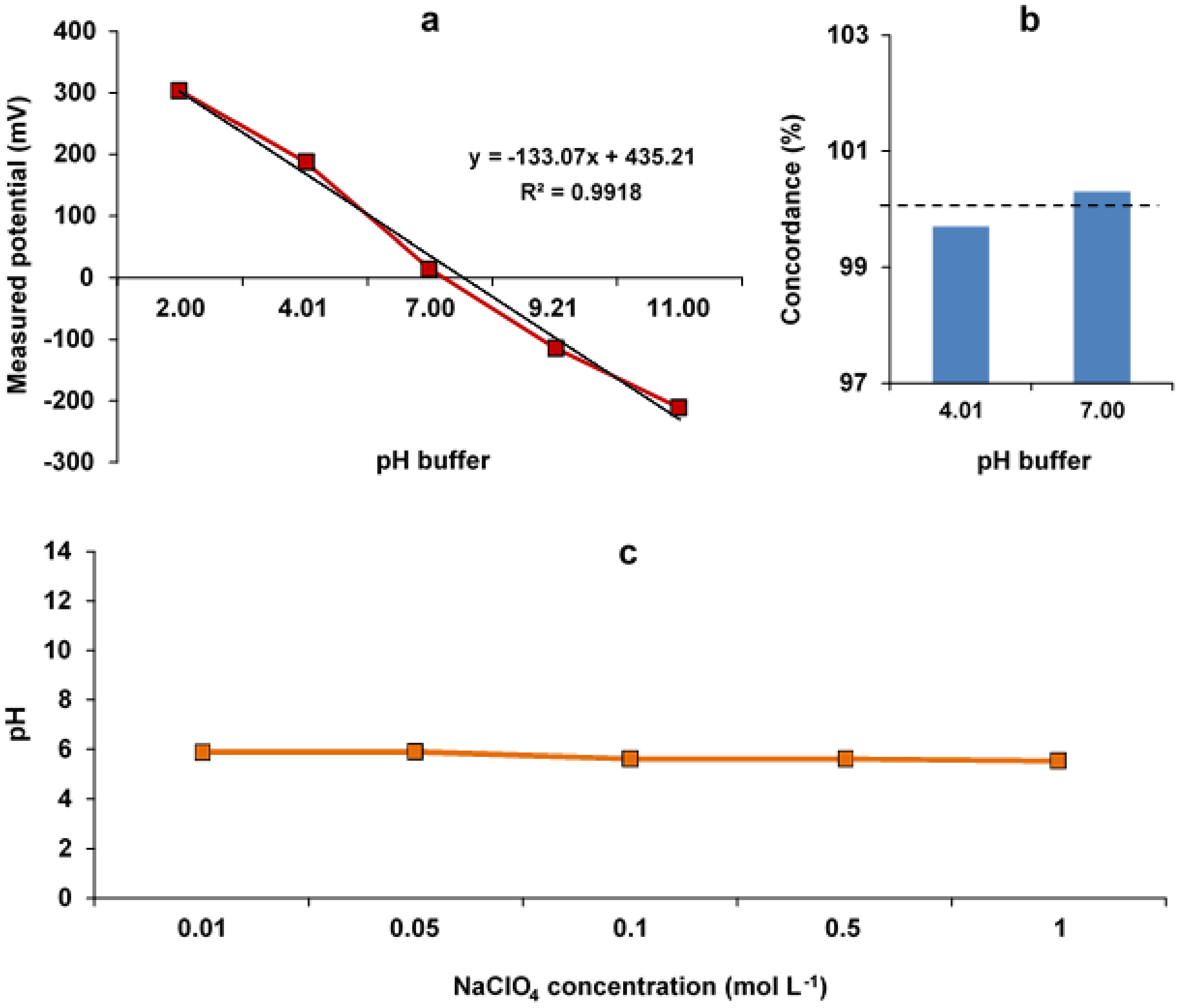

Figure 25. a) measured potential of the pH meter vs the pH of the pH buffers with trend line (in black color); b) concordance of measured pH buffers; c) measured pH for different $NaClO_4$ concentrations.

According the Pourbaix diagram for gold (presented in section 2.1.2, Figure 3), corrosion is possible at potentials around/above 1.2 V (SHE) for pH in the interval from 5.55 and 5.91. Furthermore, $NaClO_4$ solutions with lower pH than 5.55 may corrode gold only at potentials above 1.2 V (SHE). In this way, $NaClO_4$ concentrations between 0.01 and 1.0 mol L^{-1} under 1.2 V (SHE) potentials should not corrode metallic gold. In Table 5 the pH values of the electrolytes chosen for this work are listed.

Table 5. Determined pH values in different electrolytes.

Electrolyte	Concentration (mol L^{-1})	Determined pH value
H_2SO_4	0.05	1.38
$NaClO_4$	0.1	5.63
NaOH	0.1	12.71
KBr	0.1	5.45

The pH values of the selected electrolytes presented in Table 5 covers the interval from acid (H_2SO_4) to alkaline (NaOH), passing through neutral pH ($NaClO_4$).

3.6 Sample preparation and introducing into the electrochemical cell

The glass samples, before the PVD procedure, were precleaned by rinsing them with acetone and ultrapure water. Then, they were immersed in a piranha solution for approximately 10 min and finally rinsed many times with ultrapure water and dried in an Ar or N_2 stream. After preparation and before using in the experiments, the samples were stored in polystyrene boxes placed in a desiccator and handled with powder-free gloves and tweezers.

In order to provide a better adhesion of the gold layer, first a titanium layer as an adhesion layer (thickness of approximately 5-10 nm) was deposited onto the glass substrate by PVD, with a deposition rate of 2.3-2.5 Å s^{-1}. Finally, gold was evaporated (thickness of approximately 200 nm) on the substrate with a deposition rate of 0.6-0.7 Å s^{-1}. The deposition was done by use of an electron beam evaporator, using a pressure of approximately 10^{-7}-10^{-8} mbar in the chamber.

The sample fixation on the stainless steel sample holder for the electrochemical cell was carried out using conductive silver paint, Pelco® Conductive Silver Paint, cod. 16062, Ted Pella Inc., Redding, USA, http://www.tedpella.com or

Silberleitlack, cod. 530042, Ferro GmbH, Hanau, Germany, http://www.ferro.com. This silver paint was also in touch with at least one corner of the gold layer in order to provide electrical contact between sample/sample holder. After the fixation of the sample on the holder, the paint solvent was allowed to evaporate naturally during approximately 24 h before introduced into the electrochemical cell.

The sample holder with the prepared sample was placed in the device for sample introduction in the electrochemical cell according to the schematic drawing in Figure 26. With this device the sample has an electrical contact to the WE connector of the potentiostat.

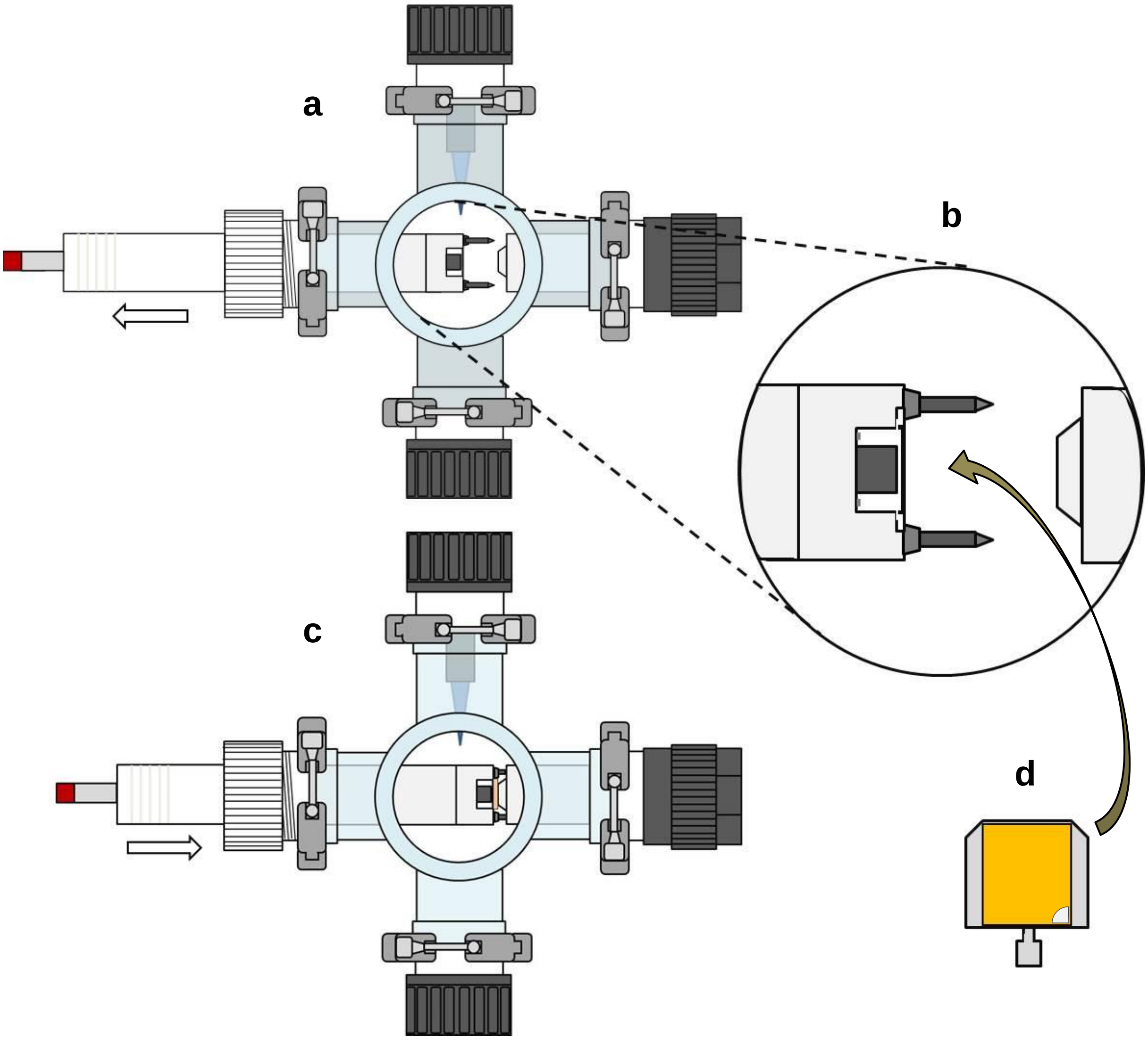

Figure 26. Representation of the electrochemical cell with the device for sample introduction into the system: a) device pulled back; b) enlarged view of the device

extremity (without sample/sample holder); c) device with sample (yellow detail) connected to the other side (sample in contact with electrolyte); d) enlarged view of a gold sample fixed on the sample holder.

After the experiments, the samples were removed from the sample holders by immersing them in a beaker containing acetone and, in sequence, they were sonicated during 5-10 min in an ultrasonic bath. This process takes off the silver paint and removes the samples from the holders. The sample holders were then rinsed many times with ultrapure water, immersed in acetone and sonicated for 10 min. Another two ultrasonic cycles were carried out using ultrapure water. Then, the sample holders were rinsed many times with ultrapure water and ethanol and, finally, dried with Ar or N_2 stream.

The sample holders used as samples in the NAP-XPS device were grinded with silicon carbide paper (first with P1000, second with P2500 and last with P4000) using the grinding/polishing machine at 120 rpm. After the grinding, they were polished using the polishing disc and the diamond suspension and lubricant solutions at 120 rpm. The sample holders were rinsed with abundant water and cleaned with an aqueous solution of neutral Extran® (5%, v/v) heated at 80 °C, ultrapure water and dried with Ar or N_2 stream. After this, they were heated during 60 min at 80 °C to eliminate remaining water on the surface. The PVD procedure for the deposition of the gold was the same as employed for the glass substrates.

3.7 Calibrating the Kelvin probe

The Kelvin probe was calibrated using a self-prepared reference electrode of Ag/AgCl/KCl. This reference electrode was prepared according the procedure adopted by Uebel *et al*.[52] with some modifications. First, a glass substrate was precleaned at the same way as described for the gold samples in section 3.6. After this, the glass substrate was introduced into the PVD system. At first, a titanium adhesion layer was evaporated with a deposition rate of 2.0 Å s^{-1} (thickness of approximately 5.0-10.0 nm) and then an Ag layer of approximately 500 nm at a deposition rate of 5.0 Å s^{-1} was evaporated onto the glass substrate. The pressure in the PVD chamber was around 3.0 x 10^{-7} mbar. A layer of AgCl was deposited onto the as prepared glass substrate covered by Ag by an electrochemical process. This was done using a three-electrode cell, composed by a platinum foil, cod. 7812031, 10 mm x 10 mm x 0.025 mm, purity 99.9%, HMW – Hauner Metalische Werkstoffe, Röttenbach, Germany, http://www.hmw-hauner.de, as counter electrode, connected by spot welding to a platinum wire, an electrode model 6.0726.110, Ag/AgCl/3M KCl, Metrohm AG, as reference electrode (filled with 3.0 mol L^{-1} KCl electrolyte solution, cod. 6.2308.020, Metrohm AG) and the glass substrate covered by Ag as working electrode. This working electrode was fixed on a self-constructed PTFE sample holder device and the connection between sample (WE) and cable from the potentiostat was done using a silver wire, cod. 4734037, 0.5 mm thickness, purity 99.99%, HMW – Hauner Metalische Werkstoffe. The cell was purged with an Ar flow of approximately 30 mL min^{-1} for 20 min before starting the polarization; the outlet of the purge system was connected to a glass trap containing inert oil, DIFFELEN ultra pump fluid, Ref.-No. 176 71, Leybold Vakuum GmbH. As electrolyte a 3.0 mol L^{-1} KCl solution was employed and the working electrode was polarized at -0.1 V for 30 s and then at 0.1 V during 120 s using the potentiostat (previously described in section 3.1.3). After the polarization, the thus prepared Ag/AgCl/KCl reference electrode was removed from the cell and dried under an Ar stream.[52] In Figure 27 a schematic drawing of the three-electrode cell used for this preparation of the Ag/AgCl/KCl reference electrode is depicted.

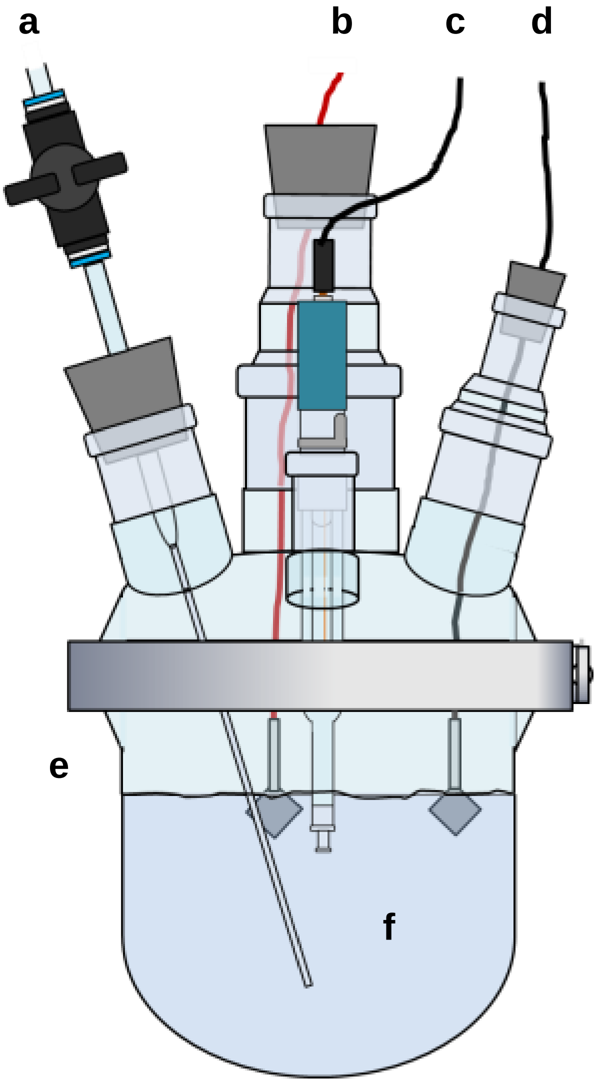

Figure 27. Sketch of the electrochemical cell set-up used for the preparation of the Ag/AgCl/KCl reference electrodes: a) Ar inlet; b) working electrode (Ag sample); c) reference electrode; d) counter electrode; e) electrochemical cell; f) electrolyte. The gas outlet is placed on the rear of the cell.

After the preparation, the Ag/AgCl/KCl reference electrode was fixed on a sample holder with conductive silver paint, inserted into the Kelvin probe/infrared beam chamber, placed under the KP tip and the Volta potential difference measured. Thus the KP tip was calibrated and the potential of emersed electrodes was measured vs this calibrated tip (Figure 28).

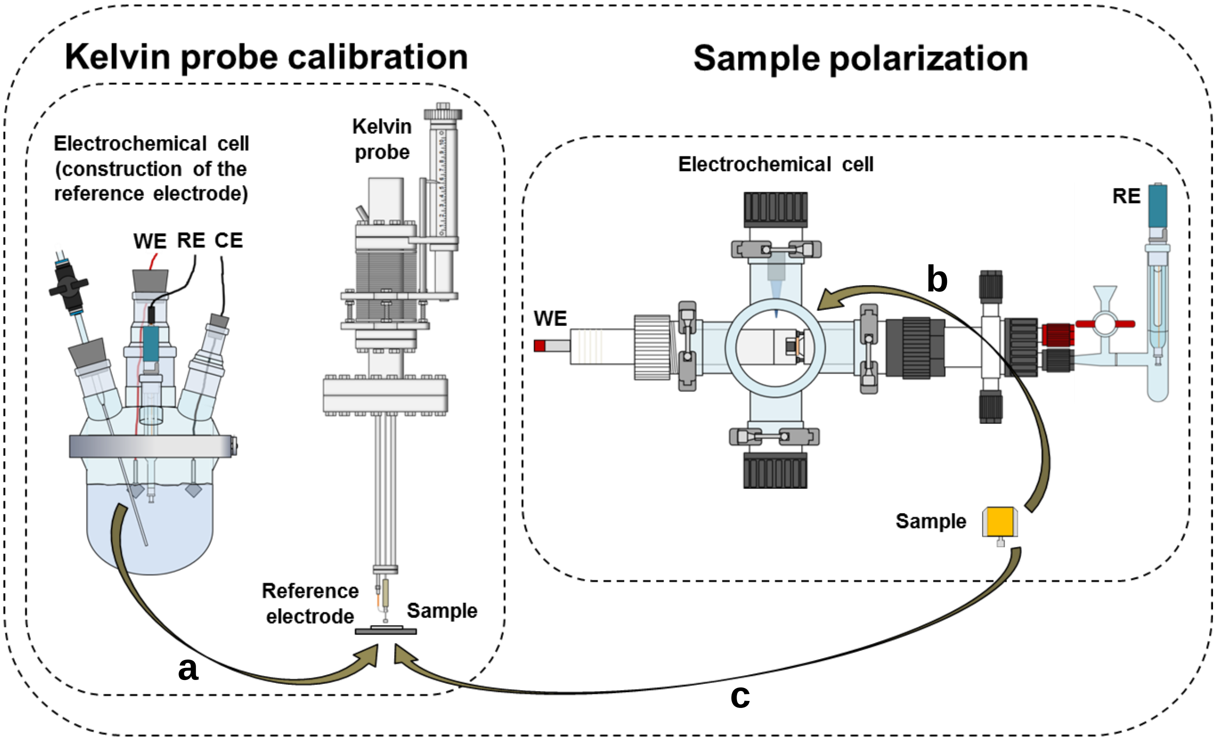
Kelvin probe calibration
Sample polarization
Electrochemical cell (construction of the reference electrode)
WE RE CE
Kelvin probe
Reference electrode
Sample
a
Electrochemical cell
WE
RE
b
Sample
c

Figure 28. Schematic representation of the Kelvin probe calibration process: a) the homemade Ag/AgCl/KCl reference electrode is removed from the electrochemical cell, dried and the Volta potential difference determined using the Kelvin probe providing the calibration of the tip; b) a sample is polarized in the electrochemical cell; c) the same polarized sample has the potential determined by the previously calibrated Kelvin probe. Cables and hoses were neglected in this representation.

Since the Volta potential differences measured in these calibrations of the KP tip vs Ag/AgCl were observed to vary quite significantly, raising the question whether this variance is mainly a problem of the tip or the reference electrodes, further tests on the stability/variance of the tip potential were carried out with highly oriented pyrolytic graphite (HOPG). The work function of HOPG is reported to be stable vs air/nitrogen gas changes. It is, however, not very stable in atmospheres of different humidity. Hence, HOPG was not tried to use for calibration, but just to obtain further information on the responsiveness of the tip on changes of the surrounding atmosphere.

HOPG, in form of a carbon foil, 10 mm x 10 mm x 2 mm, Goodfellow Cambridge Limited, Huntingdon, England, http://www.goodfellow.com, was employed for the Kelvin probe tip stability test in different atmosphere conditions. This HOPG sample was fixed on a sample holder using an adhesive film and one corner of the sample was connected to the holder with conductive silver paint. The HOPG surface was renewed for each experiment using a Scotch® Magic Tape, 3M, USA, http://www.3m.com; a piece of this tape was stuck on the surface and pulled off removing the (potentially contaminated) topmost layers, as proposed in works available in the literature.[100,101] The Volta potential difference between Kelvin probe tip and the HOPG sample was usually measured for 40 min. In this period, after every 10 min, the atmosphere inside the analysis chamber was changed: the first experiment started with "dry" N_2 and then changed to "dry" synthetic air; second experiment started with "dry" N_2 and then changed to "wet" N_2. Each experiment was repeated three times (different days). Furthermore, two other experiments were carried out during 120 min with changing atmosphere and repeated three times (different days): atmosphere inside the analysis chamber started with "dry" N_2 and then changed to "dry" synthetic air after 30 min; atmosphere inside the analysis chamber started with "wet" N_2 and then changed to "wet" synthetic air after 30 min. The "wet" atmosphere for all experiments employing HOPG was around 65-70% RH.

3.8 Open circuit potential measurement

The open circuit potential (OCP) from the Au/glass sample was determined by using the potentiostat at "Open cell mode". First, the flask containing electrolyte and the electrochemical cell were purged with a N_2 flow of 250 mL min^{-1} for approximately 1 h. Then, the potential was measured during 24 h, while electrolyte continued flowing through the cell. The N_2 flow of 250 mL min^{-1} was kept until the end of the experiment. Electrolyte used in the experiments were 0.1 mol L^{-1} $NaClO_4$ and 0.05 mol L^{-1} H_2SO_4 solutions.

3.8.1 Open circuit potential measured on the gold sample in the main electrolytes used in this work

For orientation the OCP of the gold sample (Au/glass substrate) was measured for 24 h, see Figure 29.

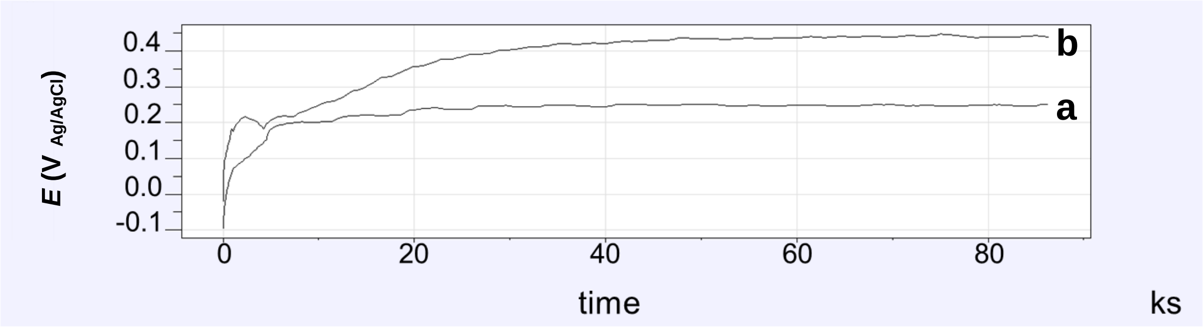

Figure 29. OCP of the gold sample for 24 h. For a) 0.1 mol L^{-1} $NaClO_4$ and b) 0.05 mol L^{-1} H_2SO_4 solutions, purged with N_2 at a flow rate of 250 mL min^{-1} during the whole time of measurement.

The OCP values on the Au/glass surface after 24 h are 0.250 V and 0.440 V when using $NaClO_4$ and H_2SO_4 as electrolyte, respectively.

3.9 Cooling the sample down to achieve higher RH values

For experiments with higher relativity humidity values inside the Kelvin probe/infrared beam chamber (for example, 90% RH or higher) a cooling system previously described in section 3.1.4 was employed. This was necessary due the impossibility to reach RH over 80% in the chamber (sample at room temperature), as such a humidity was not compatible with the Kelvin probe used here (optimized for use in UHV) which lost its signal and stopped working at relative humidity above

80%. Therefore, the sample was cooled down (between approximately 4 °C and 5 °C lower than room temperature) and the dew point/chilled mirror hygrometer was configured in order to achieve RH values lower than 70%. Thus it was possible to reach higher RH values without affect the Kelvin probe operation and accuracy.

The time needed to cooling the sample down was determined in the following way: a sample (fixed on the sample holder) was heated on a heating plate (approximately 5 °C higher than room temperature). The time for the sample surface (gold layer) to achieve the 5 °C increase was determined using a portable thermocouple and was approximately 5 min. Therefore, in order to be on the safe side, 10 min waiting time between the moment of sample placement on the manipulator and starting the cooling and the measurement of the Volta potential difference was applied.

3.10 Measurement of the potential of the emersed samples as function of the potential applied during immersion

The experiments were carried out by a procedure inspired by the experiments carried out by Samec *et al*.[7] which showed a linear correlation between the applied potential on metal surfaces emersed from liquid electrolytes and the following measurement of the Volta potential difference by KP. However, in this PhD work the inert nitrogen atmosphere into which the samples were emersed was not restricted to high relative humidity. The relative humidity was varied in order to unravel the effect of water molecules in the double layer region.

Furthermore, three electrolytes with different anions and pH values were chosen for the investigation: a 0.05 mol L^{-1} H_2SO_4 solution (acid pH), a 0.1 mol L^{-1} $NaClO_4$ solution (neutral pH) and a 0.1 mol L^{-1} NaOH solution (alkaline pH). The electrolyte flask (see Figure 16s)) and the electrochemical cell were purged with a N_2 flow of approximately 250 mL min^{-1}. Glass substrate covered with gold (previously described in section 3.6) was used as sample. Potentials from -0.4 to 1.3 V (for $NaClO_4$ and H_2SO_4 electrolytes) were applied in intervals of 0.1 V for a duration of 2 min each. These potentials were stepped in positive (from -0.4 to 1.3 V) and in negative (from 1.3 to -0.4 V) direction. The electrolyte was removed from the electrochemical cell while the potential remains applied. After each applied potential, the sample was removed from the cell and transferred to the Kelvin probe/infrared beam chamber, adjusted correctly under the KP tip and the Volta potential difference was measured for a duration of 10 min. The relative humidity inside the chamber was adjusted as “dry” N_2 (1-3% RH) and as “wet” N_2 (65-70% RH and around 90-95% RH). After each measurement by Kelvin probe the sample was transferred back to the electrochemical cell and a new potential applied.

Inside the Kelvin probe chamber also *in operando* experiments with changing atmosphere conditions were carried out. Different RH values and also the employment of synthetic air were evaluated (these experimental conditions are described in section 4.5). However, due to the high responsiveness also of the tip on changes of the atmosphere such experiments were found to be difficult to analyze.

3.11 FT-IR measurements on gold samples after applying potentials in the electrochemical cell

The LN-MCT detector was cooled down for approximately 60 min before the FT-IR measurements were started. Background measurements were taken on the gold samples surface before any electrochemical process (“clean” sample). Potentials from -0.4 until 1.3 V (in intervals of 0.1 V) were applied in the electrochemical cell for a duration of 2 min each and as electrolyte 0.1 mol L^{-1} $NaClO_4$ and 0.05 mol L^{-1} H_2SO_4 solutions were employed (the samples were emersed from the electrochemical cell while the potential remains applied). The FT-IR measurements took place in the Kelvin probe/infrared beam chamber using the external detector after each polarization step. This analysis chamber was flushed with “dry” N_2 atmosphere (< 3% RH) and also flushed with “wet” N_2 atmosphere (65-70% RH). The data acquisition was done by 1024 scans repeated 5 or 10 times. This procedure was chosen in order to reduce the signal/noise ratio as maximum as possible. The spectrometer was configured with the following settings: 4 cm^{-1} resolution, 2 mm aperture, MIR light source and KBr beamsplitter. The IR beam incident angle was 83° from the sample surface normal vector.

3.12 Ellipsometry determinations

The ellipsometer light was turned on and stabilized/warmed up before any measurement for at least 1 hour, i.e., 45 min more as recommended by the manufacturer.[95] The instrument was calibrated (sample alignment and system check) with a SiO_2 reference wafer (presented previously in section 3.1.5). The gold sample was analyzed as “blank sample” and as “flushed with electrolyte” before any electrochemical processes and then the electrochemical layer/layers thickness adsorbed on the gold electrode surface was measured after polarizing the sample (0.1 V in 0.1 mol L^{-1} $NaClO_4$ solution). Also in the ellipsometer analysis chamber different humidity conditions were employed, from dry to wet RH and this chamber was flushed with the chosen atmosphere condition for at least 24 h before the experimental procedures.

3.13 XPS measurements on gold samples after applying potentials in the electrochemical cell

The XPS technique was employed to identify chemical species present on the sample surface after emersion under potential control. The measurements were performed for selected potentials applied to the sample (0.0 and 1.0 V with $NaClO_4$; 0.1 and 0.9 V with H_2SO_4). These potentials were applied in positive and in negative direction, as explained previously. Electrolytes with different pH values were employed and the electrolyte was removed from the electrochemical cell while the potential remains applied. After this, the sample was transferred to the buffer chamber, remaining there for some hours until the pressure in this chamber reached at least a value around 10^{-6} mbar. Then, the sample was transferred to the manipulator which was inserted in the analysis chamber, where the position was adjusted to obtain an as maximum signal as possible (energy reaching the detector).

3.14 Flowchart of the processes involved in this work

In Figure 30 a summary of the processes involved in the course of this work is schematically summarized, such as the sample preparation, the electrochemical process evaluation and the data acquisition.

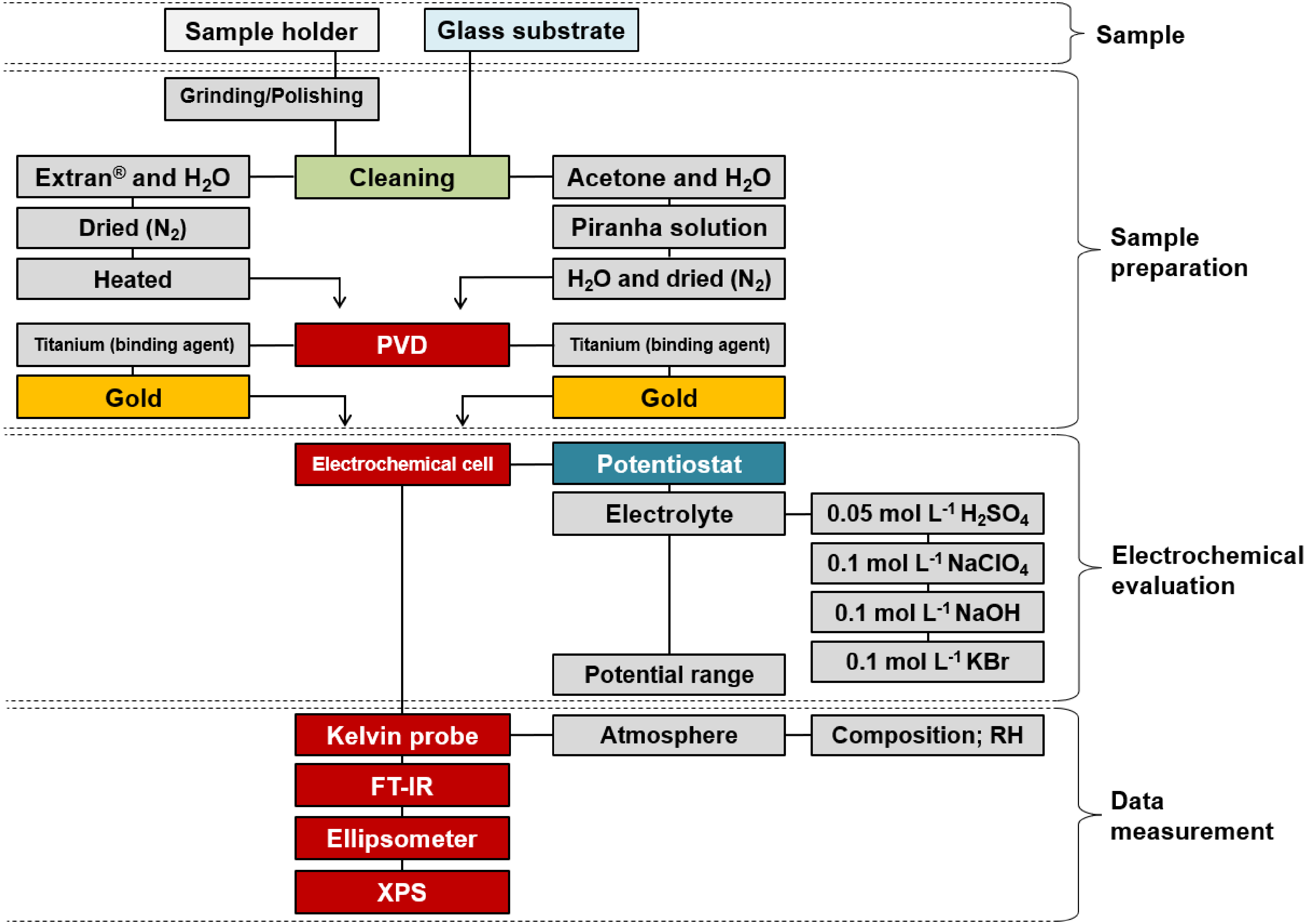
Sample holder
Glass substrate
Sample
Grinding/Polishing
Extran® and H_2O
Cleaning
Acetone and H_2O
Dried (N_2)
Piranha solution
Heated
H_2O and dried (N_2)
Sample preparation
Titanium (binding agent)
PVD
Titanium (binding agent)
Gold
Gold
Electrochemical cell
Potentiostat
Electrolyte
0.05 mol L^{-1} H_2SO_4
0.1 mol L^{-1} $NaClO_4$
0.1 mol L^{-1} NaOH
0.1 mol L^{-1} KBr
Potential range
Electrochemical evaluation
Kelvin probe
Atmosphere
Composition; RH
FT-IR
Ellipsometer
XPS
Data measurement

Figure 30. Flowchart of the processes involved in the dissertation work.

4 Results and discussions

In this chapter the results obtained during the experiments are presented and discussed. The main methods applied were Kelvin probe, infrared spectroscopy and X-ray spectroscopy, as well as some complementary analysis carried out during this work, such as ellipsometry. In the following, all electrode potentials are referred against the Ag/AgCl/3M KCl reference electrode; if potentials (often from literature references) are referred to other reference electrodes, they will be presented in parentheses.

4.1 Kelvin probe calibration by “dry” Ag/AgCl reference electrodes

4.1.1 Background

Since one of the ideas of this work is to study the effect of water on the potential of emersed electrodes and also to at least preliminary check whether there is an effect of the different amounts of water in the double layer region on the kinetics of electrochemical reactions such as oxygen reduction, it is important to makes sure that the measurements of the potential of emersed electrodes can be reliably carried out in environments of different humidity, as the amount of water in the electrochemical double layer is planned to be adjusted by controlling the relative humidity and setting it to different levels. However, this requires that there is a reliable reference that is stable in atmospheres of different relative humidity. This is, however, quite challenging. Atanasoski *et al.*[102], Ehahoun *et al.*[103] and Uebel *et al.*[52] point out that for all metal substrates such as gold, platinum, chromium, iron and also stainless steel large changes of the work function (or the respective electrode potential) are observed when the relative humidity or the oxygen partial pressure in the atmosphere are changed. In fact, since the according studies all apply the Kelvin probe for according measurements, there are always two surfaces involved in the measurements and it is difficult to conclude which surface is more or less responsive on such changes of the atmosphere. Atanasoski *et al.* showed quite convincingly by modifying a silver tip to a Ag/AgCl electrode and measuring the Volta potential difference to a Ag/AgCl sample covered by LiCl electrolyte of different concentration (thus adjusting the relative humidity in a wide range, from 40% to nearly 100% RH) that a non-immersed Ag/AgCl electrode is insensitive to changes of humidity in that investigated range of relative humidity. They even assumed that it would be stable down to 0% RH, but did not try to prove that.

They also showed a high insensitivity of the Ag/AgCl tips vs changes of the partial pressure of oxygen. This is in accordance with the work carried out by Ehahoun *et al.* who confirmed the high stability and reliability as well as the insensitivity of Ag/AgCl tips vs oxygen/nitrogen atmosphere changes.[103]

However, the insensitivity to changes of relative humidity down to 0% was never sufficiently proven. Uebel *et al.* carried out a quite extensive investigation on quite a number of different materials on the effect of relative humidity -including 0% RH- on the measured potential. They suggested the use of a paraffine coating on the tip in order to reduce its responsiveness, but also observed as a side effect the occurrence of surface charge effects, which would make problems in practice.[52]

Hence, in this PhD work it was decided to make use of a “dry”, i.e. non-immersed, Ag/AgCl reference electrode as suggested by Atanasoski *et al.* and Ehahoun *et al.* for calibration, and an additional layer of paraffine was not applied. It was also decided not to modify the tip as Ag/AgCl electrode, as it was planned that the set-up should be compatible with different gaseous environments, including e.g. hydrogen. Since hydrogen can readily reduce silver cations, it was decided not to directly modify the tip itself, but rather to regularly calibrate it against a Ag/AgCl reference. This was at least always done when a new atmosphere was adjusted.

However, since the insensitivity of this Ag/AgCl reference vs changes of relative humidity down to 0% RH was never proven, but that range was to be covered in this work, first investigations were devoted to finding out whether this reference is suited as such also in very dry atmosphere.

As discussed, it is not easy to verify the insensitivity towards humidity changes, because it is usually not known whether the second surface involved in the Volta potential measurements is sensitive or not. It was decided to use HOPG as comparison to the self-prepared Ag/AgCl electrodes.

HOPG is hydrophobic and reported to be quite insensitive towards changes of partial pressure of oxygen as well as showing only a low sensitivity to relative humidity and it is even proposed by some researchers that its work function in air may be nearly the same as in ultra-high vacuum (UHV), allowing its use in air and in vacuum.[100] Another advantage of this material is that its surface is easily refreshed by stripping off some topmost layers of graphite by use of an adhesive tape. However, being insensitive vs changes of humidity and partial pressure of oxygen does not mean that HOPG is an ideal reference electrode. It was found the work function of a freshly exposed surface shows a relatively fast shift (usually upwards), most likely due to adsorption of contamination.[100] These contaminations seem to give rise to quite considerable differences of the work function on the microscopic scale, which confirms that it may not be suitable as a reliable reference, although annealing in UHV at 700 °C seems to yield a suitable surface with homogeneous WF (of 4.6 eV) all over the sample.[104]

Also, a small sensitivity of the work function vs changes of relative humidity is reported (see Liscio *et al.*[105]); the authors observed an increase of work function of HOPG by approximately 60-70 mV when the RH was increased from 0% to 60-70% RH. The authors suggest in their study that the positive dipole moments of the water molecules which seem to adsorb at higher humidity on the HOPG are pointed towards the HOPG surface and the negative dipole moments (electron-rich oxygen atom) are pointed upwards.[105] This would lead to the increase in work function observed by them. However, the authors applied a Pt/Ir coated AFM tip for their measurements with an AFM in the Kelvin probe mode (Scanning Kelvin Probe Force Microscopy, SKPFM). Such noble metals are known to show a high sensitivity towards changes of relative humidity, and -most importantly in view of the results reported by Liscio *et al.*- water adsorption on these materials results in a decrease of work function, indicating a preferential adsorption with the oxygen towards the HOPG surface and the hydrogen atoms pointing upwards. Hence, when measuring as a consequence of increasing relative humidity an increase of contact potential difference between HOPG and a Pt/Ir tip, this could be solely due to the change of work function on the Pt/Ir (when measuring HOPG WF vs the tip). However, Liscio *et al.* assume that the major part of the observed change of contact potential is due to changes on the HOPG.[105]

In the next section typical results obtained in this PhD work concerning the stability of HOPG and “dry” Ag/AgCl vs change the environment are shown.

4.1.2 Results on stability of HOPG vs changes of relative humidity and partial pressure of oxygen

In Figure 31 the typical response of the Volta potential difference between HOPG and the stainless steel KP tip during changes of the atmosphere is shown.

Figure 31a) shows typical changes observed when changing the atmosphere between dry nitrogen atmosphere and dry oxygen atmosphere. Striking is that the potential decreases when the atmosphere is switched from nitrogen to oxygen. Since the opposite is expected, this indicates that the signal is dominated by the changes of the tip potential. More precisely, since -as discussed above- HOPG is known to be insensitive to oxygen/nitrogen changes, the observed change of potential can be safely assumed to originated nearly completely from the tip, i.e. its potential increases with changing the atmosphere from nitrogen to oxygen, as is expected. However, the observed changes are surprisingly low. In fact, the response of the tip on such changes of the atmosphere was varying of the course of the project. The native oxide layer of the tip was certainly ageing over the time and also contaminant adsorbed over time. This had an effect on tip work function itself, but also on its responsiveness on changes of atmosphere. Also much larger responses were found. The results shown in the following were obtained in a more or less the same period of time, where the tip was very stale and showed only -for stainless steel- low responsiveness on changes of the atmosphere. That is why these data were chosen.

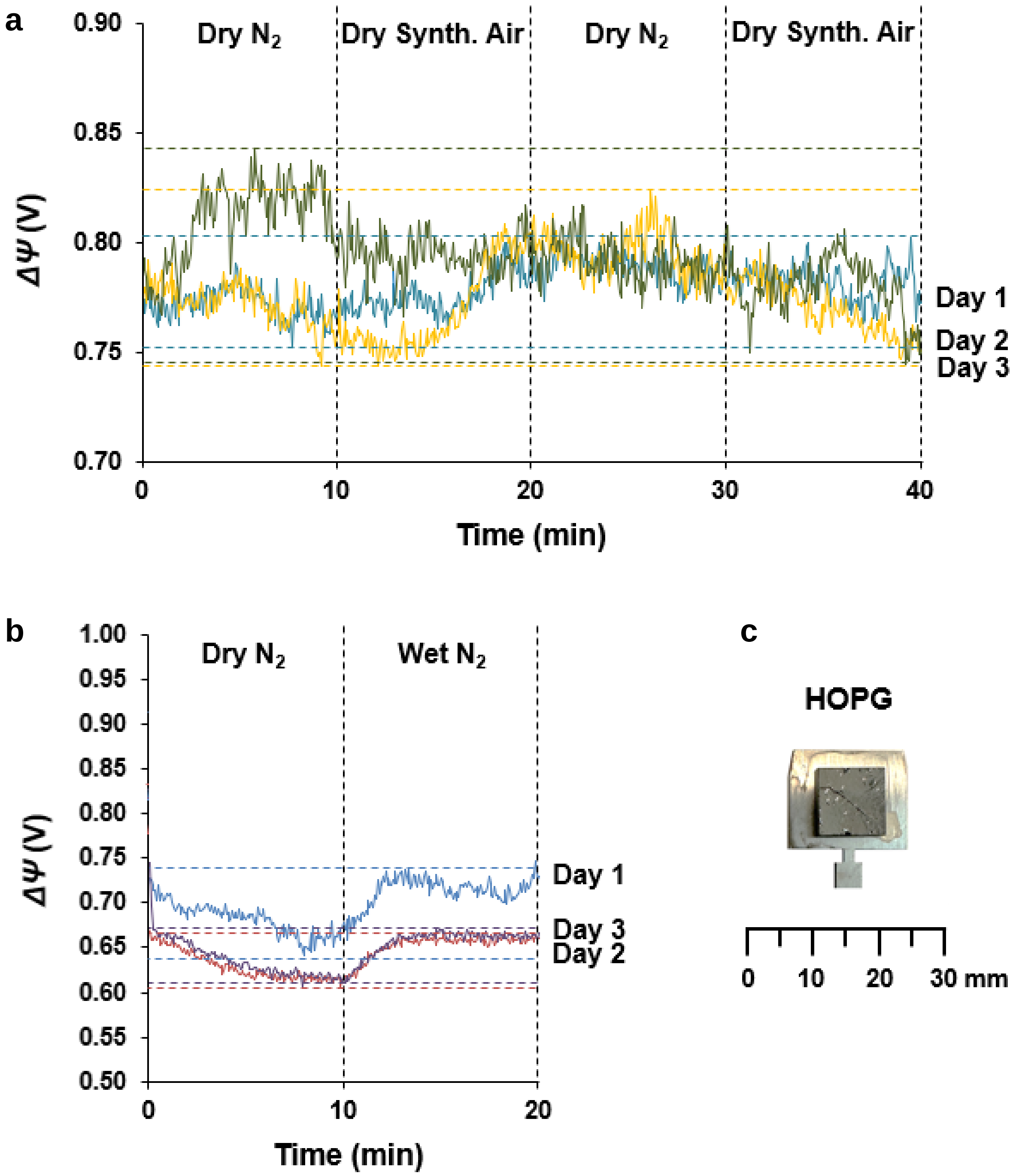

Figure 31. Diagrams representing the Volta potential difference measured between Kelvin probe tip and HOPG sample during: a) 40 min while changing the atmosphere conditions every 10 min (dry N_2 and dry synthetic air) and b) 20 min while changing the atmosphere conditions every 10 min (dry N_2 and wet N_2). Picture in c) is the real HOPG sample fixed on a sample holder and employed in the experiments presented in this section.

Also, a general downwards drift is observed over the time, which amounts to roughly 30-40 mV/h. This was unfortunately found to be a weakness of the Kelvin probe applied in the system used for these studies and will be discussed further below, as well as the strategy to overcome that problem so as to obtain reliable results on the emersed samples.

Figure 31b) shows the corresponding response of the Volta potential difference on changes between dry and humid nitrogen atmosphere. Like reported in the paper by Liscio *et al.*[105], the Volta potential difference between the HOPG and the tip increases when the atmosphere is changed to the higher humidity. As discussed above, that can be because the water molecules adsorbing on the HOPG surface are adsorbing with the hydrogen atoms of the molecule pointing towards the HOPG surface. But such a change of the Volta potential difference can also be explained by a decrease of the work function of the tip by adsorption of water, as is expected for stainless steel (see Uebel *et al.*[52], as discussed also above), or as a combination of both. Since the observed change by roughly 60 mV is not very high, it seems likely that the main part might be due to the work function change occurring on the tip, i.e. that the change of the work function of the HOPG is much smaller. This would be in accordance with the discussion made above that the change on HOPG as a consequence of change in relative humidity is expected to be very low.

In order to check that, similar studies were carried out on self-prepared “dry” Ag/AgCl electrodes: before these results are presented, first the preparation of the Ag/AgCl electrode will be shortly described.

4.1.3 Results on stability of “dry” Ag/AgCl vs changes of relative humidity and partial pressure of oxygen

The fabrication of the “dry” Ag/AgCl electrodes is described in detail in section 3.7. Figure 32 shows a typical current (*I*) vs potential (*E*) curve obtained during the electrochemical growth of the AgCl layer on the Ag surface.

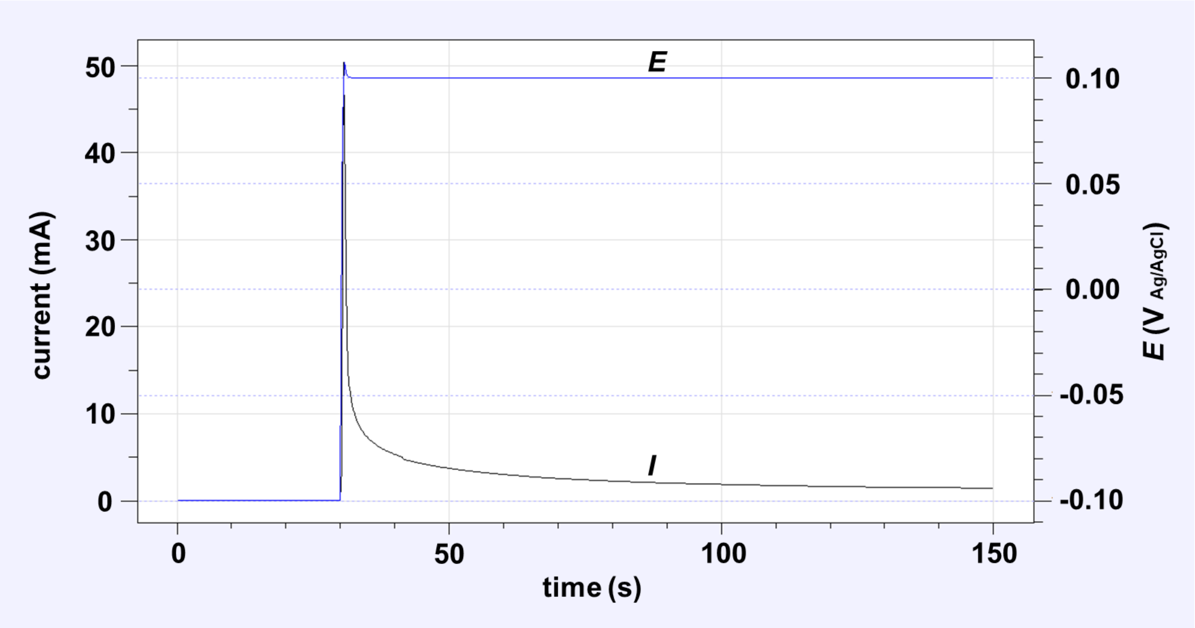

Figure 32. Diagram representing the current (*I*) vs the potential (*E*) typical behavior along time during the Ag/AgCl reference electrode fabrication process.

After the polarization ends, the potential between that electrode and the commercial Ag/AgCl reference electrodes was measured (OCP measurement). In this way, the recent new build reference electrode immersed in the electrolyte before removing it from the electrochemical cell was found to feature a potential of less than 0.002 V against Ag/AgCl after approximately 60 s. This potential observed is therefore in accordance with the expected 0.0 V potential vs Ag/AgCl reference electrode used as reference in the electrochemical cell.

After immersion, the thus prepared Ag/AgCl electrode was measured in the SKP (in humid N_2 atmosphere, approximately 100% RH) vs the potential of the $Cu/CuSO_4$ reference used in the SKP chamber. The results are shown in Figure 33 and the potential there was found to be 0.218 ± 0.004 V (SHE).

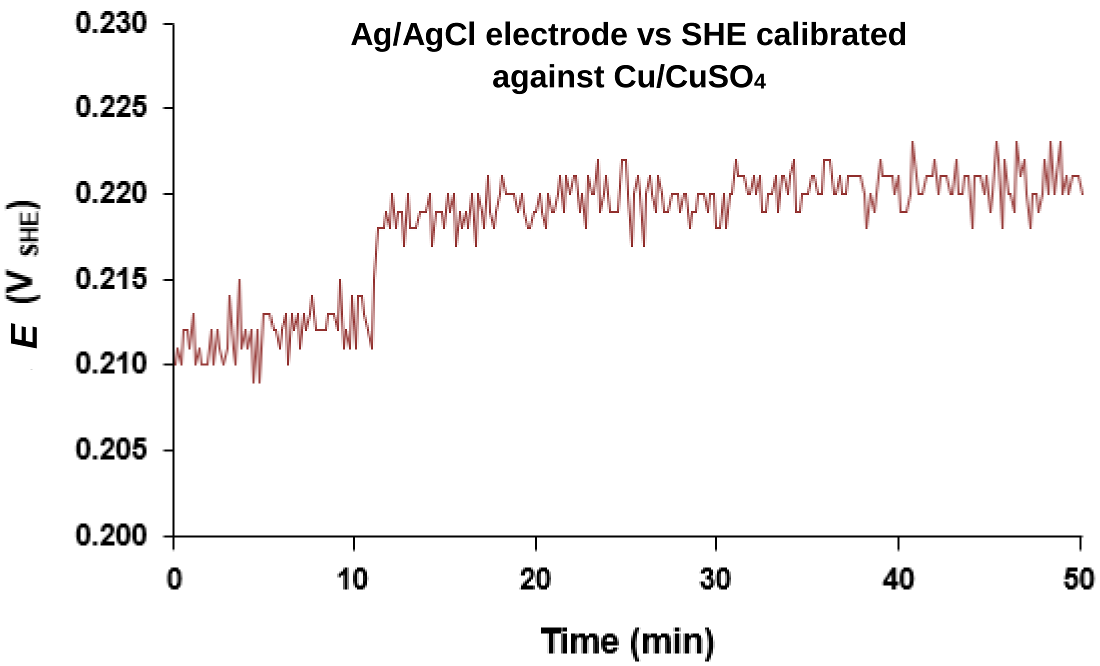

Figure 33. Prepared Ag/AgCl electrode measured in humid N_2 atmosphere inside the SKP chamber for 50 min (Ag/AgCl electrode vs SHE calibrated against $Cu/CuSO_4$).

With these thus produced Ag/AgCl reference electrodes similar tests in changing atmosphere conditions as described above for HOPG were carried out, in order to check the inertness of this electrode vs such changes. Furthermore, these were also longer-term measurements (around 120 min) to check the stability. Both experiments were carried out on the same day and in sequence with the same sample: first, dry (1-3% RH) and wet (65-70% RH) N_2 atmosphere conditions were adjusted every 30 min; second, wet (65-70% RH) N_2 and wet (65-70% RH) synthetic air were adjusted every 30 min. The results from these experiments are shown in Figure 34.

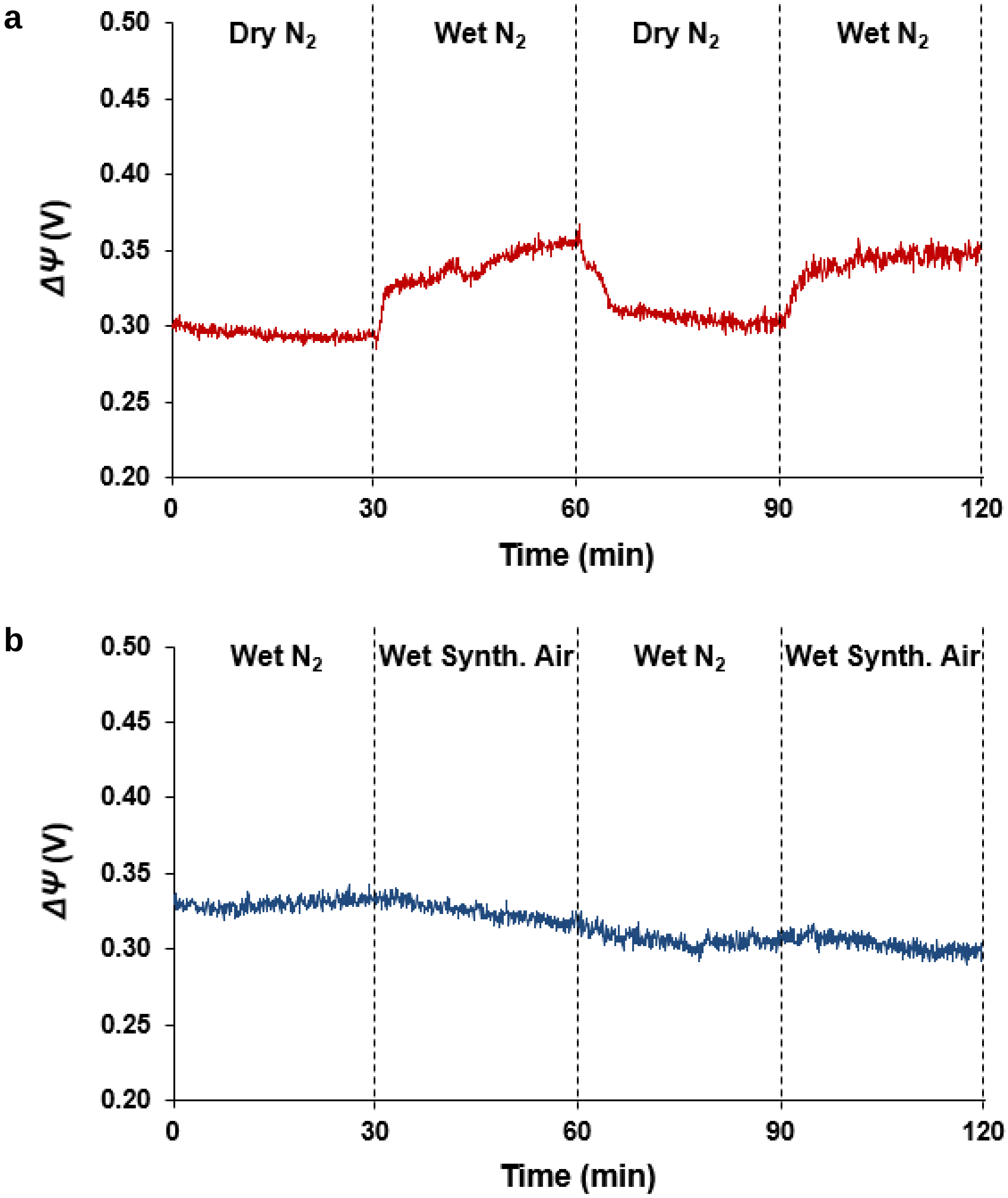

Figure 34. Volta potential difference determined by Kelvin probe on Ag/AgCl reference electrode in changing atmosphere conditions: a) dry (1-3% RH) and wet (65-70% RH) N_2 and b) wet (65-70% RH) N_2 and wet (65-70% RH) synthetic air atmosphere.

As can be seen, the changes of Volta potential difference between sample and tip upon changes of the humidity were even a bit lower than observed for HOPG (see above, Figure 31b) and text), roughly about 30-40 mV, with an increase when switching to humid and a decrease when switching to low humidity. Again, this is indicating that the signal is dominated and most likely even exclusively caused by the change of work function experienced by the tip. In view of the discussion of Figure 31b), where it was assumed that while a small part of the observed Volta potential change for HOPG upon changes of humidity may be really caused by water adsorbed on HOPG, but the dominating part is caused by the tip, it seems reasonable to assume that the slightly lower response of observed on Ag/AgCl is completely due to a decrease of work function of the tip caused by adsorption of water.

Hence, by combining these results and the results reported by Atanasoski *et al.*[102], it can be quite safely concluded that the Ag/AgCl reference is stable in the whole range of relative humidity from about 1% RH to nearly 100% RH.

Hence, in the following the Ag/AgCl reference electrode is assumed to be stable in atmospheres of different humidity.

Also the change of the Volta potential difference vs changes of oxygen partial pressure was found to be low (Figure 34b). Since the insensitivity of such Ag/AgCl electrodes -as discussed above- is already well documented, this means that during these measurements the KP tip was also very insensitive. As discussed further above, the responsiveness of metals such as stainless steel on changes of humidity and also partial pressure of oxygen depends crucially on the history of the tip and was observed to show a huge variability.

For changes of partial pressure of oxygen also much larger changes than shown here were observed during the course of this PhD work. This can be seen as an example in Figure 35, where results obtained for measurements of the Volta potential difference between HOPG and the stainless steel tip as consequence of different kind of changes of the atmosphere are shown. These measurements were carried out several months earlier than the measurements shown in Figure 31. As can be seen, the changes of Volta potential difference between dry nitrogen and dry air are much larger (for the first change at 30 min) than is observed in Figure 31.

Interestingly, the next changes at 60 and 90 min are much smaller which is associated with the ageing effects in the native oxide covering the tip. Also shown are changes in humid atmosphere where the change of Volta potential in the first switch from humid nitrogen to humid air are in the range of 150mV to 200 mV, while again in the second and third switch atmosphere much smaller changes are observed. Again, as the potential difference is observed to decrease with switch to air and HOPG is known to be insensitive to oxygen, the change of the work function of the tip is determining the complete signal change.

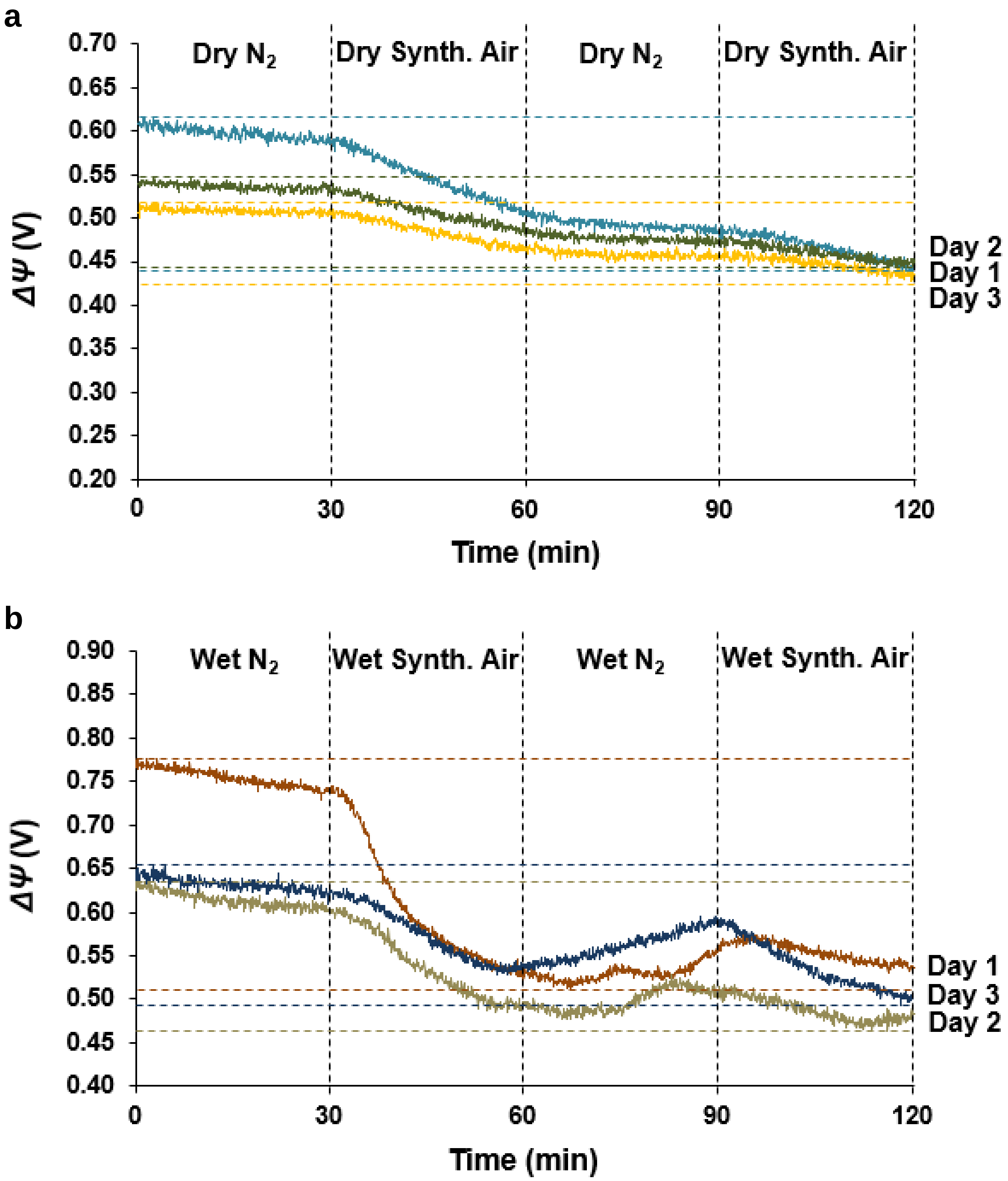

Figure 35. Volta potential difference measured between Kelvin probe tip and HOPG sample during 120 min while changing the atmosphere conditions every 30 min: a) dry N_2 and dry synthetic air and b) wet N_2 and wet synthetic air.

In Figure 36, typical results obtained a few months later are shown, where the tip was observed to be much less sensitive.

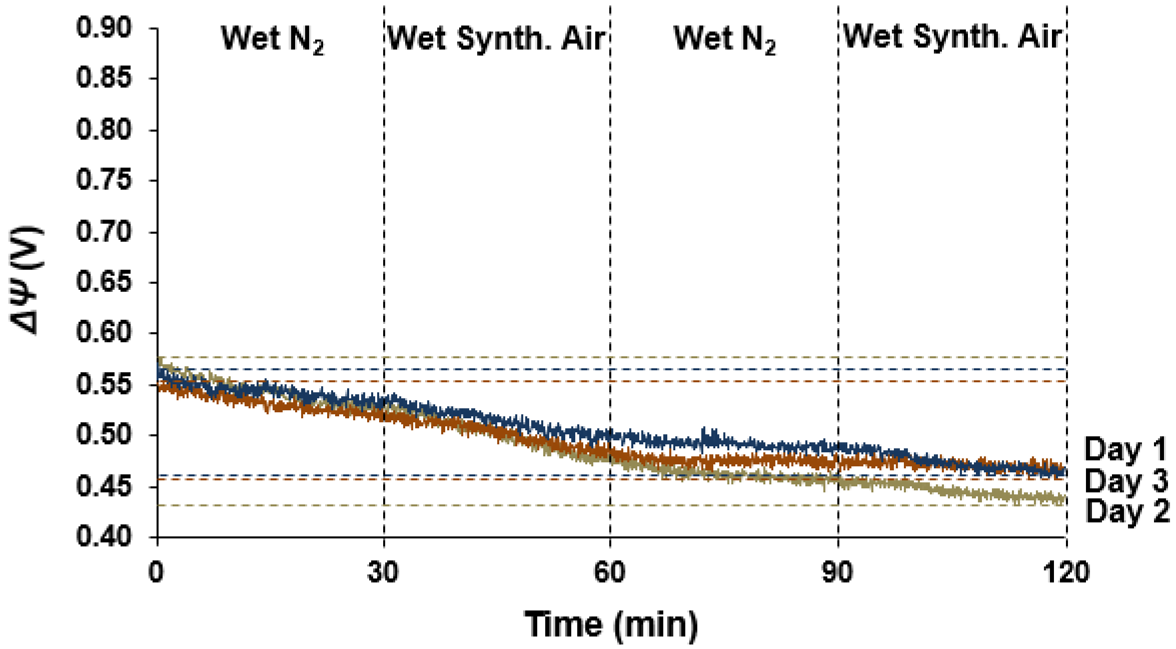

Figure 36. Volta potential difference measured between Kelvin probe tip and HOPG sample during 120 min while changing the atmosphere conditions every 30 min (wet N_2 and wet synthetic air). Experiment carried out some months later.

Since the tip was observed to be subject to large changes of its work function over time as well -as was shown here- also of its responsiveness on changes of the atmosphere, it is very important to regularly calibrate the tip. As mentioned above, this was at least always done when a new atmosphere was adjusted.

Another problem that can be seen more or less in all results shown here (Figures 31, 34, 35 and 36), there is a general tendency of the Kelvin probe signal to drift (usually downwards). This was found to be a problem of the Kelvin probe system from KP Technology applied for this work. Drifts in Kelvin probe signal can be resulting from the sample, from the Kelvin probe tip or the Kelvin probe system (motors, electronic, etc.), or from a combination of them.

Since HOPG as well as Ag/AgCl reference are very stable (at least in this time scale) and the problem is observed for measurements on both of them, it is quite obvious that the problem is the Kelvin probe system itself.

Figure 37 shows a long-term measurement where the Volta potential difference between HOPG and the tip was measured over some time, but not continuously. Instead the tip was retracted after 10 min measurement and re-approached again after 10 min. This was done again and again for more than 2 hours. As can be seen, also during the 10 min measurement the downwards drift is visible, but when withdrawing the tip and then starting a new measurement, the measured values are all in the same range as before. This means that while long-term continuous measurements are subject to continuous drift, these interrupted measurements provide constant values (see Figure 37b)), i.e. these values obtained in short measurement intervals of 10 min or so are highly reliable.

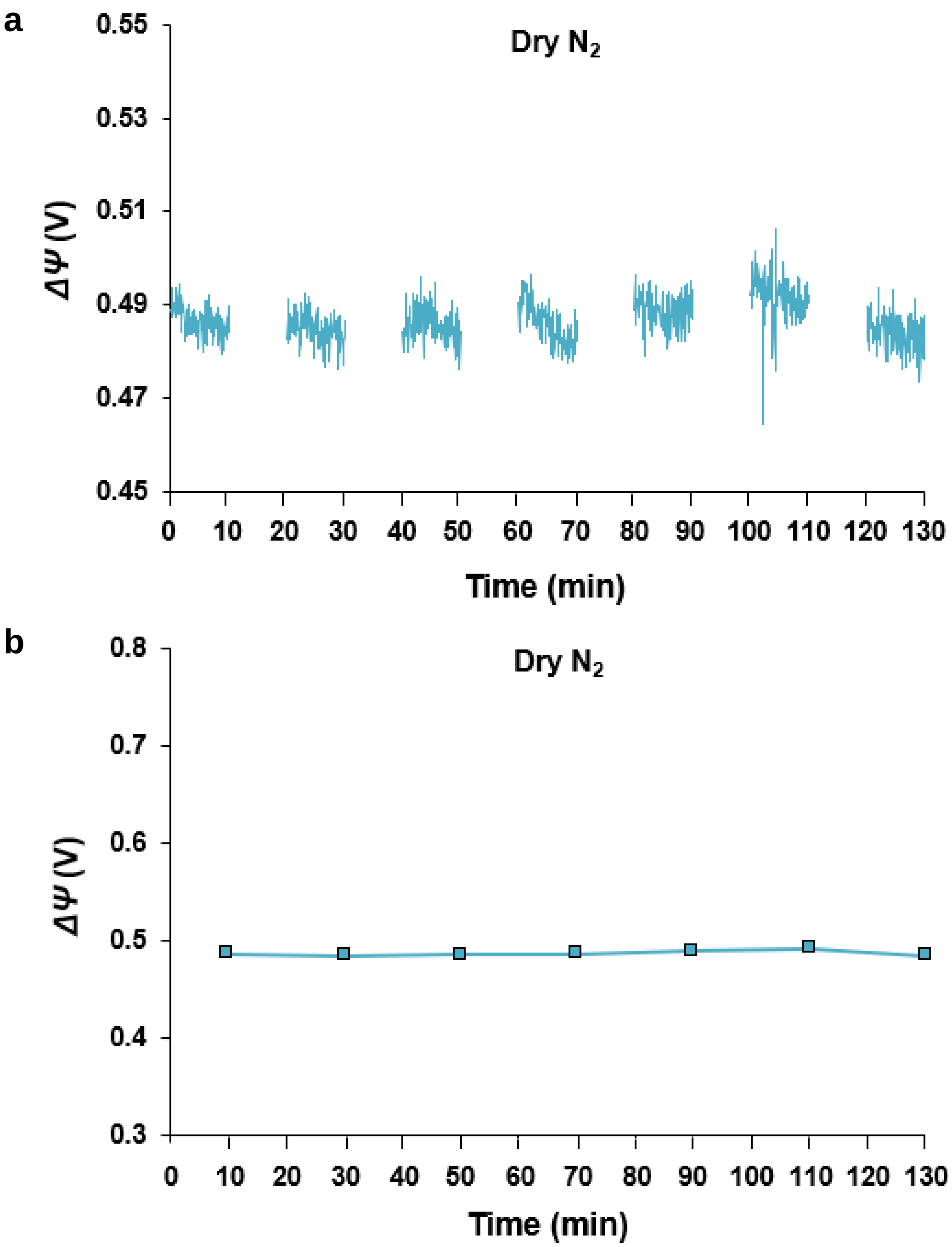

Figure 37. Diagrams representing a long-term determination of the Volta potential difference between the Kelvin probe tip and the HOPG sample surface.

Since measurements on the emersed electrodes were done exactly in this way: sample was emersed, transferred to the Kelvin probe chamber, measured about 10 min and then transferred back to the electrochemical cell and polarized anew, to be again emersed and transferred to the Kelvin probe chamber again for further measurements and so on, these results can be regarded as reliable. Also, for each series of polarization elements a calibration of the tip vs Ag/AgCl was carried out, under the respective environment adjusted. This way all measured potentials could reliably be referred to SHE.

Hence, despite the difficulty of obtaining reliably referenced values in different atmospheres, reliable results can be obtained, as will be presented in section 4.4. Furthermore, for the experiments presented in next sections, each atmosphere condition was set several hours before some Kelvin probe measurements took place, enabling a high level of atmosphere “stability” inside the analysis chamber during the determinations.

4.2 Measurement of the correlation between applied potential and the potential of the emersed gold electrode

The results presented in Tables 6 and 7 and Figure 38 were obtained from experiments in which the potential remains applied while the electrolyte was removed from the electrochemical cell, before transferring the sample into the Kelvin probe chamber. This removal of electrolyte while the electrode is remaining under potentiostatic control is equivalent to the emersion of an electrode under potential control. The potentials obtained on the emersed electrode by Kelvin probe measurements when the potential was either stepped in the positive or the negative direction (according to the procedures described in section 3.10) are listed in Tables 6 and 7, respectively. Results presented in the gray hatched areas in the both tables represent the linear ranges observed for each experiment (correlation between the potentials applied during immersion and measured on the emersed sample is approximately 1:1, i.e. plots of the emersed potentials vs the applied ones have slope of about 1). The Kelvin probe was calibrated anew for each new atmospheric condition (relative humidity) that was adjusted, with the homemade Ag/AgCl/KCl reference electrode, as described in section 3.7.

Table 6. Potentials of the emersed electrode measured by Kelvin probe and referenced vs Ag/AgCl vs the potentials applied during immersion, for stepwise polarization into the positive direction, for H_2SO_4 and $NaClO_4$ solutions as electrolyte and N_2 atmosphere with different RH values.

	E ($V_{Ag/AgCl}$)	**E ($V_{Ag/AgCl}$)**					
		0.05 mol L^{-1} H_2SO_4			**0.1 mol L^{-1} $NaClO_4$**		
		N_2 (< 3% RH)	**N_2 (65-70% RH)**	**N_2 (90-95% RH)**	**N_2 (< 3% RH)**	**N_2 (65-70% RH)**	**N_2 (90-95% RH)**
Polarization direction ↓	-0.4	0.2024 ± 0.0055	0.2923 ± 0.0112	0.1336 ± 0.0222	0.1897 ± 0.0060	0.2245 ± 0.0148	0.1114 ± 0.0063
	-0.3	0.1541 ± 0.0098	0.2944 ± 0.0081	0.0894 ± 0.0094	0.1713 ± 0.0063	0.2398 ± 0.0148	0.1004 ± 0.0103
	-0.2	0.1579 ± 0.0075	0.2987 ± 0.0116	0.1132 ± 0.0054	0.1239 ± 0.0057	0.3144 ± 0.0136	0.1159 ± 0.0069
	-0.1	0.1443 ± 0.0086	0.3477 ± 0.0143	0.1259 ± 0.0046	0.1802 ± 0.0068	0.4071 ± 0.0088	0.1955 ± 0.0070
	0.0	0.1775 ± 0.0096	0.3477 ± 0.0120	0.1764 ± 0.0046	0.2469 ± 0.0057	0.4219 ± 0.0078	0.2038 ± 0.0045
	0.1	0.1948 ± 0.0090	0.3657 ± 0.0149	0.1676 ± 0.0054	0.2482 ± 0.0064	0.4831 ± 0.0041	0.2440 ± 0.0118
	0.2	0.3429 ± 0.0045	0.3977 ± 0.0108	0.2329 ± 0.0041	0.3230 ± 0.0059	0.5248 ± 0.0057	0.2701 ± 0.0081
	0.3	0.3770 ± 0.0052	0.4753 ± 0.0112	0.3141 ± 0.0075	0.3827 ± 0.0068	0.5860 ± 0.0042	0.3096 ± 0.0082
	0.4	0.5058 ± 0.0051	0.5492 ± 0.0138	0.3921 ± 0.0053	0.4582 ± 0.0054	0.6601 ± 0.0063	0.3645 ± 0.0041
	0.5	0.6021 ± 0.0062	0.7776 ± 0.0105	0.5143 ± 0.0107	0.5778 ± 0.0070	0.8301 ± 0.0058	0.4724 ± 0.0063
	0.6	0.7365 ± 0.0078	0.8431 ± 0.0143	0.6303 ± 0.0116	0.6576 ± 0.0068	0.8812 ± 0.0076	0.5472 ± 0.0054
	0.7	0.8171 ± 0.0057	0.8967 ± 0.0126	0.6694 ± 0.0105	0.7397 ± 0.0062	0.9590 ± 0.0105	0.5909 ± 0.0085
	0.8	0.8840 ± 0.0077	0.9890 ± 0.0165	0.7448 ± 0.0112	0.8216 ± 0.0084	1.0154 ± 0.0125	0.6710 ± 0.0080
	0.9	0.9567 ± 0.0075	1.0578 ± 0.0166	0.8352 ± 0.0186	0.9086 ± 0.0089	1.0922 ± 0.0207	0.7542 ± 0.0145
	1.0	1.0294 ± 0.0100	1.1277 ± 0.0237	0.9317 ± 0.0213	0.9903 ± 0.0089	1.1978 ± 0.0174	0.7852 ± 0.0106
	1.1	1.1799 ± 0.0060	1.3254 ± 0.0163	0.9487 ± 0.0281	0.9901 ± 0.0074	1.2614 ± 0.0202	0.9263 ± 0.0113
	1.2	1.3863 ± 0.0066	1.3624 ± 0.0156	0.9155 ± 0.0300	0.9928 ± 0.0077	1.2338 ± 0.0183	0.9290 ± 0.0097
	1.3	1.3989 ± 0.0055	1.3250 ± 0.0142	1.0986 ± 0.0151	0.9587 ± 0.0095	1.2492 ± 0.0198	0.9732 ± 0.0171

Table 7. Potentials of the emersed electrode measured by Kelvin probe and referenced vs Ag/AgCl vs the potentials applied during immersion, for stepwise polarization into the negative direction, for H_2SO_4 and $NaClO_4$ solutions as electrolyte and N_2 atmosphere with different RH values.

E **($V_{Ag/AgCl}$)**	***E*** **($V_{Ag/AgCl}$)**					
	0.05 mol L^{-1} H_2SO_4			**0.1 mol L^{-1} $NaClO_4$**		
	N_2 (< 3% RH)	**N_2 (65-70% RH)**	**N_2 (90-95% RH)**	**N_2 (< 3% RH)**	**N_2 (65-70% RH)**	**N_2 (90-95% RH)**
-0.4	0.1178 ± 0.0048	0.6428 ± 0.0184	0.3129 ± 0.0062	0.2354 ± 0.0058	0.2852 ± 0.0173	0.1881 ± 0.0090
-0.3	0.1172 ± 0.0051	0.6138 ± 0.0152	0.3124 ± 0.0131	0.1016 ± 0.0063	0.2484 ± 0.0121	0.1645 ± 0.0075
-0.2	0.1028 ± 0.0056	0.4553 ± 0.0113	0.2958 ± 0.0063	0.1286 ± 0.0056	0.2645 ± 0.0114	0.1632 ± 0.0093
-0.1	0.1363 ± 0.0102	0.5247 ± 0.0109	0.3242 ± 0.0085	0.2837 ± 0.0058	0.2855 ± 0.0081	0.2032 ± 0.0042
0.0	0.1685 ± 0.0047	0.6288 ± 0.0139	0.3415 ± 0.0093	0.3394 ± 0.0053	0.4589 ± 0.0062	0.3494 ± 0.0053
0.1	0.2020 ± 0.0050	0.5656 ± 0.0115	0.3845 ± 0.0083	0.2706 ± 0.0063	0.4883 ± 0.0059	0.3462 ± 0.0043
0.2	0.2374 ± 0.0051	0.5862 ± 0.0094	0.4280 ± 0.0078	0.3498 ± 0.0059	0.5496 ± 0.0057	0.4051 ± 0.0035
0.3	0.3160 ± 0.0050	0.6532 ± 0.0115	0.5287 ± 0.0123	0.4559 ± 0.0068	0.6403 ± 0.0094	0.5134 ± 0.0055
0.4	0.4096 ± 0.0069	0.8794 ± 0.0115	0.6456 ± 0.0119	0.5163 ± 0.0057	0.7203 ± 0.0074	0.6081 ± 0.0126
0.5	0.5617 ± 0.0056	1.0509 ± 0.0137	0.8242 ± 0.0169	0.6852 ± 0.0061	0.8089 ± 0.0115	0.7343 ± 0.0066
0.6	0.7284 ± 0.0130	1.1687 ± 0.0321	0.9277 ± 0.0140	0.7983 ± 0.0075	0.9136 ± 0.0119	0.8592 ± 0.0067
0.7	0.8429 ± 0.0072	1.2354 ± 0.0254	0.9543 ± 0.0245	0.8301 ± 0.0080	1.0474 ± 0.0134	0.9518 ± 0.0107
0.8	0.9812 ± 0.0082	1.3137 ± 0.0294	1.0424 ± 0.0221	0.8677 ± 0.0082	1.0996 ± 0.0092	1.0130 ± 0.0100
0.9	1.1414 ± 0.0211	1.3685 ± 0.0271	1.1794 ± 0.0288	0.8851 ± 0.0058	1.0995 ± 0.0124	1.0332 ± 0.0091
1.0	1.2602 ± 0.0075	1.2405 ± 0.0370	1.2462 ± 0.0225	0.9268 ± 0.0068	1.1560 ± 0.0123	1.0472 ± 0.0111
1.1	1.2737 ± 0.0071	1.3410 ± 0.0369	1.2197 ± 0.0161	0.9647 ± 0.0061	1.1956 ± 0.0175	1.1001 ± 0.0119
1.2	1.2285 ± 0.0082	1.3668 ± 0.0369	1.2365 ± 0.0202	1.0039 ± 0.0071	1.2469 ± 0.0166	1.1366 ± 0.0152
1.3	1.1884 ± 0.0060	1.4020 ± 0.0148	1.2364 ± 0.0224	1.1178 ± 0.0072	1.1185 ± 0.0142	1.1183 ± 0.0116

Polarization direction ↑

The results listed in Tables 6 and 7 are represented as diagrams in Figure 38. Also trend lines and the slope and R^2 values for the linear regions are shown. In the first part of the figure (a) and b)) the results for H_2SO_4 and in the second part (c) and d)) for $NaClO_4$ as electrolyte are shown. The “color gradient effect” in the diagrams represents the humidity, i.e., the darker the color, the higher the humidity value in the corresponding atmosphere.

a

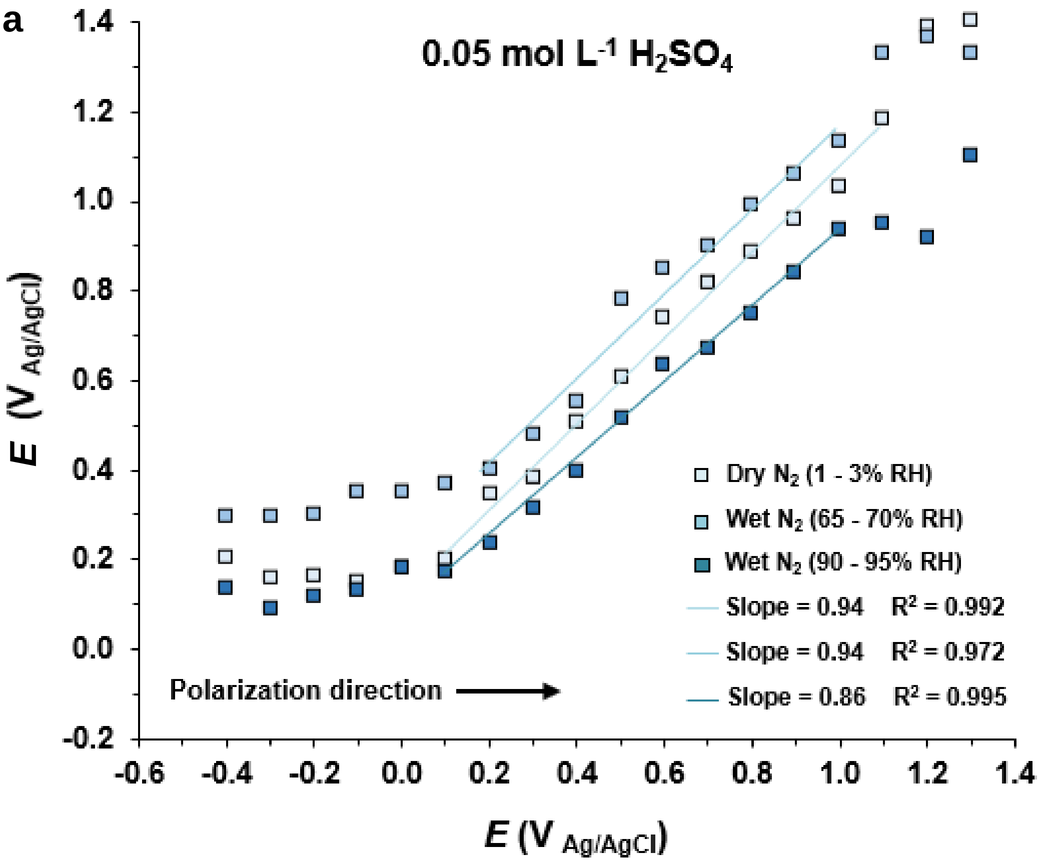
0.05 mol L-1 H2SO4
E (V Ag/AgCl)
E (V Ag/AgCl)
1.4
1.2
1.0
0.8
0.6
0.4
0.2
0.0
-0.2
-0.6
-0.4
-0.2
0.0
0.2
0.4
0.6
0.8
1.0
1.2
1.4
Dry N2 (1 - 3% RH)
Wet N2 (65 - 70% RH)
Wet N2 (90 - 95% RH)
Slope = 0.94 R2 = 0.992
Slope = 0.94 R2 = 0.972
Slope = 0.86 R2 = 0.995
Polarization direction

b

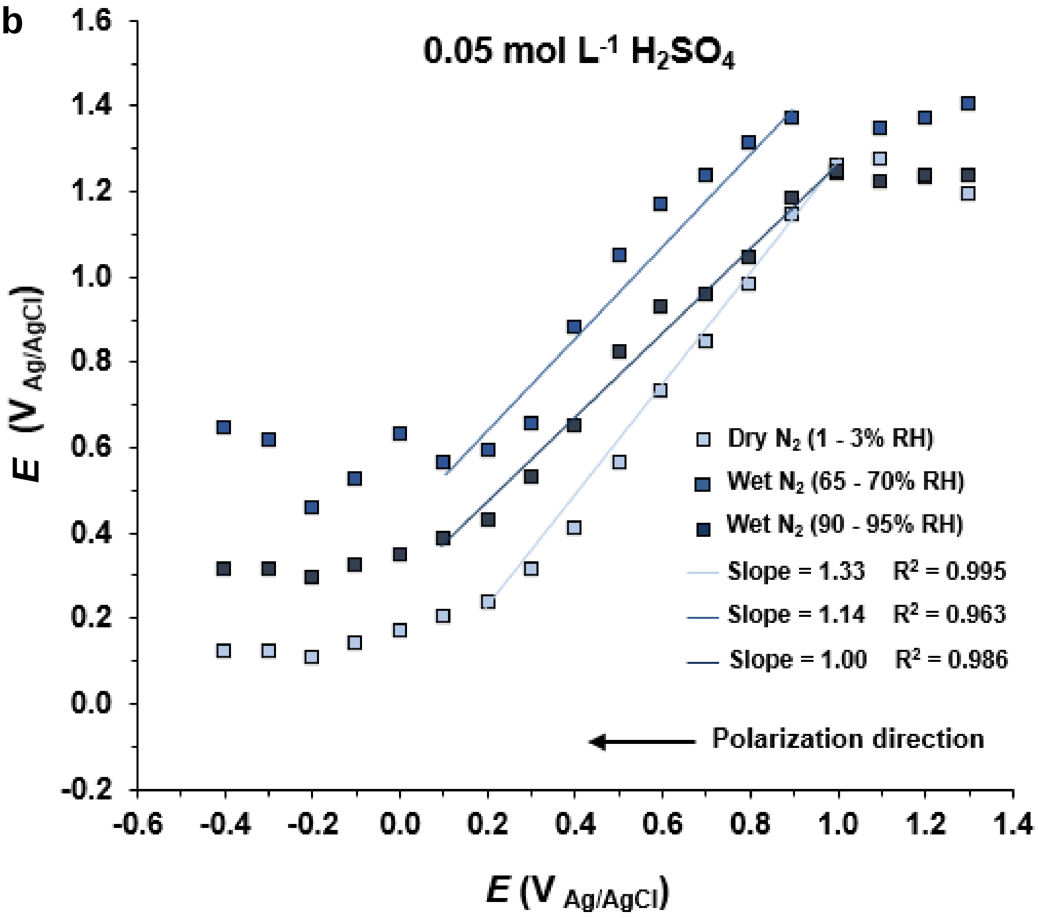
0.05 mol L-1 H2SO4
E (V Ag/AgCl)
E (V Ag/AgCl)
1.6
1.4
1.2
1.0
0.8
0.6
0.4
0.2
0.0
-0.2
-0.6
-0.4
-0.2
0.0
0.2
0.4
0.6
0.8
1.0
1.2
1.4
Dry N2 (1 - 3% RH)
Wet N2 (65 - 70% RH)
Wet N2 (90 - 95% RH)
Slope = 1.33 R2 = 0.995
Slope = 1.14 R2 = 0.963
Slope = 1.00 R2 = 0.986
Polarization direction

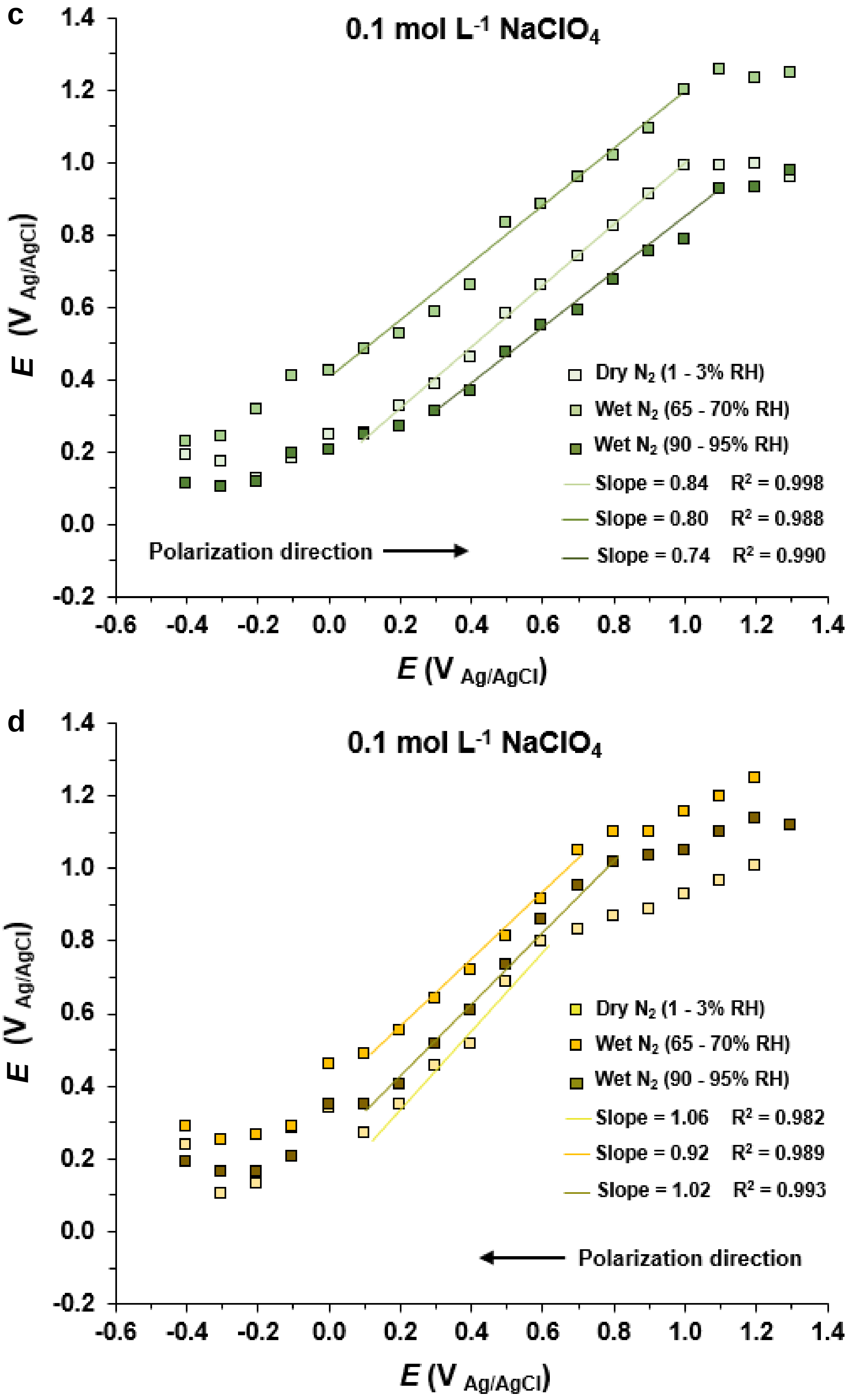

Figure 38. Plots of the potential measured by KP on the emersed electrode (vs

Ag/AgCl) vs the potentials applied on evaporated gold for emersion into nitrogen atmosphere of different relative humidity. Electrolytes were 0.05 mol L^{-1} H_2SO_4 solution (a) and b)) and 0.1 mol L^{-1} $NaClO_4$ solution (c) and d)), with the potentials stepped in a) and c) positive and in b) and d) negative direction.

In the study conducted by Samec *et al*.[7], linearity with unity slope was observed in a range of approximately 1.1 V (between about 0.0 to 1.1 V vs Ag/AgCl) when 0.05 mol L^{-1} H_2SO_4 was employed as electrolyte.[7] Such a similar range (from 0.0 to 0.9/1.1 V, depending on the atmosphere condition) was also found in this dissertation in the experiments using the same electrolyte, but using different relative humidity (Tables 6 and 7). This behavior of linearity (slope near 1) is usually interpreted to indicate that the electrical double layer after emersing the electrode from the electrolyte is more or less intact, without any loss of charge.[7,106] Hansen and Kolb[106] reported that the electrical double layer will not be retained unchanged in the "extreme" regions (very negative and very positive potentials) during emersing the electrode; in these regions, the electrical double layer is discharged by electrochemical reactions and the unity slope is no more achieved.[106] These regions with very negative and very positive potentials are the hydrogen evolution and the oxygen reduction reaction areas, respectively.

The use of 0.1 mol L^{-1} $NaClO_4$ as electrolyte and gold as electrode was also investigated by Hansen and Kolb[106]; linearity with unity slope was observed by the authors and the beyond the limits of the potential range determined by the Kelvin probe (very negative and very positive potentials) the measured potentials were independent of the applied potential (polarization).[106] The question is whether this is just due to discharging of the electrochemical double layer or also has to do with more significant re-orientation of the water molecules.

In fact, the electrochemical double layer consists of the involved charges (on the electrode surface and the according counter ions in the double layer region, as well as specifically adsorbed anions and the according countering cations) as well as the water molecules in the double layer region. Since water molecules are electric dipoles, they will play a crucial role in determining the resulting potential.

A common and quite intuitive assumption is that the work function and consequently the corresponding electrode potential of an emersed electrode should decrease with the increase of humidity. This is because of two reasons: 1) the work function of metals gets lowered by water adsorption, since usually the water molecules adsorb with the oxygen atom pointing to the electrode[107,108] and 2) the linear range observed above is more or less completely in the positively charged range (as will be further discussed below) where such an orientation is even the more expected. The extend is of course correlated to the surface coverage.[79,107] Furthermore, charge transfer between adsorbate and substrate is another factor affecting the surface coverage (water adsorption) and related change of work function/potential.[107,109] The substances involved (substrate/surface and adsorbate) will act as Lewis acids (electron acceptors) and/or Lewis bases (electron donors); the net electron transfer can be determined by the work function change, i.e., a positive change indicates net electron transfer from the surface (Lewis base) to the adsorbate (Lewis acid); on the other hand, a negative change will indicate net electron transfer to the surface (Lewis acid) from the adsorbate (Lewis base).[109]

In this dissertation the results show (see Figure 38) lower E values determined by Kelvin probe at 90-95% RH values than at 65-70% RH values, independently from the polarization direction. As mentioned recently, this behavior would be expected owing to more significant water adsorption at higher RH values.

However, the potential in dry N_2 atmosphere do not correspond “directly” to this reasoning; the E values should by higher then the other RH values applied in the experiments, however the E values for dry N_2 atmosphere were observed between 90-95% and 65-70% RH values or even below 90-95% RH values.

However, a quite plausible theory/hypothesis how this may be explained is shown in schematic drawing depicted in Figure 39. In this representation, a gold electrode potential is presented before and after a positive polarization, indicating the probable orientation of water molecules (with dependence on the humidity level and the presence of an anion) and its behavior on the potential.

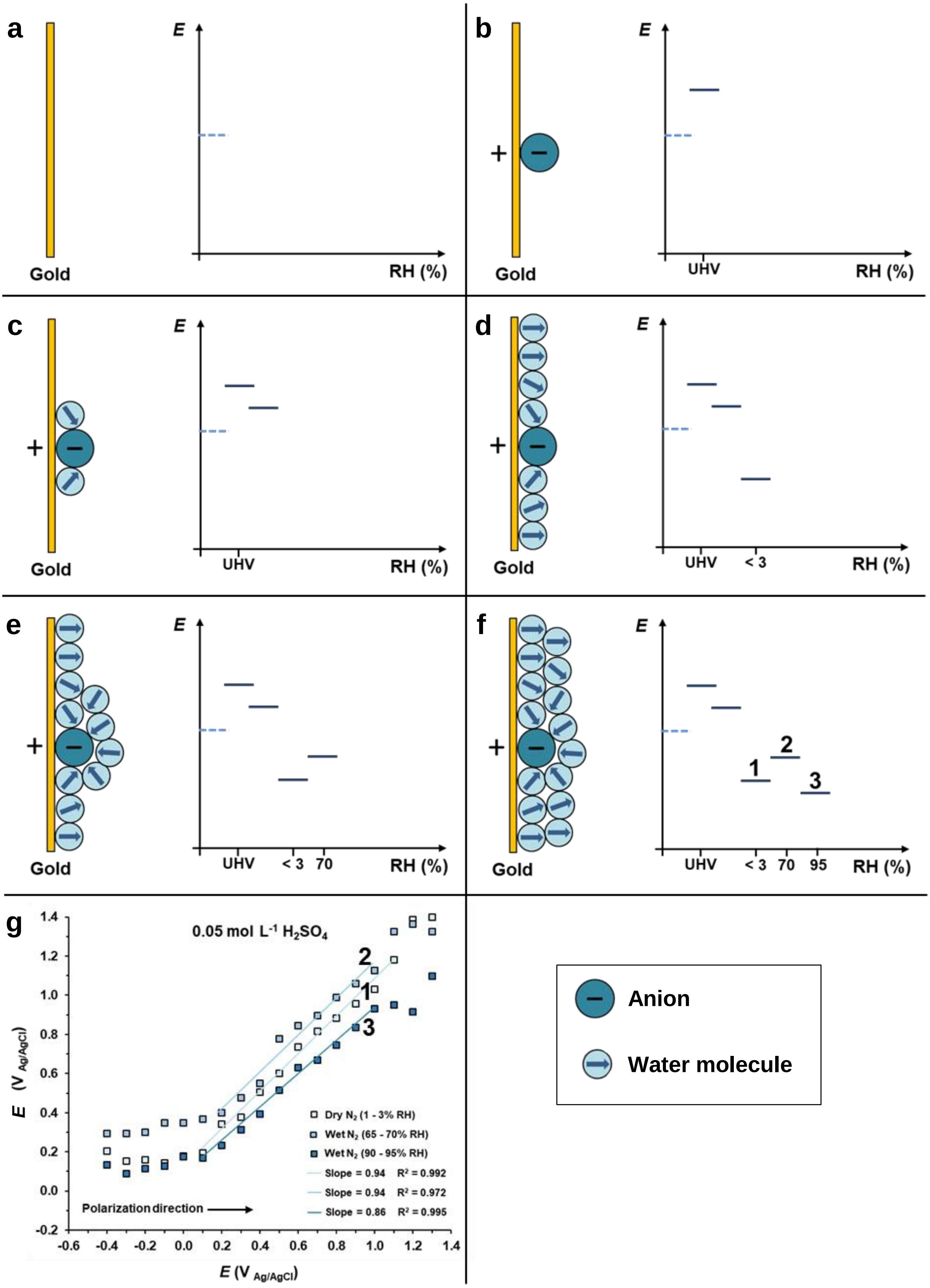
a
Gold
E
RH (%)
b
+
Gold
E
UHV
RH (%)
c
+
Gold
E
UHV
RH (%)
d
+
Gold
E
UHV
< 3
RH (%)
e
+
Gold
E
UHV
< 3
70
RH (%)
f
+
Gold
E
1
2
3
UHV
< 3
70
95
RH (%)
g
0.05 mol L-1 H2SO4
2
1
3
Dry N2 (1 - 3% RH)
Wet N2 (65 - 70% RH)
Wet N2 (90 - 95% RH)
Slope = 0.94 R² = 0.992
Slope = 0.94 R² = 0.972
Slope = 0.86 R² = 0.995
Polarization direction
E (V Ag/AgCl)
E (V Ag/AgCl)
1.4
1.2
1.0
0.8
0.6
0.4
0.2
0.0
-0.2
-0.6
-0.4
-0.2
0.0
0.2
0.4
0.6
0.8
1.0
1.2
1.4
Anion
Water molecule

Figure 39. Schematic explanation of the probable dependence of the potential

measured on the emersed electrode and relative humidity: a) clean gold (i.e. without any ions or water molecules adsorbed) in vacuum, where the measured potential is corresponding to the work function of the clean gold, b) gold polarized (anion adsorbed and corresponding positive charge on the gold surface) in UHV condition (without water molecules), c) same as b) but with a presence of a minimum amount of water molecules, assumed to be adsorbed preferentially to the charges, d) very low humidity (of 1-3% RH, which is the dry condition in this work), e) intermediate relative humidity of 65-70% RH, f) higher humidity of 90-95% RH (and with d)-f) indicated by 1-3), g) experimental example demonstrating the corresponding difference observed between the three different humidity conditions analyzed in this study.

The hypothesis presented in Figure 39 suggest an influence of the water molecules orientation on the determined potential, and this behavior is influenced by the amount of water molecules present in the system (relative humidity).

Concerning, these water molecules in the double layer, in the experiments by Neff and Kötz no indications for water present on the electrodes emersed into UHV[6], which would correspond to situation in Figure 39b) (or maybe c)), while in the experiments carried out by Samec *et al.*[7] water was definitely present on the electrodes emersed into nitrogen of high relative humidity and is proposed to play a role in the observed significantly overall lower potentials than observed by Neff and Kötz. In fact, the potentials (absolute potentials calculated from the work functions reported by Neff and Kötz and the IUPAC recommended (4.44 V) values of the absolute electrode potential of the hydrogen electrode) are shifted about +400 mV compared to the applied potentials, while Samec *et al.* observed about 200 mV lower potentials than the ones applied. Since the first and most likely also the second layer of water molecules in the electrochemical double layer are (at the positively polarized surface in the linear range) preferentially oriented with the oxygen atom pointing towards the gold surface, a lowering effect of the water molecules on potential is to be expected. In fact, it was estimated by Trasatti that the total solvent contribution to the applied potential is about 0.4 V.[110] Hence, this would fit well with the values observed in UHV by Neff and Kötz. However, it is surprising that a constant shift is observed in the whole linear range (extending over more than 1 V). This would mean that the dipole potential of the water is constant in a wide potential range, i.e. no re-orientation seems to take place form at least 0 mV to 1 V vs Ag/AgCl, which includes also the PZC. This seems in contradiction with reports on clear evidence for water re-orientation with increasing or decreasing potentials (see e.g. Ataka *et al.*[67]).

What is easier to understand are the lower potentials than applied observed by Samec *et al.* in theirs studies at very high relative humidity. They suggest that the main reason for the lower potential observed on their emersed electrodes is the missing contribution of the dipole potential at the surface of the bulk electrolyte. They assume that for the emersion into the relative high humidity close to 99% RH they transfer the first highly ordered water layers of the double layer region, so that the topmost water layer is still one with the oxygen atoms pointing towards the gold, while for bulk water the surface layer has weak dipole moment pointing in the opposite direction, leading to an increase in work function by about 130 mV (according to the most reliable estimate of the contribution of the surface potential of bulk water to the absolute electrode potential).[7,111]

This line of thought is reflected in Figure 39. As already mentioned above, the case of electrodes emersed into UHV is corresponding to the situations sketched either in Figure 39b) or c). In Figure 39c), two water molecules with their negative dipole moment pointing diagonally towards the metal cause a slight decrease of the potential compared to the situation sketched in Figure 39b). When the dry condition used in this PhD work, i.e., < 3% RH is applied (Figure 39d)), more water molecules are suggested to be present in the system, building up the first water layer, with their negative dipole pointing towards the metal surface and the potential decreases further. At 65-70% RH (Figure 39e)), additional water molecules are suggested to adsorb with their positive dipole pointing in direction of the adsorbed anion, which results in the observed increase of the potential. At the end, with 90-95% RH (Figure 39f)), even more water molecules are present in the system, building up a second water layer, with their negative dipole pointing towards the first water layer, leading again in a decrease of the potential. Figure 39g) shows typical results obtained in this work (see also Figure 38), which are showing the observed behavior of first an increase in potentials for increasing relative humidity from 1-3% RH to 65-70% RH and then again a decrease when further increasing to about 90-95% RH (Figure 39g)). All potentials are between the values reported for emersion into UHV and for emersion into very high humidity of about 99% RH, which fits well with the situations sketched in Figure 39, assuming that in the work by Samec *et al.* even further quite oriented water layers were adsorbed in the double layer region of the emersed electrodes. And nearly all of them show higher potential values than the applied ones during immersion and subsequent emersion (see also Figure 40 in the next section). Furthermore, also Figure 38 shows that there is also an effect of direction of polarization during immersion, whether it was stepped sequentially into the positive or the negative direction. This will be discussed in the following section.

4.2.1 Comparing the Volta potential difference when potentials were stepped in positive and in negative direction

Like in the work by Samec *et al*.[7], applied potentials on the samples were stepped in positive and in negative direction. In Figure 40 the potential for the emersed samples that where polarized during immersion stepwise in positive and in negative direction are compared. In these experiments 0.05 mol L^{-1} H_2SO_4 and 0.1 mol L^{-1} $NaClO_4$ solutions as electrolyte and N_2 atmosphere with various RH values inside the Kelvin probe/infrared beam chamber were used.

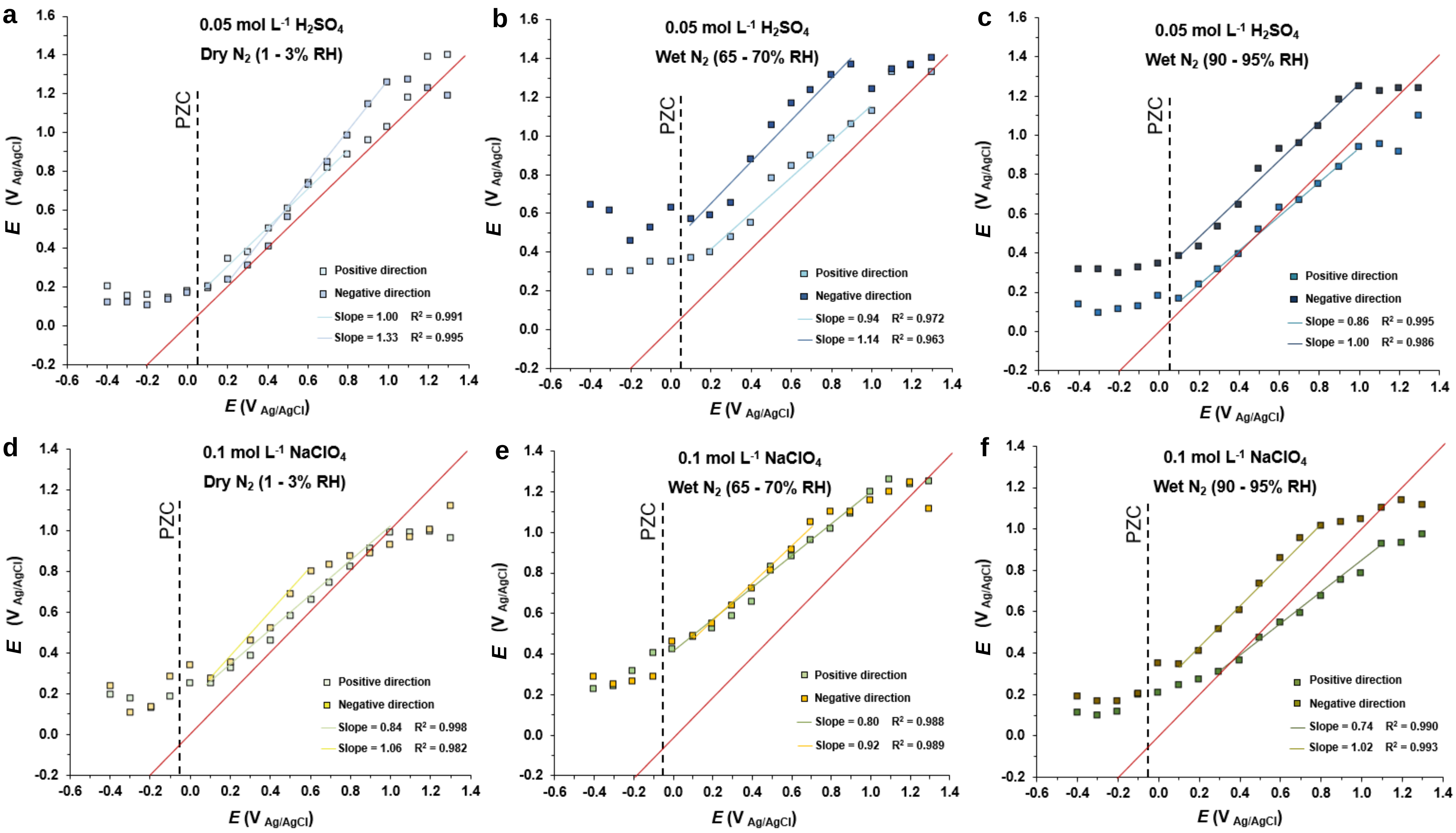

Figure 40. Comparison of potentials applied in positive and in negative direction with different electrolytes and atmosphere (RH values) conditions.

An upwards shift of the potentials between “positive direction” and “negative direction” is observed in most of the cases shown in Figure 40. Larger shifts are observed in the experiments with higher RH values (90-95% RH). Such effect (difference between “negative direction” and “positive direction”) was also observed in the work proposed by Samec *et al*.[7] Furthermore, the authors observed that when potentials were stepped in negative direction, higher values of $\Delta\psi$ (in general, about 0.2 V) were determined by the Kelvin probe.[7] This same observation can be made in Figures 40b), 40c), 40d) and 40f). The authors also compared the values of $\Delta\psi$ determined by Kelvin probe measurements of electrode potential shortly after switching off the polarization, and again a similar shift between applied potentials in “negative direction” and “positive direction” was noticed.[7]

Generally, the results in the diagrams in Figure 40 also present constant shifts for all potentials (in the linear range, which roughly starts around the PZC) with the change of the humidity. This behavior indicates a similar orientation of all water molecules above the PZC. In the study conducted by Samec *et al*.[7], the potentials obtained in a humidity around 99% are below the potentials measured for the humid atmosphere condition (90-95% RH) applied in this work, which correspond to more adsorbed water molecules in the work of Samec *et al.*, each oriented in the same way, i.e., not changing gradually with the potential.

4.2.2 Potential of zero charge and specific anion adsorption

A closer look at the plots of emersed potential vs applied potential for the different electrolytes and humidity shown in Figure 41 reveals that around 0.0 V the linear correlation between measured and applied potential starts, usually with a slope close to one; these values around 0.0 V probably correspond roughly the PZC “area”. Some reviews in the literature suggest a PZC value for gold at 0.180 V (SHE),[112] which correspond to approximately -0.02 V (Ag/AgCl). Different methods for the PZC measurement were employed and values between 0.150 and 0.180 V (SHE) using diluted solutions of $NaClO_4$ and between 0.100 and 0.150 V (SHE) using diluted solutions of $HClO_4$ were mentioned in another paper.[113] PZC values of 0.140 V (SHE) on gold electrodes were obtained using salt solutions containing SO_4^{2-} and ClO_4^- anions (Na^+ as cation) at concentrations of 0.2 and 0.1 mol L^{-1}, respectively.[88] Gold electrode potentials of zero charge in H_2SO_4 aqueous solutions are reported as following: 0.280 and 0.300 V (SHE) for 0.1 mol L^{-1} and 0.230 V (SHE) for 0.01 mol L^{-1}.[114] Resuming all these PZC values on gold surfaces presented above, a plausible PZC value (approximately) in the experiments presented in this dissertation section (employing 0.05 mol L^{-1} H_2SO_4 and 0.1 mol L^{-1} $NaClO_4$ solutions as electrolyte) could be around 0.05 V and -0.06 V vs Ag/AgCl, respectively.

Hence, for all cases investigated here the PZC is roughly at around 0 mV, for the 0.05 mol L^{-1} H_2SO_4 slightly above and the 0.1 mol L^{-1} $NaClO_4$ slightly below.

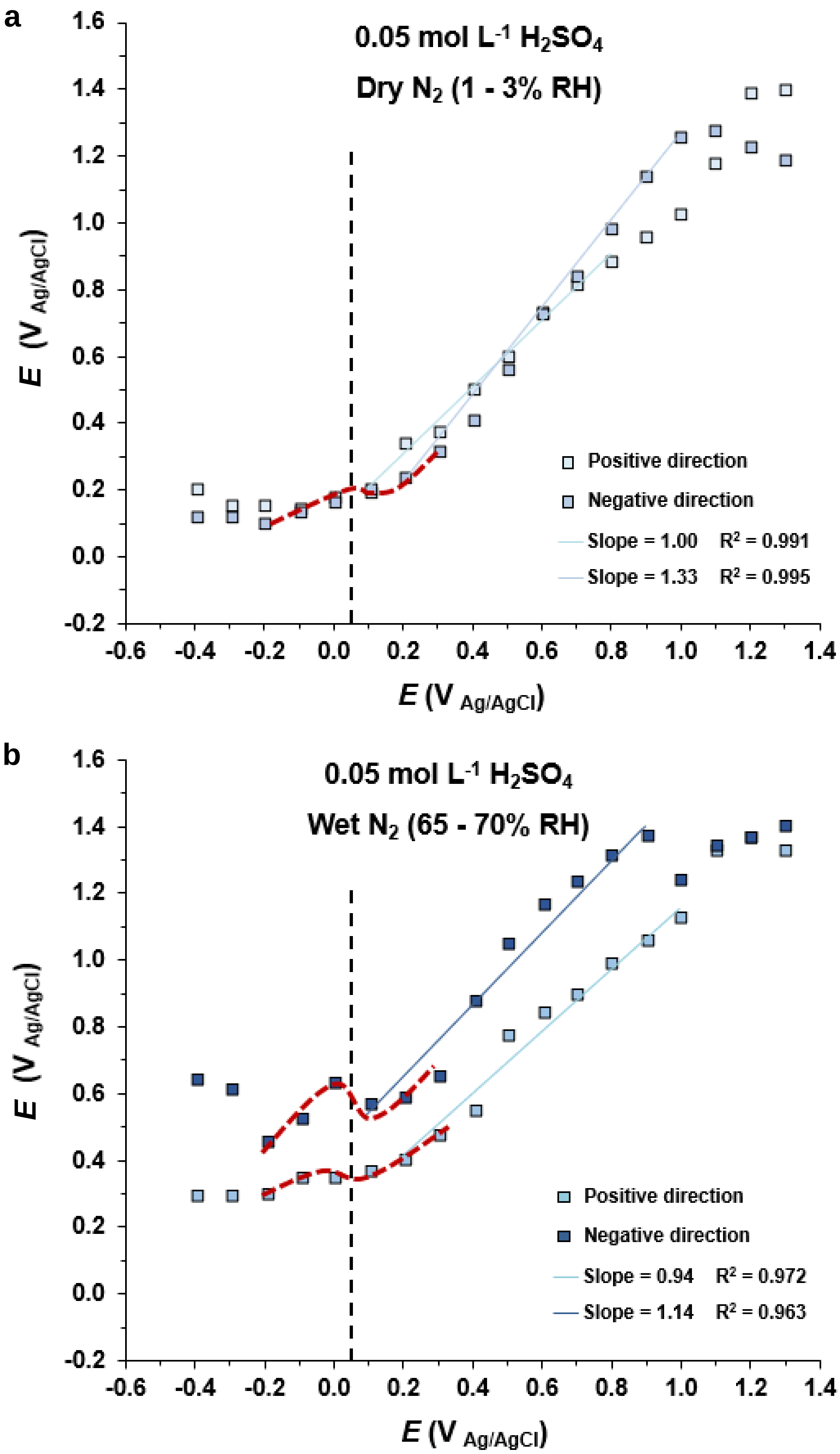
a
0.05 mol L^{-1} H$_2$SO$_4$
Dry N$_2$ (1 - 3% RH)
Positive direction
Negative direction
Slope = 1.00 R^2 = 0.991
Slope = 1.33 R^2 = 0.995
E (V Ag/AgCl)
E (V Ag/AgCl)
1.6
1.4
1.2
1.0
0.8
0.6
0.4
0.2
0.0
-0.2
-0.6
-0.4
-0.2
0.0
0.2
0.4
0.6
0.8
1.0
1.2
1.4
b
0.05 mol L^{-1} H$_2$SO$_4$
Wet N$_2$ (65 - 70% RH)
Positive direction
Negative direction
Slope = 0.94 R^2 = 0.972
Slope = 1.14 R^2 = 0.963
E (V Ag/AgCl)
E (V Ag/AgCl)

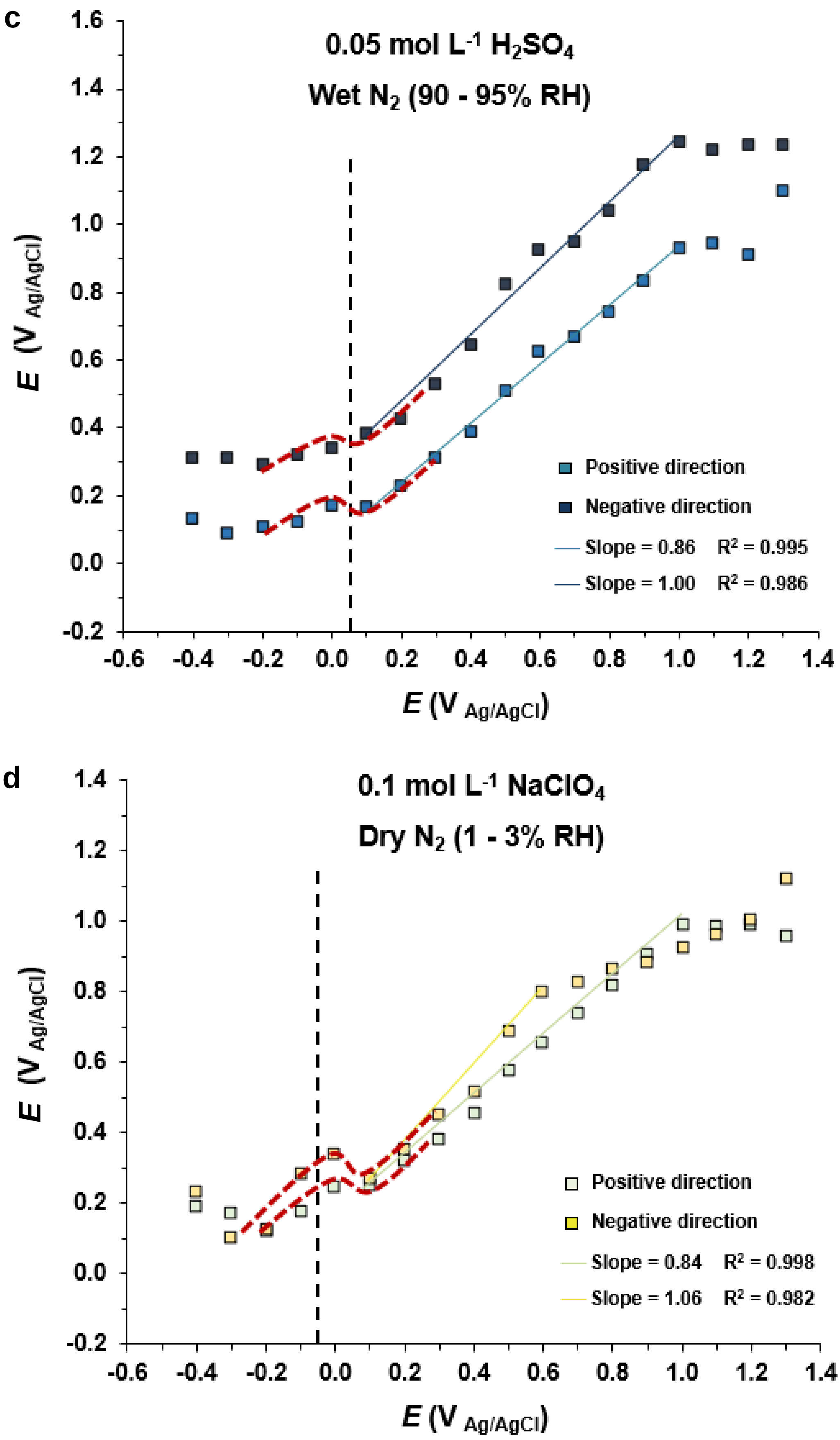
c
0.05 mol L-1 H2SO4
Wet N2 (90 - 95% RH)
E (V Ag/AgCl)
E (V Ag/AgCl)
1.6
1.4
1.2
1.0
0.8
0.6
0.4
0.2
0.0
-0.2
-0.6
-0.4
-0.2
0.0
0.2
0.4
0.6
0.8
1.0
1.2
1.4
Positive direction
Negative direction
Slope = 0.86 R2 = 0.995
Slope = 1.00 R2 = 0.986
d
0.1 mol L-1 NaClO4
Dry N2 (1 - 3% RH)
E (V Ag/AgCl)
E (V Ag/AgCl)
1.4
1.2
1.0
0.8
0.6
0.4
0.2
0.0
-0.2
-0.6
-0.4
-0.2
0.0
0.2
0.4
0.6
0.8
1.0
1.2
1.4
Positive direction
Negative direction
Slope = 0.84 R2 = 0.998
Slope = 1.06 R2 = 0.982

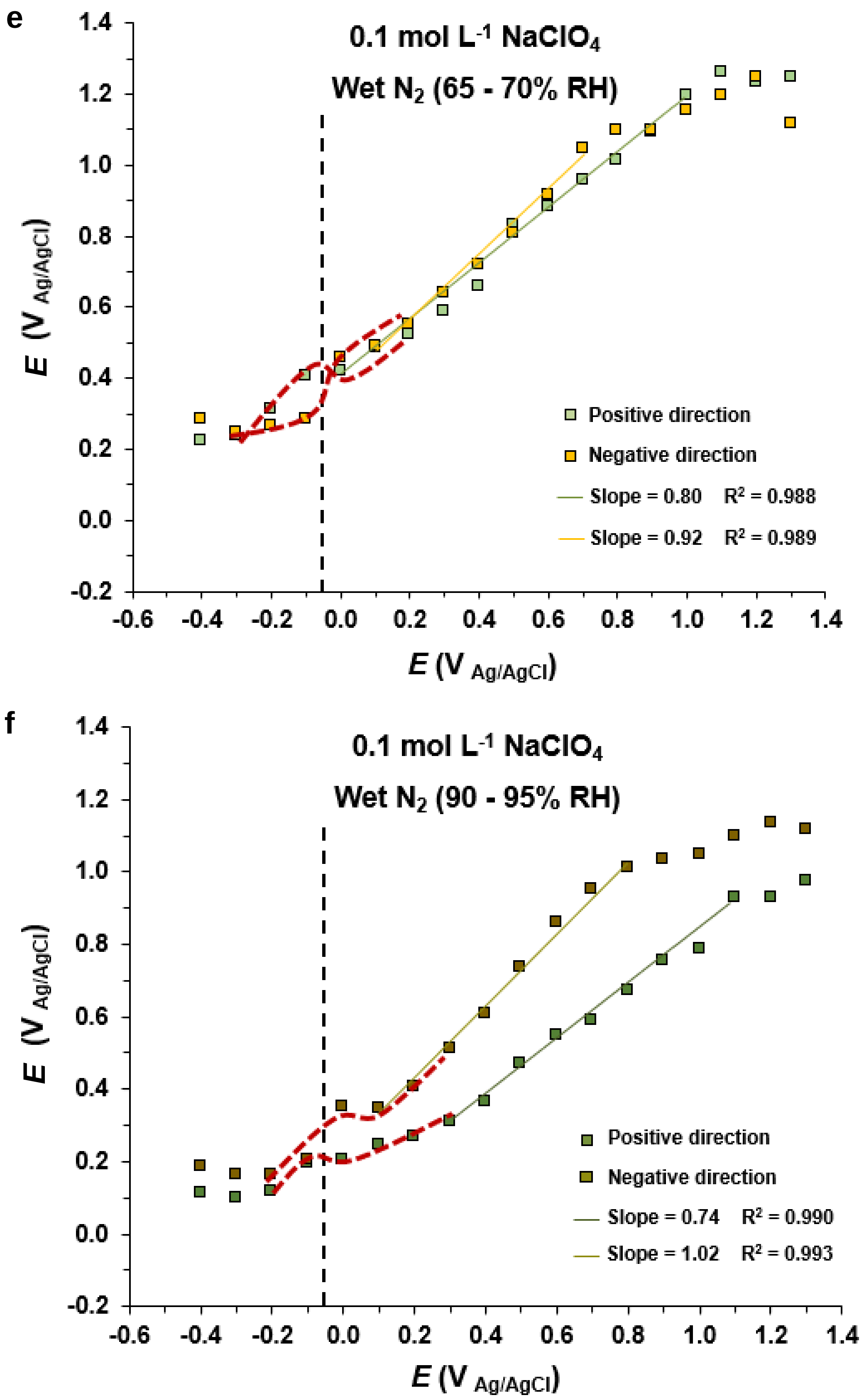

Figure 41. Plots of potential of the emersed electrode vs the applied potential, for the

different electrolytes and relative humidity: in a), b) and c) 0.05 mol L^{-1} H_2SO_4 solution and in d), e) and f) 0.1 mol L^{-1} $NaClO_4$ solution as electrolyte. The black vertical dashed lines represent the probable PZC; the red dashed lines represent a "potential variation" around the PZC value.

An effect around PZC is of course expected. Assuming no specific adsorption above the PZC, one would expect cation adsorption as counter-ions to negative charge at the surface for polarization below PZC and anion adsorption as counter-ions in the double layer above PZC, and orientation of the water molecules in the first layer(s) with oxygen pointing towards the gold a potential above PZC and in the opposite direction below PZC. Hence a change in the correlation between emersed and applied potential around PZC is expected. As already discussed, above PZC the loss of all water should result in potentials of the emersed electrode that are higher than applied during immersion, as reported by Neff and Kötz.[6] The reason is that the water in the double layer has a dipole potential contribution that should result in decreasing the work function. Below PZC, with the same reasoning one would expect lower potentials. This is not the case here. Below PZC, when following the plots of emersed vs applied potential in the negative direction, nearly in all cases first an increase in potential is observed and for about a further 200 mV the linear correlation between potential of the emersed electrode and the applied one continues. The reason for this might be that not all water is lost. Furthermore, also an effect of specific adsorption of anions has to be considered. This will be discussed in more detail further below.

The tendency for specific adsorption of anions on gold can be sorted as following: $I^- > Br^- > OH^- > Cl^- > ClO_4^- = SO_4^{2-} > F^-$; in this adsorption sequence the amount of adsorbed anions decreases and PZC increases.[88] According the study conducted by Samec *et al*.[7], when the anion becomes more adsorbing, for example I^-, the electrode potential difference determined by Kelvin probe on a gold electrode after emersion from the electrolyte was lower (i.e. the potential high) when comparing to less adsorbing anions, such as SO_4^{2-}.[7] Since for electrolytes with anions that were comparatively weakly adsorbing they observed significantly lower potentials on the emersed electrode than were applied, this means that strongly adsorbing anions caused a positive shift of the emersed potential. In the adsorption sequence listed above, the adsorption of ClO_4^- and SO_4^{2-} anions is listed as quite equally strong; this could also be a possible explanation for the relatively same potentials where the linear range with unity slope in Figure 41 starts (comparing the diagrams in Figures 41a), 41b) and 41c) with those in Figures 41d), 41e) and 41f). Indeed, as it will be shown further below, when using a stronger adsorbing anion such as bromide, the linear range extends down to at least -0.1 V. As mentioned, interfacial water is expected to reorient around the PZC value.[67] This could be a plausible explanation for the potential variation represented by the red dashed lines in the diagrams in Figure 41, as is discussed next.

4.2.3 Water molecules orientation on the metal surface and the role of specifically adsorbed anions

As already discussed above, there are estimates of the surface potential of bulk water; a value of 0.130 ± 0.02 V (SHE) is probably the closest to the real situation at the surface of an aqueous phase (gas/solution interface).[7,111] For the surface of bulk water an orientation of the water molecules with their negative dipole moment pointing preferentially towards the gas phase is expected (this is the reason of the positive potential value of the surface potential of water).[7] The relatively low value of about 130 mV for the dipole potential indicates a quite low degree of ordering.

Water molecules adsorbed on metal surfaces are normally oriented with the oxygen (negative dipole moment) preferentially pointing towards the metal[7,115] acting as a Lewis base, i.e., the bonding through the oxygen atom is accompanied by a net charge transfer to the surface, resulting in a negative work function change.[115] As mentioned previously in section 2.9, there are strong evidences that water in the double layer forms clusters in “ice-like” structures. In such arrangement, water molecules are probably organized as in the ice structure (hexagonal), with some molecules bonded directly to the metal surface and other molecules (in the second layer) held to the first layer by hydrogen bonds.[115] In Figure 42a) a plausible arrangement of water molecules in an “ice-like” structure is schematically shown. Another interesting water molecule arrangement (with the presence of specifically adsorbed anions) is represented in Figure 42b). In this last arrangement, the water molecule is attracted simultaneously by the negative pole (the oxygen atom) to the metal surface and by the positive pole (the hydrogen atoms) to the adsorbed anion.[7] For the water molecules directly on the metals surface (first layer) this is equivalent to the assumed water dipole orientation sketched in Figure 39c) and d).

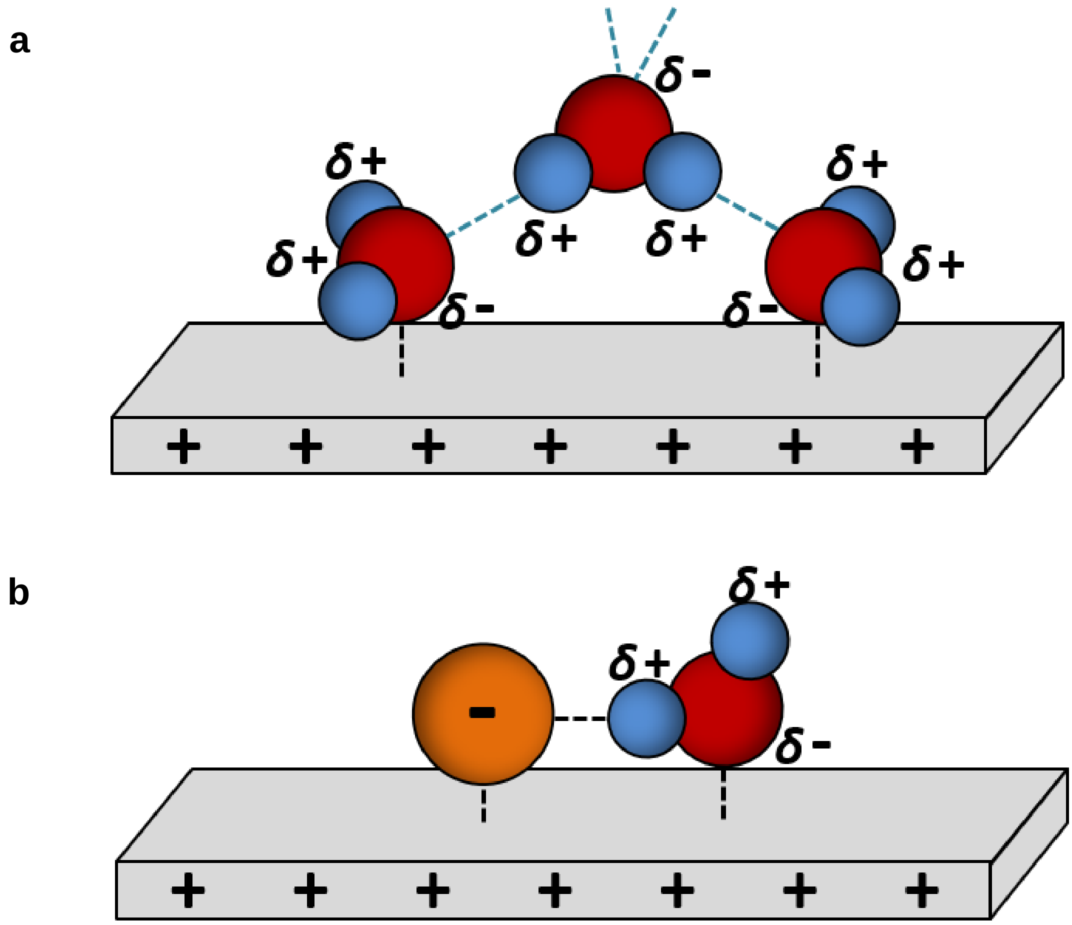

Figure 42. Sketches of possible water molecule orientation on metal surfaces: a) “ice-like” structure, with the blue dashed lines representing hydrogen bonds (adapted from reference 115); b) water molecule in the vicinity of an adsorbed anion, oriented with the oxygen atom towards the metal surface and the hydrogen atom towards the

specific adsorbed ion (adapted from reference 7). The metal surface is represented positively charged in both cases only for illustration.

One aspect to be considered regarding the “ice-like” structure is the specific adsorption of the perchlorate anion at higher potentials; this causes the break of the structure, once half of the OH from water molecules is non-hydrogen-bonded and the other half is hydrogen-bonded to another water molecule.[67] The points mentioned in this section will be discussed together with the FT-IR results (section 4.4, 4.4.1, 4.4.2, 4.4.3) obtained during this dissertation work with different electrolytes.

The water molecules positioned in the second layer sketched in Figure 42a) would cause in the orientation sketched there an increase of work function/potential. Similarly, it is then expected for water molecules in the next (third) layer interacting with these molecules in the second layer that these would again lower the work function. This is also expected to the case for water molecule adsorbing on top of an anion (see Figure 39e)).

Combined, as discussed above with help of Figure 39, the increase of potential when increasing the relative humidity from 1-3% RH to an intermediate humidity of 65-70% RH can be explained by an according orientation of water molecules in the second layer and especially on top of anions. This would also mean that when more anions are specifically adsorbed, this should cause a higher potential of the electrode emersed into intermediate humidity. It should be noted that specifically adsorbed “excess” anions, i.e. anions not needed for charging the double layer, i.e. not countered by an according positive charge on the electrode, will be accompanied by co-adsorbed cations. Water sitting on top of cations should, however, have the same orientation as water in the first layer. Hence, these accompanying cations will have no effect (above PZC at least), only the anions will have one. Since more specifically adsorbed anions can be expected on the electrode when the polarization is stepped from high to low potentials, this is the most plausible explanation for the higher potentials observed on the emersed electrode for polarization into the negative direction, compared to the ones observed for the positive direction.

For the highest humidity investigated in this work, i.e. about 90-95% RH, it is proposed that additional water molecules in the second or third layer are mainly preferentially oriented with the dipole moment pointing upwards (see Figure 39f)).

As mentioned in section 4.2.2, below PZC, when following the plots of emersed vs applied potential in the negative direction, nearly in all cases first an increase in potential is observed and for about a further 200 mV the linear correlation between potential of the emersed electrode and the applied one continues, just shifted upwards. This is proposed to be due to a re-orientation of the water molecules around PZC. Below PZC the water molecules should preferentially point with the hydrogen atoms towards the metal, thus leading to an increase in potential. It is interesting that this upward shift of potentials for the case of polarization below PZC was not observed for emersion into UHV (see e.g. Neff and Kötz[6]), where linearity was observed down to applied potentials of -0.4 V vs SCE and also not for emersion into very high humidity of about 99% RH, as was done by Samec *et al.*[7]. The results obtained by Neff and Kötz are supporting the assumption that orientation of the water molecules plays a crucial role for this phenomenon.

In the work by Samec *et al.*, the linearity between emersed and applied potential for emersion from weakly adsorbing anions (such as sulfate or perchlorate) is lost below about 0.15 V vs Ag/AgCl, below which the potentials of the emersed electrode are remaining on a constant level. This is not easy to explain, maybe traces of oxygen and corresponding onset of oxygen reduction, preventing lower potentials, might play a role here.

4.2.4 Alkaline media solution as electrolyte

Alkaline electrolyte was also applied in this study. For this a 0.1 mol L^{-1} NaOH solution was used as electrolyte. The potentials were stepped in positive direction from -1.0 until 1.0 V in 0.1 V intervals.

The experiment was conducted in dry N_2 atmosphere condition in the same way as for the other electrolytes. The results of the electrode potentials measured by

Kelvin probe after emersing the sample from the alkaline electrolyte are shown in Figure 43 (also shown there are two pictures of the gold surface after emersing the sample from H_2SO_4 and NaOH electrolytes).

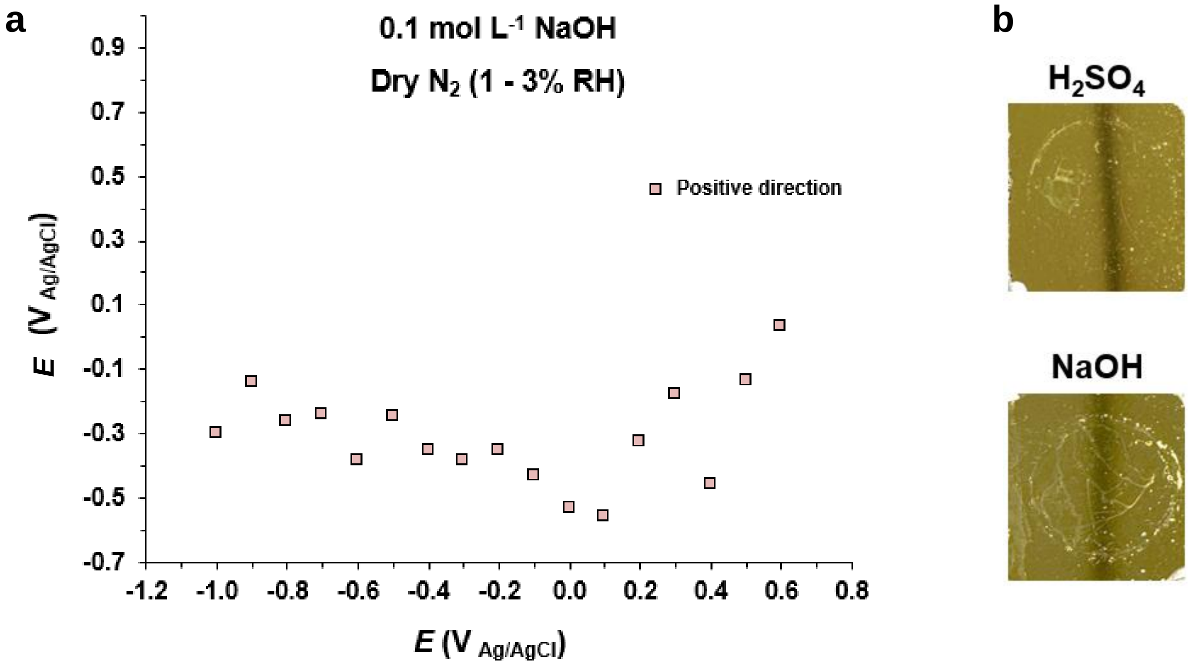

Figure 43. a) Electrode potential measured by Kelvin probe in dry N_2 atmosphere vs potential applied in 0.1 mol L^{-1} NaOH solution as electrolyte; b) pictures taken from gold samples emersed from H_2SO_4 and NaOH electrolytes.

There was no linear behavior achieved in this experiment, comparing to the experiments with H_2SO_4 and $NaClO_4$ electrolytes. The NaOH aqueous electrolyte seems to be more wetting on the gold electrode than the other electrolytes. After emersing the sample from NaOH solution, it was possible to observe (visually) many blurred marks on the whole gold surface, differently from those samples emersed from H_2SO_4, for example (Figure 43b)). The idea of emersing an electrode from aqueous electrolytes is to obtain a surface/interface free from bulk water (electrolyte) and preserve only the electrochemical double layer intact (“frozen-in”), which probably was not obtained in this experiment with alkaline media. The result shown in

Figure 44 looks a bit better, but clearly also here no reliable 1:1 correlation can be defined over a larger potential range.

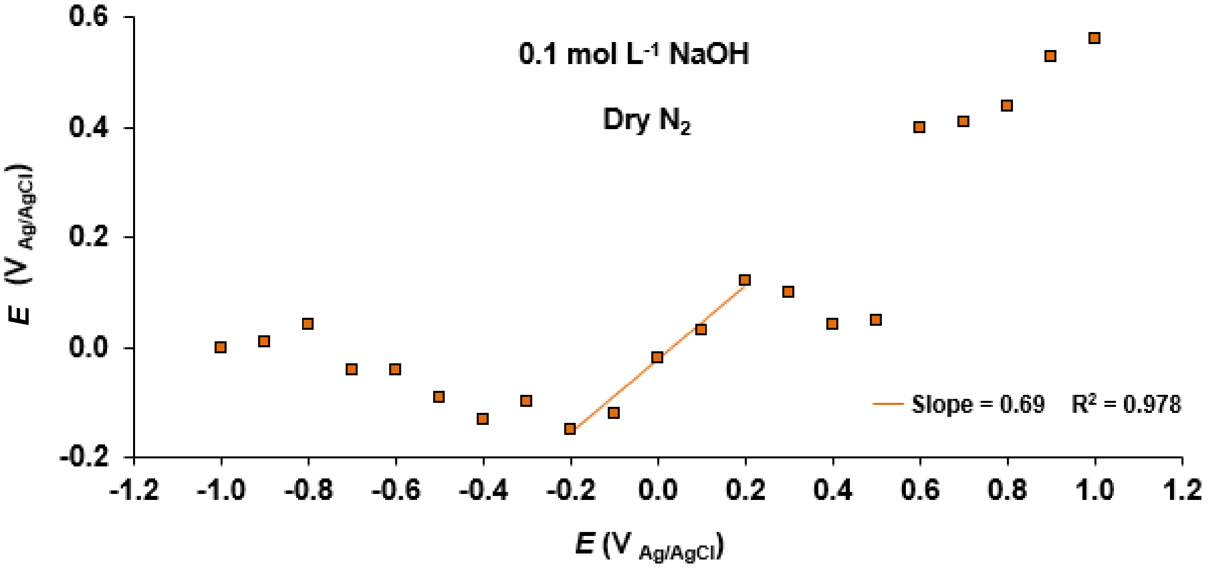

Figure 44. Another example for electrode potential measured by Kelvin probe in dry N_2 atmosphere vs potential applied in 0.1 mol L^{-1} NaOH solution as electrolyte.

Indeed reports in the literature state a PZC value of -0.09 V (SHE) for gold immersed in a 0.1 mol L^{-1} NaOH solution, suggesting a significant adsorption of the OH^- anion.[88] This fits to the observed pronounced wetting behavior on the gold electrode. Interestingly, this value corresponds to approximately -0.290 V in Figure 43 and 44, and again it is possible (at least for Figure 44 and to some extent also in Figure 43) to verify the start of the linear area with unity slope around the PZC value (like observed for electrolytes containing SO_4^{2-} and ClO_4^- anions discussed above).

However, in Figure 44 for applied potentials of between 0.2 and 0.6 V vs Ag/AgCl the potential measured on the emersed electrode seem to have lost correlation completely. Nevertheless, even though reproducibility was low, it is assumed that the results between -0.2V and 0.2 V are correct and most likely also the one below the PZC, that is below -0.2V, including the tendency of increasing values for decreasing applied potential. This would then confirm the re-orientation of the water molecules.

4.2.5 Bromide anion solution as electrolyte with higher specific adsorption

Potassium bromide (0.1 mol L^{-1} KBr aqueous solution) was chosen as electrolyte with a higher specific adsorption anion, once the experiment with NaOH in this dissertation was not successful. Potentials were applied in positive and in negative directions from -0.5 until 0.8 V. The purpose of the experiments with a higher specific adsorption anion was to observe what the effect on the measured potentials by Kelvin probe technique would be in comparison with those with less adsorbing anions, such as ClO_4^- and SO_4^{2-}. The Volta potential difference obtained when the potentials were stepped in positive and negative directions after the sample emersion from the electrolyte are presented in Table 8. Results presented in the gray hatched areas represent the linear range (slopes values of approximately 1) in each experiment. The Kelvin probe was previously calibrated with the homemade Ag/AgCl/KCl reference electrode, as described in section 3.7. For the experiments in N_2 atmosphere of higher humidity only few applied potentials in the linear range and in intervals of 0.2 V were selected.

Table 8. Polarization stepped in positive and negative directions on gold surfaces in contact with KBr solution as electrolyte and the correspondent potential measured by Kelvin probe in N_2 atmosphere with different RH values.

E (V $_{Ag/AgCl}$)	**E (V $_{Ag/AgCl}$)**					
	0.1 mol L^{-1} KBr (positive direction)			**0.1 mol L^{-1} KBr (negative direction)**		
	N_2 (< 3% RH)	**N_2 (65-70% RH)**	**N_2 (90-95% RH)**	**N_2 (< 3% RH)**	**N_2 (65-70% RH)**	**N_2 (90-95% RH)**
-0.5	0.1799 ± 0.0039			0.1801 ± 0.0035		
-0.4	0.1885 ± 0.0028			0.1866 ± 0.0031		
-0.3	0.1840 ± 0.0022			0.1875 ± 0.0039		
-0.2	0.2315 ± 0.0035			0.1823 ± 0.0035		
-0.1	0.2572 ± 0.0026			0.1916 ± 0.0049		
0.0	0.3401 ± 0.0037	0.2807 ± 0.0161	0.3489 ± 0.0093	0.2979 ± 0.0029	0.2247 ± 0.0097	0.2696 ± 0.0078
0.1	0.4291 ± 0.0037			0.3339 ± 0.0041		
0.2	0.5112 ± 0.0035	0.4422 ± 0.0158	0.5224 ± 0.0092	0.4152 ± 0.0030	0.3984 ± 0.0085	0.4474 ± 0.0058
0.3	0.6064 ± 0.0028			0.5425 ± 0.0033		
0.4	0.6901 ± 0.0031	0.6028 ± 0.0176	0.6727 ± 0.0109	0.6122 ± 0.0041	0.6045 ± 0.0110	0.6169 ± 0.0062
0.5	0.7832 ± 0.0031			0.7450 ± 0.0039		
0.6	0.9193 ± 0.0049	0.8115 ± 0.0236	0.8487 ± 0.0150	0.8845 ± 0.0050	0.7283 ± 0.0164	0.8281 ± 0.0128
0.7	1.0636 ± 0.0047			1.0139 ± 0.0094		
0.8	1.1338 ± 0.0053			1.0781 ± 0.0204		

For experiments employing $NaClO_4$ and H_2SO_4 solutions as electrolyte, the potentials were stepped up until 1.3 V; this was not done in the experiments with KBr as at 1.0 V the entire gold layer was “removed/dissolved” from the glass substrate in the first test with this electrolyte. Therefore, the experiments were only carried out until 0.8 V in order to preserve the gold layer intact. The results presented in Table 8 are represented as diagrams in Figure 45, which include the trend lines and the slope and R^2 values from the linear region. The “color gradient effect” in the diagrams represents the humidity, i.e., the darker the color, the higher the humidity value in the correspondent experiment.

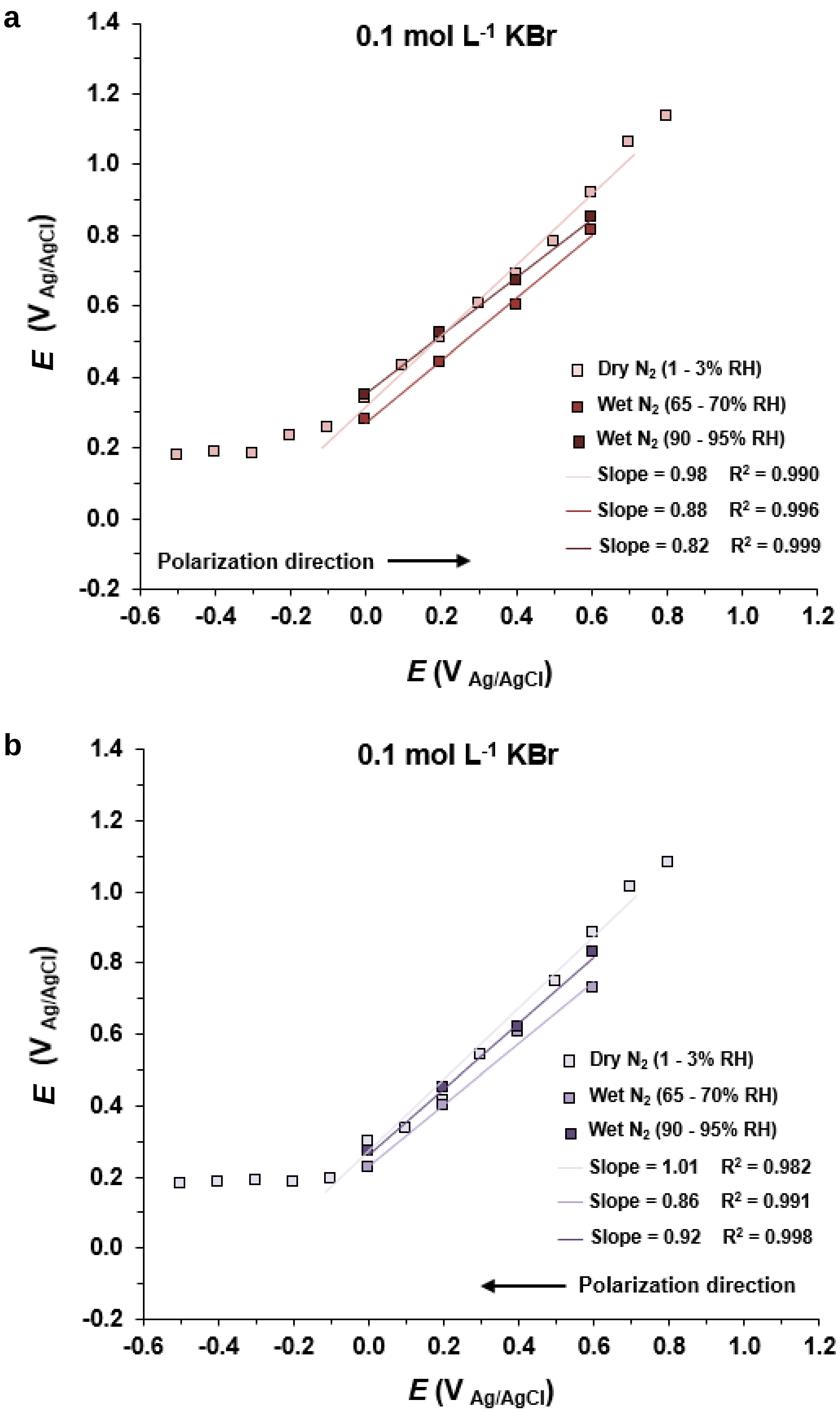

Figure 45. Potential of the emersed gold sample (calibrated vs Ag/AgCl) as function

of applied potential during immersion, measured by Kelvin probe in different RH conditions. As electrolyte was used 0.1 mol L^{-1} KBr solution, with the potentials stepped in a) positive and in b) negative direction.

Samec *et al*. observed for their experiments on electrodes emersed into high humidity nitrogen environment that the potential shifted to higher potentials for anions which are more specific adsorbing than for those with a weaker adsorption.[7] Since the results obtained by Samec *et al*. where solely obtained at very high relative humidity of close to 100% RH, the question here what the effect of the strongly adsorbing bromide would be at the lower relative humidities investigated in this work.

In Table 9 the difference (shift) in the potentials obtained when employing 0.1 mol L^{-1} KBr solution compared to 0.1 mol L^{-1} $NaClO_4$ and 0.05 mol L^{-1} H_2SO_4 solutions (in the linear range with slope around 1 for all experiments) are shown. A direct comparison of the emersed potentials as function of applied potential obtained for the three different relative humidities investigated in this work is also shown in Figure 46, where the results obtained for $NaClO_4$ and H_2SO_4 are compared to the results for KBr.

A significant positive shift of about 0.2 V is generally observed for all cases where the emersion took place into dry atmosphere of 1-3% RH, compared with the values obtained from the sulfuric acid and sodium perchlorate containing solution. Also, for the high humidity of 90-95% RH there is a clear positive shift of even up to 0.3 V for the values obtained when the polarization was towards higher potentials, i.e. in the positive direction. The latter result is in good agreement with the observations made by Samec *et al*. for close to 100% RH. However, for intermediate humidity of 65-70% RH difference is close to zero or even negative. For the high humidity very low differences were observed when the sample was polarized into the negative direction.

Figure 46 shows that the reason for the different differences in different humidity and the different polarization direction is that for emersion from KBr electrolyte the resulting potentials of the emersed electrode are much less depending on relative humidity and direction of polarization than is observed for the other two electrolytes.

Table 9. Difference of the potentials measured by Kelvin probe on the emersed electrodes when employing 0.1 mol L^{-1} KBr solution compared to 0.1 mol L^{-1} $NaClO_4$ and 0.05 mol L^{-1} H_2SO_4 solutions (in the linear range with slope around 1 for all experiments).

E **(V** $_{\mathbf{Ag/AgCl}}$**)**	**Difference in *E* (V** $_{\mathbf{Ag/AgCl}}$**)**					
	0.1 mol L^{-1} KBr / 0.1 mol L^{-1} H_2SO_4 (positive direction)			**0.1 mol L^{-1} KBr / 0.1 mol L^{-1} H_2SO_4 (negative direction)**		
	N_2 (< 3% RH)	**N_2 (65-70% RH)**	**N_2 (90-95% RH)**	**N_2 (< 3% RH)**	**N_2 (65-70% RH)**	**N_2 (90-95% RH)**
0.1	0.2343					
0.2	0.1683	0.0445	0.2895	0.1778	-0.1878	0.0194
0.3	0.2294			0.2265		
0.4	0.1843	0.0536	0.2806	0.2026	-0.2749	-0.0287
0.5	0.1811			0.1833		
0.6	0.1828	-0.0316	0.2184	0.1561	-0.4404	-0.0996
0.7	0.2465			0.1710		

E **(V** $_{\mathbf{Ag/AgCl}}$**)**	**Difference in *E* (V** $_{\mathbf{Ag/AgCl}}$**)**					
	0.1 mol L^{-1} KBr / 0.1 mol L^{-1} $NaClO_4$ (positive direction)			**0.1 mol L^{-1} KBr / 0.1 mol L^{-1} $NaClO_4$ (negative direction)**		
	N_2 (< 3% RH)	**N_2 (65-70% RH)**	**N_2 (90-95% RH)**	**N_2 (< 3% RH)**	**N_2 (65-70% RH)**	**N_2 (90-95% RH)**
0.1	0.1809			0.0633		
0.2	0.1882	-0.0826		0.0654	-0.1512	0.0423
0.3	0.2237			0.0866		
0.4	0.2319	-0.0573	0.3082	0.0959	-0.1158	0.0088
0.5	0.2054			0.0598		
0.6	0.2617	-0.0697	0.3015	0.0862	-0.1853	-0.0311
0.7	0.3239					

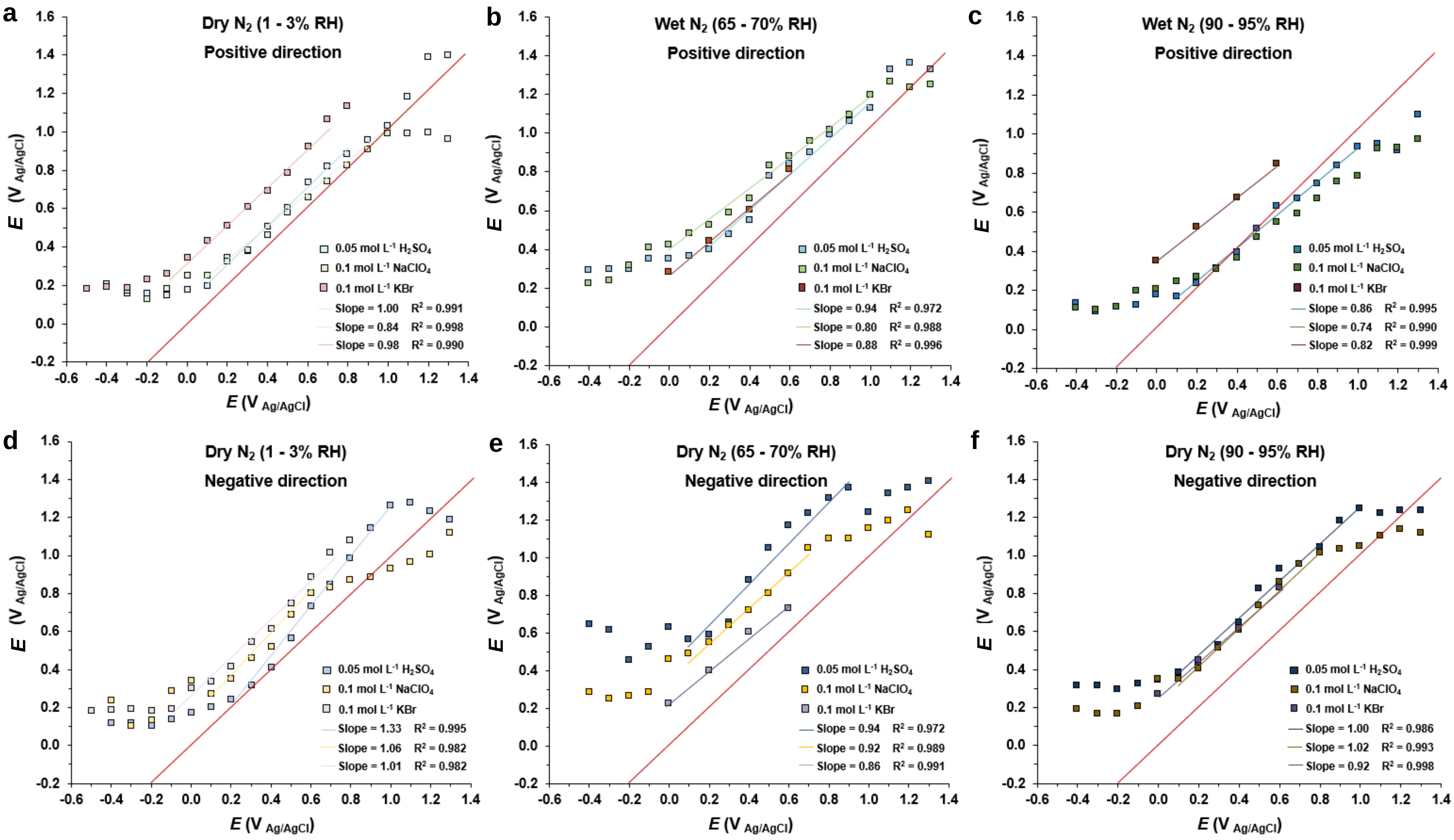

Figure 46. Comparison of measured potentials in positive and in negative direction for the electrolytes employed in this work.

Apparently, the results shown in Table 9 and especially in Figure 46 reveal a “constant” behavior when KBr was employed, which could be explained by the stronger specific adsorption of bromide that hence resulted in no pronounced changes in the potentials comparing the polarization in positive and in negative directions. Furthermore, the water molecules are also probably stronger adsorbed and on the surface are higher concentrations of K^+ and Br^- ions.

4.2.6 Evaluation of the addition of N_2 atmosphere inside the electrochemical cell during the emersing process

Generally, after emersing the gold electrode from the electrolyte sometimes some drops remaining on the surface were possible to be noticed, even for the non-alkaline electrolytes. Therefore, the experiment procedure described in section 3.10 was modified in two different ways in order to verify the reliability of the data: the electrolyte was removed as previously described and, in another test, additionally dry N_2 was introduced into the electrochemical cell through the hose shown previously in Figure 16e) and blown over the surface. This complementary experiment was done only to check if then there would be indication of presence of potential thicker electrolyte layers on the surface that would be better removed that way. Polarization and Kelvin probe measurement duration were 5 and 10 min, respectively. As electrolyte was employed 0.1 mol L^{-1} $NaClO_4$ and the potentials were stepped in positive direction from -0.4 until 1.3 V in intervals of 0.1 V. This experiment was done in dry N_2 atmosphere in the Kelvin probe chamber and the results are presented in Figure 47.

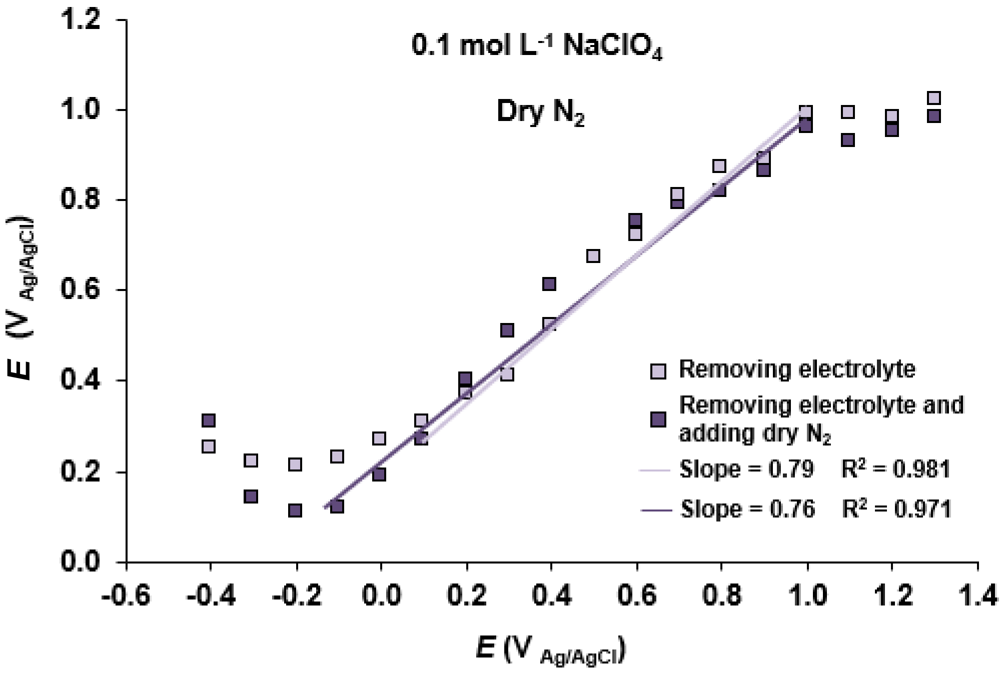

Figure 47. Potentials of the emersed gold electrode vs applied potential obtained with additional blowing of dry nitrogen. Electrolyte was 0.1 mol L^{-1} $NaClO_4$ solution. The electrolyte was removed from the electrochemical cell before the sample polarization was stopped.

No significant difference between slopes and R^2 values were observed comparing these results with the ones obtained in the earlier measurements. Very similar behavior is observed, confirming by the trendlines (from 0.1 until 1.0 V, as in Table 6), suggesting no significant influence by the addition of dry N_2 when removing the electrolyte from the electrochemical cell. In this sense, all experiments were carried out without the addition of N_2 in the electrochemical cell during the emersing process. Hence, only for the alkaline electrolyte serious problem with excess electrolyte staying on the surface was observed.

4.3 Preliminary investigation on electrochemical reactivity of the emersed electrodes

In order to assess the electrochemical reactivity of the gold electrodes emersed into atmosphere of different humidity, gas change experiments were performed. These *in operando* experiments were carried out inside the Kelvin probe chamber (these were the first *in operando* experiments employing this instrumentation).

A key problem with a non-modified tip is -as already discussed- that the work function/potential of the Kelvin probe tip may also change in such a gas change experiment. Two examples are shown in Figures 48 and 49 (where only the potential change is relevant, as the tip was not calibrated vs Ag/AgCl in these experiments). In the first case the atmosphere inside this chamber was switched from dry N_2 to dry synthetic air while the Volta potential difference was measured by Kelvin probe. First, a gold sample was polarized at -0.3 V for 2 min and then the electrolyte (0.1 mol L^{-1} $NaClO_4$) was removed from the electrochemical cell before the sample polarization ended. The sample was transferred to the Kelvin probe chamber and the Volta potential difference was measured during 6 h. The atmosphere was set to dry N_2 for the first 60 min; then the atmosphere was changed to dry synthetic air for the next 140 min; for the last 160 min, the atmosphere was changed again to dry N_2. The results of this experiment are presented in Figure 48. As mentioned, the Volta potential difference values presented in Figures 48 and 49 were not calibrated; they are only values to show the influence of a changing atmosphere. Furthermore, a steady drift can be seen in the dry nitrogen atmosphere, where a stable level is expected. This is due to the already discussed instability of the Kelvin probe during long-term continuous measurements. The focus here, however, is on the change follwing the change of atmosphere. Surprisingly the Volta potential is decreasing (by approximately 0.2 V), although it is expected that the potential of the emersed gold sample should increase. It seem reasonable to assume that the reason for this is an even larger response of the stainless steel Kelvin probe tip.

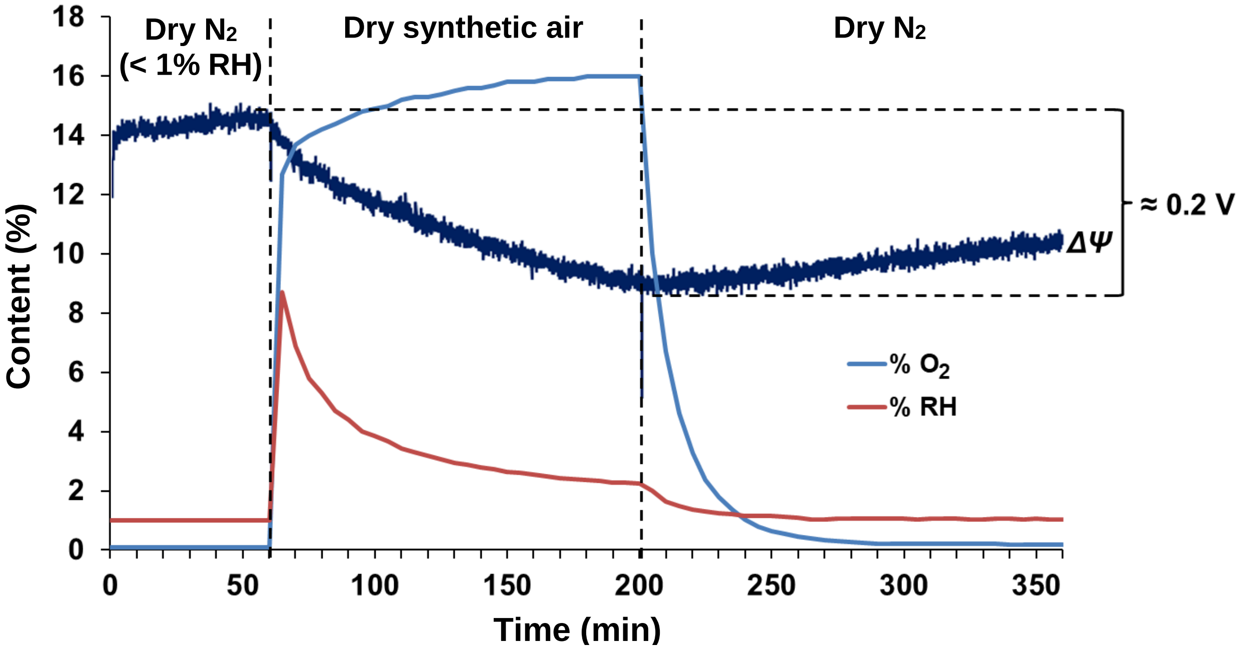

Figure 48. Volta potential difference behavior during atmosphere changing experiments. The vertical dashed lines represent the atmosphere changing time and the horizontal dashed lines represent the maximal difference between the highest and the lowest Volta potential difference value.

Another factor might be that the relative humidity is also changing. The dry N_2 atmosphere has a RH near 1%. When changing the atmosphere to dry synthetic air, the RH grows instantly to over 8% and then starts to decrease slowly, however remains over 2% until the atmosphere is changed again. In the third part of the experiment, in dry N_2 atmosphere, the RH drops again to the initial level (around 1%) and also the Volta potential difference value starts to increase. It could be possible that the higher RH value in the dry synthetic air contributes for some extent to the decrease of the Volta potential difference, however, this is most likely only a minor factor.

Also an experiment at higher humidity was performed. For this a gold sample was polarized in the same way as the previous sample. The RH in the Kelvin probe chamber was set to approximately 30%. The measurement started in wet (30% RH)

N_2; after 60 min, it was changed to wet synthetic air (30% RH) for the next 60 min. The results of this experiment are presented in Figure 49.

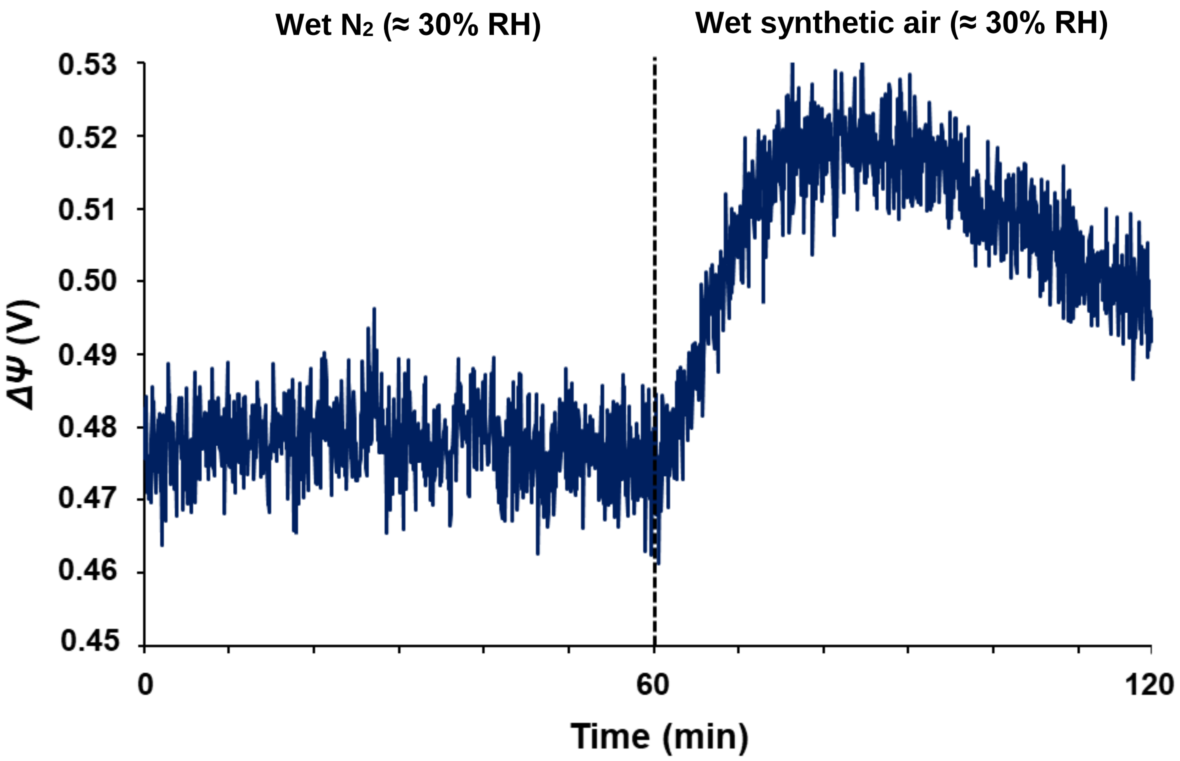

Figure 49. Volta potential difference behavior during atmosphere changing experiment. The vertical dashed line represents the atmosphere changing time.

In this case an increase of the Volta potential difference value by 0.04 to 0.05 V can be seen after changing the atmosphere from wet N_2 (approximately 30% RH) to wet synthetic air (approximately 30% RH). In this case the relative humidity stayed the same. Hence, changes of humidity should not have an influence here. Although now indeed the potential increases upon switch to synthetic air, the change is still quite small and in view of the prior experiment is seems likely that also the tip potential increased, leading to relatively small change of the Volta potential difference.

Hence, it was decided to repeat these experiments, but this time not only on samples that were emersed from negative applied potential, but also from positive applied potential where the potential was high enough as not to lead to a change due to switch from nitrogen to oxygen containing atmosphere. Gold in air has typically a potential between 0.2 and 0.3 V vs Ag/AgCl. Obviously above 0.3 V the oxygen reduction reaction is too slow as to further increase the potential. Hence it was decided to perform such gas change experiments on samples emersed from -0.3 V and from +0.4 V vs Ag/AgCl. The changes seen for the Volta potential difference for the samples emersed from +0.4 V vs Ag/AgCl can be assumed to originate solely from the tip.

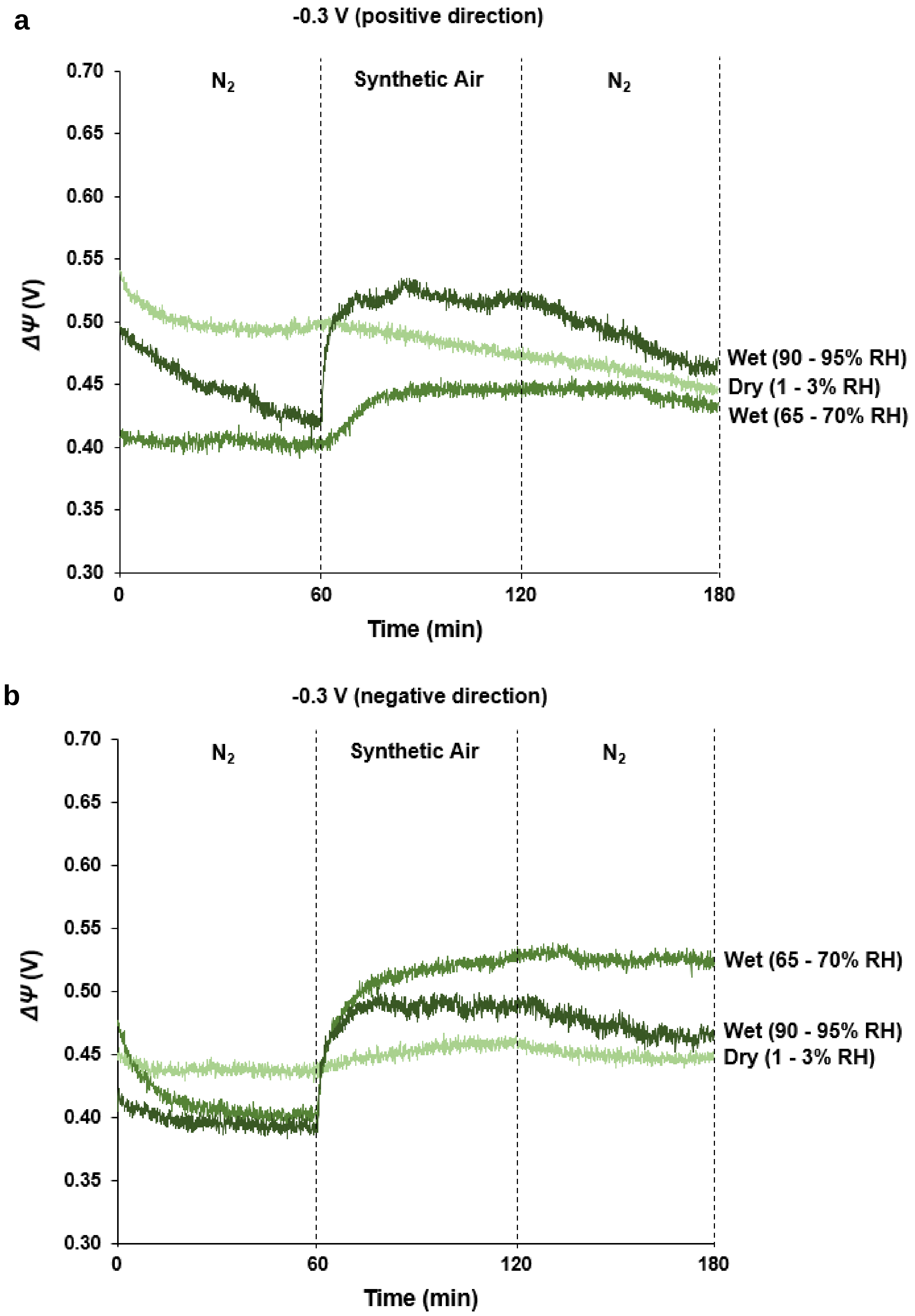

Figure 50. Volta potential difference between emersed electrode and Kelvin probe for

different gas change experiments and for applied potential of -0.3 V corresponding to potential change: a) in positive and b) in negative direction.

Figure 50 show the Volta potential difference between emersed electrode and Kelvin probe for different gas change experiments and for applied potential of -0.3 V corresponding to potential change in positive and in negative direction. In all cases after about 60 min in nitrogen atmosphere, the nitrogen was exchanged for synthetic air and after further 60 min the atmosphere was changed back to nitrogen. The difference was just the relative humidity: dry (1-3% RH), intermediate (65-70% RH) and high (90-95% RH).

In these experiments even in dry atmosphere a slight positive change of the Volta potential difference is observed, indicating a higher inertness of the Kelvin probe tip. It is obvious that the magnitude of the potential increase is increasing with increasing humidity. The increase is proposed to be caused by oxygen reduction which is accompanied by an electron transfer from the electrode to the oxygen molecule, which causes then the shift towards higher potentials. The first and rate determining step in oxygen reduction under bulk electrochemistry conditions is the formation of superoxide O_2^-. Most likely this superoxide gets better stabilized by the presence of higher amounts of water in the double layer region. Strikingly, the potential changes for -0.3 V adjusted by coming from higher applied potentials (negative direction) show higher changes, which would in this logic correspond to more adsorbed water.

This will be discussed in more detail later on the basis of the results obtained from the further characterization of the water on the emersed electrodes by FT-IR and ellipsometry. Since further reaction products such as OH^- cannot diffuse away into bulk electrolyte, it is assumed that the overall reaction stops here at the superoxide level.

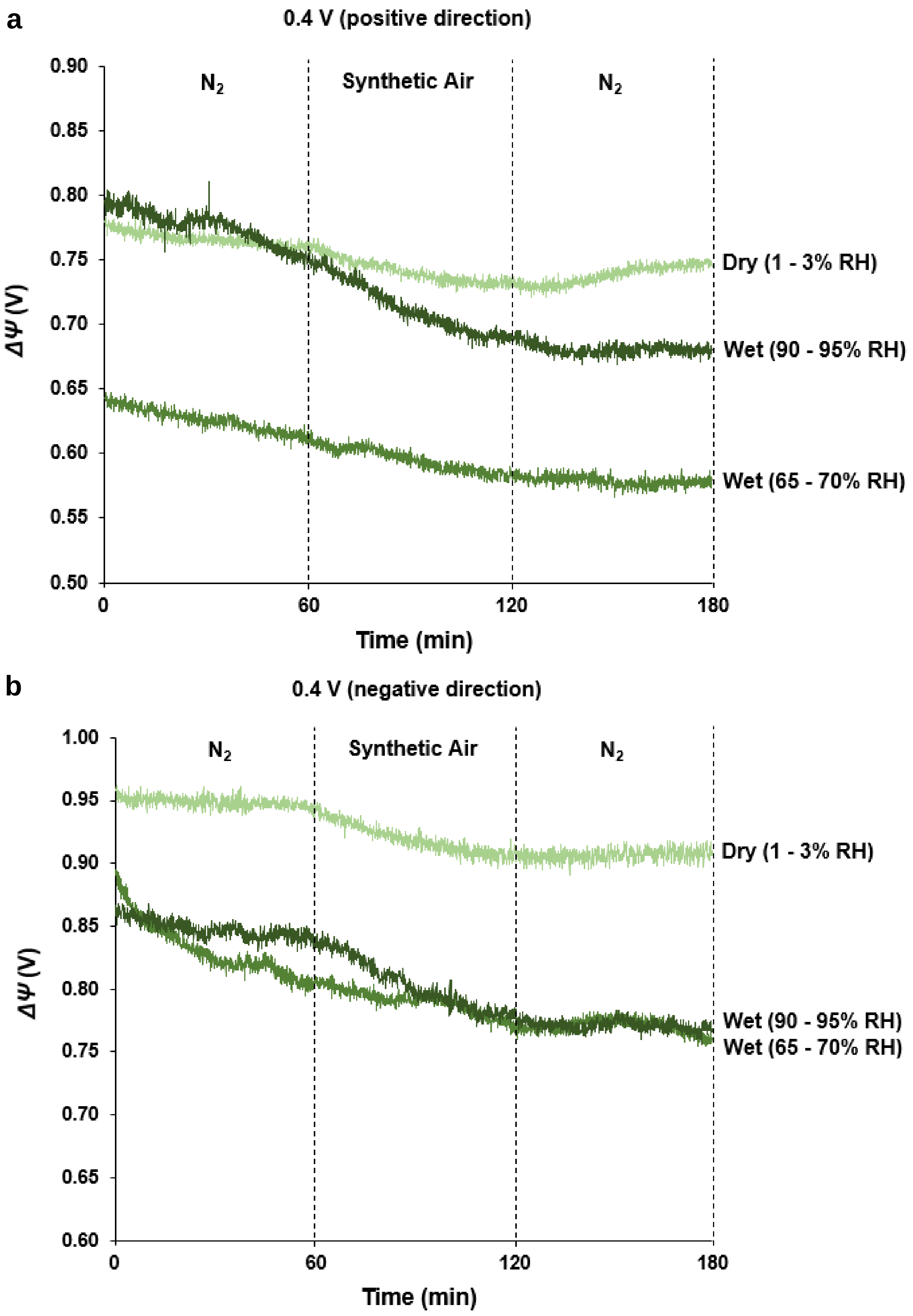

Figure 51. Volta potential difference between emersed electrode and Kelvin probe for

different gas change experiments and for applied potential of +0.4 V corresponding to potential change: a) in positive and b) in negative direction.

In Figure 51 also the results obtained for the case of an applied potential of +0.4 V vs Ag/AgCl is shown for the same three humidity levels as used above and the two polarization directions. In fact, for each of the different humidity levels the experiment with +0.4 V applied potential was carried out right after the one with -0.3 V. As discussed above, the changes in Volta potential difference is in this case expected to be solely from the Kelvin probe tip.

Hence, in a first approximation these can be used as a reference level for obtaining the “pure” potential change of the emersed electrode, by subtracting these curves from the ones obtained for the electrodes emersed at -0.3V vs Ag/AgCl. These curves, thus corrected for the change of the tip potential, are shown in Figure 52.

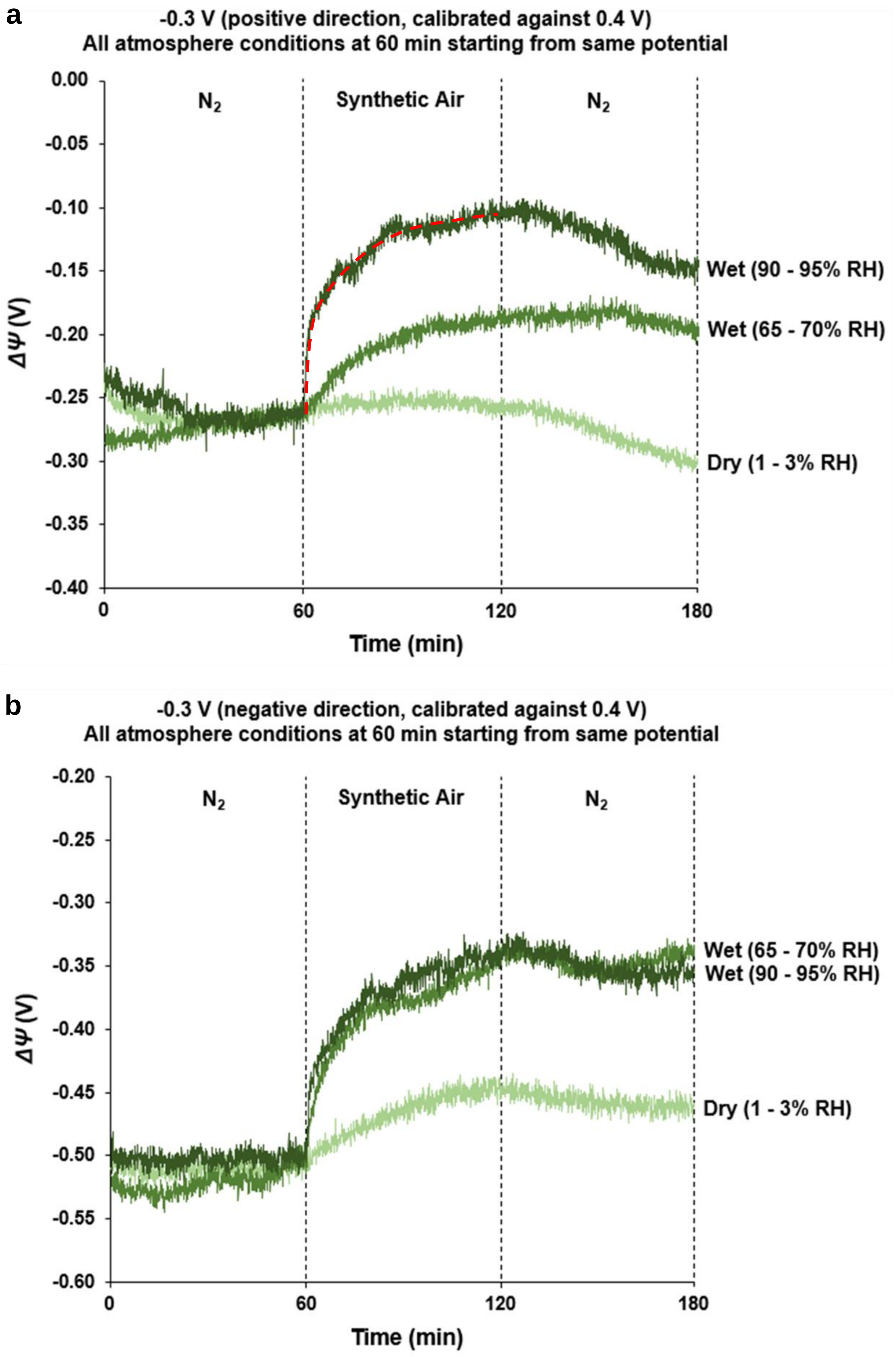

Figure 52. Potential change of the emersed electrode during change of the

atmosphere between nitrogen and synthetic air for different humidity (see indicated in the figure), corrected vs the tip (Volta potential change obtained on electrodes emersed at +0.4 V vs Ag/AgCl). The vertical dashed lines represent the atmosphere changing time. The applied potential during immersion was -0.3 V vs Ag/AgCl adjusted in: a) positive and b) negative direction. The dashed red curve indicates the fitting curve used further below for calculating Tafel plots.

The steeper the potential change, the more significant will be the rate of oxygen reduction. For the absolute electrode potential, we can write:[56,57]

$$E_{\mathrm{abs}} = -\frac{\mu_e}{e} + \Delta\varphi^{\mathrm{Me}}{}_{\mathrm{El}} + \chi_{\mathrm{S}} \qquad \text{(Equation 22)}$$

where μ_e is the chemical potential of the electron in the gold electrode, $\Delta\varphi^{\mathrm{Me}}{}_{\mathrm{El}}$ the potential drop across the metal/electrolyte layer interface and χ_{S} the surface potential of the electrolyte layer.

Assuming a constant capacitance C of the electrochemical double layer, the relation between surface charge σ, capacity and $\Delta\varphi^{\mathrm{Me}}{}_{\mathrm{El}}$ can be written as:

$$C = \sigma/\Delta\varphi^{\mathrm{Me}}{}_{\mathrm{El}} \qquad \text{(Equation 23)}$$

This can be rewritten as:

$$\Delta\varphi^{\mathrm{Me}}{}_{\mathrm{El}} = \sigma/C \qquad \text{(Equation 24)}$$

If the charge of the electrochemical double layer is now changed by electrochemical reactions, assuming a constant capacitance, the potential drop across the interface between metal and electrolyte will also change. Since chemical potential of the electron in the electrode and surface potential of the electrolyte layers can be assumed to remain constant, this change of $\Delta\varphi^{\mathrm{Me}}{}_{\mathrm{El}}$ is also the change of the absolute electrode potential. Hence, it can be written:

$$C \cdot dE/dt = d\sigma/dt = i \qquad \text{(Equation 25)}$$

where i is the current (or current density, if C is the capacitance per unit area).

According to the Butler Volmer equation and assuming only the cathodic current density as relevant here:

$$\frac{\partial\, ln(i)}{\partial E} = -\frac{(1-\beta)\cdot n \cdot F}{RT} \qquad \text{(Equation 26)}$$

where β is the so-called geometric factor (usually assumed to be 0.5), n is the number of electrons transferred in the electron transfer step, F is the Faraday constant, R the gas constant and T the temperature. Hence:

$$\frac{\partial\, ln(dE/dt)}{\partial E} = -\frac{(1-\beta)\cdot n \cdot F}{RT} \qquad \text{(Equation 27)}$$

And with $\ln(i) \approx 2.3 \cdot \lg(i)$, this can be rewritten as:

$$\frac{\partial\, lg(dE/dt)}{\partial E} = -2.3\,\frac{(1-\beta)\cdot n \cdot F}{RT} \qquad \text{(Equation 28)}$$

The inverse of that is $2.3\ RT/(1-\beta)\ nF \approx 59\ \text{mV}/(1-\beta)\ F$ is called the Tafel slope for the cathodic reaction.

Assuming $\beta = 0.5$ and $n = 1$, this would provide result in a change of the current density or here dE/dt by a factor of 10 when the potential changes by 120 mV.

For oxygen reduction on noble metal electrodes in bulk electrolyte, Tafel slope of about 60 mV/decade at low current densities is found, for the higher current densities 120 mV/decade, as is also reported for ORR on Pd in bulk electrolytes.[116] Recently similar Tafel slopes were also found -by use of a hydrogen permeation based approach- on non-immersed palladium surfaces exposed to humid oxygen atmosphere.[3]

Plots of d*E*/d*t* vs *E* are shown in logarithmic scale in Figure 53 for the electrode emersed to intermediate and high humidity (for -0.3 V obtained by polarizing in the positive direction). The d*E*/d*t* values were for the electrode emersed into high humidity determined pointwise for 7 selected potential values along the fitted curve shown in red in Figure 52a). This was done because the measured curve was extremely noisy and hence allowed only a rough evaluation. Interestingly these values show in the logarithmic plot a linear dependence on the potential and the corresponding Tafel slope is about 65 mV/decade. The data quality obtained for the emersed electrode at intermediate humidity (also Figure 52a)) showed much less noisy behaviour and was accordingly fitted in the whole range (see Figure 53b)). Initially, (i.e. at the low potentials) a linear behaviour can be seen, with a Tafel slope of about 120 mV/decade (indicated by a yellow line), but the Tafel slope (if small potential ranges are selected) then quickly decrease (see 60 mV/decade). This change in Tafel slope is also present for the electrode emersed into the high humidity, but is not shown as the data for potentials in the slowly increasing range of about 25 min after the switch to air does not allow a reliable evaluation (potential changes are comparable to the noise level).

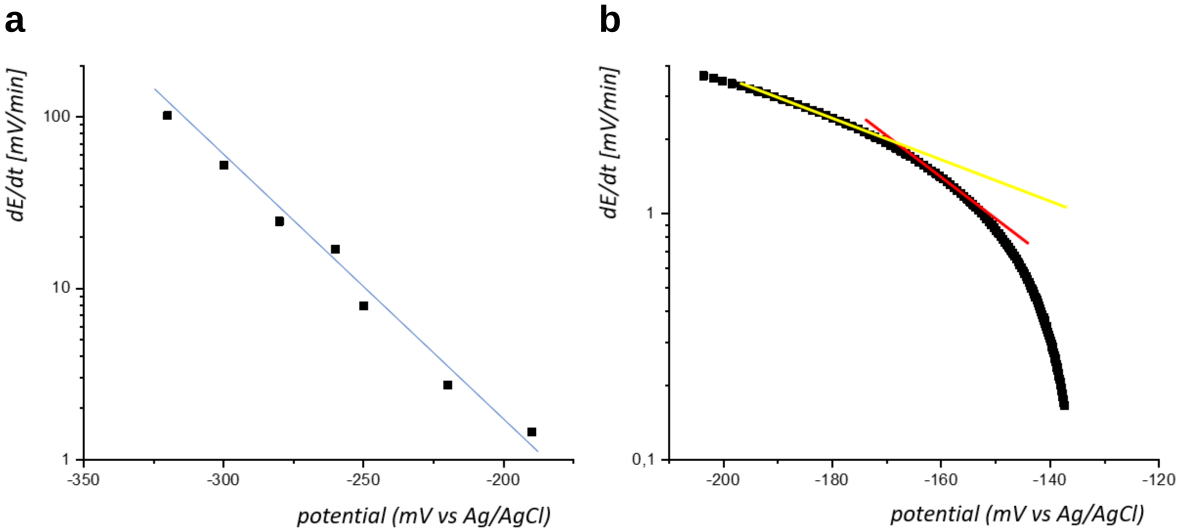

Figure 53. d*E*/d*t* vs *E* plots for a) the electrode emersed at -0.3 V vs Ag/AgCl into a) high humidity of 90-95% RH and b) intermediate humidity of 65-70% RH. The data

were obtained from the data of potential vs time upon switching to synthetic air (between 60 and 120 min; data from Figure 52a)).

Hence, the results shown here just serve to demonstrate that this approach of monitoring the change of potential upon change of the atmosphere from nitrogen to oxygen containing atmosphere seems to be a feasible method of investigating the kinetics of oxygen reduction on emersed electrodes. Of special interest is certainly the effect of the amount of anions and water in the electrochemical double layer.

4.4 Results obtained by FT-IR measurements on the gold electrodes after emersion

The gold sample surface was analyzed using the FT-IR spectroscopy technique as previously described in section 3.11. The main goal of this analysis was observing the presence of water molecules and IR sensitive anions adsorbed on the sample surface. The first FT-IR spectra obtained with the new assembled instrumentation are presented in Figure 54. These first spectra were only calculated by subtracting the background spectra, obtained on the gold sample surface before the electrochemical process (“clean” sample) in the same atmosphere (dry N_2) as the subsequently performed measurement after immersion, polarization and emersion. The potentials were stepped in positive direction in intervals of 0.2 V from -0.2 until 1.0 V.

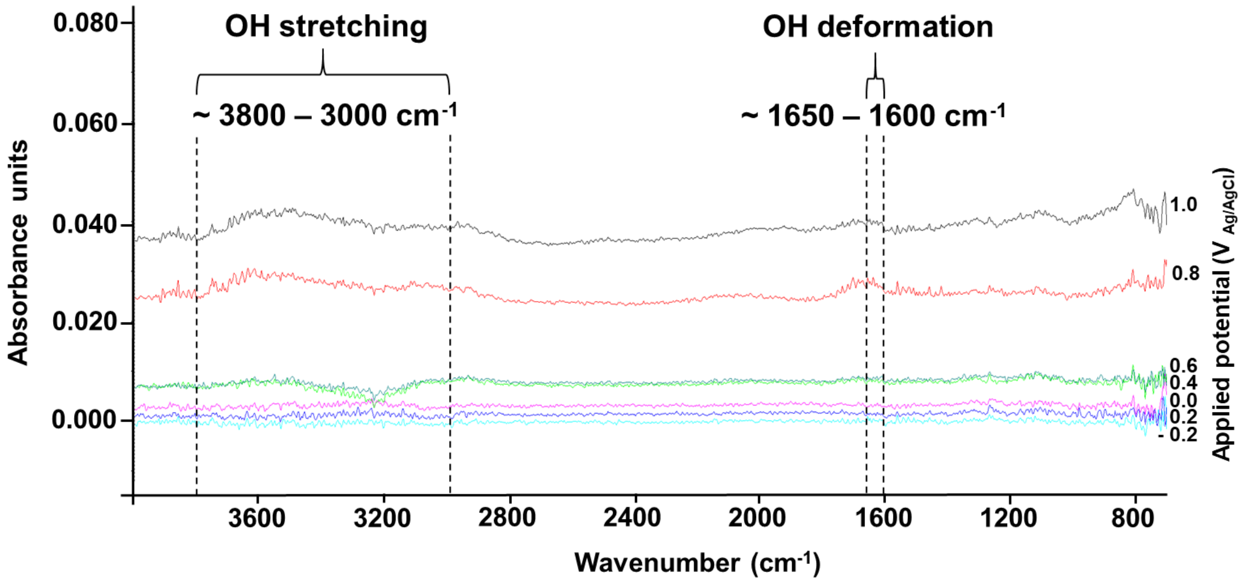

Figure 54. FT-IR spectra obtained stepwise with an emersed gold sample surface, after polarizing stepwise from -0.2 until 1.0 V employing 0.1 mol L^{-1} $NaClO_4$ solution as electrolyte.

The ClO_4^- anion is a tetrahedral compound and features following vibrational frequencies: 459, 625, 928, 1119 cm^{-1}.[117,118] Hence in the spectra in Figure 54, the vibrational frequency band between approximately 1030 – 1110 cm^{-1} can be attributed to the perchlorate ion. These results are also compatible with the interval between 1130 – 1090 cm^{-1}, which is attributed to perchlorate ion adsorbed on gold surfaces.[67]

As can be seen the intensity of the 1030 – 1110 cm^{-1} band increases with increasing potential as is expected for the counter-anion to the increasing positive charge on the electrode.

Two other important regions of analysis are the spectra zones at approximately 3756 and 3652 cm^{-1} and at approximately 1596 cm^{-1}. As presented previously in section 2.5 (Table 4), these vibrational frequencies are attributed to the water molecule, more specifically, to the ν_a, ν_s and δ, respectively, of the OH group.[64] Therefore, the band in the spectra between approximately 3800 and 3000 cm^{-1} and at approximately 1600 cm^{-1} shown in Figure 54 correspond to H_2O. These stretching and deformation vibrations at the same spectra zones were also reported by Ataka *et al*. on gold surface studies.[67]

The relatively low signals at the spectra could be assigned, in parts, to the small sample surface (approximately 0.64 cm^2 of polarized area) and to the device set-up; as presented previously in section 3.1.4 (Figure 18c)), the infrared beam is guided from the spectrometer through an external guide chamber. Here two mirrors and a polarizator are placed in the optical path. Furthermore, the Kelvin probe/infrared beam chamber is separated by two KBr windows from the other parts of the system. All these “extra” optical components could play a role in the signal attenuation. In Figure 55 the optical components and the IR beam path are shown schematically.

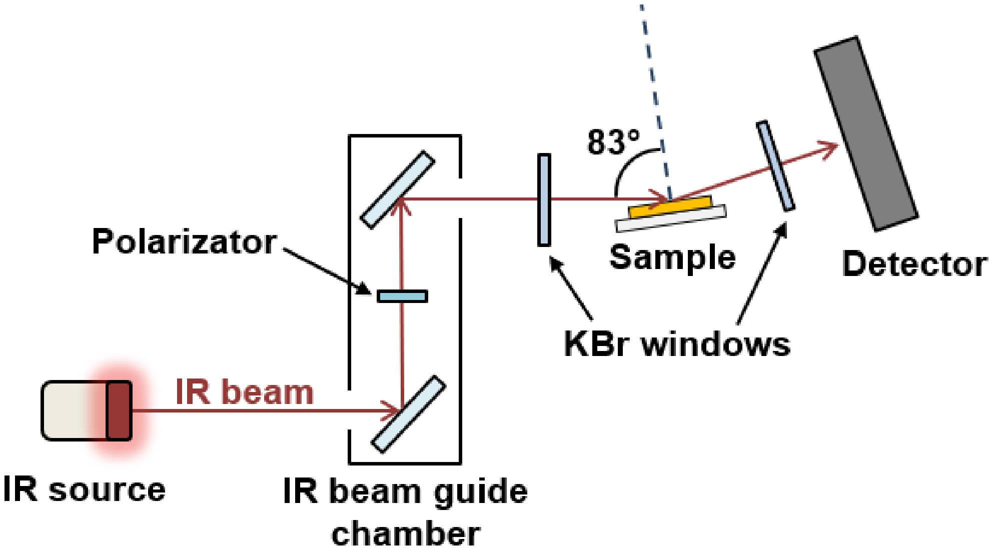

Figure 55. Infrared beam path guided outside the spectrometer through the IR beam guide chamber and analysis chamber (sample location) with the instrumentation optical components.

Another important aspect to be noticed is the possibly very low thickness of the water layer adsorbed on the sample surface. This will be described and discussed in section 4.5. One attempt to increase the signal amplitude was changing the aperture configuration by the spectrometer, increasing it from 2.0 to 4.0 mm. This resulted in spectra as shown in Figure 56.

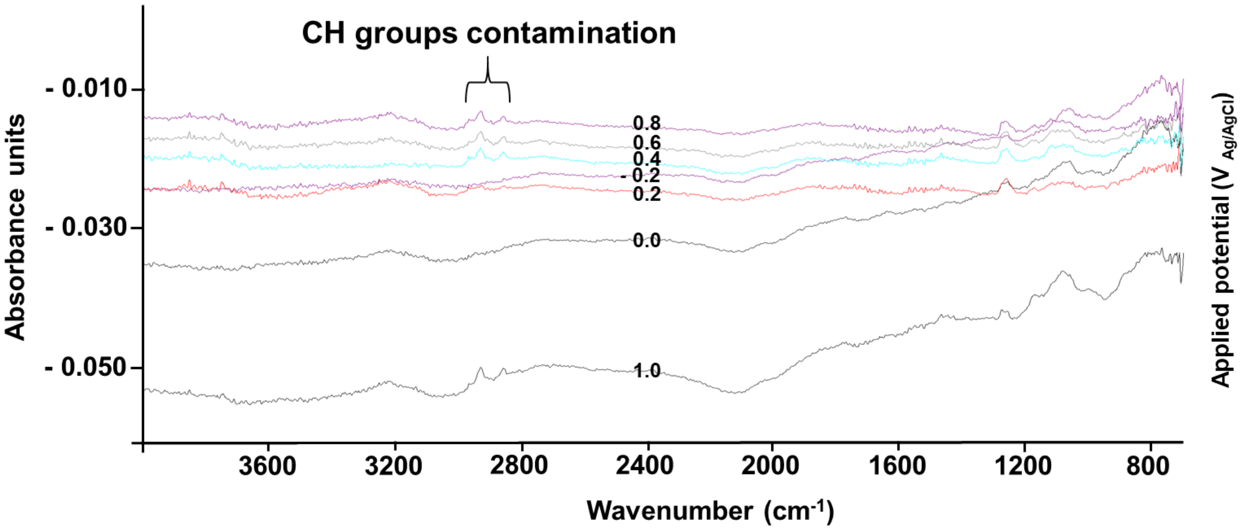

Figure 56. FT-IR spectra of a gold sample surface polarized from -0.2 until 1.0 V using 0.1 mol L^{-1} $NaClO_4$ solution as electrolyte and spectrometer aperture configured to 4.0 mm.

As can be observed in Figure 56, increasing the spectrometer aperture value from 2.0 to 4.0 mm did not achieve an expected better signal increase, instead, the signal amplitude for bands correlated to water molecules was lower than observed in Figure 54. Furthermore, increasing the aperture value also increases more absorbance from the sample surroundings, which could contribute for more contamination signals. The bands at approximately 2931 and 2850 cm^{-1} can be attributed to CH groups (stretching modes).[64]

The spectra region below 800 cm^{-1}, in both last figures, can be explained by the relatively low single beam spectra signals, as presented in Figure 57.

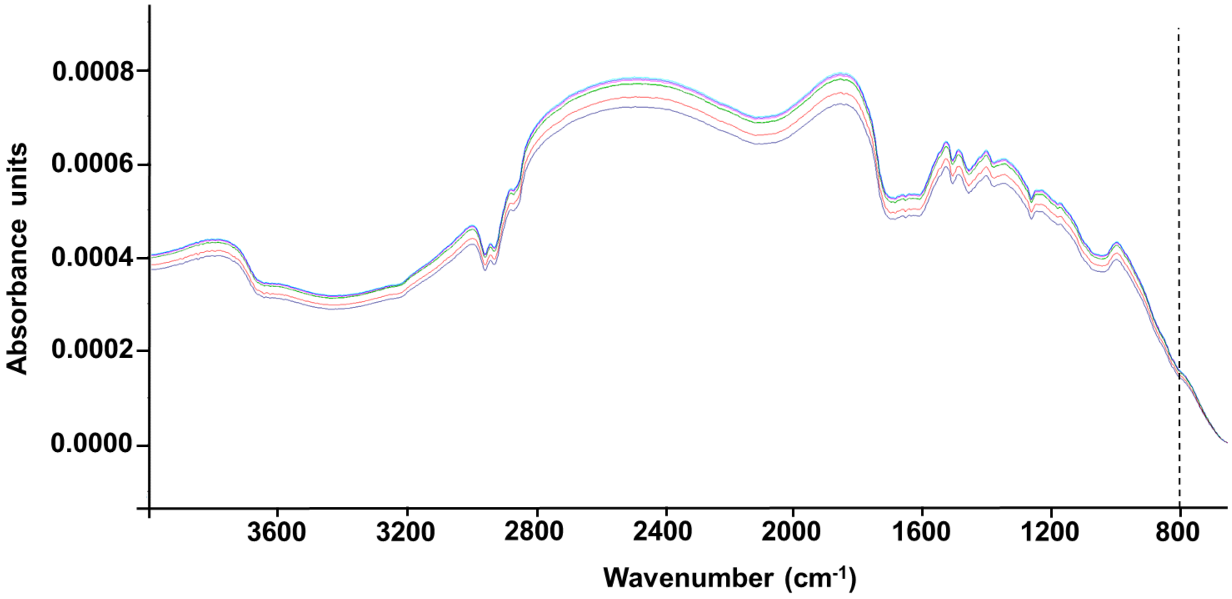

Figure 57. Single beam spectra of a gold sample surface polarized from -0.2 until 1.0 V using 0.1 mol L^{-1} $NaClO_4$ solution as electrolyte.

These single beam spectra show relatively low intensities below 800 cm^{-1} when compared to the other wavenumbers (4000 – 800 cm^{-1}). This could explain the high “noise” signal at the FT-IR spectra below 800 cm^{-1}. One solution to reduce this noise of the FT-IR spectra in that range could be to increase the measuring time, however this was not done in this study, since the most important spectra regions here are the ones related to the water molecule, which have a relatively good signal quality.

One important aspect to be considered during the FT-IR determinations is the time needed for a complete spectra acquirement, including the stepwise polarization and emersion (for example, from -0.4 until 1.3 V in intervals of 0.1 V, as will be presented in sections 4.4.1, 4.4.2 and 4,4,3). The whole experiment requires around four days, once the LN-MCT detector remains cooled for approximately 9 hours (measurement time available). In order to check the instrument stability during the different days (especially the detector), the following procedure was carried out: the last measurement of the prior day was repeated next day, without removing the sample from the chamber, as shown in Figure 58.

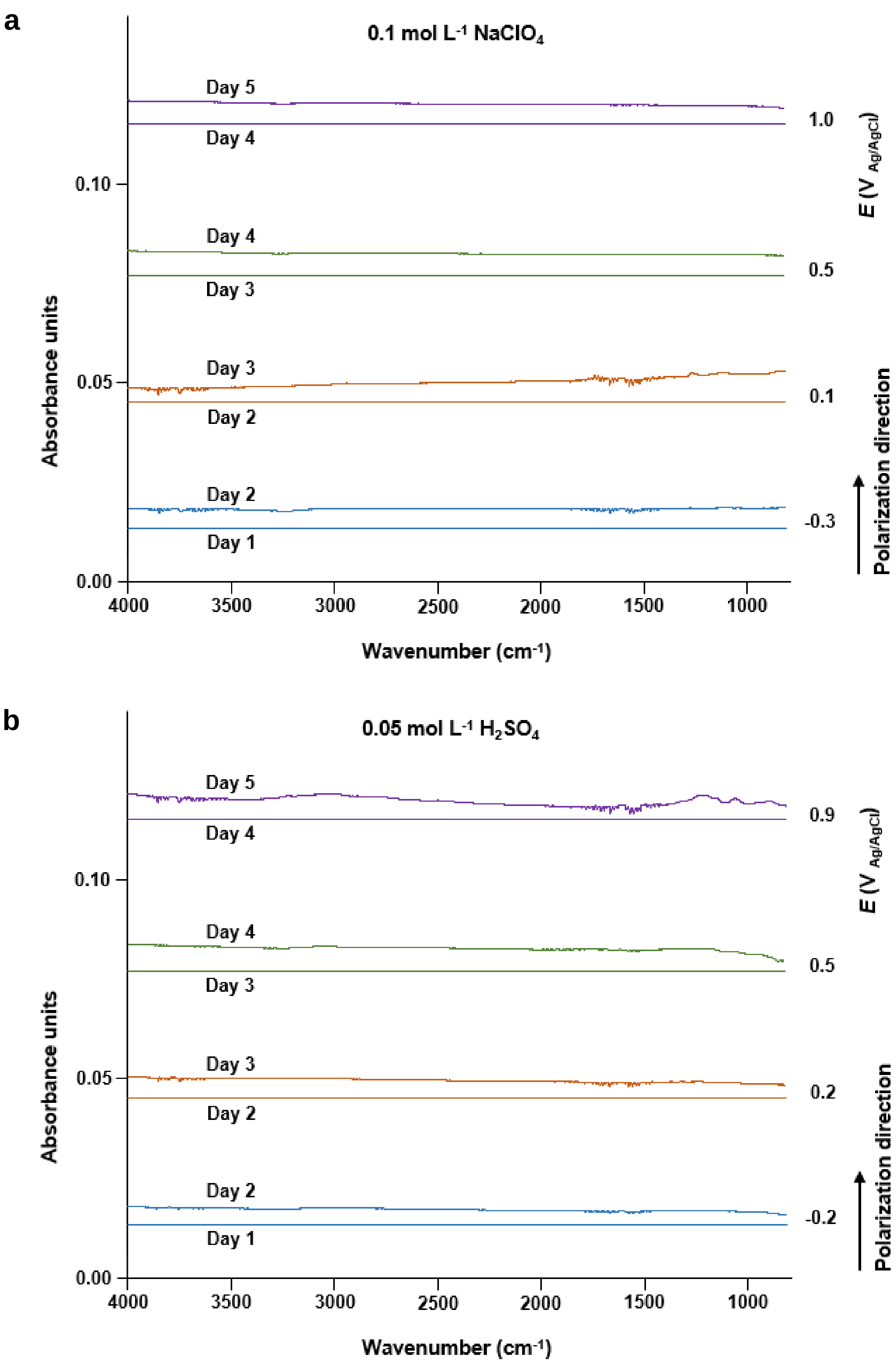

Figure 58. LN-MCT detector stability test experiment along 5 days. A gold sample

was polarized using a) 0.1 mol L^{-1} $NaClO_4$ and b) 0.05 mol L^{-1} H_2SO_4 solution as electrolyte. As reference the spectra from the previous day was employed (resulting in a perfect horizontal line, signaling high reproducibility and stability) and the next day spectra can be directly compared.

Comparing the results from two consecutive days in Figure 58, in general the detector shows high stability. Only in some cases minimal imperfections can be observed in the results; these could probably be related to noise. The small and sharper imperfections present in some spectra between 3500 – 4000 cm^{-1} and 1500 – 1800 cm^{-1} are probably originating from water vapor; as these measurements were done with dry nitrogen atmosphere slight variations in humidity had huge effects. For instance, after removing the sample from the electrochemical cell and blowing off, some water drops sometimes were found to be remaining on the sample surface (at the edges), which could have wet the sample holder. As soon the sample holder is introduced in the chamber, the water could be evaporated in the dry N_2 atmosphere and was detected by the FT-IR.

4.4.1 FT-IR spectra from gold surfaces employing $NaClO_4$ solution as electrolyte

The gold sample was polarized employing 0.1 mol L^{-1} $NaClO_4$ solution as electrolyte with the potentials stepped in positive (from -0.4 until 1.3 V) and in negative (from 1.3 until -0.4 V) directions in 0.1 V intervals. The atmosphere inside the analysis chamber was first set as “dry” N_2 (< 3% RH). In Figure 59 the spectra from these experiments are shown. The spectra shown in Figure 59 were obtained with the detector providing quite low signal intensities.

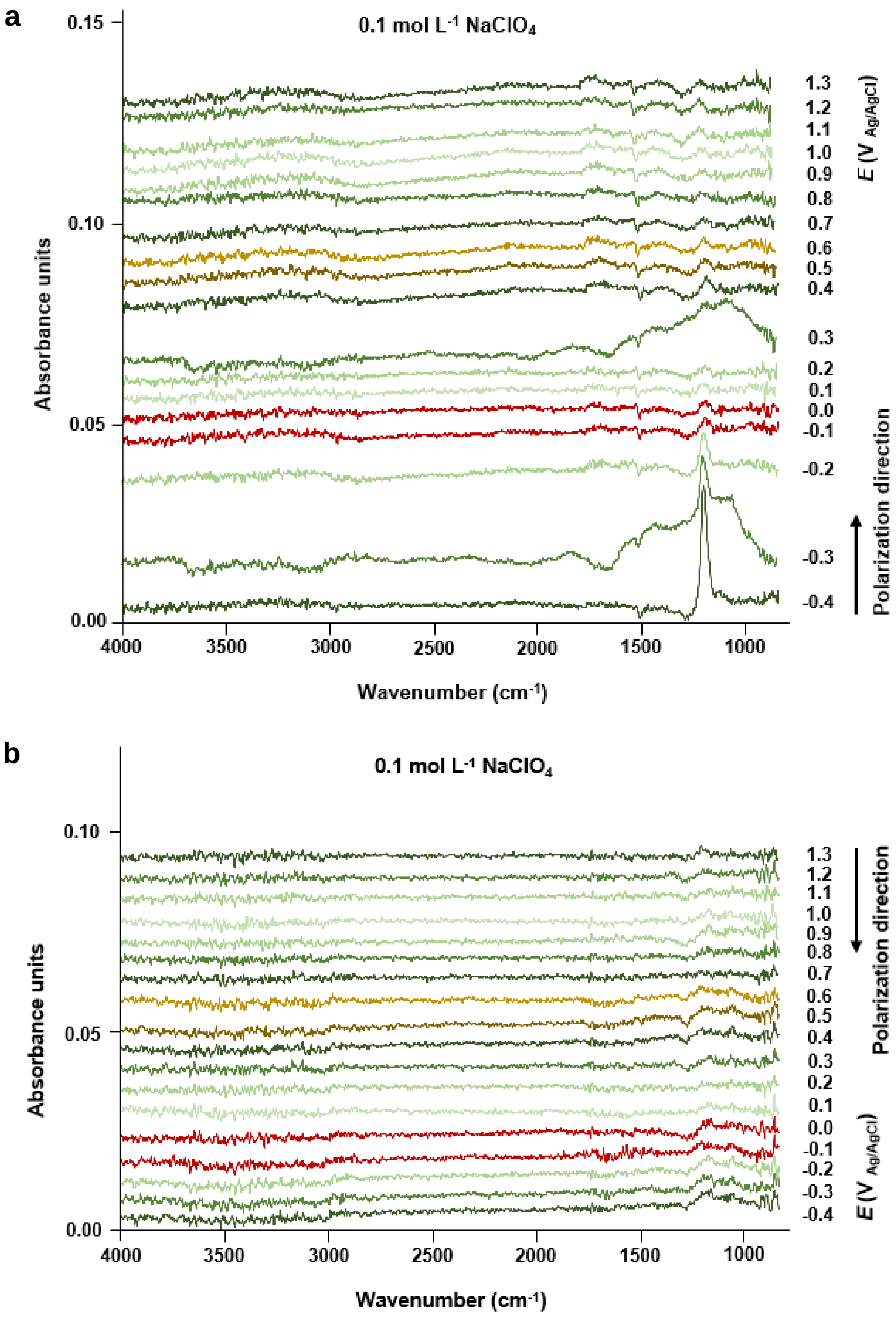

Figure 59. FT-IR spectra obtained on gold surface after polarizing the sample in 0.1

mol L^{-1} NaClO$_4$ solution with the potentials stepped in: a) positive and b) negative directions.

The spectra presented in Figure 59 were calculated by subtracting the background spectra, obtained on the fresh gold sample surface before took place the first immersion (“clean” sample). It is important to remark that even a clean sample freshly introduced into the system could have some adsorbed water molecules coming from the atmosphere due the transportation and transferring to the system, before it was introduced to a controlled atmosphere condition (more details on this will be discussed in section 4.5, on the results obtained by ellipsometry). The spectra in red colors represent the potential region of the possible PZC value (as discussed in section 4.2.2). Peaks/bands around 1030 – 1240 cm^{-1} in Figure 59a) can be attributed to the perchlorate anion. This wavenumber interval was reported for perchlorate ion adsorbed on gold surfaces, under immersed as well as emersed conditions.[67,119] As mentioned previously in section 2.11, many reports in the literature suggest a weak adsorption of perchlorate ions on gold surfaces at potentials more positive than the PZC.[67,86,87]

The spectra obtained on the sample polarized stepwise in positive direction show more pronounced peaks than the ones obtained when polarization occurred into the negative direction.

Striking are the very intense peaks/bands obtained after polarization into positive direction at -0.4, -0.3 and -0.2 V vs Ag/AgCl, i.e., at potentials more negative than the PZC (represented by red color spectra). It is unclear why so high intensities that clearly seem to be related to perchlorate are observed here. Such significant adsorption is certainly not expected for the negative perchlorate anion on the negatively charged surface. Quite notable is the sharp peak at around wavenumber 1160 cm^{-1}, which is also almost identical with literature reports.[67,119] This perchlorate peak is due Cl-O stretch vibration.[119] Also striking is that at potentials more positive than the PZC the perchlorate peak is much less intense. This will be further discussed below. When the potentials were stepped in negative direction (Figure

59b)), no relevant changes along the different potentials were observed in the waveband region correlated to the perchlorate anion at the 1030 – 1240 cm^{-1} region.

With reference to bands related to water molecules (OH stretching between approximately 3800 – 3000 cm^{-1}), Figure 59b) shows a negative-going behavior at potentials more negative than the PZC, suggesting some change on the water vibrational properties.[67] This effect was not clearly observed in the same spectral region in Figure 59a), although also there negative going intensities are observed below PZC and positive going ones above PZC, with no clear tendency of further increase when the potentials were stepwise increasing to higher potentials. As mentioned before (section 4.4), the instrumentation set-up could play a role in the low intensities observed.

Besides the water bands also the perchlorate peaks around 1030 – 1240 cm^{-1} in Figure 59a) are especially at potentials higher than the PZC not very clear, i.e. the overall quality of the spectra seems to be quite low. Therefore, it was tried to optimize the alignment of all components in order to obtain less noisy data. Thus results with higher intensity were obtained (for the region attributed to perchlorate peaks). Typical results are presented in Figure 60. In Figure 60b) the spectra from Figure 60a) were replotted by employing the 0.0 V (PZC region) spectra as reference. This procedure was carried out in order to achieve a better visualization of changes in the spectra below and above the PZC region.

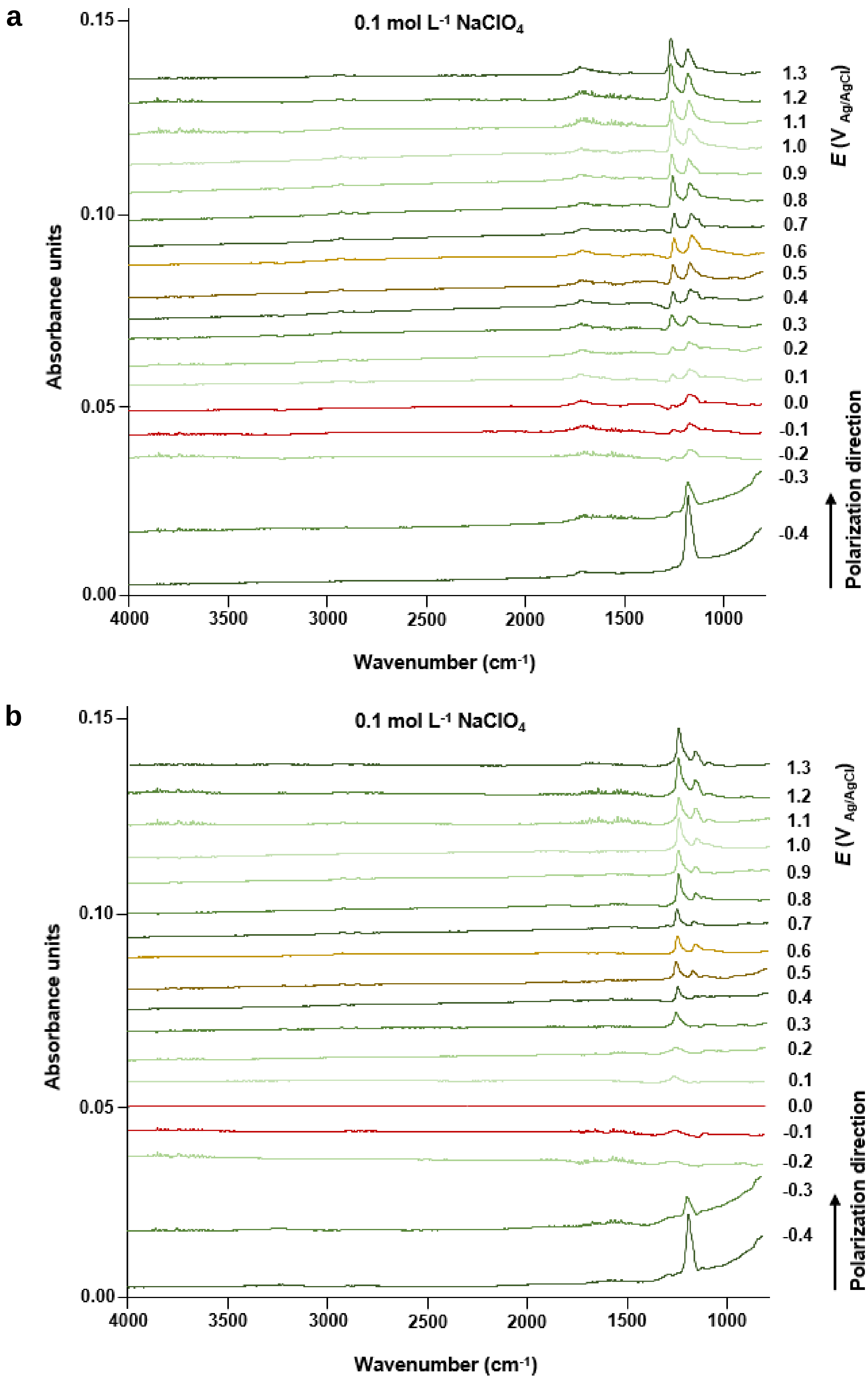

Figure 60. FT-IR spectra obtained on gold surface after polarizing the sample in 0.1

mol L^{-1} $NaClO_4$ solution with the potentials stepped in positive direction. As reference spectra were used: a) spectra of clean sample (background) and b) spectra obtained after emersion from 0.0 V (PZC region).

The spectra depicted in Figure 60 appear much less noisy. Most notably, the spectra between 1000 and 1500 cm^{-1} exhibit two distinguished and very sharp peaks around 1160 and 1240 cm^{-1}, which can be probably attributed to perchlorate ions, as already discussed above. Above PZC, the peak around 1240 cm^{-1} in Figure 60a) shows an increase in intensity for increasing potentials. Regarding the spectra more negative than the PZC (Figures 60a) and 60b)), especially for -0.4 and -0.3 V, an intense perchlorate peak can be seen at 1160 cm^{-1}.

This peak, but much smaller, is also observed above PZC where it systematically growing alongside the peak at 1240 cm^{-1}. Such split perchlorate peak was not reported in the literature yet. However, so far the reports on FT-IR spectra of perchlorate on gold were either restricted to immersed conditions or for emersion into very high humidity.[67,119] It is thinkable, that interaction with water at higher amounts of water in the double layer regions smears out this splitting. Again, striking is that at very low potentials, especially -0.4 V, the peak at 1160 cm^{-1} is the most intense (just as observed in the Figure 59), which then first decreases. At PZC it is still larger than the peak at 1240 cm^{-1}. Then it gets smaller. While this peak splitting could be caused by the electric field in the double layer region and the changes in the relative intensities by a possible reorientation of the molecule as a consequence of the changing field, the high intensity of the peak at very low potentials is difficult to understand. However, it was very reproducible on gold surfaces emersed from perchlorate electrolyte into nitrogen atmosphere of low humidity, i.e. dry atmosphere.

The bands attributed to water molecules around 3800 – 3000 cm^{-1} are more or less missing in these spectra (very low intensity, but also very low noise). However, around 1600 cm^{-1} some intensity could be identified. This is more visible in Figure 60a) and less in Figure 60b), i.e. no systematic differences for the different potentials can be identified here. In general, the water bands show very low intensity, which could be resulting from the low humidity inside the Kelvin probe/infrared beam chamber (1-3% RH) and the consequently low amount of adsorbed water. Notable, however, is that also the noise level in the range of the expected water bands is very low, indicating that it is unlikely that the water bands from water adsorbed on the surface are not visible because of higher contributions from the gas phase. Hence, very probably the water layer in this case is in the sub-monolayer range (as will be discussed further on the basis of the results obtained by ellipsometry, section 4.5).

Figure 61 shows corresponding spectra to Figure 60, but now from the experiments with the potentials stepped in negative direction.

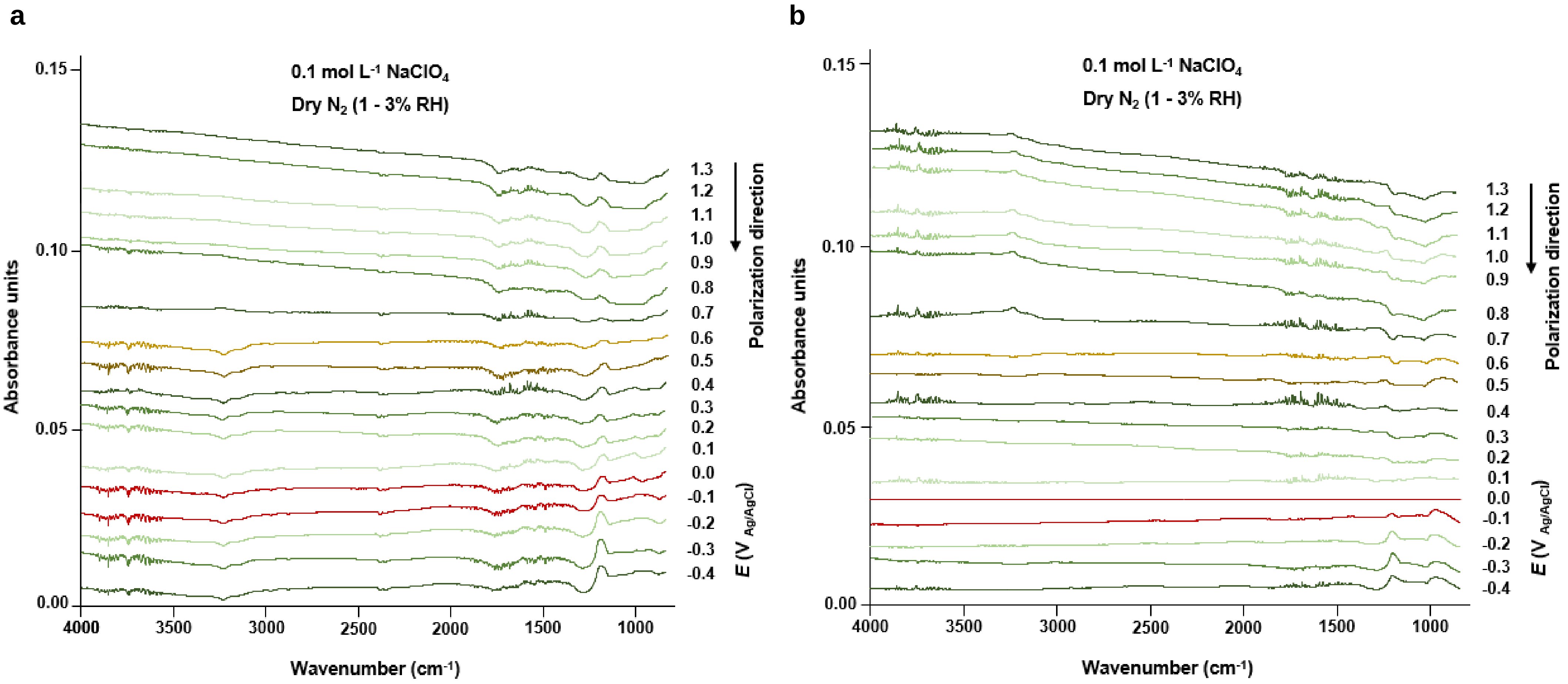

Figure 61. FT-IR spectra obtained on gold surface after polarizing the sample in 0.1 mol L^{-1} $NaClO_4$ solution with the potentials stepped in negative direction. As reference spectra were used: a) spectra of clean sample (background) and b) spectra obtained after emersion from 0.0 V (PZC region).

As in the spectra shown in Figure 60, peaks attributed to perchlorate around 1240 – 1030 cm^{-1} are present in the spectra shown in Figure 61. These peaks show lower signal intensities (height of the peaks) than for the spectra obtained for stepwise polarization in the positive direction, especially the 1240 cm^{-1} peak compared to the spectra in Figure 60 is missing, i.e. no splitting is observed here. Only the 1160 cm^{-1} peak appears here. Above PZC not much changes are observed, indicating a strong specific adsorption of the perchlorate, exceeding the effect of anions necessary as counter anions in the double layer.

4.4.2 FT-IR spectra from gold surfaces employing H_2SO_4 solution as electrolyte

The gold sample was also polarized employing 0.05 mol L^{-1} H_2SO_4 solution as electrolyte with the potentials stepped in positive (from -0.4 until 1.3 V) and in negative (from 1.3 until -0.4 V) directions in 0.1 V intervals before emersion. The atmosphere inside the analysis chamber was again set as “dry” N_2 (< 3% RH). In Figure 62 spectra obtained from these experiments are shown. The spectra shown in Figure 62 and 63 were obtained with the detector presenting low signal intensities.

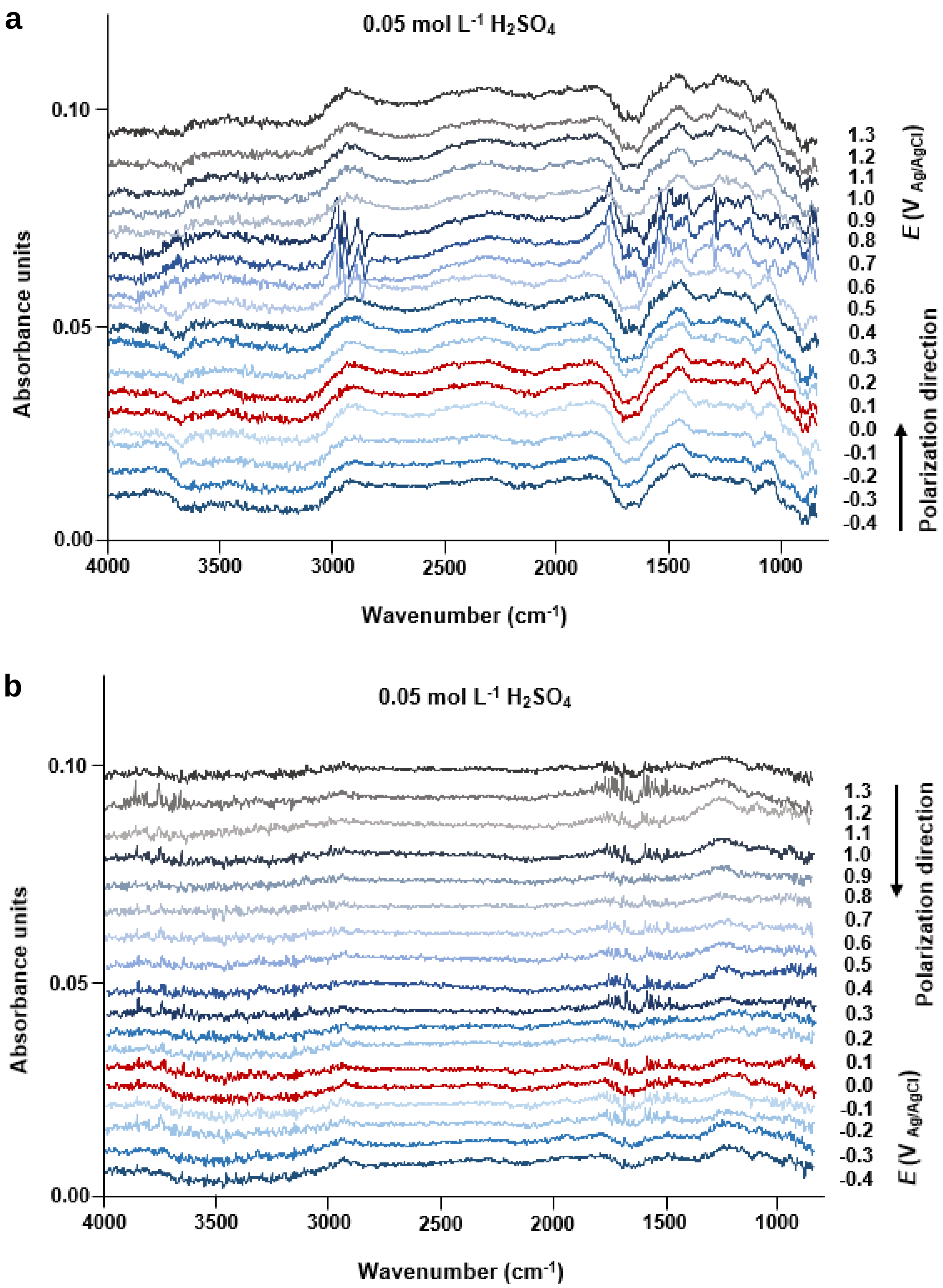

Figure 62. FT-IR spectra obtained on gold surface after polarizing the sample in 0.05 mol L^{-1} H_2SO_4 solution with the potentials stepped in: a) positive and b) negative directions.

In the same way as for the $NaClO_4$ experiments, the spectra from Figure 62 were recalculated employing the 0.1 V (PZC region) results as reference. This procedure was also carried out in order to improve a better visualization of changes in the spectra below and above the PZC region. These recalculated spectra are presented in Figure 63.

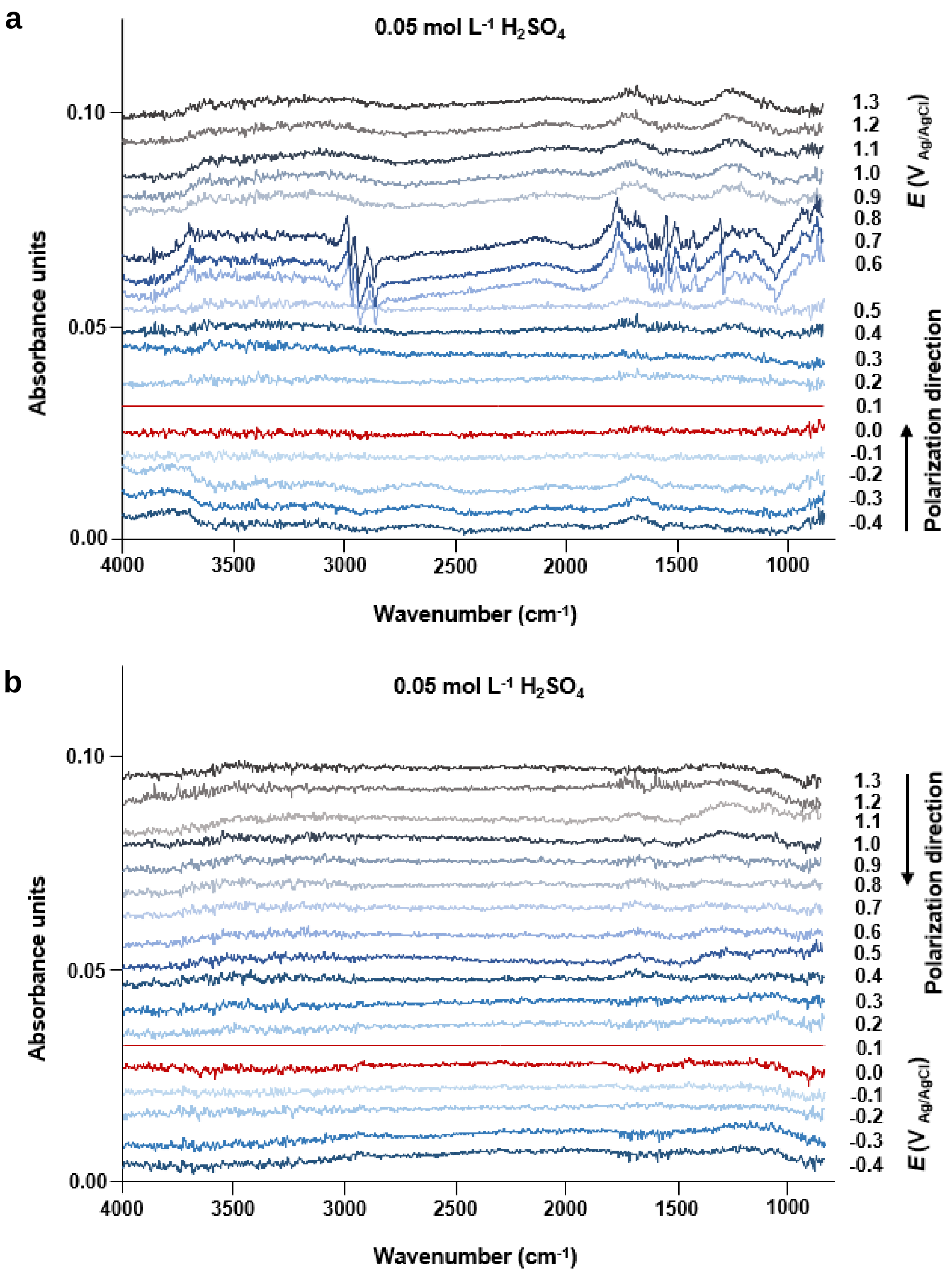

Figure 63. FT-IR spectra obtained on gold surface after polarizing the sample in 0.05 mol L^{-1} H_2SO_4 solution with the potentials stepped in: a) positive and b) negative

directions. Same data as used for Figure 62 above, but as reference were employing the 0.1 V (PZC region) spectra.

The spectra presented in Figure 63 were calculated in the same way as mentioned previously in section 4.4.1 and the spectra in red colors represent the potential region of the possible PZC value (also mentioned previously in section 4.2.2). Around this potential region it is possible to notice a change in the intensities related to water bands (OH stretching between approximately 3800 – 3000 cm^{-1}), especially for the spectra obtained by stepwise polarizing into the positive direction (Figure 63a)); around 3750 cm^{-1} the bands start to decrease at potentials lower than the PZC and to increase at potentials higher than the PZC. This change of vibrational bands of the water molecule around the PZC value was expected and can be attributed to the interfacial water reorientation.[67] When the potentials were stepped in negative direction (Figure 63b)), this behavior was not so pronounced, although there is a slight tendency of the absorption band between approximately 3800 – 3000 cm^{-1} to get "flatted" at potentials more positive than the PZC value.

Measuring infrared spectra from aqueous electrolytes is not a simple task; some adjustments are needed, such as choosing the correct window material to assure compatibility with vapors coming from the liquid, especially if the electrolytes are corrosive, such as acids. When trying to obtain information on sulfate related bands for comparison with the spectra obtained here, this has to be considered. Generally, infrared spectra/wavenumbers corresponding to sulfate are often from crystals, such as sodium and potassium sulfate, for example.[120] The authors assign infrared antisymmetric stretching vibrations to sulfate between approximately 1172 – 1120 cm^{-1} and symmetric stretching vibrations between 1100 – 1000 cm^{-1}, depending on the crystal.[120] These values were chosen for comparison with the results obtained here. With respect to vapor of substances containing sulfate, such as H_2SO_4 vapor, reports suggest infrared vibrations assigned to H_2SO_4 around 1222 and 1465 cm^{-1} (symmetric and antisymmetric stretching, respectively).[121] Hence, the bands observed in Figure 63a) around 1080 – 980 cm^{-1} and around 1480 – 1360 cm^{-1} could be probably assigned to sulfate anions. Similarly, as for the electrodes emersed form perchlorate electrolyte, there seem to be more changes in positive direction that in negative direction. This could be explained by the presence of more specific adsorption of anions when decreasing the potential stepwise form high potentials into the negative direction. However, for the case of sulfate the peaks are much less resolved here.

The nature of the unusual sharp peaks from 0.6 until 0.8 V around 3000 – 2800 and 1800 – 1640 cm^{-1} in Figure 63a) compared to the other spectra is not clear. Due the long time needed for a complete analysis, i.e., for the measurement of all spectra from -0.4 until 1.3 V and the refiling of the LN-MCT detector after approximately 9 hours measurement time, it is only possible to finish the complete analysis sequence after some days. In this sense, the measurement on different days could here play some influence in the results (as explained in section 4.4 for the detector stability). Another plausible explanation could be the presence of CH groups (approximately 2931 and 2850 cm^{-1})[64]; this contamination could be resulting from the organic compounds present in the conductive silver paint employed on the sample surface corner for the electrical contact with the sample holder during the polarization procedure. But these should have had no contact with the electrolyte.

Comparing the spectra for potentials stepped in negative direction (Figure 61b) with 0.1 mol L^{-1} $NaClO_4$ and Figure 63b) with 0.05 mol L^{-1} H_2SO_4 solutions as electrolyte), similar behavior could be observed in the 3800 – 3000 cm^{-1} region corresponding to water molecule OH stretching.

As mentioned in section 4.4, spectra bellow 800 cm^{-1} present relatively higher noise than spectra between 4000 – 800 cm^{-1}; in one experiment, however, it was possible to perform vibrational assignments around 770 – 620 cm^{-1}, which could be perfectly identified. These results are presented in Figure 64 and are attributed to sulfate anions.

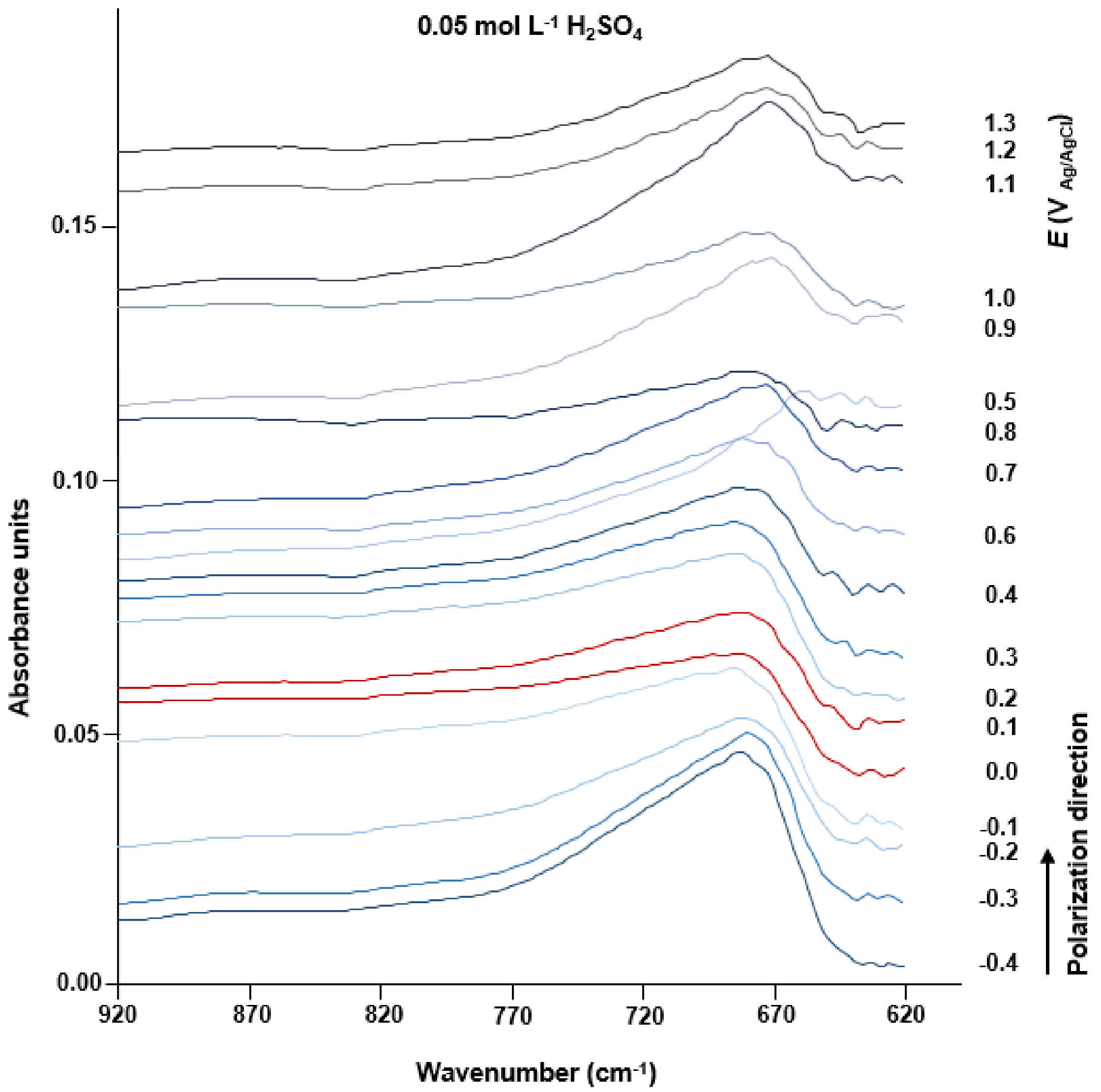

Figure 64. FT-IR spectra presenting the sulfate vibrational assignments around 770 – 620 cm^{-1} obtained on gold surface after polarizing the sample in 0.05 mol L^{-1} H_2SO_4 solution with the potentials stepped in positive direction.

The results presented in Figure 64 show a quite clear signal around 680 cm^{-1}, which can be assigned to sulfate. In the literature many vibrational assignments between 637 – 736 cm^{-1} related to sulfate anions in different crystals are suggested, such as Na_2SO_4 and K_2SO_4.[120] Beside the presence of sulfate anions, the spectra also demonstrate similar behavior as the presented by the perchlorate peak (1160 cm^{-1}) in Figure 60a), i.e., higher intensities for negative potentials, specially at -0.4

and -0.3 V, which could probably be associated to some chemisorption process. For most of the potentials more positive than the PZC value, the correspondent spectra present higher intensities, like observed for perchlorate at 1240 cm^{-1} in Figure 60a). Only the spectra corresponding to 0.5 V in this experiment does not fit in with the ones obtained after polarization at all other potentials. It is unclear what went wrong in that case. A peak splitting is not observed, but there seems to be a shift towards lower wavenumbers at very positive potentials.

Likewise, as for the measurements with perchlorate, results with higher intensity were obtained than shown in Figure 62 and 63. These are shown in Figure 65. The same spectra from Figure 65a) were recalculated employing the 0.1 V (PZC region) results as reference. This procedure was carried out in order to achieve a better visualization of changes in the spectra below and above the PZC region.

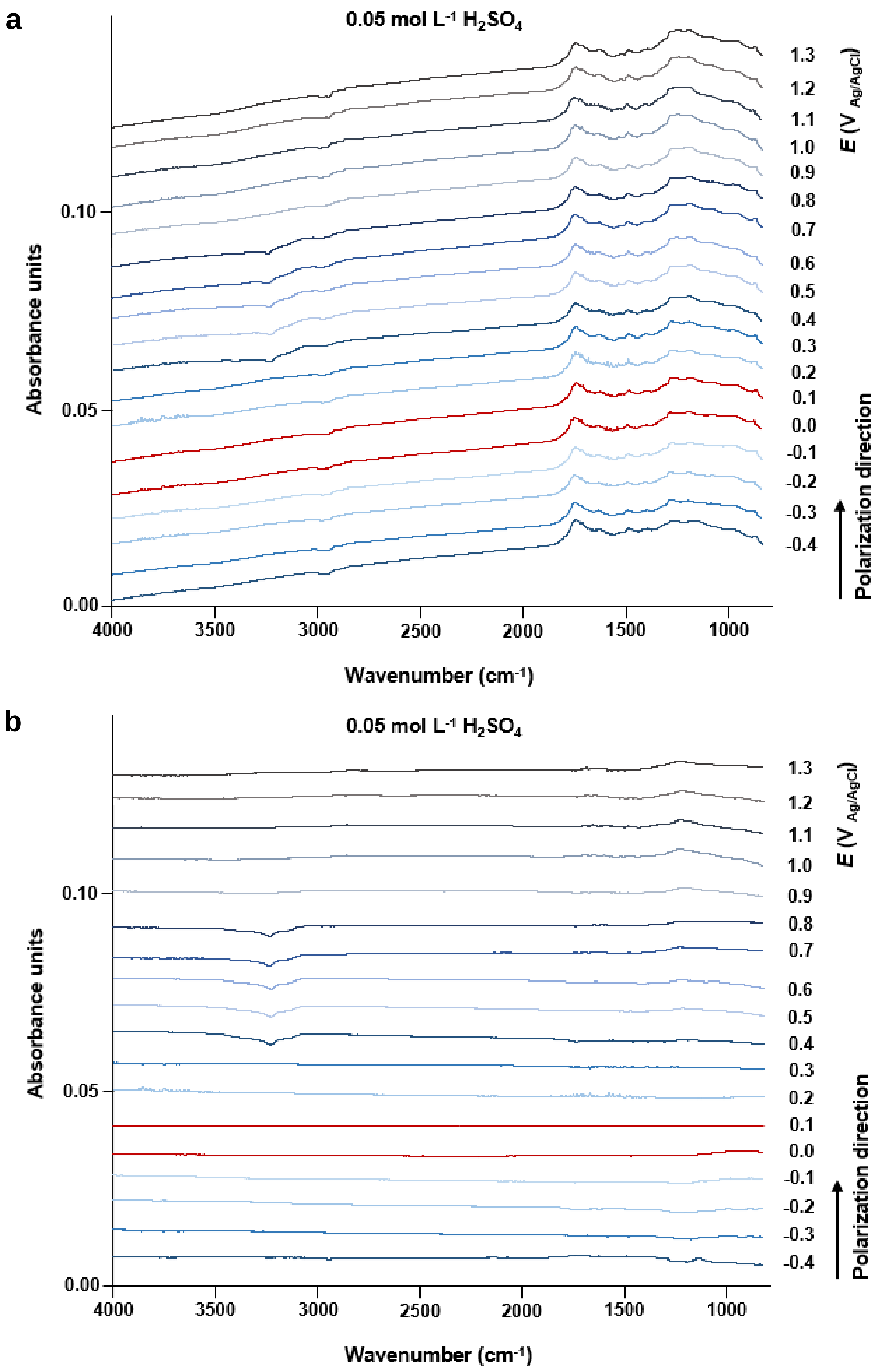

Figure 65. FT-IR spectra obtained on gold surface after polarizing the sample in 0.05

mol L^{-1} H_2SO_4 solution with the potentials stepped in positive direction. As reference spectra were used: a) spectra of clean sample (background) and b) spectra obtained after emersion from 0.1 V (PZC region).

Again, above PZC the peak associated with sulfate is slightly increasing for increasing potentials. The assignment for the pronounced peak at around 1700 cm^{-1} is not certain. It is also reported in literature. According to the authors, this peak is not due to water.[119]

Figure 66 shows spectra from the experiment with the potentials stepped in negative direction. The same spectra from Figure 66a) were also recalculated employing the 0.1 V (PZC region) results as reference.

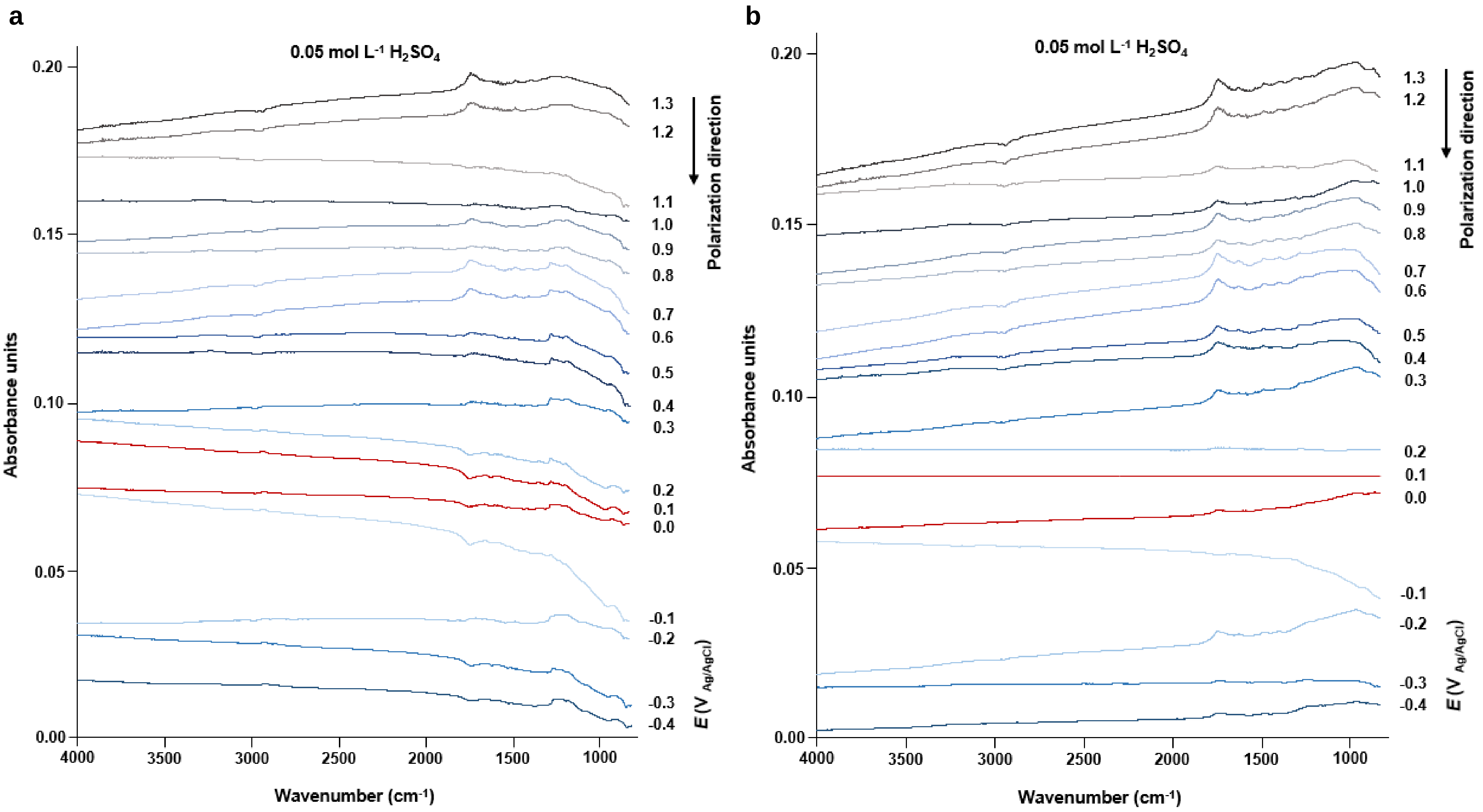

Figure 66. FT-IR spectra obtained on gold surface after polarizing the sample in 0.05 mol L^{-1} H_2SO_4 solution with the potentials stepped in negative direction. As reference spectra were used: a) spectra of clean sample (background) and b) spectra obtained after emersion from 0.1 V (PZC region).

In the spectra shown in Figure 66 the peak around 1700 cm^{-1} is also present like in the spectra shown in Figure 65. Now, however, it is clearly showing a remarkable change in the intensity (upwards) for increasing potentials more positive than the PZC.

In sum, concerning adsorbed water, for electrodes emersed from the sulfuric acid electrolyte quite similar observations are made as for the ones emersed form perchlorate: the amount of adsorbed water seems to be very low. Hence, also emersion into higher humidity was investigated. Also, above PZC anions seem to increase in amount for increasing potentials when the potential is stepped in positive direction. For negative direction much smaller changes are observed with change of the potential.

4.4.3 FT-IR spectra from gold surfaces emersed into humid atmosphere

Also experiments on electrodes emersed into humid atmosphere inside the infrared beam chamber were carried out. The gold sample was polarized employing 0.1 mol L^{-1} $NaClO_4$ and 0.05 mol L^{-1} H_2SO_4 solutions as electrolyte with the potentials stepped in positive (from -0.4 until 1.3 V) direction in 0.1 V intervals. The atmosphere inside the analysis chamber was set as “wet” N_2 (65-70% RH). In Figure 67 spectra from experiments with 65-70% RH employing $NaClO_4$ electrolyte are shown. These were obtained with the detector providing low signal intensities.

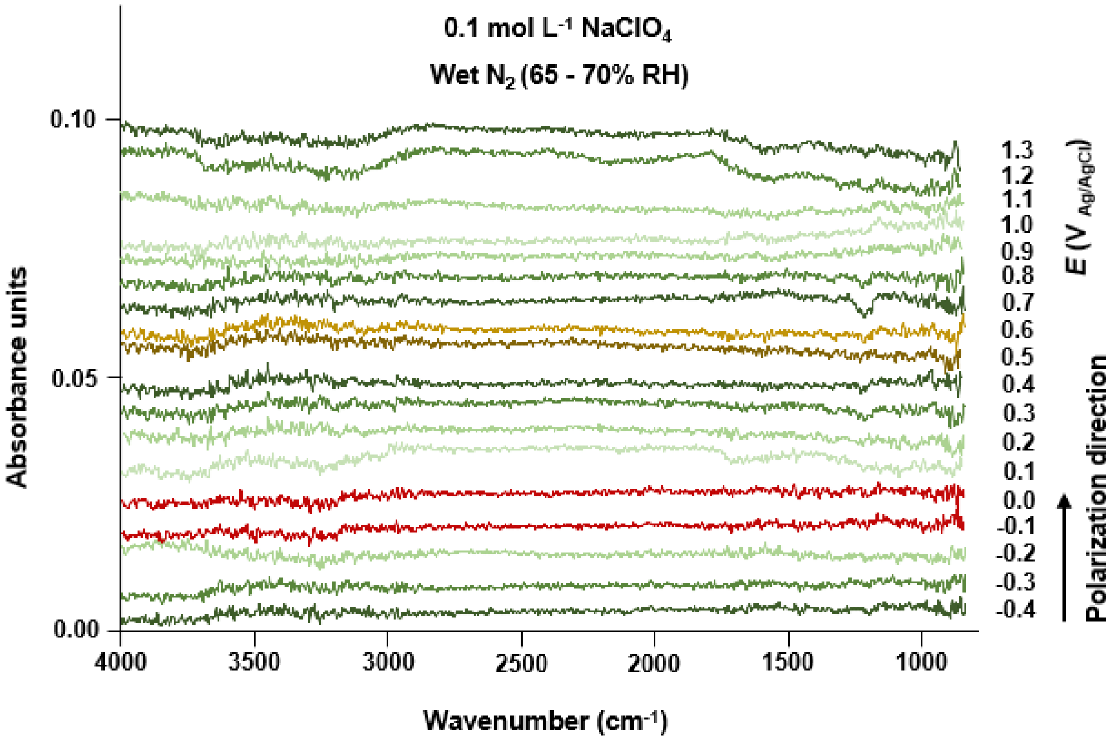

Figure 67. FT-IR spectra obtained on emersed gold surface after polarizing the sample in 0.1 mol L^{-1} $NaClO_4$ solution with the potentials stepped in positive direction. The atmosphere inside the analysis chamber was set to humid N_2 (65-70% RH).

The spectra presented in Figure 67 were calculated in the same way as mentioned previously in the last two sections and the two spectra in red color represent the potential region of the possible PZC value. The water spectral region from 3800 – 3000 cm^{-1} in Figure 67 shows a “flat” profile around the PZC value; potentials more positive than 0.0 V presented this region as positive-going (at least until 1.0 V). This could be an evidence for water molecules reorientation at potentials more positive than the PZC value as mentioned in previous discussions involving the FT-IR results in this dissertation. Although in this experiment was employed $NaClO_4$ as electrolyte, the peaks/bands around 1030 – 1240 cm^{-1} related to perchlorate anions were not pronounced in the results obtained with the electrode emersed from aqueous $NaClO_4$.

This experiment in humid atmosphere was also repeated with potentials stepped in positive direction (between -0.4 and 0.6 V) with higher intensity, see Figure 68.

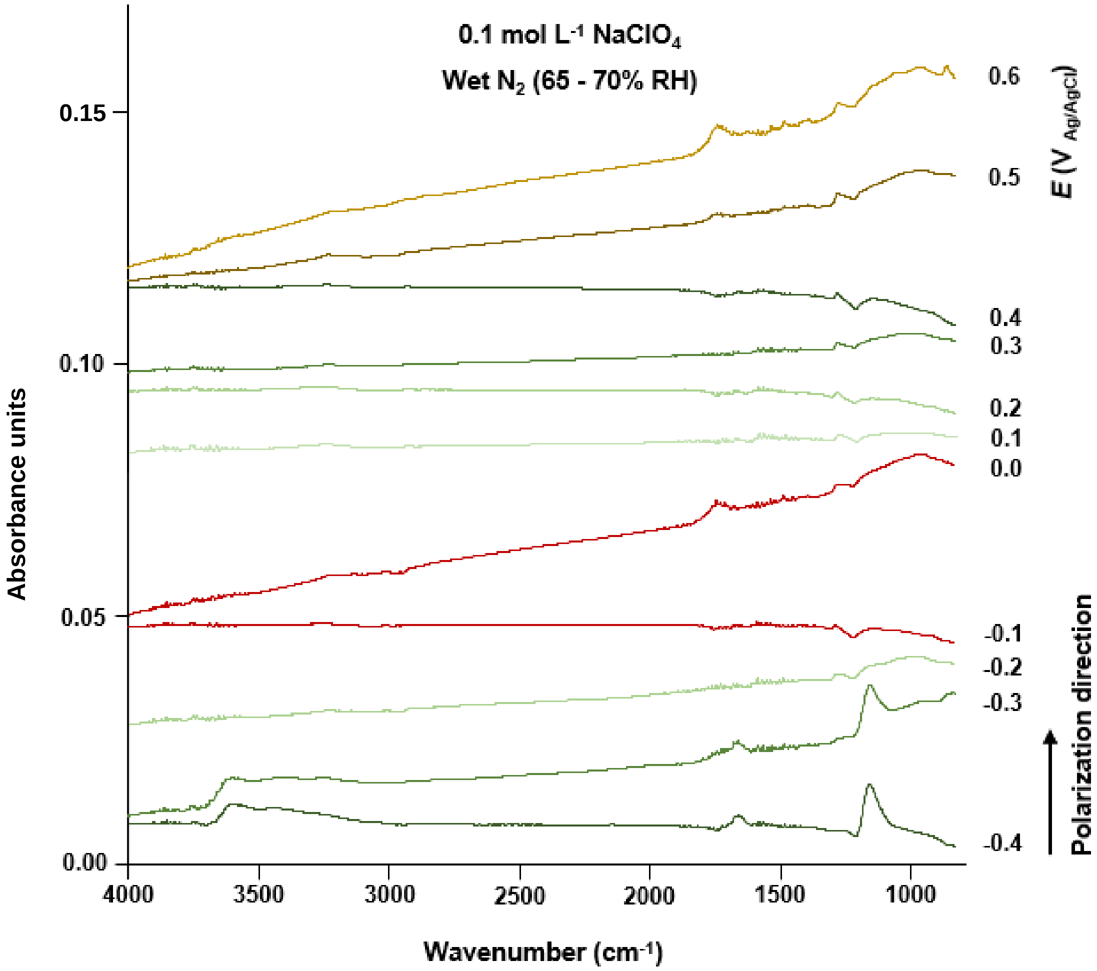

Figure 68. FT-IR spectra obtained on emersed gold surface after polarizing the sample in 0.1 mol L^{-1} $NaClO_4$ solution with the potentials stepped in positive direction (between -0.4 and 0.6 V). The atmosphere inside the analysis chamber was set to humid N_2 (65-70% RH).

The spectra around PZC (-0.1 and 0.0 V) present different profile (i.e. underlying slope); therefore, it is difficult to employ these spectra as reference (as was done so for the spectra so far). However, it is clearly visible that the spectra in Figure 68 shown the same pronounced peaks related to perchlorate at -0.4 and -0.3

V as in Figure 59a) and 60a). Furthermore, also here the perchlorate peak shows the splitting that was already seen in dry atmosphere (see Figure 60), but not so well pronounced and of lower intensity. Water bands are not well visible here. However, the pronounced peak at around 1700 cm^{-1} as discussed already above is again visible.

Sulfuric acid also was used as electrolyte in the FT-IR experiments in humid atmosphere. Figure 69 shows spectra from the experiment with the potentials stepped in positive direction. The same spectra from Figure 69a) were also recalculated employing the spectra obtained for emersion at 0.1 V (PZC region) as reference.

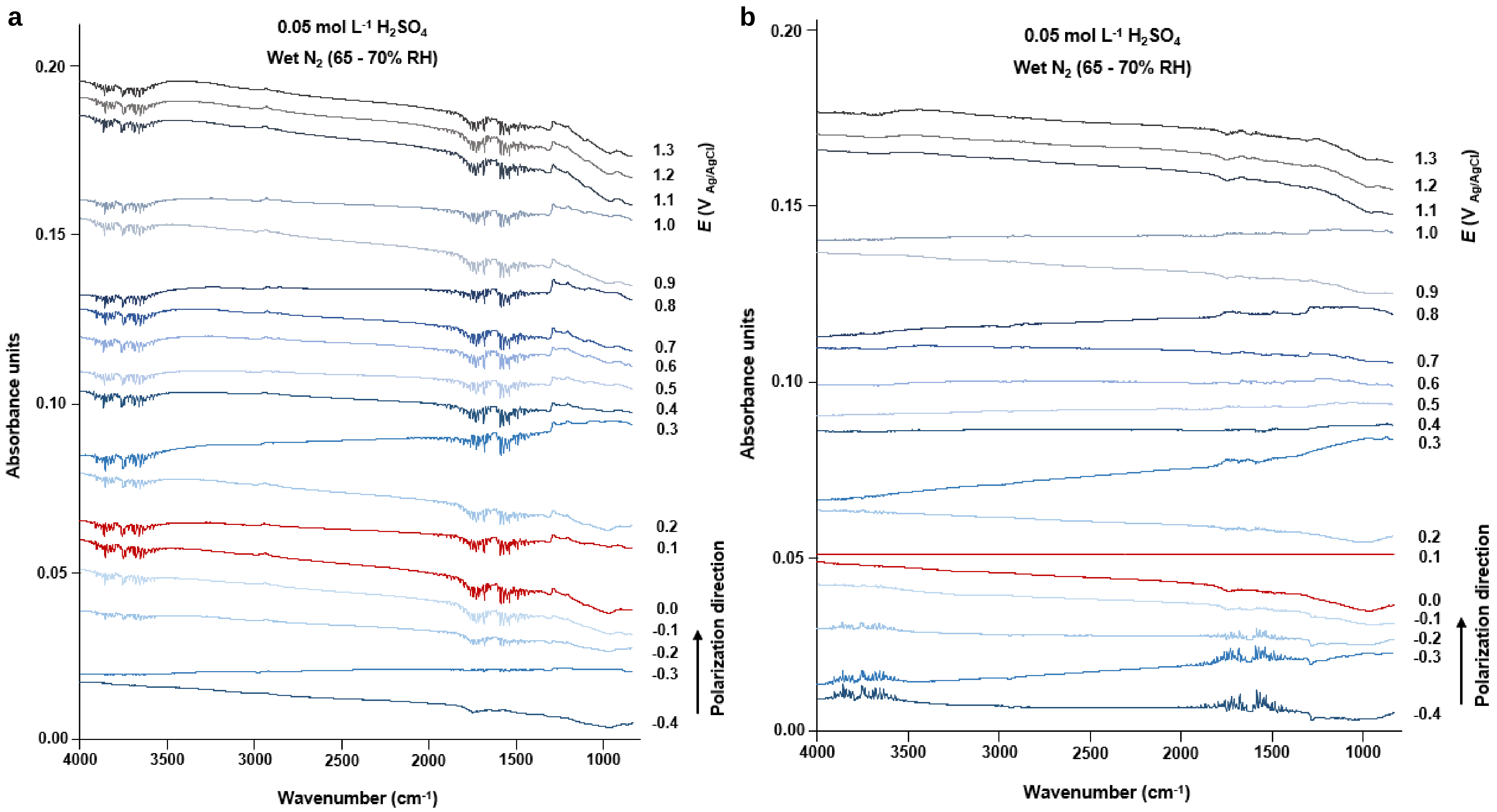

Figure 69. FT-IR spectra obtained on gold surface in humid atmosphere after polarizing the sample in 0.05 mol L^{-1} H_2SO_4 solution with the potentials stepped in positive direction. As reference spectra were used: a) spectra of clean sample (background) and b) spectra obtained after emersion from 0.1 V (PZC region).

The many sharp peaks around 4000 – 3500 cm^{-1} and 1800 – 1400 cm^{-1} shown in Figure 69a) are probably attributed to water vapor inside the FT-IR analysis chamber. This last spectral region with such sharp peaks was also reported in the literature and attributed to gaseous water.[119]

Comparing the results obtained by FT-IR measurements with the ones obtained by Kelvin probe, generally lower relative humidity conditions inside the chamber result in lower difference between potentials stepped in positive and in negative directions. This could be related to the low amount of water adsorbed on the emersed electrode in the dry atmosphere.

For higher relative humidity conditions, the potentials measured by Kelvin probe resulted in higher difference between potentials stepped in positive and in negative directions. This may be due to the higher amount of specifically adsorbed anions on the electrode when stepping the potential in the negative direction, in combination with higher amount of adsorbed water (see also Figure 39). While the difference in adsorbed anions could be confirmed by the FT-IR measurements, the information about the water molecules in the double layer region that could be derived from the FT-IR measurements was quite weak. Strangely, especially the spectra obtained at improved high intensity showed only little information about water.

4.5 Results obtained by ellipsometry

Ellipsometry measurements were performed in order to obtain information about the thickness of the water (electrolyte) layer at different relative humidity. For this, first calibration measurements (sample alignment and system check) were carried out with a SiO_2 reference wafer in different atmosphere conditions. The results of these calibrations are shown in Table 10.

Table 10. SiO_2 layer thickness determined by ellipsometry in N_2 atmosphere of different relative humidity.

N_2 atmosphere composition	SiO_2 layer thickness (nm)	Δ thickness between wet and dry conditions (nm)
1-3% RH	20.53 ± 0.021	-
65-70% RH	20.65 ± 0.025	0.12 ± 0.026
90-95% RH	20.70 ± 0.032	0.17 ± 0.036

The SiO_2 layer thickness results in Table 10 were obtained from three measurements for each atmosphere condition. According the manufacturer, the SiO_2 layer thickness on the reference/calibration sample varies significantly from wafer to wafer; 25 nm are provided by the manufacturer as the nominal thickness and the employed wafer in this dissertation may have SiO_2 thickness thinner or thicker than the nominal value (between 20 and 30 nm).[95] Hence, value of about 20 nm shown in Table 10 are in accordance with the range provided by the manufacturer. The thickness difference measured between wet and dry atmosphere conditions suggest an influence of the humidity, i.e., the higher the RH inside the analysis chamber, the larger the thickness of the water layer adsorbed on the SiO_2 surface.

Then a potential of 0.1 V was applied on the gold sample, while immersed in 0.1 mol L^{-1} $NaClO_4$ solution. The water layer thickness adsorbed on the emersed gold sample surface was then determined by ellipsometry in N_2 atmosphere of different relative humidity. As reference for this experiment a gold sample was flushed with electrolyte (in the electrochemical cell) without any polarization (i.e. at OCP) and analyzed in dry N_2 (1-3% RH) condition. This procedure was carried out in order to assure a clean gold surface as reference once the ellipsometry technique is very sensible. The results for the experiment after applying 0.1 V on the gold sample and emersing it from $NaClO_4$ electrolyte are shown in Figure 70 and the thickness was obtained from the calibration at 900.296 nm. The calculation was done using light incident angle of 68.9° from the sample surface normal vector.

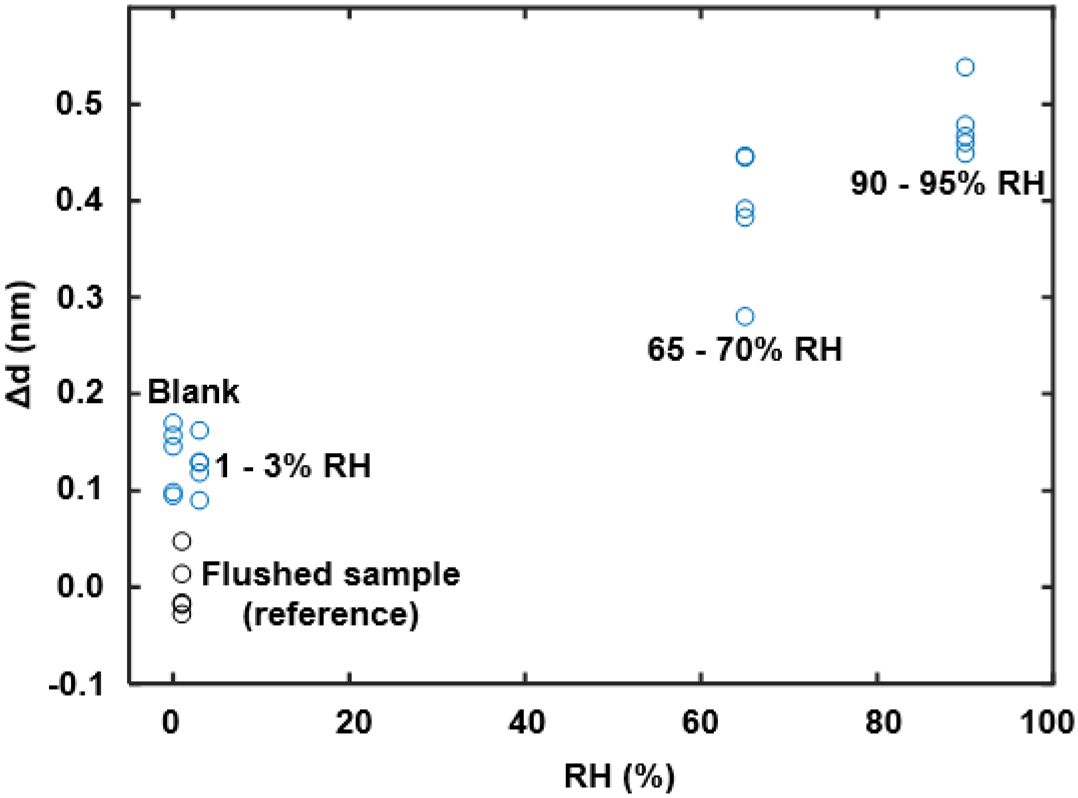

Figure 70. Thickness of the water layer adsorbed on gold surface after applying 0.1 V and emersion from 0.1 V. Prior to the measurements, the ellipsometry chamber was flushed for 24 h with N_2 atmosphere with following RH values: 1-3, 65-70 and 90-95%, which were thus maintained at high stability throughout the according measurement. It should be noted that while the relative difference of thickness obtained at different relative humidity is quite reliable, the value at 1-3 % RH is subject to high uncertainty, i.e. there might be an offset error.

The results shown in Figure 70 show a clear dependence of the water layer thickness on the relative humidity, namely an increase with increasing relative humidity. According to the widely accepted thickness of a water monolayer of about 0.286 nm (see Karslioğlu *et al.*[122]) at 1-3% RH the water layer thickness is roughly in the range of about a third to half monolayer, at 65-70% RH a bit above one monolayer and at 90-95% RH about 1.5 monolayers.

Hence at the dry condition (1-3% RH) the thickness of the water layer is probably in the sub-monolayer range. Unfortunately, it is difficult to obtain absolute thickness values in this experiment, as it is complicated to assure a perfect reference value. Hence, while the relative difference of thickness obtained at different relative humidity is quite reliable, the value at 1-3 % RH is subject to high uncertainty, i.e. there might be an offset error.

But interestingly, the values obtained here are in quite good agreement with the assumptions made for explaining the response of the potential measured by Kelvin probe on the emersed electrodes at different relative humidity.

4.6 Preliminary investigations by XPS

For this work also the use of the XPS and NAP-XPS system was planned. Furthermore, combining XPS with the other part of instrumentation (electrochemical cell, Kelvin probe and FT-IR) via an UHV suitcase for sample transfer was part of the laboratory concept, as explained in section 3.1.4. For the preliminary XPS the focused X-ray source of the NAP-XPS was used, which has only low power. Unfortunately, no satisfactory results were obtained. Hence, according measurements need further development work that could not be done anymore in this work.

4.7 Measurement of OCP after stopping polarization without removing the electrolyte from the electrochemical cell and after emersion and re-immersion of the sample

Measurements of the OCP after stopping the polarization were carried out in order to further assess the dynamics of the electrochemical double layer. These experiments were done in two different ways, employing 0.05 mol L^{-1} H_2SO_4 as electrolyte: first, a potential was applied and after the polarization (120 s), polarization was stopped and the OCP was measured for 10 min. Polarization was carried out at selected potentials (0.0, 0.3, 0.6 and 0.9 V vs Ag/AgCl) and applied in positive and in negative direction in order to observe if there might be some difference when the potentials are applied in both directions. This was done with the sample staying immersed. The second part of the experiment consisted in removing the electrolyte (emersing the sample) and after 60 s to refill the electrochemical cell again with electrolyte (re-immersing the sample). This part of the experiment was also conducted with potentials stepped in positive and in negative directions. Furthermore, an unpolarized sample was also analyzed (OCP of the just immersed sample without any prior polarization, in the electrolyte and after emersion and re-immersion). In Figures 71 – 74 the results for these experiments are shown.

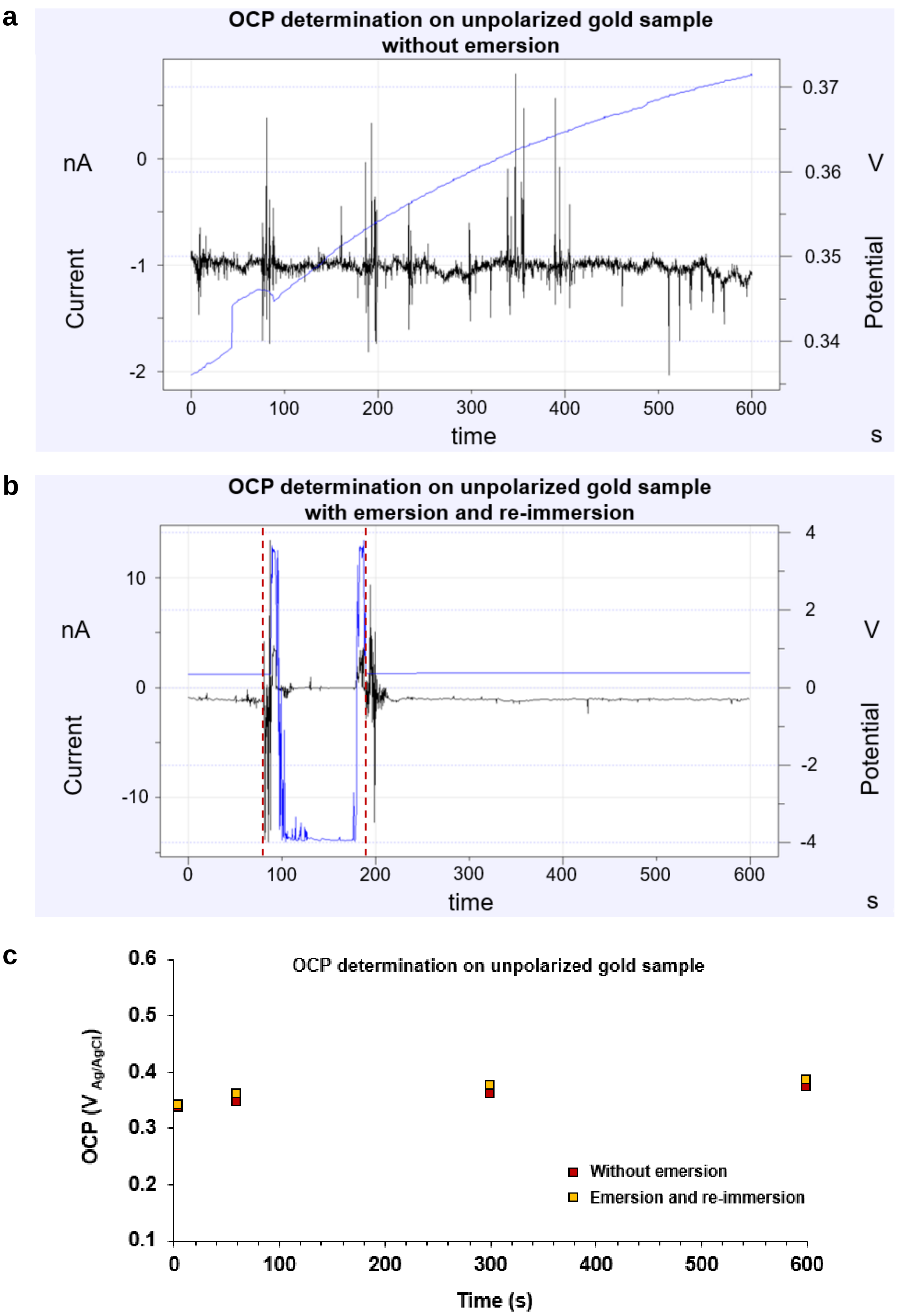

Figure 71. OCP measurement on the unpolarized gold sample: a) without emersion; b)

with emersion and re-immersion; c) after 5 or 10, 60, 300 and 600 s. The red dashed lines in b) represents the start of the emersion and re-immersion processes.

The results obtained with the unpolarized gold sample are presented in Figure 71. The potential shows a relative stable level in both evaluated situations, i.e., without emersing the sample and after emersing and re-immersing the sample. Thereafter, the sample was polarized and the OCP determined as explained previously; these results are presented in Figure 72. A similar potential is measured for the as-prepared sample in dry nitrogen atmosphere by Kelvin probe. It should be noted that the PZC is at about 150 mV lower and hence the non-polarized sample is positively charged. This could be due to oxygen adsorption on the surface. Although the electrolyte is purged by nitrogen and hence should be oxygen-free, this is thinkable as the sample was prior immersion transported through air. However, as will be seen in the following, the same potential was established on the samples polarized to significantly lower potentials after polarization was stopped. Hence, a prior polarization by oxygen cannot be the explanation for this OCP values.

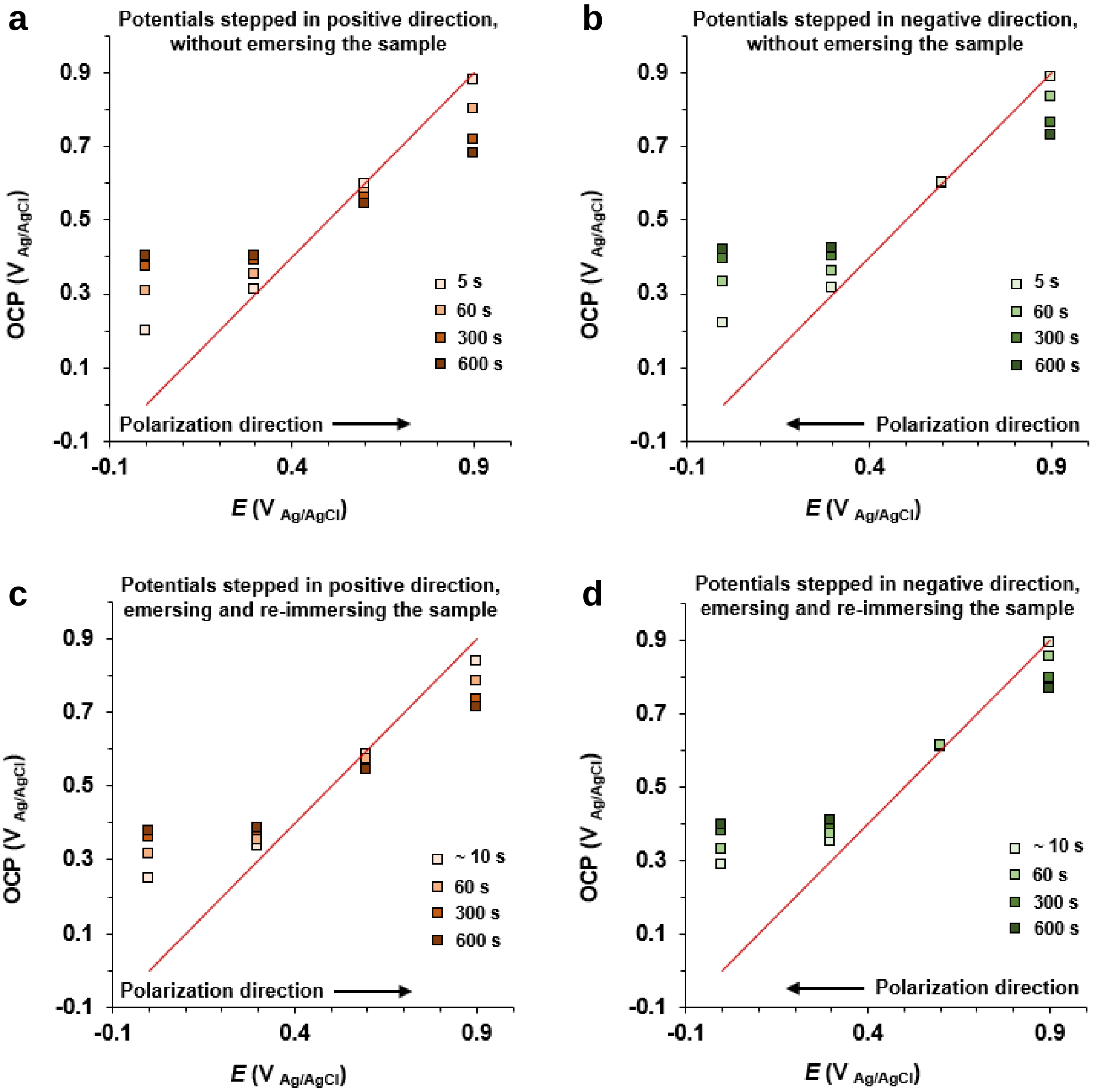

Figure 72. OCP determination on the polarized gold sample: a) and b) without emersion; c) and d) with emersion and re-immersion. Electrolyte was 0.05 mol L^{-1} H_2SO_4.

In Figure 72 results are shown of an experiment where the potentials were stepped in both directions. Then the polarization was stopped and the evolution of the OCP monitored. Four different values for the waiting time were selected and the corresponding potentials plotted in the diagrams, for 5, 60, 300 and 600 s waiting time. For the emersion and re-immersion experiment 10 s time of waiting time were chosen; this was done in order to guarantee the “stop” of the electrolyte pumping into the cell and minimizing of the “turbulence” inside the cell, caused by electrolyte filling. The OCP values show the expected behavior: the shorter the waiting time, the closer the measured potentials are compared to the originally applied potentials (especially for 5 and 10 s). Furthermore, the correlation between OCP values and corresponding applied potentials shows nearly perfect trend lines (slope 1) between 0.3 and 0.9 V. It is also important to mention the relative stability of the electrochemical double layer after the emersion and re-immersion processes, as can be seen in Figures 72c) and 72d), confirming the idea of the “frozen-in” structures during the emersion process under controlled potential, as also there a very good correlation is preserved throughout the process.

Interestingly, the correlation between OCP and the potential applied prior to stopping the polarization is lost for applied potentials below the PCZ, just as it is observed also for the emersed samples measured by Kelvin probe. Furthermore, the potential that these reach after a while is the OCP of the samples emersed in electrolyte without polarization. Interestingly, the same potential was measured by Samec *et al.*[7] for samples when the polarization was stopped when they were polarized below PZC.

In the same way as for many other experiments presented in this dissertation, the results from Figure 72 are replotted so that potentials obtained in positive and in negative directions can directly be compared. These diagrams are plotted and presented in Figures 73 (without emersion process) and 74 (with emersion and re-immersion processes).

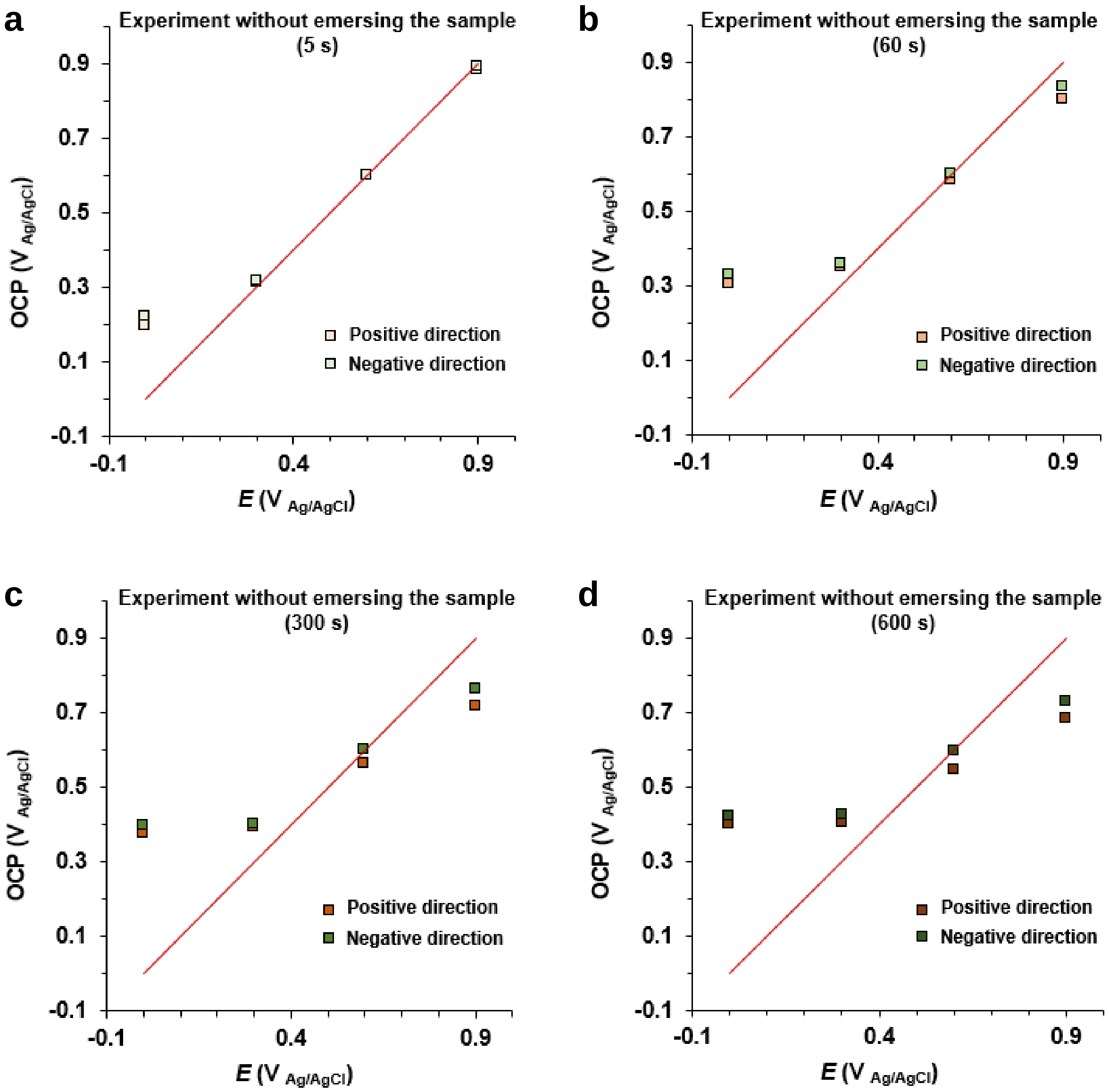

Figure 73. Plots of OCP at different waiting times after the polarization was stopped vs applied potential during polarization, with the potentials stepped in positive and in negative directions. Electrolyte was 0.05 mol L^{-1} H_2SO_4.

The results in Figure 73 show a very little shift to higher potentials when the potentials were stepped in negative direction, but for the 5 s OCP this difference was practically no detectable. After 600s up to about 50 mV difference were measured. In the next Figure are presented the results for the OCP determinations with emersion and re-immersion processes.

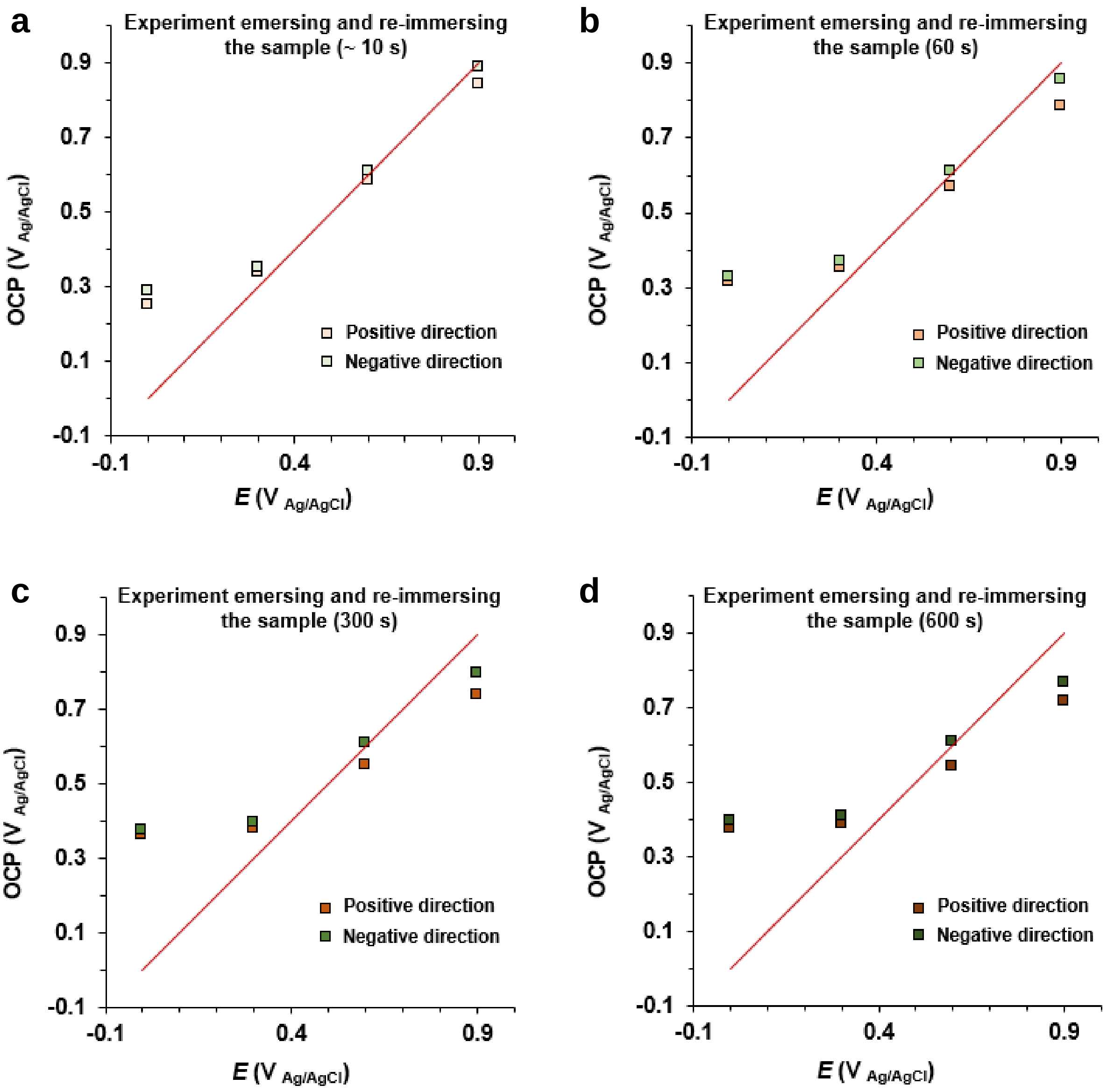

Figure 74. Plots of OCP of re-immersed samples at different waiting times after emersion vs applied potential during polarization, with the potentials stepped in positive and in negative directions. Electrolyte was 0.05 mol L^{-1} H_2SO_4.

For the emersed and re-immersed samples the difference between potentials obtained in positive and in negative direction are already in the 50 mV range even after 10 s waiting time and reach a final level of about 80 mV after 60 s. Similar values were reported by Samec *et al.* for the OCP values after stopping polarization.[7]

However, in this work the difference of the OCP values for positive and negative direction are a bit smaller than reported there.

For potentials measured directly on the emersed samples by Kelvin probe much higher values of up to 200 mV were obtained at high relative humidity. This was also observed by Samec *et al.* for the very high relative humidity that they used. For lower relative humidity investigated in this PhD work much smaller differences were observed, as previously presented in the Kelvin probe measurement section.

5 Summary and Outlook

In this dissertation a methodology for tailoring the electrochemical double layer of electrodes covered by electrolyte layers in the sub-monolayer and monolayer range was developed and first studies on these so-called “electrodes in the dry” were performed. This methodology is based -under maintenance of the polarization- on the emersion of an electrode into inert nitrogen atmosphere of different relative humidity. The idea was that by adjusting the relative humidity to different level, the thickness of the resulting electrolyte layer in the double layer can be controlled.

For these studies, first a novel complex experimental set-up was planned, built-up and taken into service. This set-up realizes the combination of an electrochemical cell with a number of optical spectroscopic techniques, such as FT-IR and ellipsometry, Kelvin probe and an ultra-high vacuum system featuring electron spectroscopies such as XPS (NAP-XPS) and UPS.

Potentials applied on the sample during immersion were stepped in a wide range: from -0.4 until 1.3 V vs Ag/AgCl (positive direction) and from 1.3 until -0.4 V vs Ag/AgCl (negative direction). After polarization at a given potential the electrode was emersed into nitrogen atmosphere of relative humidity values of 1-3%, 65-70% and 90-95%. From the measured Volta potential difference between sample and Kelvin probe the corresponding electrode potentials of the emersed electrodes were obtained, based on a calibration of the Kelvin probe with a Ag/AgCl reference at the relative humidity of interest. For the plots of potential of the emersed electrode vs the applied potential, a linear range with unity slope after emersing the electrode from the electrolyte was generally observed for applied potentials between about 0.1 until 1.0 V. This potential range corresponds to the potential window from about PZC to gold oxidation. The potentials of the emersed electrode were close to the applied values or higher, depending on the relative humidity. This dependence on relative humidity is attributed to the role of the amount water molecules and their orientations and the contribution of the corresponding dipole moments to the potential. In humid nitrogen atmosphere up to 0.2 V higher potentials were observed on the emersed electrode when the potentials were stepped during the polarization in the negative direction compared to the experiments in which the potentials were stepped in positive direction. This is similar to what was observed by Samec *et al.*[7], who suggest that this difference between the potentials of the emersed electrode polarized stepwise into positive and stepwise into negative direction might be due to a difference in the amount of specifically adsorbed anions. As it seems unlikely that specifically adsorbed excess anions per se (i.e. anions not needed as countercharge to the positive charge on the electrode) whose charge will be compensated by corresponding cation adsorption will gave a significant effect on the potential, it is proposed here that this effect is caused by adsorbed water that is adsorbed on these anions in an orientation with the hydrogen atoms pointing towards the anion and the oxygen atom pointing upwards, which indeed should result in a higher potential.

This fits well with the observation that for electrodes emersed into dry condition no difference in the potentials of emersed electrode polarized in positive and polarized in negative direction was found.

In general, the potentials obtained were higher than the ones reported by Samec *et al.*, who found that their values were about 0.3 V lower than the applied potentials[7], while for electrodes emersed into UHV values of about 0.4 V higher than applied were reported.[123] The higher potentials observed on electrodes emersed into UHV is explained by the more or less complete loss of water, which is assumed to contribute in total with 0.4 V to the potential, by decreasing it accordingly. In the case of Samec *et al.* the electrodes were emersed into very high humidity, where it is assumed that the thickness of the electrolyte layer comprises several monolayers, which are decreasing the potential and are still relatively oriented at the topmost layer with dipole orientation reducing the potential, while on the bulk electrolyte the water molecules show a net orientation increasing the potential. Hence, this difference could explain the lower potentials obtained on the electrodes emersed into very high relative humidity.

Since the relative humidity range investigated in this work is in between these two extremes, it seems reasonable that the potentials obtained here are in between the corresponding values reported for emersion into UHV and in very high humidity.

However, what seems remarkable is that the correlation observed here between potentials of the emersed electrode and the potential applied before emersion shows for most cases a clear linear dependence with slope close to 1. This would mean that there cannot be a meaningful re-orientation of the adsorbed water molecules with a change of potential, and that throughout the full linear range of about 1 V!

In that context it has to be pointed out that a 1:1 correlation between potential of the emersed electrode and the potential prior applied during immersion was observed only for applied potentials above PZC. Around PZC it seems that a re-orientation of the water molecules occurred, resulting in an often visible step in the plots of potential of the emersed electrode vs applied potential. For potential slightly below PZC still some correlation, but with much less than 1:1, was observed. With increasing negative potentials a plateau seems to be reached with even a tendency to increasing potentials measure on the emersed electrode with decreasing applied potentials. This is especially pronounced for samples emersed from alkaline electrolyte. However, since wetting of the alkaline electrolyte on the gold surface was quite strong, it was quite difficult to avoid transfer of bulk electrolyte during emersion. Hence, the electrodes emersed form alkaline electrolyte were not further investigated.

Concerning the effect of different electrolyte, for the aqueous electrolytes with sulfuric acid and the sodium perchlorate quite similar correlations between the potentials of the emersed electrode and the applied ones were observed. Both anions are weakly adsorbing on gold. In both cases, in dry atmosphere the resulting potentials show in the linear range values close to the applied ones. When going to intermediate relative humidity (of 65-70% RH), the potentials shift to higher values, more for the ones obtained when stepwise polarizing negatively, leading to a potential difference between emersed electrodes polarized in the two different directions. Precisely, this first occurs for the electrodes emersed from sulfuric acid and then is also observed at the higher humidity of 90-95% RH also for perchlorate. At this higher humidity for both cases again lower overall potentials are observed.

This is explained as follows: water in the range of a monolayer or below is present in the double layer of the electrode transferred into low relative humidity. This leads to potentials that are in the linear range more or less the same as the ones applied. And that is the case for samples stepwise polarized into positive and negative direction (maybe with the latter ones showing a slight tendency towards higher potentials). For electrodes emersed into intermediate relative humidity, additional water molecules are adsorbed on the adsorbed anions in the double layer in an orientation with the hydrogen atoms pointing towards the anion and the oxygen atom pointing upwards, which results in a higher potential (see Figure 75). A difference for electrodes stepwise polarized in the two directions is explained by more anions specifically adsorbed for polarization coming from high potentials (i.e. into the negative direction). At the highest humidity investigated (90-95% RH) more water molecules are adsorbed, mainly on the water layer directly adsorbed on the gold surface, which means preferentially in an orientation with the oxygen atom pointing downwards, i.e. decreasing now the potential (see Figure 75). This is in accordance with the results obtained by ellipsometry, that at 1-3% RH the water layer thickness is roughly in the range of about a third to half monolayer, at 65-70% RH a bit above one monolayer and at 90-95% RH about 1.5 monolayers.

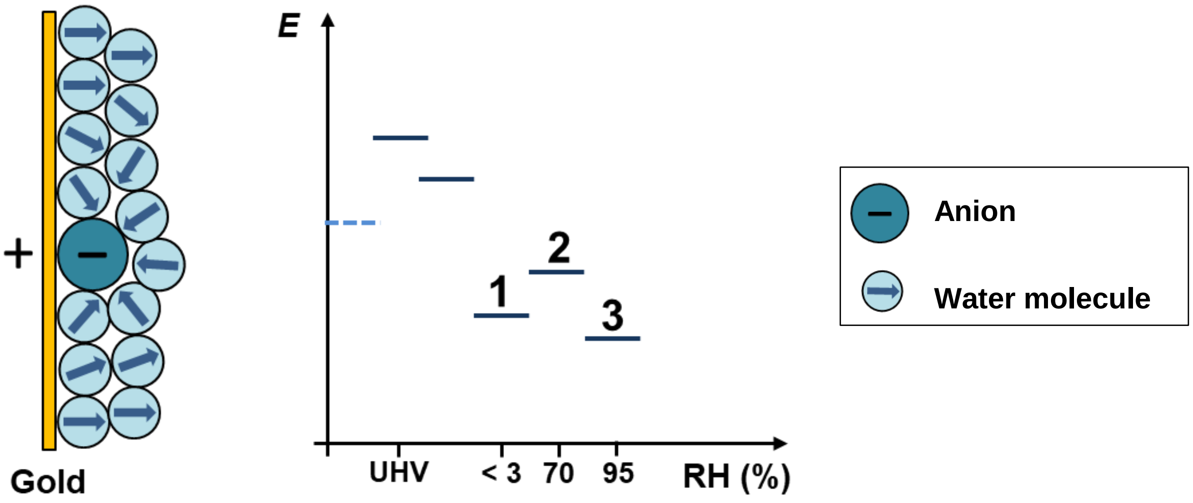

Figure 75. Schematic representation of water adsorption at different relative humidity and how it is affecting the potential of the emersed electrode (1, 2, 3 denoting 1-3% RH, 65-70% RH and 90-95% RH, respectively).

The higher amount of specifically adsorbed anions for the electrodes polarized in the negative direction, i.e. coming from higher potentials, is confirmed by the results obtained by FT-IR. While stepwise increases from lower to higher potentials (i.e. into the positive direction) clearly shows an increase of the bands associated with perchlorate or sulfate anions, for the negative direction much less changes are observed which indicates a higher specific adsorption of anions. Also, in negative direction and especially at higher humidity, the according bands are broader. While e.g. on electrodes emersed form perchlorate containing electrolyte in dry atmosphere a very sharp peak associated with the perchlorate is observed, at higher humidity this is much broader. This is assumed to be possibly due to the interaction with the water molecules. In dry atmosphere and for emersed electrodes obtained by stepwise positive polarization, even a split peak is observed in the FT-IR, which might be associated with re-orientation of the perchlorate at different field strength in the double layer region.

Surprisingly, bands that can be associated with water are more or less not discernible in the FT-IR spectra, even at 65-70% RH, where about a monolayer of water should be present, as indicated by the results obtained by Kelvin probe and by ellipsometry. Hence, no conclusions can be drawn about possible water re-orientation with changing potential. However, that a correlation close to 1:1 in the potential range where the potential of the emersed electrode shows a linear dependence on applied potential (i.e. above PZC to about 1 V) was found for different humidity levels, indicates that water molecules do not re-orient much with changes in the field. This is at least the case for potentials above PZC. Below PZC strong indications for a re-orientation were found, which even resulted in higher potentials for samples polarized prior to emersion to very negative potentials than for electrodes polarized to somewhat higher ones.

Finally, first investigations on the electrochemical reactivity of these emersed electrodes were carried out. For this the change of potential of a negatively polarized sample (-0.3 V vs Ag/AgCl) upon a change of the atmosphere from nitrogen to air was investigated for different levels of relative humidity. It was found that at low humidity of 1-3% RH only a very slow increase in potential due to oxygen reduction can be observed. For intermediate humidity of 65-70% RH the response is faster and much faster at the highest humidity. This shows that the water in the double layer region plays a crucial role for electrochemical reactions, e.g. for stabilizing ions formed during the reaction, intermediately or final. Interestingly, for the electrodes polarized coming from higher potentials (negative direction), the response of the electrode emersed into intermediate humidity was nearly the same as the one of the electrode emersed into high humidity, which supports the assumption that -at same potential- due to the higher amount of specifically adsorbed anions (and corresponding cations needed for charge neutrality) also more water is adsorbed.

Concluding, this work has demonstrated that the novel experimental set-up built at MPIE for electrochemical surface science studies of “dry electrodes” that was put into operation here is working well. Furthermore, the results obtained in this work clearly show that it is possible to control the amount of water in the double layer region and that this has an effect on the resulting potential and electrochemical reactivity. The “dry electrode” system seems to be a very promising platform for electrochemical surface science studies in order to obtain a better in-depth study of the correlation of structure and reactivity of the electrochemical interface.

As outlook, it would be desirable to be able to better characterize the water in the electrochemical double layer. One way would be to enhance the sensitivity of the FT-IR. Although XPS and especially NAP-XPS was planned to be a part of this work, these studies were not started yet. Besides a better quantified information about anions and cations on the emersed electrode, especially NAP-XPS at different relative humidity could also provide more information about the amount of water. By shifts of the XPS peaks for oxygen one might also learn about different (vertical) position of the water in different layers. Another approach would be to try also thermal desorption spectroscopy to analyze possible differences of desorption energies caused by different binding energies of the water molecules in different positions in the electrochemical double layer region.

Bibliography

1. Evers, S., Rohwerder, M., The hydrogen electrode in the “dry”: A Kelvin probe approach to measuring hydrogen in metals. *Electrochemistry Communications* 24 (2012) 85-88.

2. Evers, S. Senöz, C., Rohwerder, M., Hydrogen detection in metals: a review and introduction of a Kelvin probe approach. *Science and Technology of Advanced Materials* 14(1) (2013) 014201.

3. Zhong, X., Schulz (née Uebel), M., Wu, C.-H., Rabe, M., Erbe, A., Rohwerder, M., Limiting Current Density of Oxygen Reduction under Ultrathin Electrolyte Layers: From the Micrometer Range to Monolayers. *ChemElectroChem* 8(4) (2021) 712-718.

4. Hansen, W. N., Wang, C. L., Humphryes, T. W., Electrode emersion and the double layer. *Journal of Electroanalytical Chemistry and Interfacial Electrochemistry* 90 (1978) 137-141.

5. Kolb, D. M., Electrochemical Surface Science. *Angewandte Chemie International Edition* 40 (2001) 1162.

6. Neff, H., Kötz, R., Photoelectron spectroscopic study of emersed gold electrodes. *Journal of Electroanalytical Chemistry* 151 (1983) 305-310.

7. Samec, Z., Johnson, B. W., Doblhofer, K., The absolute electrode potential of metal electrodes emersed from liquid electrolytes. *Surface Science* 264 (1992) 440-448.

8. Debe, M. K., Tutorial on the Fundamental Characteristics and Practical Properties of Nanostructured Thin Film (NSTF) Catalysts. *Journal of The Electrochemical Society* 160(6) (2013) F522-F534.

9. McBreen, J., Voltammetric Studies of Electrodes in Contact with Ionomeric Membranes. *Journal of The Electrochemical Society* 132 (1985) 1112-1116.

10. Liu, J., Zenyuk, I. V., Proton transport in ionomer-free regions of polymer electrolyte fuel cells and implications for oxygen reduction reaction. *Current Opinion in Electrochemistry* 12 (2018) 202-208.

11. Tsuru, T., Tamiya, K.-I., Nishikata, A., Formation and growth of micro-droplets during the initial stage of atmospheric corrosion. *Electrochimica Acta* 49 (2004) 2709-2715.

12. de Oliveira, A. R. B., Estudo eletroquímico da corrosão de aço revestido com a liga $Al_{90}Si_{10}$, Faculdade de Ciências – Universidade do Porto, Porto, 2012.

13. European Federation of Corrosion (EFC), Definition of Corrosion, http://efcweb.org/Definition+of+Corrosion.html (accessed 02/03/2018).

14. Strehblow, H.-H., Phenomenological and Electrochemical Fundamentals of Corrosion. In: Schütze, M. (Ed.), *Corrosion and Environmental Degradation*, Volume I, Wiley-VCH, Weinheim, 2000, pp. 1-66.

15. Strehblow, H.-H., Marcus, P., Fundamentals of Corrosion. In: Marcus, P. (Ed.), *Corrosion Mechanisms in Theory and Practice*, Third Edition, CRC Press, Boca Raton, 2012, pp. 1-104.

16. Brett, C. M. A., Brett, A. M. O., *Electrochemistry: Principles, Methods, and Applications*, Oxford University Press, New York, 1993, pp. 427.

17. Jones, D. A., *Principles and Prevention of Corrosion*, Second Edition, Pearson Education Limited, Essex, 2014, pp. 572.

18. Craig, B. D., *Fundamental Aspects of Corrosion Films in Corrosion Science*, Plenum Press, New York, 1991, pp. 192.

19. Gokcen, N. A., *Thermodynamics*, Techscience Incorporated, Hawthorne, 1975, pp. 460.

20. Pourbaix, M., *Atlas of Electrochemical Equilibria in Aqueous Solutions*, Second Edition, National Association of Corrosion Engineers, Houston, 1974, pp. 644.

21. Huayhuas-Chipana, B. C., Gomero, J. C. M., Sotomayor, M. D. P. T., Nanostructured Screen-Printed Electrodes Modified with Self-Assembled Monolayers for Determination of Metronidazole in Different Matrices. *Journal of the Brazilian Chemical Society* 25(9) (2014) 1737-1745.

22. Weast, R. C. (Ed.), *Handbook of Chemistry and Physics*, Fifty-second Edition, Chemical Rubber Publishing Company, Cleveland, 1971, pp. 2319.

23. Combrade, P., Crevice Corrosion of Metallic Materials. In: Marcus, P. (Ed.), *Corrosion Mechanisms in Theory and Practice*, Third Edition, CRC Press, Boca Raton, 2012, pp. 449-498.

24. Kucera, V., Mattsson, E., Atmospheric Corrosion. In: Mansfeld, F. (Ed.), *Corrosion Mechanisms*, Marcel Dekker, Inc., New York, 1987, pp. 211-284.

25. Knotková-Čermáková, D., Bartoň, K., Corrosion Aggressivity of Atmospheres (Derivation and Classification). In: Dean, S. W., Rhea, E. C. (Eds.), *Atmospheric Corrosion of Metals*, ASTM STP 767, Philadelphia, 1982, pp. 225-249.

26. Chico, B., de la Fuente, D., Díaz, I., Simancas, J., Morcillo, M., Annual Atmospheric Corrosion of Carbon Steel Worldwide. An Integration of ISOCORRAG, ICP/UNECE and MICAT Databases. *Materials* 10(6) (2017) 601.

27. Baker, E. A., Lee, T. S., Calibration of Atmospheric Corrosion Test Sites. In: Dean, S. W., Rhea, E. C. (Eds.), *Atmospheric Corrosion of Metals*, ASTM STP 767, Philadelphia, 1982, pp. 250-266.

28. Eiselstein, L. E., Caligiuri, R. D., Atmospheric Corrosion of the Suspension Cables on the Williamsburg Bridge. In: Dean, S. W., Lee, T. S. (Eds.), *Degradation of Metals in the Atmosphere*, ASTM STP 965, Philadelphia, 1986, pp. 78-95.

29. Graedel, T. E., The Chemistry of Precipitation: Perspectives on Potential Impacts on the Corrosion of Metals. In: Dean, S. W., Lee, T. S. (Eds.), *Degradation of Metals in the Atmosphere*, ASTM STP 965, Philadelphia, 1986, pp. 327-335.

30. Leygraf, C., Atmospheric Corrosion. In: Marcus, P. (Ed.), *Corrosion Mechanisms in Theory and Practice*, Third Edition, CRC Press, Boca Raton, 2012, pp. 669-704.

31. Prabhakar, J. M., Kerger, P., de Vooys, A., Rohwerder, M., Migration of ions on oxygen-deficient chromium oxide electrodeposited from trivalent chromium electrolyte. *Corrosion Science* 199 (2022) 110185.

32. Khayatan, N., Rohwerder, M., A new insight into the rate determining step of cathodic delamination. *Corrosion Science* 202 (2022) 110311.

33. Ito, M., Ooi, A., Tada, E., Nishikata, A., In Situ Evaluation of Carbon Steel Corrosion under Salt Spray Test by Electrochemical Impedance Spectroscopy. *Journal of The Electrochemical Society* 167 (2020) 101508.

34. Simillion, H., Dolgikh, O., Terryn, H., Deconinck, J., Atmospheric corrosion modeling. *Corrosion Reviews* 32(3-4) (2014) 73-100.

35. Van der Steen, N., Simillion, H., Dolgikh, O., Terryn, H., Deconinck, J., An integrated modeling approach for atmospheric corrosion in presence of a varying electrolyte film. *Electrochimica Acta* 187 (2016) 714-723.

36. Stratmann, M., Streckel, H., Kim, K. T., Crockett, S., On the atmospheric corrosion of metals which are covered with thin electrolyte layers – III. The measurement of polarization curves on metal surfaces which are covered with thin electrolyte layers. *Corrosion Science* 30 (1990) 715-734.

37. Nishikata, A., Ichihara, Y., Hayashi, Y., Tsuru, T., Influence of Electrolyte Layer Thickness and pH on the Initial Stage of the Atmospheric Corrosion of Iron. *Journal of The Electrochemical Society* 144 (1997) 1244-1252.

38. Peschka, W., *Liquid Hydrogen: Fuel of the Future*, Springer-Verlag, Vienna, 1992, pp. 303.

39. Godula-Jopek, A., Jehle, W., Wellnitz, J., *Hydrogen Storage Technologies: New Materials, Transport, and Infrastructure*, First Edition, Wiley-VCH, Weinheim, 2012, pp. 254.

40. Airbus, Airbus ZEROe (zero-emission aircraft concept), https://www.airbus.com/newsroom/stories/these-new-Airbus-concept-aircraft-have-one-thing-in-common.html (accessed 30/09/2020).

41. Airbus, Airbus reveals new zero-emission concept aircraft, Press Release, Toulouse, France, 2020, pp. 3.

42. Haseli, Y., Maximum conversion efficiency of hydrogen fuel cells. *International Journal of Hydrogen Energy* 43 (2018) 9015-9021.

43. Khotseng, L., Fuel Cell Thermodynamics. In: Vizureanu, P. (Ed.), *Thermodynamics and Energy Engineering*, IntechOpen, Rijeka, 2020, pp. 1-17.

44. Kaesche, H., *Die Korrosion der Metalle: Physikalisch-chemische Prinzipien und aktuelle Probleme*, Springer-Verlag, Heidelberg, 2011, pp. 555.

45. Louthan Jr., M. R., The Effect of Hydrogen on Metals. In: Mansfeld, F. (Ed.), *Corrosion Mechanisms*, Marcel Dekker, Inc., New York, 1987, pp. 329-365.

46. Sparnaay, M. J., The Electrical Double Layer. In: Everett, D. H. (Ed.), *The International Encyclopedia of Physical Chemistry and Chemical Physics – Topic 14: Properties of Interfaces*, Pergamon Press Ltd., Oxford, 1972, pp. 415.

47. Souza, A. K. P., Desenvolvimento de potenciostatos para caracterização de células eletroquímicas, Faculdade de Tecnologia – Universidade Federal do Amazonas, Manaus, 2016.

48. Atkins, P., de Paula, J., *Physical Chemistry*, Tenth Edition, Oxford University Press, Oxford, 2014, pp.1008.

49. Vijayshankar, D., Tran, T. H., Bashir, A., Evers, S., Rohwerder, M., Hydrogen Permeation as a Tool for Quantitative Characterization of Oxygen Reduction Kinetics at Buried Metal-Coating Interfaces. *Electrochimica Acta* 189 (2016) 111-117.

50. Grundmeier, G., Jüttner, K.-M., Stratmann, M., Novel Electrochemical Techniques in Corrosion Research. In: Schütze, M. (Ed.), *Corrosion and Environmental Degradation*, Volume I, Wiley-VCH, Weinheim, 2000, pp. 285-381.

51. KP Technology, Ultra-High Vacuum (UHV) Kelvin probe system manual: For software series 11 and hardware versions UHV-KP020-50/UHV-KP020-100, KP Technology, Wick, United Kingdom, 2017, pp. 52.

52. Uebel, M., Vimalanandan, A., Laaboudi, A., Evers, S., Stratmann, M., Diesing, D., Rohwerder, M., Fabrication of Robust Reference Tips and Reference Electrodes for Kelvin Probe Applications in Changing Atmospheres. *Langmuir* 33 (2017) 10807-10817.

53. Lägel, B., The application of the Kelvin Probe in materials science, Robert Gordon University, Aberdeen, 2000.

54. Herring, C., Nichols, M. H., Thermionic Emission (Chapter I. Thermodynamics of Emission from Uniform Surfaces). *Reviews of Modern Physics* 21 (1949) 187-199.

55. Baikie, I. D., Grain, A. C., Sutherland, J., Law, J., Dual Mode Kelvin Probe: featuring Ambient Pressure Photoemission Spectroscopy and Contact Potential Difference. *Energy Procedia* 60 (2014) 48-56.

56. Trasatti, S., Structure of the metal/electrolyte solution interface: new data for theory. *Electrochimica Acta* 36(11/12) (1991) 1659-1667.

57. Rohwerder, M., Turcu, F., High-resolution Kelvin probe microscopy in corrosion science: Scanning Kelvin probe force microscopy (SKPFM) versus classical Kelvin probe (SKP). *Electrochimica Acta* 53 (2007) 290-299.

58. Gomer, R., Tryson, G., An experimental determination of absolute half-cell emf's and single ion free energies of solvation. *The Journal of Chemical Physics* 66 (1977) 4413-4424.

59. The Kelvin Probe Principles, http://www.kelvinprobe.info/technique-principles.htm (accessed 03/07/2018).

60. Cook, A. B., Barrett, Z., Lyon, S. B., McMurray, H. N., Walton, J., Williams, G., Calibration of the scanning Kelvin probe force microscope under controlled environmental conditions. *Electrochimica Acta* 66 (2012) 100-105.

61. Burgstaller, W., Schimo, G., Hassel, A. W., Challenges in hydrogen quantification using Kelvin probe technique at different levels of relative humidity. *Journal of Solid State Electrochemistry* 21 (2017) 1785-1796.

62. Schrader, B. (Ed.), *Infrared and Raman Spectroscopy: Methods and Applications*, VCH Verlagsgesellschaft mbH, Weinheim, 1995, pp. 786.

63. Hercules, D. M., Surface Analytical Techniques – An Overview. In: Randell, D. R., Neagle, W. (Eds.), *Surface Analysis Techniques and Applications*, Royal Society of Chemistry, Cambridge, 1990, pp. 173.

64. Silverstein, R. M., Webster, F. X., Kiemle, D. J., *Identificação Espectrométrica de Compostos Orgânicos*, Seventh Edition, LTC, Rio de Janeiro, 2006, pp. 530.

65. Choong, Y.-K., Fourier Transform Infrared and Two-Dimensional Correlation Spectroscopy for Substance Analysis. In: Nikolic, G. (Ed.), *Fourier Transforms – High-tech Applications and Current Trends*, IntechOpen, London, 2017, pp. 175-190.

66. Skoog, D. A., Leary, J. J., *Instrumentelle Analytik: Grundlagen – Geräte – Anwendungen*, Springer-Verlag, Berlin, 1996, pp. 898.

67. Ataka, K., Yotsuyanagi, T., Osawa, M., Potential-dependent reorientation of water molecules at an electrode/electrolyte interface studied by surface-enhanced infrared absorption spectroscopy. *Journal of Physical Chemistry* 100 (1996) 10664-10672.

68. Fujiwara, H., *Spectroscopic Ellipsometry – Principles and Applications*, Wiley, Chichester, 2007, pp. 369.

69. Tompkins, H. G., McGahan, W. A., *Spectroscopic Ellipsometry and Reflectometry – A User's Guide*, Wiley, New York, 1999, pp. 228.

70. Sirohi, R. S., Genshaw, M. A., Electrochemical Ellipsometric Study of Gold. *Journal of the Electrochemical Society* 116(7) (1969) 910-914.

71. McCrackin, F. L., Passaglia, E., Stromberg, R. R., Steinberg, H. L., Measurement of the Thickness and Refractive Index of Very Thin Films and the Optical Properties of Surfaces by Ellipsometry. *Journal of Research of the National Bureau of Standards – A. Physics and Chemistry* 67A(4) (1963) 363-377.

72. Hofmann, S., *Auger- and X-Ray Photoelectron Spectroscopy in Materials Science*, Springer-Verlag, Berlin, Heidelberg, 2013, pp. 528.

73. SPECS, PHOIBOS 150 NAP – Near Ambient Pressure Hemispherical Energy Analyzer, SPECS Surface Nano Analysis GmbH, Berlin, Germany, 2010, pp. 8.

74. Starr, D. E., Liu, Z., Hävecker, M., Knop-Gericke, A., Bluhm, H., Investigation of solid/vapor interfaces using ambient pressure X-ray photoelectron spectroscopy. *Chemical Society Reviews* 42 (2013) 5833-5857.

75. Van der Heide, P. A. W., *X-Ray Photoelectron Spectroscopy – An Introduction to Principles and Practices*, Wiley, Hoboken, 2012, pp. 241.

76. Young, V. Y., Hoflund, G. B., Photoelectron Spectroscopy (XPS and UPS), Auger Electron Spectroscopy (AES), and Ion Scattering Spectroscopy (ISS). In: Rivière, J. C., Myhra, S. (Eds.), *Handbook of Surface and Interface Analysis – Methods for Problem-Solving*, Second Edition, CRC Press, Boca Raton, 2009, pp. 19-64.

77. IUPAC. Compendium of Chemical Terminology, 2nd ed. (the “Gold Book”). Compiled by A. D. McNaught and A. Wilkinson. Blackwell Scientific Publications, Oxford (1997). Online version (2019-) created by S. J. Chalk. ISBN 0-9678550-9-8. https://doi.org/10.1351/goldbook (accessed 11/08/2021).

78. Lützenkirchen-Hecht, D., Strehblow, H.-H., Surface analytical investigations of the electrochemical double layer on silver electrodes in alkaline media. *Electrochimica Acta* 43 (1998) 2957-2968.

79. Heras, J. M., Viscido, L., Work function changes upon water contamination of metal surfaces. *Applications of Surface Science* 4 (1980) 238-241.

80. Wells, R. L., Fort Jr., T., Adsorption of water on clean gold by measurement of work function changes. *Surface Science* 32 (1972) 554-560.

81. Zettlemoyer, A. C., Micale, F. J., Klier, K., Adsorption of Water on Well-Characterized Solid Surfaces. In: Franks, F. (Ed.), *Water: A Comprehensive Treatise*, Volume 5, Springer Science + Business Media, LLC, New York, 1975, pp. 249-291.

82. Burke, L. D., Nugent, P. F., The Electrochemistry of Gold: I The Redox Behaviour of the Metal in Aqueous Media. *Gold Bulletin* 30(2) (1997) 43-53.

83. Nguyen Van Huong, G., Hinnen, C., Lecoeur, J., Spectroscopic investigation of single crystal gold electrodes: Part II. The incipient oxidation of gold electrode. *Journal of Electroanalytical Chemistry* 106 (1980) 185-191.

84. Cherevko, S., Topalov, A. A., Zeradjanin, A. R., Katsounaros, I., Mayrhofer, K. J. J., Gold dissolution: towards understanding of noble metal corrosion. *RSC Advances* 3 (2013) 16516-16527.

85. Ujvári, M., Láng, G. G., On the stability of perchlorate ions against reductive attacks in electrochemical systems and in the environment. *Journal of Electrochemical Science and Engineering* 1(1) (2011) 1-26.

86. Angerstein-Kozlowska, H., Conway, B. E., Barnett, B., Mozota, J., The role of ion adsorption in surface oxide formation and reduction at noble metals: general features of the surface process. *Journal of Electroanalytical Chemistry* 100 (1979) 417-446.

87. Angerstein-Kozlowska, H., Conway, B. E., Hamelin, A., Stoicoviciu, L., Elementary steps of electrochemical oxidation of single-crystal planes of Au-I.

Chemical basis of processes involving geometry of anions and the electrode surfaces. *Electrochimica Acta* 31 (1986) 1051-1061.

88. Bodé Jr., D. D., Andersen, T. N., Eyring, H., Anion and pH Effects on the Potential of Zero Charge of Gold and Silver Electrodes. *Journal of Physical Chemistry* 71 (1967) 792-797.

89. Samec, Z., Johnson, B. W., Cappadonia, M., Jauch, M., Doblhofer, K., Kelvin probe measurements for chemical analysis: interfacial structure of electrodes exposed to the gas phase containing water vapour. *Sensors and Actuators B* 13-14 (1993) 741-742.

90. Zhang, W., Bas, A. D., Ghali, E., Choi, Y., Passive behavior of gold in sulfuric acid medium. *Transactions of Nonferrous Metals Society of China* 25 (2015) 2037-2046.

91. Zhang, Y., Gao, X., Weaver, M. J., Nature of Surface Bonding on Voltammetrically Oxidized Noble Metals in Aqueous Media as Probed by Real-Time Surface-Enhanced Raman Spectroscopy. *Journal of Physical Chemistry* 97 (1993) 8656-8663.

92. Bruker Optics, VERTEX 70v User Manual, Bruker Optik GmbH, Ettlingen, Germany, 2007, pp. 146.

93. Ivium Technologies, http://www.ivium.nl/filez/documents/Ivium%20Manual.pdf (accessed 27/02/2018).

94. Haider, C., Electrodes in Potentiometry, Metrohm AG, Herisau, Switzerland, 2004, pp. 27.

95. J.A. Woollam, iSE Spectroscopic Ellipsometer Hardware Manual, J.A. Woollam Co., Lincoln, USA, 2018, pp. 98.

96. Pfeiffer Vacuum, HiPace 700 Turbopump Operating Instructions, Pfeiffer Vacuum GmbH, Aßlar, Germany, pp. 42.

97. Pfeiffer Vacuum, HiPace 300 Turbopumpe Betriebsanleitung, Pfeiffer Vacuum GmbH, Aßlar, Deutschland, pp. 85.

98. Pfeiffer Vacuum, HiPace 80 Turbopumpe Betriebsanleitung, Pfeiffer Vacuum GmbH, Aßlar, Deutschland, pp. 74.

99. Milli-Q Reference System, User Manual, Millipore SAS, Molsheim, France, 2010, pp. 90.

100. Hansen, W. N., Hansen, G. J., Standard reference surfaces for work function measurements in air. *Surface Science* 481 (2001) 172-184.

101. Kim, C., Bae, C., Ryu, K., Lee, B., Shin, H., Local Work Function Measurements on Various Inorganic Materials Using Kelvin Probe Force Spectroscopy. *Solid State Phenomena* 124-126 (2007) 607-610.

102. Atanasoski, R. T., Huang, S.-M., Albani, O., Oriani, R. A., A dry redox couple employed as the reference material in work function and corrosion potential measurements by the Kelvin technique. *Corrosion Science* 36(9) (1994) 1513-1521.

103. Ehahoun, H., Stratmann, M., Rohwerder, M., Ag/AgCl/KCl micro-electrodes as O_2-insensitive reference tips for dynamic scanning Kelvin probe measurement. *Electrochimica Acta* 50 (2005) 2667-2674.

104. Garrillo, P. A. F., Grévin, B., Chevalier, N., Borowik, Ł., Calibrated work function mapping by Kelvin probe force microscopy. *Review of Scientific Instruments* 89 (2018) 043702.

105. Liscio, A., Palermo, V., Müllen, K., Samori, P., Tip-Sample Interactions in Kelvin Probe Force Microscopy: Quantitative Measurement of the Local Surface Potential. *Journal of Physical Chemistry C* 112 (2008) 17368-17377.

106. Hansen, W. N., Kolb, D. M., The work function of emersed electrodes. *Journal of Electroanalytical Chemistry* 100 (1979) 493-500.

107. Kaur, J., Kant, R., Theory of Work Function and Potential of Zero Charge for metal Nanostructured and Rough Electrodes. *Journal of Physical Chemistry* 121 (2017) 13059-13069.

108. Macdonald, J. R., Barlow Jr., C. A., Work Function Change on Monolayer Adsorption. *Journal of Chemical Physics* 39 (1963) 412.

109. Stair, P. C., The Concept of Lewis Acids and Bases Applied to Surfaces. *Journal of the American Chemical Society* 104 (1982) 4044-4052.

110. Trasatti, S., The “absolute” electrode potential – the end of the story. *Electrochimica Acta* 35(1) (1990) 269-271.

111. Trasatti, S., Relative and Absolute Electrochemical Quantities – Components of the Potential Difference across the Electrode/Solution Interface. *Journal of* *the Chemical Society, Faraday Transactions 1: Physical Chemistry in Condensed Phases* 70 (1974) 1752-1768.

112. Trasatti, S., Potentials of zero charge and "electrochemical" work functions. *Journal of Electroanalytical Chemistry* 33 (1971) 351-378.

113. Bockris, J. O'M., Argade, S. D., Gileadi, E., The determination of the potential of zero charge on solid metals. *Electrochimica Acta* 14 (1969) 1259-1283.

114. Holze, R., Electrode potentials of zero charge of metal electrodes in contact with electrolyte solutions. In: Lechner, M. D. (Ed.), *Electrochemical Thermodynamics and Kinetics*, Springer-Verlag, Berlin Heidelberg, 2007, pp. 191-231.

115. Thiel, P. A., Madey, T. E., The interaction of water with solid surfaces: fundamental aspects. *Surface Science Reports* 7 (1987) 211-385.

116. Sepa, D. B., Vojnovic, M. V., Vracar, Lj. M., Damjanovic, A., Different views regarding the kinetics and mechanisms of oxygen reduction at Pt and Pd electrodes. *Electrochimica Acta* 32(1) (1987) 129-134.

117. Siebert, H., Kraftkonstante und Strukturchemie – Struktur der Sauerstoffsäuren. *Zeitschrift für anorganische und allgemeine Chemie* 275 (1954) 225-240.

118. Nakamoto, K., *Infrared and Raman Spectra of Inorganic and Coordination Compounds – Part A: Theory and Applications in Inorganic Chemistry*, Sixth Edition, Wiley, Hoboken, 2009, pp. 419.

119. Hansen, G. J., Hansen, W. N., Infrared Spectroscopy of the Electrochemical Double Layer Via Electrode Emersion. *Berichte der Bunsengesellschaft für physikalische Chemie* 91 (1987) 317-320.

120. Periasamy, A., Muruganand, S., Palaniswamy, M., Vibrational studies of Na_2SO_4, K_2SO_4, $NaHSO_4$ and $KHSO_4$ crystals. *Rasayan Journal of Chemistry* 2(4) (2009) 981-989.

121. Hintze, P. E., Feierabend, K. J., Havey, D. K., Vaida, V., High-resolution spectroscopy of H_2SO_4, $HDSO_4$, and D_2SO_4 vapor in the region 1200-10000 cm^{-1}. *Spectrochimica Acta Part A* 61 (2005) 559-566.

122. Karslioğlu, O., Nemšák, S., Zegkinoglou, I., Shavorskiy, A., Hartl, M., Salmassi, F., Gullikson, E. M., Ng, M. L., Rameshan, Ch., Rude, B., Bianculli, D., Cordones, A. A., Axnanda, S., Crumlin, E. J., Ross, P. N., Schneider, C. M., Hussain, Z., Liu, Z., Fadley, C. S., Bluhm, H., Aqueous solution/metal interfaces investigated *in operando* by photoelectron spectroscopy. *Faraday Discussions* 180 (2015) 35-53.

123. Kötz, E. R., Neff, H., Müller, K., A UPS, XPS and work function study of emersed silver, platinum and gold electrodes. *Journal of Electroanalytical Chemistry* 215 (1986) 331-344.

All drawings presented in the figures (including the instruments/equipment) were made by the author of this dissertation. Some shapes, colors and details may have a small difference between the drawings and the real instruments/equipment. The instruments/equipment represented in different figures are not necessarily in the same scale.

The constant values presented in the glossary were referenced from: Atkins, P., Jones, L., *Princípios de Química: Questionando a vida moderna e o meio ambiente*, Bookman, Porto Alegre, 2001, pp. 914.

Appendix A: Configuring and testing the electrochemical cell

In order to optimize parameters, such as the time needed to fill the electrochemical cell with electrolyte, according tests were carried out. These experiments helped to explain some observations made during the experiments.

In order to assess the reliability of the electrochemical control under the operation conditions of this work, the potentiostat was tested using the testcell (Figure 1) provided by the manufacturer in order to check the linearity of the equation $R = U / i$. In some of these tests relevant oscillations were observed, affecting directly the desired linearity. After checking the cables and connections, it was noticed that “instable signal”/oscillations (i.e. noise) was present always when the diaphragm pump for the electrolyte was on. The vibration caused by this pump was also transmitted to the entire electrolyte hose system and affected directly the reference electrode cable.

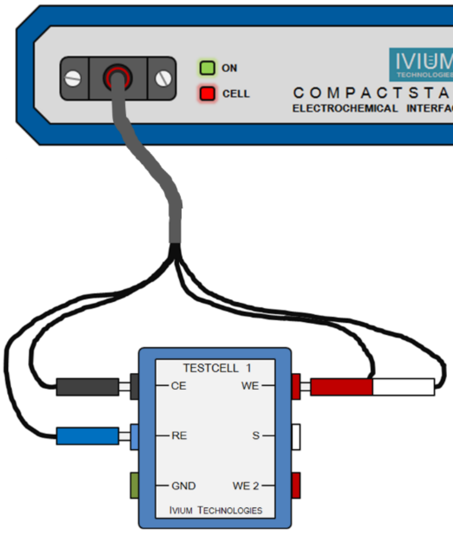

Figure 1. Potentiostat connected to the testcell through the cables for working, reference and counter electrodes. This testcell operates at 1000 Ω resistivity.

The diaphragm pump for the electrolyte (as introduced in section 3.1.3) was operated according the description presented in Figure 2.

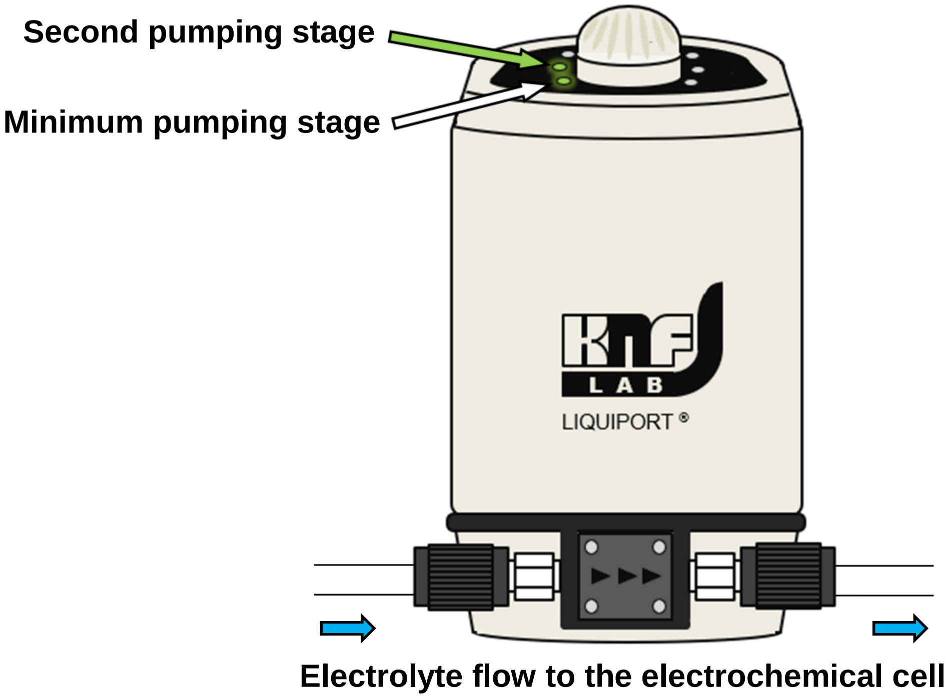

Figure 2. Diaphragm pump employed in the electrochemical cell system: the rate of the electrolyte flow from the reservoir to the electrochemical cell was controlled through ten stages (indicated by green LED lights), from minimum to maximum. For the experiments in this dissertation, the pump was always set on the second pumping stage.

This pump was operated in the low flow stage (second pumping stage) in order to avoid higher pressures in the hoses and connections system and also to minimize a turbulent electrolyte flow to the electrochemical cell. The electrolyte was removed from the cell while the pump was turned totally off or it was set to the minimum pumping stage; the removal of the electrolyte was controlled by the valves presented previously in section 3.1.3 (Figures 16m) and 16n)).

The time needed for the processes from filling the electrochemical cell with electrolyte until removing it from the cell were determined using ultrapure water and monitoring its behavior in the hoses and connections system. Values for the duration of key steps in operating the electrolyte in the cell are presented in Table 1.

Table 1. Processes involved in the electrochemical cell study, from filling until removing the electrolyte.

Process step	Time needed (s)	Observations
Filling electrolyte	30 – 40	
Flow stabilizing	20	
Pump turned off	30	After electrolyte flow stabilizing
Polarization	80	Started 30 s after pump was turned off
Removing electrolyte	20 – 40	Potential maintained applied

The polarization time was not influenced by these experiments; it was stablished for 120 s (total time for the applied potential) and after 80 s the valve for changing the electrolyte flow from the electrochemical cell back to the electrolyte flask was opened. The electrolyte had up to 40 s to be removed from the electrochemical cell while the potential was maintained applied on the working electrode (gold sample). It was not possible to assure exactly when the electrochemical cell was completely empty (without electrolyte), since it was made entirely of PTFE and its construction does not allow a look inside. Nevertheless, the time evaluated between 20 and 40 s was sufficient to empty the cell; this was confirmed by pulling the device for sample introduction back and no electrolyte leak was observed.

After setting the time for all the processes presented in Table 1, the potentiostat (using the testcell) was configured in the “Linear Sweep (Standard)” mode. As mentioned earlier, some interferences from the diaphragm pump were noticed. The results of different experiments employing the testcell are presented in Figure 3.

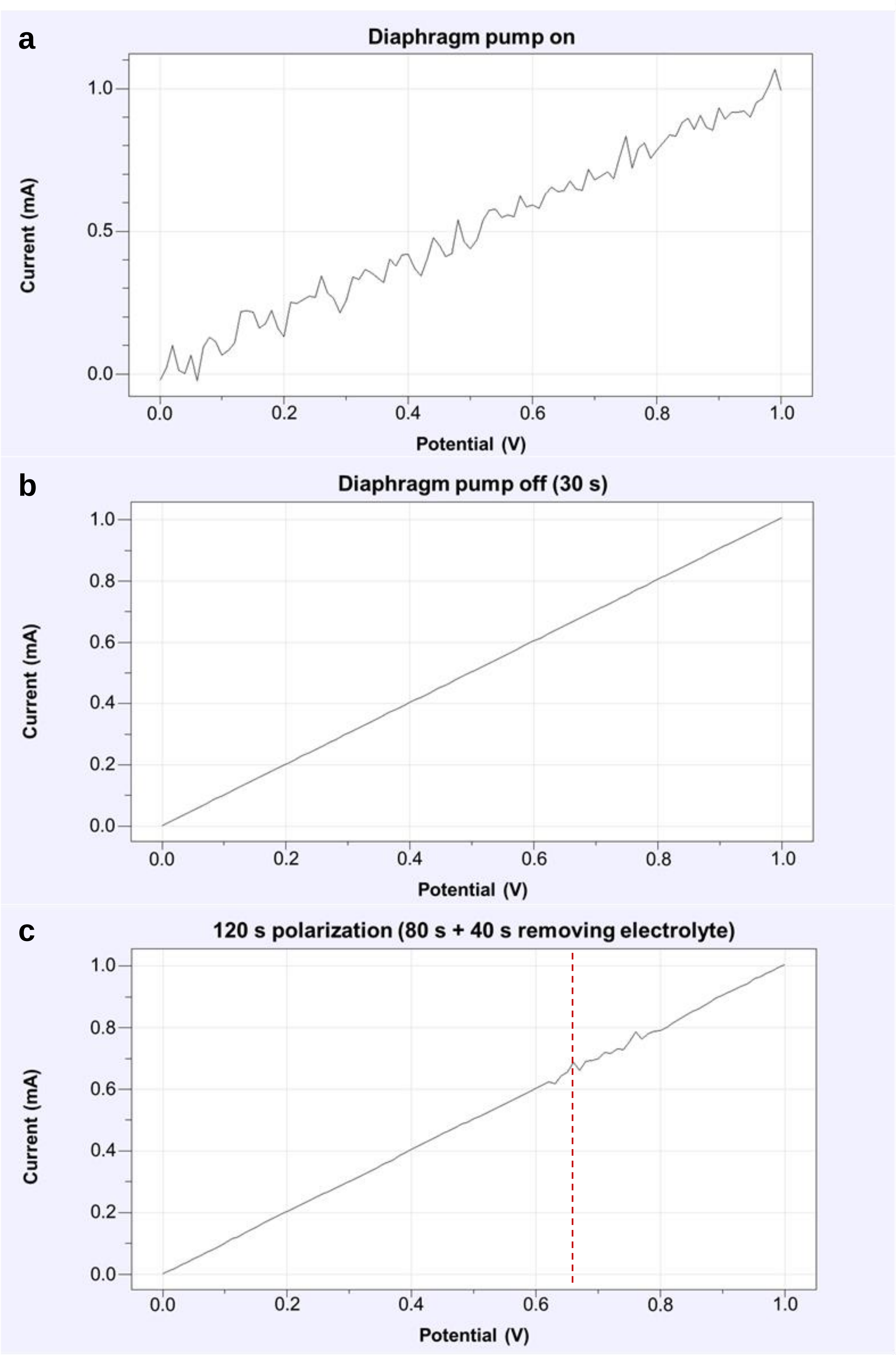

Figure 3. Results to check the linearity of the equation $R = U / i$ employing the testcell: a) diaphragm pump turned on (second pumping stage); b) diaphragm pump

turned off and waited 30 s to start the measurement; c) simulation of 120 s polarization, opening the valve for changing the electrolyte flow from the electrochemical cell back to the electrolyte flask after 80 s (red dashed line). All experiments were done employing ultrapure water instead real electrolyte.

As shown in Figure 3a), visible oscillations are present, however, when the diaphragm pump is turned off the result is more stable, as shown in Figure 3b). This behavior suggests an influence of the pump vibrations on the stability of the potential measurement. The small oscillations near the red dashed line in Figure 3c) were probably caused when the valve was opened and the water removed from the electrochemical cell.

Curriculum Vitae

Personal information

Name: Cristiano Kasdorf Giesbrecht

Birth information: 09.09.1984 - Bagé/RS - Brazil

e-Mail: cristiano.k.giesbrecht@gmail.com

Formal education

2017 - 2023 **Doctorate degree (Dr.-Ing.)**

Max-Planck-Institut für Eisenforschung GmbH (MPIE), Düsseldorf, Germany / Ruhr-Universität Bochum (RUB), Bochum, Germany

Thesys title in German: Elektrochemie von „trockenen“ Metalloberflächen im Hinblick auf atmosphärische Korrosion.

Lectures: ***Surface Science and Corrosion (electrochemistry principles with thermodynamics and kinetics, corrosion types, corrosion prevention techniques, coatings and inhibitors, delamination study, hydrogen embrittlement, analytical tools for surface science).***

2015 - 2017 **Master's in Chemistry (M. Sc.)**

Universidade Federal de Santa Maria (UFSM), Santa Maria, Brazil

Dissertation title in Portuguese: Determinação de Elementos do Grupo da Platina em Carvão com Alto Teor de Cinzas por ICP-MS ***“Determination of Platinum Group Elements in High Ash Content Coal by ICP-MS”***.

Lectures: ***Instrumental Methods in Analytical Chemistry, Advanced Analytical Chemistry, Experimental Application of Atomic Absorption Spectroscopy, Special Topics in Analytical Chemistry, Seminars in Chemistry.***

2004 - 2010 **Graduation in Industrial Chemistry (Diplom)**

Universidade Federal de Santa Maria (UFSM), Santa Maria, Brazil

Internship report title in Portuguese: Formação de monocamadas auto-organizadas de ácido octadecilfosfônico sobre a superfície de placas de nióbio ***“Formation of octadecylphosphonic acid Self-Assembled Monolayers on niobium surfaces”***. Work developed during an internship at the Max-Planck-Institut für Eisenforschung GmbH (MPIE) and presented at the UFSM.

2000 - 2002 **High Education**

Escola Estadual de Ensino Médio Dr. Carlos Antônio Kluwe, Bagé, Brazil

1992 - 1999 **Primary and Secondary Education**

Escola de 1º Grau Menno Simons, Colônia Nova, Bagé, Brazil

Professional experience

Max-Planck-Institut für Eisenforschung GmbH (MPIE) - Düsseldorf, Germany

2017 - present Contract: Researcher/PhD Student

Development of the PhD thesys and instrumentation assembling in the laboratory, with main emphasis in Surface Science, Corrosion, Instrumentation (FT-IR, XPS, Kelvin probe technique), Electrochemistry.

2008 - 2008 Contract: Internship (DAAD scholarship)

Internship fulfilled during October and November in a project related to surface modifications (Self-Assembled Monolayers on niobium surfaces) employing infrared spectroscopy for the characterization.

Fundação de Apoio à Tecnologia e Ciência (FATEC/RS) - Santa Maria, Brazil

2015 - 2015 Contract: Laboratory technician

Working contract during the Master in Chemistry with main emphasis in crude oil sample preparation and analysis.

2010 - 2014 Contract: Laboratory technician

Worked with vegetable sample preparation for nutrient and water analysis (ion chromatography and atomic spectrometry).

Languages

German (Hochdeutsch): Understanding Fluent, Speaking Fluent, Writing Fluent, Reading Fluent

English: Understanding Fluent, Speaking Fluent, Writing Fluent, Reading Fluent

Plattdeutsch (Dialekt): Understanding Fluent, Speaking Fluent, Writing Basic, Reading Functional

Portuguese (Native): Understanding Fluent, Speaking Fluent, Writing Fluent, Reading Fluent

Spanish: Understanding Basic, Speaking Basic, Reading Basic

Online Version

Additional information to this CV, like publications and participation in events, you will find on:

Plataforma Lattes / Currículo Lattes:
http://buscatextual.cnpq.br/buscatextual/visualizacv.do?id=K4710016T6&tipo=completo&idiomaExibicao=2
(Portuguese and English)

LinkedIn:
www.linkedin.com/in/cristianokasdorfgiesbrecht
(English)

Düsseldorf, 22 August 2023

Cristiano Kasdorf Giesbrecht